HOLDUP STUDIES IN THREE-PHASE FLUIDIZED BEDS AND RELATED SYSTEMS

by

VINAY KUMAR BHATIA

B. Sc. (Chem. Eng.), Agra University, India, 1963

M. Tech. (Chem. Eng.), I.I.T., Kharagpur, India, 1965

A THESIS SUBMITTED IN PARTIAL FULFILMENT OF THE REQUIREMENTS FOR THE DEGREE OF DOCTOR OF PHILOSOPHY

in the Department of CHEMICAL ENGINEERING

We accept this thesis as conforming to the required standard

THE UNIVERSITY OF BRITISH COLUMBIA

December, 1972

In presenting this thesis in partial fulfillment of the requirements for an advanced degree at the University of British Columbia, I agree that the Library shall make it freely available for reference and study. I further agree that permission for extensive copying of this thesis for scholarly purposes may be granted by the Head of my Department or by his representatives. It is understood that publication, in part or in whole, or the copying of this thesis for financial gain shall not be allowed without my written permission.

VINAY K. BHATIA

Department of Chemical Engineering

The University of British Columbia

Vancouver 8, Canada

Date Jan. 19, 1973.

ABSTRACT

Previous research in three-phase fluidization has provided some experimental data on individual phase holdups, but no unified bed model for predicting these holdups under a variety of circumstances. A step in this direction is made here with the development of a "generalized wake model", which builds upon the earlier analyses of Østergaard, of Efremov and Vakhrushev, and of Rigby and Capes. The present analysis takes into account

1. the effect of size and particle content of the bubble wakes,
2. the circulation of solids initiated by particle entrainment in the bubble wakes, and
3. the relative motion between the continuous phase and the dispersed phases.

It does not take into account any surface effects, especially the solids wettability. The expression used for estimating the wake volume fraction was necessarily arbitrary, due to the paucity of relevant information on bubble wakes, especially in the presence of solids.

Comparison of the generalized wake model with previous analyses indicates that the earlier models are special cases of the generalized wake model. Where the wake volume fraction can be neglected, the generalized model reduces

to the "gas-free model," which follows from the mechanism proposed by Volk. This simplified model gives good prediction of solids holdup for previous experimental data on three-phase fluidization of heavy and/or large particles, in which the paradoxical bed contraction on introduction of gas is no longer observed.

Experiments to test the generalized wake model were carried out over a particle diameter range of 1/4 - 3 mm and a particle density range of 2.5 - 11.1 gm/cm^3, using water (1 c.p.), aqueous glycerol (2.1 c.p.) and aqueous polyethylene glycol (63 c.p.), covering the particle Reynolds number range of 0.36 - 1800. The experiments were performed in 20 mm and 2 inch diameter transparent columns. The liquid superficial velocity was varied from 0.4 to 39 cm/sec and the gas (air) superficial velocity from 0.2 to 21.0 cm/sec. Holdups in the three-phase fluidized bed, as well as in the gas-liquid regions above and below the bed, were measured by the pressure drop gradient method and by the valve shut-off technique. Attempts were made to analyze, as well as to modify, the methods used for measuring holdups. Thus, whereas the expanded bed height in the 20 mm glass column was obtained from somewhat arbitrary visual observations, the expanded bed height in the 2 inch perspex column was obtained by the intersection of two straight lines, one of positive (three-phase region) and one of negative (two-phase region) slope, resulting

from a plot of the pressure drop profile in the axial direction. Similarly, attempts to improve upon the gas holdup measurement techniques produced an electro-resistivity probe with a slight variation in design from that employed by Nassos and Bankoff, well suited for measurements in air-water flow. The subsequent use of the probe for measuring gas holdups in three-phase fluidized beds was not as successful.

For the beds of small light particles, the knowledge of wake characteristics--the size as well as the particle content of the bubble wakes--was shown to be of critical importance for solids holdup predictions and of little consequence for gas holdup predictions. On the other hand, for the large or heavy particles, the gas-free model again sufficed for predictions of solids holdup, thereby suggesting the insignificant role of bubble wakes in these systems. The operation of the three-phase fluidized beds in the Stokes regime, though subject to particle elutriation, similarly showed no apparent effect of bubble wakes. The generalized wake model was thus vindicated by the experiments, as was a proposed correlation for bubble rise velocity in the absence or presence of solids, which was incorporated into the model.

ACKNOWLEDGEMENTS

I gratefully acknowledge the meaningful assistance provided by Dr. Norman Epstein, under whose quidance this investigation was conducted. I am indebted to him for reviewing the progress of this work both patiently and critically.

Thanks are due to Dr. S.D. Cavers for helping with the wake size data in liquid-liquid systems, to Drs. R.M.R. Branion and G.H. Neale for helping with some theoretical analyses, and to Dr. K.B. Mathur for helpful discussions at various stages of preparation of this thesis.

I acknowledge with gratitude the help rendered by the Workshop Staff in construction of experimental facilities at various stages of the work and in building parts of the apparatus.

The financial assistance provided by National Research Council of Canada and the University of British Columbia are gratefully and most cordially acknowledged.

My very special thanks are due to Mr. P.M.G. Rao for timely assistance in preparation of all the diagrams in this dissertation. Last but not the least, thanks are due to my colleagues and friends for contributing to my "knowledge" over the years.

And to my family, I owe it all.

TABLE OF CONTENTS

CHAPTER PAGE

CHAPTER PAGE

CHAPTER PAGE

CHAPTER PAGE

CHAPTER PAGE

LIST OF FIGURES

FIGURE PAGE

FIGURE PAGE

FIGURE PAGE

FIGURE PAGE

FIGURE PAGE

LIST OF TABLES

TABLE PAGE

TABLE PAGE

NOTATION

The analysis of multiphase flow, in which several phases flow simultaneously, has drawn considerable attention in recent years. For two-phase flow, the simplest case of multiphase flow, the information available in the literature, though often contradictory, is staggering. Since no standard definitions of the terms used for describing the multiphase flow phenomenon exist, the terminology adopted by various researchers is often vague and sometimes very confusing. Zuber and Findlay [39] tried to develop a rigorous terminology which gives a physical meaning to each of the terms. Later the same terminology was used extensively by Wallis [27]. The terminology employed in this thesis follows closely that adopted by Wallis, and recently extended by Bhaga [1]. Although the nomenclature is listed at the end, some explanation of the more common terms is given here in order to provide some familiarity with the simple relationships among these terms.

The three phases involved in three-phase fluidization are identified by subscripts 1, 2 and 3 in general. Subscript 1 describes the continuous liquid phase, while subscripts 2 and 3 represent the dispersed gas and solid phases respectively. For the three-phase system considered in this

study the gas and liquid phases flow cocurrently upwards in a vertical cylindrical pipe. A cylindrical coordinate system is used in which Z represents the distance measured vertically upwards and r denotes the radial distance from the pipe axis.

The volumetric flow rate is represented by the symbol Q. The total volumetric flow rate is then the sum of the individual component flows:

$$Q = Q_1 + Q_2 + Q_3 \qquad \text{(i)}$$

Since in this investigation flow of solid particles is not considered, Q_3 is zero and equation (i) reduces to

$$Q = Q_1 + Q_2 \qquad \text{(ii)}$$

In a three-phase fluidized bed, every part of the three-phase region will be occupied by one phase or another at any instant of time. If we consider an element of volume which is very much smaller than the volume of either a gas bubble or a solid particle, then $\alpha(t)$, representing the fraction of elemental volume occupied by one phase, can practically only be either 0 or 1. The temporal average of this event (occupation by one phase) occurring over a long period will represent the statistical average volume fraction of the given phase for that spatially fixed elemental volume:

$$\alpha = \frac{1}{T}\int_0^T \alpha(t)\, dt \qquad \text{(iii)}$$

For homogeneous distribution of the given phase, $\langle\alpha\rangle = \alpha$.

However, if the three-phase region is not of homogeneous distribution, it becomes necessary, in order to obtain a truly significant value of the average volumetric fraction, that the averaging process be carried out both in space and time. Then

$$\langle\alpha\rangle = \frac{\int\int \alpha(r,t) r\, dr\, dt}{\int r\, dr \int dt} \qquad \text{(iv)}$$

Thus in order to avoid any ambiguities about the measurement of average volumetric fraction of a phase, it is essential to define explicitly how the averaging process was carried out.

For many purposes the distribution of phases in the entire field is not required; therefore the averaging can be done over a much larger volume of the three phase region, and α then represents the average volumetric fraction (hold-up) of one phase. In this case α is measured over the entire cross-section of the conduit and over sufficient length to eliminate any spurious longitudinal variations. Thus, if a batch of solid particles of mass, W, is expanded to a height, L_b, in a pipe of cross-sectional area, A, the average volumetric fraction of solids (solids holdup) in the flow region will be

$$\langle\alpha_3\rangle = W/\rho_3 A L_b \qquad (v)$$

Similarly if we isolate the three-phase flow region by cutting off the gas and the liquid flow rates simultaneously, then the average volumetric fraction of gas (gas holdup) can be obtained by measuring the ultimate volume of gas collected, Ω_2, at the top:

$$\langle\alpha_2\rangle = \Omega_2/A L_b \qquad (vi)$$

The symbol j is used to represent the volumetric flux or volumetric flow rate per unit area of conduit, and is equivalent to what has been commonly called "superficial" velocity in the literature. Flux is indeed a vector quantity, but in this study j will be used to represent the scalar component in the direction along the pipe. Then by definition,

$$\langle j_1\rangle = Q_1/A \qquad (vii)$$

$$\langle j_2\rangle = Q_2/A \qquad (viii)$$

$$\langle j_3\rangle = Q_3/A = 0 \qquad (ix)$$

and the total average volumetric flux is

$$\langle j\rangle = \langle j_1\rangle+\langle j_2\rangle+\langle j_3\rangle \qquad (x)$$

The local volumetric flux is related to local phase volumetric fraction and velocity as follows:

$$j_1 = \alpha_1 v_1 \qquad \text{(xi)}$$

$$j_2 = \alpha_2 v_2 \qquad \text{(xii)}$$

$$j_3 = \alpha_3 v_3 \qquad \text{(xiii)}$$

and the total local volumetric flux is

$$j = j_1 + j_2 + j_3 \qquad \text{(xiv)}$$

The relative velocity between the fluid phases is defined as

$$v_{21} = v_2 - v_1 = -v_{12} \qquad \text{(xv)}$$

Drift velocities are defined as the difference between the phase velocities and the total volumetric flux. Thus

$$v_{1j} = v_1 - j \qquad \text{(xvi)}$$

$$v_{2j} = v_2 - j \qquad \text{(xvii)}$$

$$v_{3j} = v_3 - j \qquad \text{(xviii)}$$

The drift flux of phase i represents the volumetric flux of that phase based on drift velocity:

$$j_{ij} = \alpha_i v_{ij} = \alpha_i (v_i - j) \qquad \text{(xix)}$$

The symbol Δp is used to describe the pressure drop in a pipe. If dp/dZ represents the rate at which pressure increases with distance in the Z direction, then pressure drop over a length of pipe L will be

$$-\Delta p = -\int_0^L (dp/dZ)\, dZ \qquad \text{(xx)}$$

The following brief citation on Indian Philosophy is presented to illuminate "thought":

. . . One of the most important topics of orthodox Indian philosophy was the question of *pramāṇa* -- "means of reliable knowledge." Four means of reliable knowledge were recognized: perception (*pratyakṣa*), inference (*anumāna*), inference by analogy or comparison (*upmāna*), and "word" (*śabda*), the pronouncement of reliable authority, such as the Vedas. The materialists allowed only perception, but India developed her own system of logic in the study of the process of inference.

A correct inference was established by syllogism, of which the Indian form (*pañcāvayava*) comprises five members: proposition (*pratijña*), reason (*hetu*), example (*udāharaṇa*), application (*upnaya*), and conclusion (*nigamaṇa*). The classical example of Indian syllogism may be paraphrased as follows:

1. There is fire on the mountain,
2. because there is smoke above it,
3. and where there is smoke there is fire, as, for instance, in a kitchen;
4. such is the case with the mountain,
5. and therefore there is fire on it.

The Indian syllogism reversed the order of that of classical logic (Aristotelian: major premiss (3), minor premiss (2), and conclusion (1)), the argument being stated in the first and second clauses, established by the general rule and example in the third, and finally clinched by virtual repetition of the first two clauses. The "example" (in the above syllogism the kitchen) was generally looked on as an essential part of the argument, and helped to strengthen its

rhetorical force. The basis of generalization (for example "where there is smoke there is fire") on which every inference rests was believed to be the quality of universal concomitance (*vyāpti*). . . .

But the world is more complex and subtle than we think it, and that what is true of a thing in one of its aspects may at the same time be false in another.

Basham, A.L., "The wonder that was India," Grove Press, Inc., New York (1959).

CHAPTER 1

INTRODUCTION

1.1 Three-phase fluidized beds

A large number of chemical and process engineering systems require bringing two or more phases (gas, liquid and solid) into intimate contact with each other. The chemical characteristics of the phases involved are determined by the requirements of the process itself, but the dynamic behaviour of these phases is principally governed by the relative motion between the lighter and the heavier phases.

Fluidization is a phenomenon involving relative motion between a fluid phase and a solid phase in such a manner that solid particles are supported and maintained in a suspended state by upward flowing fluid. Under these conditions gravity forces on the particles, modified by buoyancy, are balanced by drag forces arising from the relative motion between the fluid and the solid particles.

The geometrical structure of a fluidized bed is very much dependent on the nature of the fluidizing medium. If the fluid used is a liquid, a fluidized bed of single sized spherical particles will generally appear to be homogeneously distributed. There are then no inter-particle collisions, each particle appears to have its individual identity and therefore such a liquid-solid fluidized bed is described as

"particulately fluidized". The gross expansion characteristics of a particulately fluidized bed under these ideal conditions can be predicted theoretically by various cell models (Happel, Kuwabara), but is best represented by an empirical relation developed by Richardson and Zaki [2]. However, if the fluid used is a gas, large or small solid-free aggregates usually rise up through the bed, giving it the appearance of a boiling liquid, and therefore such a gas-solid fluidized bed is described as "aggregatively fluidized". The solid-free aggregates or gas bubbles give rise to heterogeneous particle distributions in gas-solid fluidized beds, and therefore the description of bed expansion becomes more difficult and complex.

In three-phase fluidization, a mixture of gas and liquid is used as the fluidizing medium to maintain solid particles in the suspended state. Three phases (gas, liquid and solid) are thereby brought into contact simultaneously. The term 'three-phase fluidization' has been used rather loosely to describe the process of bringing gas, liquid and suspended solid particles into contact, where the gas and the liquid may be flowing either cocurrently or countercurrently. As defined in this thesis, however, the term is restricted to the fluidization of solid particles by a mixture of gas and liquid flowing cocurrently and vertically upwards The term 'gas-liquid' fluidization has also been used to describe this mode of contacting. The prediction of holdup

for each phase of a three-phase fluidized bed requires a knowledge of equilibrium conditions between the three phases, which in turn is governed by the local relative velocities between the phases. The geometrical structure and physical appearance of the bed will depend on the local holdup of each phase in the bed. The bed will appear to be particulately fluidized at low gas-to-liquid ratios [7,8] and aggregatively fluidized at large gas-to-liquid ratios, as has been visually observed by various investigators [13]. Jackson [3] and Bhatia [4] observed qualitatively that for suspension of granular particles in a pool of liquid by gas injection, the resulting bed consists of solid particles dispersed in a continuous liquid phase, with the gas rising through the medium as discrete bubbles, transferring its momentum to the liquid phase during the ascent. Thus it is envisaged that in a three phase fluidized bed the solid particles are supported entirely by the liquid phase alone, which suggests that the characteristic properties of a three-phase fluidized bed can be synthesized on the basis of the properties of two simpler two-phase systems, namely, cocurrent gas-liquid flow and liquid-solid fluidization.

The analysis of the complex behaviour of three-phase fluidized beds becomes somewhat simplified in view of the above observations, since the holdup of liquid-solid fluidized beds is very well described by the empirical relation of Richardson and Zaki, as well as by other similar correlations.

However, knowledge of local holdup distributions of the gas and the liquid phases, and their interaction, is also very important in order to analyse the phenomenon completely. The study of the distribution of gas and liquid phases in three-phase fluidized beds requires knowledge of two-phase gas-liquid flow and the effect of solid particles in perturbing the distribution of phases in the gas-liquid flow. The field of gas-liquid flow has been investigated by a large number of researchers, but still the understanding of the effect of interaction of the two phases on their respective flow and holdup profiles is far from complete [39]. This incomplete understanding of the two phase gas-liquid flow phenomenon puts attempts to analyse the behaviour of three-phase fluidized beds at some disadvantage.

Nevertheless, the three-phase fluidization technique has already found its way into certain process industries involving gas-liquid reaction in the presence of a suspended solid catalyst. In such reaction systems, where interphase mass transfer is not the controlling resistance, cocurrent gas-liquid flow is employed since much higher throughputs can be achieved without flooding than for countercurrent flow, while the higher mass transfer driving force obtainable from the latter is not required.

The applicability of the three-phase fluidization technique of bringing three phases into contact simultaneously has not been completely investigated [54] but three-phase

fluidized beds have the industrial potential of being employed in any of the following combinations:

1. gas reacting with liquid in the presence of solids as the catalyst, viz. hydrogenation of vegetable oil in the presence of nickel or other powdered catalysts.
2. gas and liquid reacting with solid particles, e.g. in the production of calcium bi-sulfite cooking liquor from solid limestone particles in the presence of water and sulfur dioxide [55].
3. gas reacting with solid particles in the presence of liquid catalyst; certain esterification reactions could be classified as specific examples.
4. gas reacting with liquid to form the solid phase which is kept in suspension [3].

Besides its applications in chemical reaction systems, three-phase fluidization can also be employed for physical operations. Thus a three-phase crystallizer has been designed to regulate the crystal growth of ammonium-sulfate [5].

1.2 Gas holdup and expansion characteristics of three-phase fluidized beds

The actual and potential uses of three-phase fluidization in various industrial processes have led various investigators to study it experimentally. Thus, Turner [6]

suggested the possibility of using the three-phase fluidization technique in desulfurizing higher molecular weight residual petroleum feedstocks. He therefore carried out preliminary hydrodynamic experiments on the air-water-sand system and thus demonstrated for the first time the peculiar behaviour of three-phase fluidized beds.

Turner observed that introducing a small flow rate of gas to a liquid-solid fluidized bed, keeping the liquid velocity constant, resulted in contraction of the bed. Stewart and Davidson [7], Østergaard [8], and Adlington and Thompson [9] then investigated this unexpected behaviour of three-phase fluidized beds, using air and water as gas and liquid respectively, with spherical, single-sized solid particles of various densities. They too observed the contraction of a liquid-solid fluidized bed on introduction of gas at constant liquid flow rate in all the systems which they investigated. The degree of contraction observed was, however, found to depend on the initial degree of expansion of the liquid-solid fluidized bed.

A similar investigation had been carried out earlier by Volk [10], using nitrogen as gas, heptane as liquid and extruded cylindrical catalyst pellets as solids in different columns varying from 0.625 inch to 6 inches in diameter. Volk, however, observed that under all conditions studied the liquid-solid fluidized bed expanded further on introduction of gas at constant liquid flow rate. This contradictory

behaviour of three-phase fluidized beds can perhaps be ascribed to the difference in physical properties and especially surface tension of the liquid phase used.

The effect of liquid properties on the behaviour of three-phase fluidized has not been investigated systematically, but recently Dakshinamurty et al. [11], using kerosene as the liquid phase, air as the gas phase and single-sized glass beads as the solid phase, observed that the smoothly fluidized liquid-solid fluidized bed expanded further on introduction of gas at constant liquid velocity. Contrary behaviour was observed with water as liquid.

It should be noted that the organic liquids used by Volk and by Dakshinamurty et al. have surface tensions about one-third that of water, and that these investigators paid no attention to the possible presence of trace impurities in their technical grade liquids. It is known that minute organic impurities could change the surface characteristics of the solid particles, such as rendering them non-wettable by the liquid phase. The importance of solids wettability was pointed out earlier by Guha et al. [13] in their study of the suspension of solid particles in a liquid medium by means of a gas flow. In carefully planned experiments to show the effect of wettability of particles in three-phase fluidization, Evans [12] observed that a bed of liquid and wettable particles contracted, while the same bed with the

particles rendered non-wettable expanded further, on introduction of gas at a fixed liquid rate. It is, then, believed that the physical properties of the liquid, especially surface tension, and the nature of the particle surface are probably interrelated and play an important role in determining the behaviour of three-phase fluidized beds [83]. However, since no systematic investigation has yet been carried out to elucidate the effect of liquid and solid surface properties, no generalizations can be made with any confidence. Almost all studies, including the present one, have been carried out using solid particles which were fully wettable by the liquid phase.

Michelsen and Østergaard [14], in conducting detailed experiments on 3 mm and 6 mm glass beads, found that water fluidized beds consisting of such relatively large particles did not show any contraction when air was introduced as observed for smaller particles. Almost all of the earlier works were carried out using only very small gas flow rates, since it was difficult to discern the expanded bed height at high gas rates. Michelsen and Østergaard extended the range of gas velocities studied, though they did not indicate how the height of expanded bed was measured. They observed that a liquid-solid fluidized bed of 1 mm particles contracted on introducing the gas at small flow rates. On further increasing the gas velocity at a fixed liquid velocity, the bed height tended to reach a definite minimum

and then increase with increase of gas velocity.

Another important aspect of three-phase fluidized bed operation is the behaviour of the gas phase inside the bed. Numerous attempts have been made to study this aspect, but it is not yet fully understood. Massimilla et al. [15] studied the rise velocity of a single gas bubble in a liquid-solid fluidized bed, using water as the liquid. They observed that the rise velocity was a function of the bubble diameter, but that the functional dependence for small bubbles (bubble diameter up to 8 mm), was radically different than in pure water. However, for larger bubbles the rise velocity in the liquid-solid fluidized beds approached the rise velocity in pure water. Another important observation to be made from their measurements is that, although the rise velocity of bubbles in pure water is practically constant for bubble diameters in the range 3 mm - 20 mm, the rise velocity of bubbles in a liquid-solid fluidized bed for the same range of bubble diameters increases monotonically. This observation then leads to the possibility of vertical bubble coalescence in a liquid-solid fluidized bed, if the bed contains bubbles of various sizes. Thus large bubbles, with their characteristic high velocity, would be prevalent if coalescence were the predominant phenomenon inside the bed, while small bubbles, with their characteristic low velocity, would prevail if bubble break-up were the predominant phenomenon. The role of the solid particles can then be characterized by noticing

how the gas holdup, defined as the volumetric fraction of the bed occupied by the gas bubbles, is affected.

To compare the gas holdup in a three-phase fluidized bed with that in two-phase gas-liquid flow it is necessary that they both be referred to a common solids free basis. The gas holdup in a three-phase fluidized bed on a solids-free basis is given by

$$\varepsilon_2''' = \varepsilon_2/(1-\varepsilon_3) \qquad (1.1)$$

The gas holdup from equation 1.1 can then be compared to the gas holdup in two-phase gas-liquid flow, ε_2'', to elucidate the effect of the solid particles.

Most investigators [14,16,17] have, however, compared the directly measured absolute gas holdup in a three-phase fluidized bed, ε_2, with that in two-phase gas-liquid flow, at the same flow rates of both the gas and the liquid phases. Thus from such a comparison Michelsen and Østergaard [14], who obtained the gas holdup inside the bed from the static pressure drop measurements in a 6 inch diameter column, concluded that in beds of 3 mm and 6 mm glass beads break-up of bubbles takes place in the lower portion of the bed, whereas in beds of 1 mm glass beads coalescence takes place in the same region. No mechanistic correlation was, however, obtained between the gas holdup in a three-phase fluidized bed and the gas holdup in two-phase gas-liquid flow.

Efremov and Vakhrushev [16] used the same principle of static pressure drop measurement to obtain the gas holdup inside the bed in a 10 cm diameter column, although the accuracy of their static pressure drop measurement technique, using a static tube immersed in the bulk of the fluid, is questionable [82]. They employed narrow fractions of glass beads with mean diameters ranging between 0.32 mm and 2.15 mm and they observed that for all sizes of particles studied, the gas holdup in a three-phase fluidised bed was considerably smaller than in two-phase gas-liquid flow under identical gas and liquid flow rates, respectively. They were furthermore able to empirically correlate the gas holdup inside the three-phase fluidized bed with the gas holdup in two phase gas-liquid flow.

Vail et al. [17] used the method of isolating the test section by simultaneously cutting off the gas and the liquid flows and then recording the amount of gas collected at the top of the bed. As will be discussed under "Experimental Technique," this method has inherent errors, which were not fully corrected for by these investigators. They studied 0.73 mm glass beads and two different catalyst powders of the same size, the measurements being carried out in a 14.6 cm diameter column. They found that for all the three solid particles studied, the gas holdup in three-phase fluidization was always smaller than the gas holdup in two-phase gas-liquid flow under identical flow conditions. They attributed

this result to the fact that the solid phase displaces part of the liquid, while the gas bubbles can rise and exist only within the liquid phase. Based on this reasoning,an empirical correlation between the gas holdup in a three-phase fluidized bed and in two-phase gas-liquid flow was presented.

In view of the reported works [14,15,79] it would seem to be correct that if the particle size is small as compared to the bubble size, bubble coalescence will result, whereas if the particle size is comparable or bigger than the bubble size, bubble break-up will occur, in the bed. Østergaard and Theisen [18] observed that this does not seem to affect the contraction or expansion behaviour of the bed, since particle size does not seem to influence the distribution of liquid between the liquid-solid fluidized (particulate) phase and the gas-liquid (bubble) phase. However, since no detailed study has been done of flow distribution or solids circulation in three-phase fluidized beds, it is rather important to understand the characteristic behaviour of each phase and the mutual interaction between phases, at least qualitatively.

1.3 Wake model for three-phase fluidized beds

The qualitative description of the behaviour of individual phases can provide the basis for a mathematical model describing the gross behaviour of three-phase fluidized beds. However, to keep the mathematical model realistic, assumptions

have to be made about those aspects of three-phase fluidized beds which are not well understood.

One aspect of three-phase fluidized beds which, although it plays an important role in determining the behaviour of such beds, has not been sufficiently investigated, is the phenomenon of wake formation behind the dispersed gas phase. It is very well recognized now that a dispersed phase, when moving through a continuous medium, carries along with it some continuous phase as its wake. The average amount of continuous phase carried as the wake of the dispersed gas phase will depend upon the size and shape of the wake [8] and on the mode, frequency and rate of wake shedding [80]. Thus, in a three phase fluidized bed, gas bubbles rising through the continuous liquid medium will carry part of the liquid phase in their wake, making that part of the liquid phase unavailable for support of the solid particles. On the basis of this wake phenomenon, Stewart and Davidson [7] were able to explain the observed contraction in three-phase fluidized beds.

Using a two-dimensional liquid-fluidized bed contained between perspex plates spaced 0.25 inch apart, Stewart and Davidson observed photographically that when an air bubble rises through the bed, some liquid follows the bubble as its wake. They also observed that the liquid wake was practically free of solid particles. The resulting combined gas-liquid bubble rises through the bed at a much greater velocity than the

average velocity of liquid through the interstices of the bed, thus removing some liquid from the continuous phase and, according to the reasoning of these investigators, thereby reducing the overall fluidizing force. Because of this reduction, the bed settles to a lower depth. No phenomenological correlation was attempted to represent the observed bed behaviour.

The model subsequently proposed by Østergaard [8] was in its main features the same as that suggested by Stewart and Davidson, but it was based on representing a three-phase fluidized bed as consisting of a liquid-fluidized particulate phase, a gas bubble phase and a wake phase. The wake phase was assumed to follow the bubble phase at the bubble velocity and have a porosity identical to that of the particulate phase. This last assumption, based on photographic observation of a bubble emerging from a liquid-solid fluidized bed being followed by a long trail containing solids, contradicts the observation of Stewart and Davidson that a bubble is followed by a wake of liquid devoid of particles. There is, unfortunately, no conclusive evidence available yet to support or repudiate either claim. The model proposed by Østergaard is presented here in its entirety, since it is felt that this model attempts to consider the fundamental distribution of the liquid between the particulate phase and the wake phase. Further, it is hoped that deficiencies of the model can be identified so that modifications can be incorporated to

explain three-phase bed behaviour more realistically.

Let us consider a bed of particles of weight, W, expanded to a height, L_b, in a column of cross-sectional area, A, under the influence of gas and liquid volumetric fluxes $\langle j_1 \rangle$ and $\langle j_2 \rangle$ respectively. Then the average volumetric solids fraction or solids holdup will be

$$\varepsilon_3 = \frac{W}{\rho_3 A L_b} \tag{1.2}$$

The bed porosity, ε, defined as the fraction of the bed volume occupied by gas and liquid, will be

$$\varepsilon = \varepsilon_2 + \varepsilon_1 = (1-\varepsilon_3) \tag{1.3}$$

If it is assumed that the porosity of the wake phase is identical to the porosity of the particulate (i.e. the liquid-solid fluidized) phase, it follows that

$$\varepsilon = \varepsilon_1''(1-\varepsilon_2) + \varepsilon_2 \tag{1.4}$$

where ε_1'' is the volume fraction of liquid in the particulate phase and is related to the volumetric flux through this region, j_1'', by the well known Richardson - Zaki [2] equation, i.e.,

$$\varepsilon_1'' = (j_1''/V_\infty)^{1/n} \tag{1.5}$$

where

$$n = f(Re_p, d_p/D) \qquad (1.6)$$

Let us assume that the volume fraction of the three-phase bed occupied by the wake phase is ε_k. If we consider the three-phase fluidized bed to be macroscopically homogeneous, then the fraction of any cross-sectional area occupied by the gas bubble phase and the wake phase will be ε_2 and ε_k respectively. Therefore on the basis of the physical picture assumed by Østergaard for a three-phase fluidized bed, the area occupied by the particulate or liquid-solid fluidized phase in the plane perpendicular to the principle flow axis will be

$$A_{LS} = (1-\varepsilon_2-\varepsilon_k)A \qquad (1.7)$$

The distribution of liquid phase between the particulate phase and the wake phase is obtained by carrying out a material balance across any cross-section inside the three-phase bed:

$$\begin{pmatrix}\text{Total volumetric flow rate of}\\ \text{liquid through the column}\end{pmatrix} = \begin{pmatrix}\text{Volumetric flow rate of}\\ \text{liquid through the}\\ \text{particulate phase}\end{pmatrix} + \begin{pmatrix}\text{Volumetric flow rate of}\\ \text{liquid through the wake}\\ \text{phase}\end{pmatrix}$$

or

$$Q_l = Q_{lf} + Q_{lk} \tag{1.8}$$

If it is assumed that the wake phase travels with the gas bubble phase at the bubble velocity, a good assumption if one disregards the wake shedding phenomenon, then equation 1.8, with the aid of equation 1.7, may be rewritten as

$$\langle j_l \rangle A = j_l''(1-\varepsilon_2-\varepsilon_k)A + \bar{v}_2 \varepsilon_k A \varepsilon_l'' \tag{1.9}$$

Solving equation 1.9 for j_l'' gives the volumetric flux through the particulate phase as

$$j_l'' = \frac{\langle j_l \rangle - \bar{v}_2 \varepsilon_k \varepsilon_l''}{1-\varepsilon_2-\varepsilon_k} \tag{1.10}$$

In order to predict the behaviour of a three-phase fluidized bed from the above set of equations, one requires independent knowledge of ε_2 and ε_k. The fraction of the bed volume occupied by the gas phase is related to the average rise velocity of the bubbles by

$$\varepsilon_2 = \langle j_2 \rangle / \bar{v}_2 \tag{1.11}$$

As discussed in the preceding section, the rise velocity of a single bubble in a liquid-solid fluidized bed was

studied by Massimilla [15]. However, no data on the rise velocity of a swarm of bubbles in a liquid-solid fluidized bed are available. Østergaard therefore obtained an estimate of bubble rise velocity in a three-phase fluidized bed from the data of Nicklin [19] for two-phase gas-liquid flow, which Østergaard correlated by the empirical equation,

$$\bar{v}_2 = 21.7 - 4.6 \ln \langle j_2 \rangle + \langle j_1 \rangle \qquad (1.12)$$

However, since equation 1.12 is based on two-phase data, it could hardly be expected to accurately represent the gas bubble phase in a three-phase bed.

The phenomenon of wake formation behind a gas bubble has not been studied extensively. The importance of the wake phenomenon in controlling transport processes was first realized in liquid-liquid operations [36]. Subsequently, therefore, attempts were made to obtain information regarding the shape and size of wakes behind liquid drops [84], while study of the mode, frequency and rate of wake shedding in liquid-liquid systems is currently in progress [85]. Generalizable quantitative information regarding the wake characteristics in liquid-liquid systems, however, is rather limited, whereas even specific information on the wake characteristics in gas liquid systems is minimal and in three-phase systems almost non-existent. Therefore in

order to obtain an estimate for the volume fraction occupied by the wakes, ε_k, Østergaard [8] postulated qualitatively that

1. ε_k increases with increasing ε_2, the rate of increase in ε_k being slower at large values of ε_2.
2. ε_k increases with increasing liquid flow rate, that is, with increasing bed fluidity.

These two assumptions were then incorporated by trial and error into the following equation in such a way as to satisfy the data for bed contraction:

$$\varepsilon_k = 0.14\ \varepsilon_2^{0.5}\ (\langle j_l \rangle - \langle j_l \rangle_{mf}) \qquad (1.13)$$

where $\langle j_l \rangle_{mf}$ is the minimum volumetric liquid flux required to initiate fluidization of the solid particles.

Østergaard thus presented the set of equations 1.2 - 1.10, which when used in conjunction with equations 1.11 - 1.13, satisfied a limited quantity of experimental data on bed contraction. But later, in a more detailed investigation, Østergaard and Theisen [18] reported that the model proposed by Østergaard could not satisfactorily predict the observed contraction of three-phase fluidized beds over a wider range of operating variables. Furthermore, the model fails to describe fully the observed bed behaviour of three-phase

fluidized beds as outlined in the preceding section, viz. that the bed height drops on introduction of gas at a constant liquid flow rate, then reaches a definite minimum on increasing the gas flow rate, and finally slowly expands again as the gas flow rate is further increased. Only the initial bed contraction is predicted by the model. Nevertheless Østergaard's model for a three-phase fluidized bed does have the virtue of describing, albeit approximately, the distribution of liquid between the particulate phase and the wake phase. The equations used for estimating the volumetric gas fraction and the volumetric wake fraction cannot be expected to accurately predict these quantities in a three-phase fluidized bed, since they were obtained from a very limited range of data. Even in two-phase gas-liquid flow the information on gas holdup is non-conclusive and ambiguous, while the information on volumetric wake fraction and its role in determining velocity profiles in gas-liquid flow is almost non-existent.

It is useful at this point to digress from Østergaard's model and consider the simple model proposed by Davidson [20] to explain the bubble phenomenon in gas solid fluidization, and the modification introduced to this simple model by Kunii and Levenspiel [21] to explain bubble behaviour in gas-solid fluidized beds more realistically. Davidson postulated that a bubbling gas-solid fluidized bed can be considered as being constituted of a gas bubble phase and a

gas-solid emulsion phase. Davidson also assumed the bubbles in the bubble-phase to be spherical and the flow around the spherical cavities to be irrotational and incompressible. The flow pattern of gas and solid and the pressure distribution in the vicinity of the rising bubble predicted by this model have been shown to be essentially correct [21]. However, Rowe and Partridge [22] observed that the rising bubbles each carry a wake behind them containing solid particles. The reason given for the presence of this wake was that the pressure in the lower part of the bubble is less than in the nearby emulsion phase, a reason predictable by Davidson's model. Gas is thereby drawn into the bubble, resulting in an instability, partial collapse of the bubble, and turbulent mixing behind it. This turbulence results in solids being drawn up behind the bubble and forming a wake. The wake of the bubble exchanges solid material continually during its rise, depending on the mode, frequency and rate of wake shedding, but ultimately the solid particles carried in the wake of the bubble are deposited at the bed surface when the bubble emerges from the bed, thus giving rise to downward solid movement in the emulsion phase.

Kunii and Levenspiel [21] modified Davidson's simple model by incorporating the wake phenomenon. They considered the bubbling gas-solid fluidized bed as consisting of a gas bubble phase, a gas-solid emulsion phase, and a wake phase. This model is analogous to that proposed by Østergaard for a

three-phase fluidized bed. Kunii and Levenspiel pointed out that the solid particles in the emulsion phase develop a circulatory motion promoted by the rising bubble wakes, containing solid particles. However, they also showed that solids movement did not affect the behaviour of the bubble phase markedly, but that the movement of the entire emulsion phase could be reversed due to the motion of the particles.

In a three-phase fluidized bed as pictured in Østergaard's model, it is the relative velocity between the liquid and the solid particles in the particulate phase that would control the expansion or contraction of the bed. Østergaard considered the distribution of liquid between the particulate phase and the wake phase, but the circulatory motion of the solids in the particulate phase as induced by the gas bubbles, was not considered. By analogy with gas-solid fludization, a circulatory motion of solid particles would also exist in three-phase fluidized beds, if it is assumed that the wake accompanying a gas bubble contains solid particles.

Thus the main drawbacks in the simple but elegant model proposed by Østergaard seem to be:

(i) The assumption that the porosity of the wake phase is equal to that of the particulate phase.

(ii) The neglect of solids circulation induced by the motion of gas bubbles carrying wakes containing solid particles.

(iii) The quantitative representation of wake volume fraction by equation 1.13 and of bubble rise velocity by equation 1.12.

1.4 Importance of turbulence phenomena in three-phase fluidized beds

Turbulence is known to exert significant influence on momentum transfer (and other transfer processes) from a particle immersed in a fluid by altering the flow field around the particle. However, very little effort has gone in to quantitatively correlating these effects with the measureable fundamental properties of a turbulent field, viz. intensity and scale of turbulence. The importance of turbulence in a fluidized bed can be appreciated if we consider that the bed consists of solid particles of finite size. Then a flow field is developed around each particle due to the relative motion between the fluid and the particle and the no slip condition to be satisfied at the particle surface. The latter causes generation of vorticity at the particle surface, the growth and decay of which determines whether the flow field near the particle is either turbulent or non-turbulent. At high relative velocity, the vorticity is convected downstream with the flow and is concentrated at the rear of the particle, causing a backward flow to be induced near the surface. This backward flow counters the forward moving fluid and deflects it away from the rear,

strengthening the rotational motion in the standing eddy. The term wake is commonly applied to this whole region of non-zero vorticity on the downstream side of the particle. At still higher relative velocities the wake no longer remains permanently attached to the particles but is shed at regular intervals in an otherwise uniform stream of fluid. Thus formation of a sufficiently high vorticity wake behind a particle can be considered as the onset of a turbulence field in the fluid medium around the particle. The turbulence field in a fluidized bed, which is constituted of an assemblage of particles, can then be considered as the composite effect of the wakes of individual particles [87].

However, in three-phase fluidized beds as in two-phase gas-liquid systems, it is the gas bubbles which play the dominant role in creating turbulence in the fluid phase. The mechanism for generation of turbulence is principally the same as described above, viz. the formation of wakes behind the bubbles and consequent wake shedding at higher relative velocities. Thus a cocurrent gas-liquid flow under non-laminar flow conditions may be considered as a system which generates fluid phase turbulence through the presence of randomly moving bubbles. The presence of solid particles in such a turbulence generating system may suppress the liquid phase turbulence in varying degrees, depending on the relative inertia of the particles and the intensity of

turbulence. A large density difference between the particle and the liquid will tend to damp out turbulence [88], so that the liquid-phase intensity of turbulence in a three-phase fluidized bed may be much smaller than in the corresponding cocurrent gas-liquid flow, for equal fluid phase velocities. A systematic investigation of the expansion characteristics of a fluidized bed should then involve a study of turbulence generation in the bed and the influence of fundamental turbulence properties on the drag coefficient of an individual particle.

The knowledge of wake formation behind the bubble and the mode, frequency and rate of wake shedding has not been examined to any extent. Stewart and Davidson [7], in their investigation of a three-phase fluidized bed in a two dimensional column, observed the wake shedding phenomenon photographically. Rigby and Capes [80], following up their investigation of a two-dimensional three-phase fluidized bed, successfully explained the observed contraction phenomenon on the basis of a few measurements of wake shedding and the consequent rise of shed vortices through the bed. Their work thus indirectly demonstrates the possible relevance of turbulence, generated by shedding of wakes from the rising bubbles, in the study of three-phase fluidized beds. Studies [14,17] on the state of mixing in three-phase fluidized beds have also demonstrated indirectly the dominant role of

turbulence in multiphase flow. However, attempts to gain better insight into the mechanisms controlling other transport phenomena cannot be entirely satisfactory until the flow fields around both the dispersed phases are fully understood.

Thus we see that turbulence probably plays a role in defining the behaviour of three-phase fluidized beds. Given the present state of knowledge of three-phase systems, however, it appears sufficient to know the size and shape of a wake behind an isolated bubble, the influence of other bubbles and particles on the size and shape of the wake, and the mode, frequency and rate of wake shedding--in order to quantify the contraction phenomenon. Nevertheless, in order to gain complete knowledge of the fluid dynamics of three-phase fluidized beds, it is important that the turbulence phenomenon be systematically examined. The present state of knowledge of turbulence can be used to describe single phase flow, but it has not advanced enough to predict fundamental quantities for multiphase flow.

1.5 Scope of research

The information available on three-phase fluidized beds is rather scanty. Therefore the primary aim of this research was to devise and carry out an experimental programme for collecting reliable and accurate data on the holdup of solids and gas in a three-phase fluidized bed

under a wide range of flow conditions. As has been suggested earlier [3,4], a three-phase fluidized bed can be considered as a complex system, the properties of which are a composite of two simpler systems: gas-liquid cocurrent flow and a liquid-solid fluidized bed. The parameters to be studied were selected on the basis of information about the two-phase systems. Thus, since it had been established in various studies on two-phase gas-liquid flow that variation in the properties of the gas phase does not play an important role under normal atmospheric conditions, it was decided to use atmospheric air as the gas phase for the entire programme.

Water was chosen as the liquid phase for most of the study for simplicity and for purposes of comparing the data collected in this study with the data available in the literature from the work of various investigators, most of whom used water as the liquid and air as the gas. In order to study three-phase fluidized beds under conditions where turbulence in the continuous phase is insignificant, water was replaced by a high viscosity liquid. A 30% (by weight) solution of polyethylene glycol in water was selected because it gives high viscosity ($\simeq$ 60 c.p.) without affecting density and surface tension of the solution markedly. Surface tension of the liquid phase, though an important parameter in gas-liquid flow systems and found to be even more important for three-phase systems [11], was not deliberately varied because of the experimental difficulty of keeping traces of

impurities from entering the system and thus radically changing the static equilibrium (contact angle) between the phases.

Solid particles selected for the study had to be non-reacting with the liquids chosen and of well defined shape. The behaviour of irregularly shaped particles in liquid-solid fluidized beds is not entirely understood and therefore closely sized spherical particles of various densities and sizes were chosen. Also the behaviour of particulately fluidized beds with spherical particles lends itself to satisfactory explanation by simple mathematical models.

The secondary aim of this research was to derive a mathematical model which, when coupled with some empirical information, would yield better understanding of the behaviour of a three-phase fluidized bed. For this purpose the wake model proposed by Østergaard was chosen as a starting point, since it describes the distribution of liquid between the wake phase and the particulate phase. However, as pointed out earlier, it was expedient to incorporate into the model the recirculation of solids induced by movement of gas bubbles in order to explain not only the observed contraction, but also the subsequent expansion, of three-phase fluidized beds.

To develop a model for three-phase fluidized beds, knowledge of gas holdup in cocurrent gas-liquid flow is essential. Since the models available in the literature for predicting gas holdup in gas-liquid flow are mostly empirical in nature, there is quite a variability and ambiguity in their range of applicability. It therefore became

necessary to study two-phase gas-liquid cocurrent flow from the point of view of developing a logical and reasonable physical model for gas holdup in two-phase gas-liquid flow.

Attempts were also made to develop a model for three-phase fluidized beds under conditions in which the turbulence phenomenon can be neglected. Experimental measurements carried out with small particles in a highly viscous liquid to support such a model were not entirely successful, but the model is presented herein for possible future investigations.

CHAPTER 2

THEORY

This chapter is divided into three sections--dealing with holdup in gas-liquid flow, in liquid-solid fluidized beds and in three-phase fluidized beds, respectively. These dispersed phase operations have been investigated in the past to varying extents. Mathematical models purporting to predict the desired quantities have been presented, often without any understanding of the phenomena involved. Therefore, an attempt is made to outline the mechanisms of these phenomena from the knowledge available in the literature and then, on the basis of these mechanisms, to propose either new models or modifications to existing models, in order to describe the characteristics of the dispersed phase operations more satisfactorily.

2.1 Holdup in gas-liquid flow

Two-phase gas-liquid flow has been studied for many years, so that the amount of information currently available in the literature, though often inconclusive, is staggering. Excellent treatises [23,24,25] have been written on the subject and an index of over 5000 articles, reports and books on two-phase gas-liquid flow has been prepared by Gouse [26].

Recently, the book by Wallis [27] has put the subject into some perspective. Due to the complex nature of two-phase flow phenomena, it has become necessary to rely heavily on experimental data, since a realistic analysis has been lacking. For example, the presence of wakes behind a rising bubble swarm has been recognized but as yet no analysis has adequately taken the wake phenomenon into consideration. It is, therefore, necessary that all the basic information available be carefully studied, and that the salient features found to be controlling the behaviour of gas-liquid flow in a given regime be identified. A realistic model can then be developed based on those parameters found to be relevant in the physical observations. To test the applicability and limitations of the model so developed, carefully planned and statistically designed experimental data will be required. Only an approach which is appropriately balanced between theoretical and experimental efforts will lead to better understanding of two-phase gas-liquid flow.

2.1.1 Holdup studies

When we are considering a dispersed two-phase system in which the gas is uniformly distributed in a liquid medium as discrete bubbles, the rise velocity of the swarm of bubbles is subject to two influences, one arising from the motion of the bubbles and the other from their presence. The

relationship between the average rise velocity of the bubble swarm, $\bar{v}_2$, and the average volume fraction of gas in the swarm, $\langle\alpha_2\rangle$, is simply

$$\bar{v}_2 = \langle j_2\rangle / \langle\alpha_2\rangle \qquad (2.1)$$

where $\langle j_2\rangle$ is the average volumetric flux of the gas through the system. Thus in order to predict the rise velocity of the bubble swarm, and consequently the gas holdup, it is necessary to understand the motion of a bubble and how it is affected by the proximity of other bubbles.

2.1.1.1 Bubble dynamics

The rise velocity of a single bubble in an infinite medium has been studied extensively. Haberman and Morton [29] presented a comprehensive review of bubble motion studies up to 1956. Although the work of Haberman and Morton [28] and of Peebles and Garber [30] elucidates the importance of the physical properties of the liquid (the properties of the gas phase are found not to be important under normal pressure) on the rise velocity of a bubble, most of the experimental data available for the rise velocity of single bubbles is for bubble motion in water. In the following description the data obtained for bubble motion in water [31] are used to illustrate the important aspects of the rise of a gas bubble through a pool of stagnant liquid.

It has been observed that small gas bubbles ($r_e < 0.4$ mm), which are almost perfect spheres because of the dominant surface tension forces, behave very much like small solid particles. However, the Stokes solution for the terminal rise velocity of a bubble, V_∞, can be used only for still smaller bubbles ($r_e < 0.2$ mm, $Re_b < 2$):

$$V_\infty = d_b^2 \, g \, (\rho_1-\rho_2)/18 \, \mu_1 \tag{2.2}$$

Equation 2.2 assumes that the liquid velocity at the bubble surface relative to the bubble is zero, an assumption which, however, breaks down for bubbles with internal circulation. Hadamard [32] and Rybczynski [33] modified the above equation for perfect fluid spheres with complete transference of shear stress at the bubble-liquid interface, and obtained

$$V_\infty = \frac{d_b^2 \, g(\rho_1-\rho_2)}{18\mu_1} \cdot \frac{3\mu_1 + 3\mu_2}{2\mu_1 + 2\mu_2} \tag{2.3}$$

which for $\mu_1 >> \mu_2$ reduces to

$$V_\infty = d_b^2 \, g(\rho_1-\rho_2)/12\mu_1 \tag{2.4}$$

Equation 2.4 applies to small bubble sizes ($Re_b<2$), but only in the complete absence of surface impurities.

At the other extreme, when the bubbles are very large ($r_e > 9.0$ mm, $Re_b > 5000$) and show a spherical cap shape,

the Reynolds and Weber numbers are known to characterize the motion of such bubbles. For predicting the shape of the bubble in this regime, the surface tension and viscous forces are normally considered to be negligible as compared to the gravity and inertia forces. Based on these assumptions, Davies and Taylor [34] considered the motion around the front stagnation point to be irrotational and obtained

$$V_\infty = \frac{2}{3} (g\ R_s)^{1/2} \qquad (2.5)$$

where R_s is the radius of curvature of the bubble at the front stagnation point. It is important to note here that although Davies and Taylor observed a sizable wake region behind spherical cap bubbles, the irrotational flow model was applied to the region around the front stagnation point only and no attempt was made to consider the detailed structure of the wake itself. The ability of equation 2.5 to predict the terminal rise velocity of large bubbles (r_e > 9.0 mm) stems from the fact that the bubble shape, the bubble velocity and the rate of energy dissipation are inter-related.

For the intermediate bubble sizes(0.6 < r_e < 9.0 mm), where the surface tension and viscous forces are comparable to the gravity and inertia forces, the bubble shape and bubble velocity are difficult to model. In this range the gas

bubbles are neither spherical nor do they rise rectilinearly. Although no study has considered the wake structure behind a rising bubble in this range, the studies on rise or fall of a liquid drop through a liquid medium with which it is immiscible by Edge and Grant [35], Letan and Kehat [36], and Magarvey and Bishop [37] all suggest that wake activity in this region of Reynolds number is quite predominant. The bubbles with $r_e > 0.8$ mm are quite noticeably deformed and their path of ascent is helical. Because of the helical path, the rise velocity of these bubbles in the vertical direction decreases slowly as the bubble size increases until $r_e \simeq 2.4$ mm, which corresponds to the minimum in the rise velocity vs. bubble size relationship. Peebles and Garber [30], from their extensive experimental data, observed that the average bubble rise velocity for $1.0 < r_e < 2.4$ mm is best represented by the equation

$$V_\infty = 1.35(\sigma/\rho_l r_e)^{0.5} \qquad (2.6)$$

For bubbles with $r_e > 2.4$ mm, the bubble shape is not regular but pulsates around an oblate spheroid. The path of rise of such bubbles becomes less helical and therefore the vertical rise velocity of the bubble once again begins to slowly increase with increasing bubble size. Nevertheless Peebles and Garber [30], Haberman and Morton [28], and Levich [38] termed the bubble movement to be turbulent in

this range and found that the average vertical rise velocity is governed mainly by the physical properties of the gas-liquid system and is therefore approximately a constant for a given system. The empirical equation suggested by Haberman and Morton, which has been vindicated[39] for gas-liquid systems with $2.4 < r_e < 4.0$ mm is

$$V_\infty = 1.53 \left(\frac{\sigma g}{\rho_l}\right)^{0.25} \tag{2.7}$$

For bubbles with $r_e > 4$ mm, the transition from an oblate spheroid to a spherical bubble cap becomes noticeable and is manifested by an almost rectilinear path of rise. Bubbles with $r_e > 9.0$ mm rise rectilinearly and have a well defined spherical cap with a flat undulating tail. Their rise velocity is controlled not by the volume of the bubble but by the curvature of the leading edge of the spherical cap.

Rigorous theoretical analyses of bubble motion in this intermediate bubble size range ($0.4 < r_e < 9.0$ mm) have met with little success because of the difficulty in defining (a) the shape of the bubble and (b) the flow field around the bubble. Levich [38] postulated that in low viscosity systems the energy is dissipated into a thin boundary layer around the bubble and the flow field outside the thin boundary layer is essentially unaffected by the bubble. Moore [40] presented a model based on this postulate and found it to predict the rise velocity satisfactorily for suitably sized bubbles with fore and aft symmetry in a high

surface tension low viscosity liquid. Because of the difficulty of defining the bubble boundary, the applicability of this model is limited to bubble sizes of $r_e \leq 2.0$ mm. Most of the bubble sizes encountered in two-phase gas-liquid flow are generally greater than 2.0 mm. Therefore we cannot expect Moore's theoretical model to be of much practical use.

Mendelson [41], on the other hand, considered the large bubbles ($r_e > 1.5$ mm) as being analogous to interfacial disturbances whose dynamic motion is assumed to be similar to those of waves on an ideal liquid, because of the inviscid nature of the motion of large bubbles [38]. For waves of small wave length, λ, compared to the depth of the liquid, the wave velocity, C_∞, is given by Lamb [42] as

$$C_\infty = \sqrt{\frac{2\pi\sigma}{\lambda\rho_l} + \frac{g\lambda}{2\pi}} \tag{2.8}$$

Mendelson replaced the wave length in equation 2.8 by the circumference of the equivalent bubble defined by the relation

$$\lambda = 2\pi r_e \tag{2.9}$$

and obtained the bubble rise velocity, V_∞ ($\simeq C_\infty$) as

$$V_\infty = \sqrt{\frac{\sigma}{\rho_l r_e} + g r_e} \tag{2.10}$$

On comparing the rise velocity predicted by equation 2.10 with experimental data [28,30], Mendelson observed that this simplistic model predicts the rise velocity of a bubble in an infinite medium quite satisfactorily for $r_e > 1.5$ mm.

Therefore it is recommended that, in order to predict the rise velocity of bubbles in low viscosity liquids, the following relations be used :

Theoretical solutions of Moore [40], $r_e < 1.5$ mm and $Re_b < 800$.

$$V_\infty = (gr_e + \sigma/\rho_l r_e)^{0.5} \quad r_e > 1.5 \text{ mm} \quad \text{and} \quad Re_b > 800 \qquad (2.10)$$

The rise velocity of large gas bubbles in narrow ducts is yet another interesting aspect of two-phase gas-liquid flow, as it forms a flow regime quite distinct from the discrete bubble flow regime, and has been studied by Dumitrescu [43] and by Davies and Taylor [34]. These bubbles occupy almost the entire cross-section of the duct and are called slugs. The rise velocity of an individual slug is given by Dumitrescu's equation,

$$V_\infty = k_1 \sqrt{gD} \qquad (2.11)$$

where k_1 is in general a complex function of viscosity and surface tension, but for a low viscosity liquid is well approximated by a constant value of 0.35 [44].

The rise velocity of a particular bubble in a bubble swarm, with respect to the column boundaries, is influenced by the walls of the containing vessel as well as by the bubbles around it. The rise of a gas bubble in a confined liquid medium is somewhat analogous to the corresponding sedimentation of a solid particle; but this analogy has been misinterpreted in the past by various authors who were therefore obliged either to set narrow operating limits on the validity of their equations [45] or to correct them by means of empirical factors [46]. These authors used the basic equation desired for the sedimentation of a solid particle in a confined liquid medium on the assumption that, due to the return flow caused by the displacement of the liquid by the falling particle, additional resistance would be encountered by the particle and thus it would settle at a lower velocity. Therefore

$$V/V_{\infty} \propto (1-d_p/D)^k \qquad (2.12)$$

For $d_p/D \to 1$, it can be seen from equation 2.12 that $V \to$ zero. However, for large bubbles rising in a narrow conduit ($d_b \to D$) it is well known that the bubble rise velocity is not zero but is given by equation 2.11. Thus it is not surprising that an empirical correlation of the basic form of equation 2.12 does not satisfactorily predict the rise velocity of a gas bubble in a restricted liquid medium, despite the fact that the above form has been successfully used to predict

the wall effect in liquid-solid fluidization [47]. Mendelson and Maneri [48], therefore, questioned the theoretical basis for such formulations, and suggested again that a bubble can be considered as an interfacial disturbance whose dynamic behaviour is analogous to the motion of surface waves on an ideal liquid. The extension of this analogy to account for wall proximity effects was obtained by arguing that a dynamic similarity should exist between the propagation of waves over shallow water and the rise velocity of a bubble in a restricted medium. In shallow liquids, the wave velocity is given by [42]

$$C = \sqrt{\left(\frac{2\pi\sigma}{\lambda\rho_l} + \frac{g\lambda}{2\pi}\right)\left(\tanh\frac{2\pi h}{\lambda}\right)} \qquad (2.13)$$

where h is the depth of the undisturbed liquid. Substituting for the wave length in equation 2.13, as before, the circumference of the equivalent bubble defined by equation 2.9, Mendelson and Maneri[48] obtained the bubble rise velocity V(=C) in conjunction with equation 2.10 as

$$V/V_\infty = \sqrt{\tanh(h/r_e)} \qquad (2.14)$$

The parameter h, which by analogy should be related to some effective liquid depth, was assumed by Mendelson and Maneri to be directly proportional to the tube radius. Then

$$V/V_\infty = \sqrt{\tanh C_1 (R/r_e)} \qquad (2.15)$$

The value of the constant C_1 was then obtained from the known rise velocity of slugs, assuming that large bubbles with $r_e = R$ behave like slugs, an assumption already shown to be valid by Dumitrescu [43] and many other investigators. For comparatively large tubes, at large N_{Eo}, containing low viscosity and high surface tension liquid, the constant C_1 was found to be 0.25. Thus the rise velocity of a single bubble in a confined medium is given by

$$V/V_\infty = \sqrt{\tanh [0.25(R/r_e)]} \qquad (2.16)$$

The effect of the presence of other bubbles on the motion of a bubble has not been investigated systematically. A theoretical analysis has not been possible since the flow field around the conglomeration of bubbles can not be defined except for very small spherical bubbles. However, the motion of solid particles singularly and in groups undergoing laminar flow within a confined space has been extensively studied by Happel, Brenner and co-workers [49] utilizing cell model techniques. This involves the concept that an assemblage of solid particles can be divided into a number of identical cells, each of which contains a particle surrounded by a fluid envelope containing a volume of fluid sufficient to

make the fractional void volume in the cell identical to that in the entire assemblage. The cell model technique was found to apply with greatest success for concentrated assemblages where the particles in the assemblage are distributed more or less randomly and the effect of the container walls is not important. Happel [49] assumed a typical cell envelope to be spherical. Then for a spherical particle,

$$\varepsilon_3 = (r_e/r_{cell})^3 = (\gamma)^3 \qquad (2.17)$$

Happel and Ast [50], however, considered the typical cell envelope to be cylindrical. To characterize the individual cell completely, both the cell radius and the cell length are then required. They still assumed the applicability of equation 2.17, so that the length of their cylindrical cell would have to be $4/3(r_{cell})$. They found that the predicted values of settling velocities for their cylindrical cell model agreed reasonably well with the values predicted by the concentric sphere cell model up to a solids holdup of $\varepsilon_3 = 0.216$ (corresponding to $r_e/r_{cell} = 0.6$). Thus Happel concluded that the shape of the fluid envelope to be used in such cellular representations of assemblages is of no significant importance up to substantial solids holdups. A similar cell model representation is subsequently applied in the present work to swarms of bubbles.

2.1.1.2 Bubble column

If a two-phase gas-liquid operation is carried out in a vertical column under conditions of zero net liquid flow rate through the column, then the contacting device is called a "Bubble Column". The controlling parameters for the operating characteristics of a bubble column are the residence time of the gas phase (determined by the rise velocity of the swarm), the interfacial area (determined by the size of the bubbles in the swarm) and the mixing characteristics (determined by the wake phenomenon and by the geometric structure of the containing vessel).

Freedman and Davidson [51] presented a summary of data obtained in bubble columns of diameters ranging from 1 inch to 42 inch which is shown in Figure 2.1. As can be seen, a wide spread in gas holdup exists but the data can mainly be divided into two distinct regions, that is, a region in which liquid circulation is prevalent (column diameter $\geq$ 4 inch) and a region where liquid circulation is not important (column diameter $\leq$ 2 inch). The studies of Hughmark [52] and of Shulman and Molstad [53] for small diameter columns (1 inch to 4 inch) have shown that the gas holdup is primarily a function of the volumetric flux of gas, $\langle j_2 \rangle$, through the column and can be predicted from a knowledge of bubble size in the swarm. However, the information concerning bubble sizes is not readily available except at small gas flow rates. At higher gas flow rates, dispersion of the gaseous phase

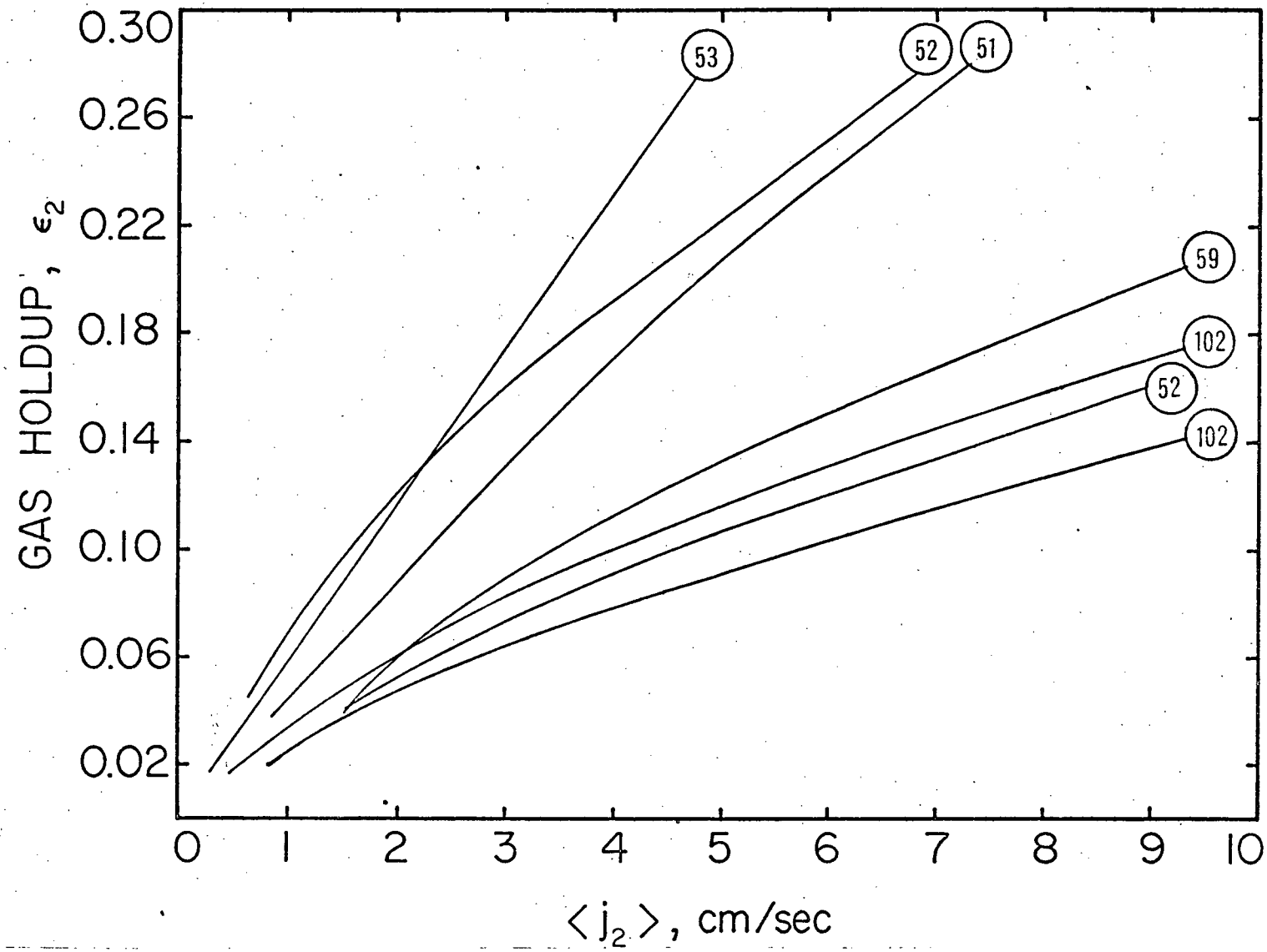

FIGURE 2.1 GAS HOLDUP DATA FROM LITERATURE FOR AIR-WATER SYSTEM IN BUBBLE COLUMNS OF 1-42 INCH DIAMETER (curves are numbered in accordance with references)

into the liquid phase is brought about by induced turbulence, and the breakup and coalescence of the dispersed phase occurs continuously. The size of bubbles in the swarm under these turbulent conditions had not been studied conclusively but it is believed that in columns of diameter up to 4 inch, the bubble size increases with gas flow rate [53] until the bubbles are large enough ($r_e \geq 9.0$ mm) to become spherically capped [58]. Then, if the liquid pool is deep enough, these spherically capped bubbles coalesce to form slugs which occupy almost the entire cross-section of the column.

Towell et al. [59] studied the bubble size and gas holdup in a 16 inch diameter column. With the help of high speed cine photography, they observed that liquid circulation in such large diameter columns is very significant and is responsible for a high degree of mixing and a lowering of gas holdup relative to smaller columns. Small diameter columns (up to 4 inch in diameter), on the contrary, were shown [60] not to have significant liquid circulation and were, therefore, found to exhibit very insignificant axial mixing and much larger gas holdups. Various explanations have been provided for the presence of liquid circulation in large diameter columns. Freedman and Davidson believe that it is caused by the maldistribution of the gas at the bottom of the column. De Nevers [61] suggests that density differences between those parts of the column which are rich and those which are poor in dispersed phase cause the

liquid circulation to set in. Yoshitome and Shirai [62] measured the intensity of circulation in a 15 cm diameter column and found a strong upward flow of continuous phase in the central core region and a downward flow near the walls of the column.

As observed by these authors [59-62], the turbulent activity in large columns is quite significant and under such conditions the size of the bubbles in the swarm is controlled by the energy dissipation in the two-phase system [63]. Calderblank [64], in studying the dispersion of gas in a mechanically stirred tank, utilized this concept to obtain the average bubble size in the tank by balancing the surface tension forces with the turbulent energy dissipation. Towell et al. recommended that Calderblank's correlation be extended to predict average bubble size for bubble columns by assuming that the power dissipated per unit volume in a bubble column can be taken as

$$\text{Power input per unit volume} = \langle j_2 \rangle \rho_1 / g \qquad (2.18)$$

They then substituted equation 2.18 into Calderblank's correlation for stirred tanks and obtained the following relationship to predict the average bubble size in a swarm:

$$d_b = 0.25 \left[(\langle j_2 \rangle)^{-0.4} (\sigma/\rho)^{0.6} \right] \varepsilon_2^{0.5} + 0.09 \qquad (2.19)$$

Good agreement was reported between equation 2.19 and the limited amount of data obtained by Towell et al. photographically for large (> 4 inch) diameter columns.

2.1.1.3 Vertical cocurrent flow

The flow of the gas and the liquid phases cocurrently in a vertical conduit has been studied and a number of methods have been suggested to predict the gas holdup. It is important to note that the bubble dynamics as observed in bubble columns is not radically changed due to the flow of the liquid phase. Baker and Chao [65] observed that the rise velocity of a bubble in a vertically moving liquid stream is not affected by the velocity of the liquid stream inasmuch as the relative velocity of the bubble is found to be the same as the bubble velocity in the quiescent liquid stream. It has also been observed [66] that bubble formation from an orifice in a vertically moving liquid stream is unaffected by the velocity of the liquid stream. Thus the phenomenon of relative velocity could be used to generalize the behaviour of two-phase flow, as suggested by Lapidus and Elgin [67].

The effect of column diameter on the mixing characteristics and gas holdup in cocurrent gas-liquid flow was investigated by Reith et al [68] in 5, 14 and 29 cm columns. They found that a 5 cm column displays very little axial mixing and high gas holdup, as was observed earlier for bubble columns. But for larger vessels, although no systematic

circulation of the liquid stream was observed, the rates of axial mixing were found to be much higher, and the gas holdup much lower, than for the 5 cm column. Therefore they suggested that axial mixing in large columns is caused by the generation of large scale eddies in the liquid phase due to passage of the bubbles.

The average bubble size in cocurrent gas-liquid flow has not been investigated systematically. However, Patrick [69], based on a limited amount of data obtained in a 5 cm column, reported that the average bubble size in two-phase gas-liquid flow is a function of the average linear liquid velocity, the following relationship representing the data for the cocurrent bubble flow regime:

$$d_b = 5.074/\bar{v}_1^{0.666} \qquad 15 < \bar{v}_1 < 150 \tag{2.20}$$

The transition point from the bubble flow regime to the slug flow regime has been studied only qualitatively. Reith et al. suggested that for a 5 cm column, slug flow occurred at gas velocities above $\langle j_2 \rangle = 5$ cm/sec. Ellis and Jones [60] observed the transition point visually and found the following relationship to describe the transition approximately:

$$\langle j_2 \rangle = 0.2 \langle j_1 \rangle + 3.05 \tag{2.21}$$

Although no slugs were actually observed in pipes greater than 10 cm in diameter up to $\langle j_2 \rangle = 45$ cm/sec [68], Ellis

and Jones classified the flow to be in the slug flow regime if the average relative velocity of the gas phase was found to be greater than the velocity of rise of a single slug as given by Dumitrescu's relation, equation 2.11, for the given column diameter.

Several methods have been suggested to predict the gas holdup in cocurrent gas-liquid flow. Of all the empirical correlations available, that of Lockhart and Martinelli [70], originally developed for horizontal flow but subsequently applied also to vertical flow, is still the most convenient to use when information concerning the detailed flow structure is either not available or not desired [71]. Duckler et al. [72] compiled all the available data and checked the validity of various empirical correlations that have been recommended in the literature. They found that Hughmark's [73] correlation represents most of the data reported over a wide range of operating limits very satisfactorily. Therefore, Hughmark's correlation will be used to check the validity of the model proposed herein, in conjunction with equations 2.20 and 2.21.

2.1.2 Models for gas holdup predictions

The relative velocity between the dispersed and the continuous phases has been suggested by Lapidus and Elgin [67] as the single parameter required to completely describe the behaviour of an ideal dispersed phase system. They did

not provide a definition of an ideal system, but it can be inferred from their work that if the dispersed phase is uniformly distributed throughout the continuous phase in such a manner that each particle has an individual identity, yet its behaviour is identical to that of all the other particles, then the dispersed phase system is ideal. The local relative velocity is then uniform and identical to the average relative velocity of the whole assemblage. In a non-ideal system the concept of relative velocity can only be employed locally. Since the data on local relative velocity are not easily available, Zuber and Findlay [39] recommended that the concept of local drift velocity be used instead. The property of constancy of drift velocity for certain specific regimes can then be utilized, the information on relative velocity in various flow regimes being often vague and incomplete.

The local drift velocity, as defined earlier, represents the local velocity of the bubble with respect to the local volumetric flux of the mixture:

$$v_{2j} = v_2 - j \tag{2.22}$$

In a two-phase system, data on the average values are more readily available; thus the average volumetric flux of the gas phase, $\langle j_2 \rangle$, which is readily measurable, is

$$\langle j_2 \rangle = \langle \alpha_2 v_2 \rangle = Q_2/A \tag{2.23}$$

The weighted mean velocity of the gas phase, $\bar{v}_2$, which is obtained by integration across the cross-section, is given by

$$\bar{v}_2 = \frac{\langle j_2 \rangle}{\langle \alpha_2 \rangle} = \frac{\langle \alpha_2 v_2 \rangle}{\langle \alpha_2 \rangle} \tag{2.24}$$

In view of equation 2.22, the weighted mean velocity of the gas phase can also be expressed as

$$\bar{v}_2 = \frac{\langle \alpha_2 j \rangle}{\langle \alpha_2 \rangle} + \frac{\langle \alpha_2 v_{2j} \rangle}{\langle \alpha_2 \rangle} \tag{2.25}$$

Equation 2.25 can be put in several alternate forms which are most useful for analyzing experimental data and for determining the average volumetric gas fraction, $\langle \alpha_2 \rangle$. Thus, multiplying and dividing the first term on the right hand side by $\langle j \rangle$, we obtain

$$\bar{v}_2 = C_0 \langle j \rangle + \frac{\langle \alpha_2 v_{2j} \rangle}{\langle \alpha_2 \rangle} \tag{2.26}$$

where C_0 is the distribution parameter [39] and is given by

$$C_0 = \frac{\langle \alpha_2 j \rangle}{\langle \alpha_2 \rangle \langle j \rangle} \tag{2.27}$$

The distribution parameter takes into account that both the volumetric flux of the mixture and the gas holdup are not uniform over the cross-section. However, if either the volumetric flux of the mixture or the gas holdup is uniform over the cross-section, it can be easily seen from equation 2.27 that C_0 will be unity. Thus where

$$\varepsilon_2 = \langle\alpha_2\rangle = \alpha_2 \tag{2.28}$$

Equation 2.26 can be simplified to

$$\bar{v}_2 = \langle j\rangle + \langle v_{2j}\rangle = \langle j_1\rangle + \langle j_2\rangle + \langle v_{2j}\rangle \tag{2.29}$$

Combination of equation 2.29 with equation 2.24 yields

$$\langle j_2\rangle = \frac{\varepsilon_2(\langle j_1\rangle + \langle v_{2j}\rangle)}{1 - \varepsilon_2} \tag{2.30}$$

For ideal bubbly flow, all the averaging brackets on the velocities can also be dropped. If, however, neither the volumetric flux of the mixture nor the volumetric gas fraction is uniform over the cross-section, the distribution parameter for axially symmetric flow through a circular duct, assuming flow and gas holdup profiles in the radial direction to be

$$\frac{j}{j_c} = 1 - (R^*)^M \tag{2.27a}$$

and

$$\frac{\alpha_2}{\alpha_{2C}} = 1 - (R^*)^{M'} \tag{2.27b}$$

respectively, is given by [39]

$$C_0 = \frac{M + M' + 4}{M + M' + 2} \tag{2.27c}$$

For positive values of $(M + M')$, C_0 is obviously greater than unity.

Zuber and Findlay have pointed out that the main problem in two-phase flow is determining the correct equation for the drift velocity, v_{2j}, with particular regard to the flow regime. In general, the local drift velocity is found to be affected by the bubble spacing or the gas holdup. Thus for the bubble flow regime, Zuber and Hench [74] reported that

$$v_{2j} = V_\infty (1 - \alpha_2)^m \tag{2.31}$$

where m was found to vary between 0 and 3 depending on the bubble size.

As a basis for considering the more complicated case of three-phase flow, Bhaga [1] developed a model for two-phase gas-liquid flow by considering the relative velocity between the phases. The local relative velocity is related to the local drift velocity by the equation

$$v_{2j} = (1 - \alpha_2)\, v_{21} \tag{2.32}$$

Thus, combining equations 2.31 and 2.32, we get

$$v_{21} = V_\infty\, (1 - \alpha_2)^{m-1} \tag{2.33}$$

which is the relationship used by Bhaga [1] who expected the exponent (m-1) to vary between -1 and 2. For the limited data tested, however, Bhaga found that a value of m = 2 best represented his results for both cocurrent and countercurrent air-water flow in a vertical conduit. Nevertheless, the model proposed by Bhaga provides no advantage over the original model proposed by Zuber and Findlay, at least for two-phase flow.

Marrucci [75] utilized the concept of energy dissipation in irrotational flow [38,40] in conjunction with the cellular representation of a bubble swarm suggested by Happel [49] to predict the rise velocity of a bubble swarm. His method, applicable in the bubble flow regime, assumes that the vorticity generated in the wake of a bubble is not transferred far enough downstream to affect the motion of any downstream bubbles. Based on these assumptions he found that the energy-destroying velocity (due to buoyancy alone), or the drift velocity, is given by

$$v_{2j} = V_\infty (1 - \alpha_2)^2/(1 - \alpha_2^{5/3}) \qquad (2.34)$$

He noted qualitatively that the sparse data of Nicklin [19] and his own data indicated a relatively small decrease in rise velocity with increasing α_2, in conformity with equation 2.34. Although no explicit mention is made of the radius of bubbles which make up the swarm, Marrucci's model does implicitly indicate the effect of bubble radius on the rise velocity of the swarm through the term V_∞.

Another model has been proposed by the present author [76] for predicting the drift velocity in the bubble flow regime, based on the method of Maneri and Mendelson [48] for predicting the rise velocity of large bubbles in confined media. The latter authors showed that for large N_{Eo} $(=g\rho_l R^2/\sigma)$, that is, for large tube diameters such that $1/N_{Eo} << 1$, the rise velocity of a single bubble is given by

$$V/V_\infty = \sqrt{\tanh [0.25 (R/r_e)]} \qquad (2.35)$$

Equation 2.35 was found by Maneri and Mendelson to correlate experimental data well for $1/\gamma = R/r_e$ between 1 and 10, the lower limit of which corresponds to a slug. This equation gives the drift velocity of a single spherical bubble in a cylindrical tube. Happel and Ast [50] suggested a sphere-in-cylinder-type cell model to represent an assemblage of solid

particles. Thus, if we use the approach of Happel and Ast, we have the necessary relationship between γ and the volumetric gas fraction, α_2, as follows:

$$\alpha_2 = \gamma^3 \tag{2.36}$$

Now, combining equations 2.35 and 2.36, we get

$$v_{2j} = V_\infty \sqrt{\tanh\ [0.25\ (1/\alpha_2)^{1/3}]} \tag{2.37}$$

Thus equation 2.37 would predict the drift velocity [or the energy-destroying velocity as defined by Nicklin [19]] of a bubble swarm in tubes of large diameters for low viscosity systems e.g. water. It should, however, be pointed out that equation 2.37 will not give the drift velocity for slugs, but equation 2.35 with $r_e = R$ does represent the rise velocity of slugs in a quiescent medium, for which it then simplifies [48] in combination with equation 2.10 for large N_{Eo} to

$$v_{2j} = \sqrt{gr_e\ (\tanh\ 0.25)} \tag{2.38}$$

or

$$v_{2j} = 0.35\ \sqrt{gD} \tag{2.39}$$

which is the Dumitrescu equation for drift velocity in the slug flow regime recommended by several investigators [39,27].

Equation 2.26, derived originally by Zuber and Findlay, is quite general and applicable to all gas-liquid flow regimes if the distribution parameter, and the weighted mean drift velocity can be obtained independently. This requires simultaneous measurements of velocity and gas holdup profiles, which have not generally been made, and thus local drift velocity profiles are not available. The lack of experimental measurements of local properties thus necessitates suitable assumptions for the distribution parameter and the weighted mean drift velocity in order to advance a meaningful empirical or semi-empirical model for two-phase gas-liquid flow. Zuber and Findlay assumed smooth and symmetric profiles for velocity and gas holdup and thus found the distribution parameter to be between 1.0 and 1.5 (see equation 2.27c). They did not appreciate the possibility of systematic circulation, which persists in bubble columns [59] and which may render these profiles to be neither smooth nor symmetric. Thus, the models above cannot be used successfully to predict the gas volume fraction in columns where circulation exists. At the present time not enough information is available to predict the rate of circulation, but a possible mechanism is suggested in the next section.

2.1.3 Circulation and turbulence in two-phase gas-liquid flow

It has been shown above that for a bubble column greater than 10 cm in diameter, a systematic circulation develops in the liquid phase with an upward liquid flow in the central core of the column and a downward liquid flow near the walls. From all the evidence presented, the following description of circulation can be given:

At very small gas flow rates and low Reynolds number ($Re_b < 10$) the bubbles are uniformly distributed and rise in distinguishable bubble chains [77]. Crabtree and Bridgwater [78] showed that the rising bubble chains drag liquid by viscous shear and thus induce circulation in the liquid phase. This circulation is further enhanced by the presence of both low density (high gas fraction) and high density (low or zero gas fraction) regions. At higher Reynolds number ($Re_b \simeq 400$), a distinguishable wake behind the bubbles appears and the liquid in the attached wake travels at the bubble velocity. The liquid in the wake is deposited near the surface of the main liquid when the bubble reaches this surface and breaks up. Because of the rise of liquid in the wake of the bubble, the circulation becomes quite intense, affecting the radial bubble distribution and giving rise to more regions of high and low density, which help to sustain the circulation. At still higher Reynolds number, it is believed

that the wake no longer remains attached to the bubble but is shed at regular intervals [79], as observed by Letan and Kehat [36] for drops in liquid-liquid systems. Under these conditions the liquid circulation appears to be chaotic as it is superimposed on random eddying [59], but in fact a systematic circulation is maintained in which the liquid moves upwards in the central region and downwards near the wall. The bubbles mainly rise in the high upward velocity region, but the circulation is so intense that a bubble could be trapped in the downward flow region or even swept back with the downward flow, as observed by Freedman and Davidson [51].

A similar physical model can be advanced for cocurrent gas-liquid flow. Baker and Chao [65] have shown that the dynamics of an individual bubble is not affected by the upwards liquid velocity. It is therefore to be expected that a similar general model should be applicable to cocurrent flow, where the circulation and the wake shedding patterns are superimposed on a net liquid flow in the vertical direction. However, Reith et al. [68] observed no systematic circulation of liquid in cocurrent flow; nevertheless, axial mixing was found to occur and was apparently caused by the wake shedding phenomenon. The same effect has also been observed by Letan and Kehat [36] for the study of axial mixing in liquid-liquid extraction (spray) columns. It is therefore probable that in cocurrent flow the circulation is contained in cellular regions.

It has been observed for the rise or fall of a drop through a liquid medium that the wake behind the drop is shed at regular intervals [36]. Though vortex shedding from behind a bubble has not been studied, it is believed to occur on very similar patterns as behind a drop. The shed vortices will initially rise in the liquid at the bubble velocity, but will subsequently be dissipated by viscous stresses [79]. The interaction of the mean flow with these ejected vortices would create intense and chaotic velocity fluctuations in the mean flow. These fluctuations are believed to be responsible for the generation and maintenance of turbulence in the liquid phase at the expense of the energy of the mean flow. Delhaye [81] had reported some measurements of intensity of turbulence induced in a liquid due to passage of gas bubbles. He observed that even at small gas flow rates, the turbulence generated in the liquid phase by the gas bubbles is quite significant.

2.2 Voidage in liquid-solid fluidized beds

The hydrodynamics of fluid flow through a bed of granular material has been researched quite successfully in the past. Basically, three distinct approaches have been developed and used to study the hydrodynamics of fluidized beds:

(i) Using the relationship between pressure drop and fluid flow rate of a fixed bed at the fludization transition point to study incipient fluidization and subsequent bed expansion [56].

(ii) Using the concept suggested by Lapidus and Elgin [67] that the relative velocity between the liquid and the solid particles alone can predict the voidage in liquid-solid fluidized beds. The actual form of the relationship between the relative velocity and the bed voidage has, however, to be determined experimentally.

(iii) Using a cell model to represent an assemblage of particles as suggested by Happel and Brenner [49]; then solving the full Navier-Stokes equations within the cell analytically for low Reynolds numbers ($Re_p < 1$), when the inertial terms are not important, or numerically for moderately high Reynolds numbers [65,66].

All three techniques have been found to predict the relationship between voidage and volumetric liquid flux quite satisfactorily over a wide range of system variables. Since all these techniques have been treated quite eloquently by various investigators [56,2,49], no attempt is made here to present them in detail. However, a summary of these techniques is given below.

Andersson [56] studied the applicability of the pressure drop equation for fixed beds to obtain a relationship

between the liquid velocity and the bed voidage for liquid-solid fluidized beds. The applicability of this technique mainly depends on the experimentally observed fact that the pressure drop in fluidized beds is always equal to the buoyed weight of the bed per unit area, i.e.,

$$-\Delta p = \varepsilon_3(\rho_3-\rho_1)\, L_b\, g \tag{2.40}$$

Ergun [57] successfully represented the pressure drop through a fixed bed of spherical particles by an equation which, at the transition point to fluidization, is

$$-\frac{\Delta p}{L}\left(\frac{d_p}{\rho_1 \langle j_1\rangle^2}\right) g \left(\frac{\varepsilon_1^3}{\varepsilon_3}\right)_{mf} = 150\,(\varepsilon_3)_{mf}\,\frac{\mu}{\langle j_1\rangle \rho_1 d_p} + 1.75 \tag{2.41}$$

Since the pressure drop through a fixed bed of particles must equal the buoyed weight of the bed per unit area in order to initiate fluidization, combination of equations 2.40 and 2.41 provides the desired relationship between the void fraction and the volumetric liquid flux. However, the knowledge of bed voidage at incipient fluidization, $(\varepsilon_1)_{mf}$, is still required. A value of 0.4 is recommended for spherical particles [21,49]. Neuzil and Hrdina [47] observed that the voidage at minimum fluidization, $(\varepsilon_1)_{mf}$, is affected by the d_p/D ratio and recommended the following relationship for spherical particles:

$$(\varepsilon_1)_{mf} = 0.404 + 0.429\ (d_p/D) \tag{2.42}$$

The second approach utilizes the concept of relative velocity between the liquid and the solid particles to describe the relationship between the voidage and the volumetric liquid flux. Richardson and Zaki [2], based on a dimensional analysis of the relevant variables involved in fluidization, demonstrated that

$$\frac{v_{13}}{v_\infty} = \frac{v_1 - v_3}{v_\infty} = f_1(Re_p,\ \varepsilon_1,\ d_p/D) \tag{2.43}$$

Since in batch fluidization the net velocity of the solid particles is zero, the relative velocity between the liquid and the solid particles is simply

$$v_{13} = v_1 = \langle j_1 \rangle / \varepsilon_1 \tag{2.44}$$

Now, combining equations 2.43 and 2.44, the functional relationship can be written as

$$\frac{\langle j_1 \rangle}{v_\infty} = f_2\ (Re_p,\ \varepsilon_1,\ d_p/D) \tag{2.45}$$

On the basis of a large amount of data obtained for sedimentation and fluidization of particles for a wide range of

system variables, Richardson and Zaki [2] found that the following simple relationship represented the results in the best manner:

$$\langle j_l \rangle / V'_\infty = \varepsilon_l^n \tag{2.46}$$

where $V'_\infty = V_\infty$ and exponent n was found to be a function of particle Reynolds number (Re_p) alone, only if the ratio d_p/D was sufficiently small. The following values of n were reported by Richardson and Zaki over a wide range of Re_p, in the absence of wall effect:

$$n = 4.65 \qquad Re_p < 0.2 \tag{2.47}$$

$$n = 4.35\, Re_p^{-.03} \qquad 0.2 < Re_p < 1 \tag{2.48}$$

$$n = 4.45\, Re_p^{-0.1} \qquad 1 < Re_p < 500 \tag{2.49}$$

$$n = 2.39 \qquad 500 < Re_p \tag{2.50}$$

Richardson and Zaki [2] also observed that the ratio d_p/D affected the fluidization quite markedly. However, Neuzil and Hrdina [47] found that the correction factors reported by Richardson and Zaki to take wall effects into account were not adequate. They, therefore, questioned the basis on which Richardson and Zaki had formulated their wall effect correction factors. Neuzil and Hrdina, following an

approach similar to that suggested by Steinour [93], obtained the following semi-empirical relationship to describe the bed expansion:

$$\langle j_l \rangle / V_\infty = 0.67\ Re_p^{0.03}\ [1-1.27(d_p/D)^{1.15}]\ \varepsilon_l^{2.7} \qquad (2.51)$$

which is based on a large quantity of experimental data in the range $0.0454 < d_p/D < 0.3$ and $75.5 < Re_p < 1795$. The correlation for minimum fluidization of spherical particles was obtained by combining equations 2.42 and 2.51, the result being

$$\frac{\langle j_l \rangle_{mf}}{V_\infty} = [1-1.27(d_p/D)^{1.15}]\,[0.348+0.370(d_p/D)]^{2.7}\ Re_p^{0.03} \qquad (2.52)$$

However when the wall effects are not important, e.g. for $d_p/D = 0.1$ the relative error in the liquid phase volume fraction is only 3.5% [47]. Equation 2.46 proposed by Richardson and Zaki [2], with the value of the exponent n obtained from equations 2.47 -2.50, should be used because it has been checked for a wider variety of data and is generally more acceptable.

Thus the equation proposed by Neuzil and Hrdina, when the wall effects are important, and the equations proposed by Richardson and Zaki, when the wall effects are negligible, will be used in this work to predict the relationship between

the voidage and the volumetric liquid flux for the liquid-solid systems investigated.

The third method for liquid-solid fluidization is essentially analytical in its approach, and depends on the ability of representing an assemblage of particles by a unit cell consisting of one spherical particle surrounded by a concentric spherical envelope, which contains a volume of liquid such that the liquid phase volume fraction in the cell is the same as that for the entire assemblage [49]. This approach then requires solving the full Navier-Stokes equations of motion within the cell for appropriate boundary conditions. The Navier Stokes equations, with the required boundary conditions, can be solved analytically if the inertial terms in the equations can be neglected ($Re_p < 0.2$). However, when the inertial terms are important, solution of the complete Navier-Stokes equations can only be obtained by numerical techniques. Such techniques have been developed and used by Masliyah and Epstein [82] and by Leclair and Hamielec [90] to obtain solutions for an assemblage of spherical or spheroidal particles up to quite large Reynolds numbers ($Re_p \simeq 100$).

2.2.1 Effect of turbulence on voidage in liquid-solid fluidized beds

Free-stream turbulence has been shown to have a significant effect on the drag coefficient of a single particle

[94-96]. Changes in the drag coefficient of a particle were found to be influenced by the free-stream Reynolds number, based on the relative velocity of free stream with respect to the particle, and the characteristics of the free-stream turbulence, viz., the intensity of turbulence [94,95] and the scale of turbulence relative to the particle size [96]. Torobin and Gauvin [95] measured drag coefficients of aerodynamically smooth spheres by studying their velocity history in a wind tunnel, in which turbulence was generated by screen grids. They observed that, at constant Reynolds number, an increase in the intensity of turbulence at first produced a moderate increase and then a sharp decrease in the drag coefficient of the particle. The increase was assumed to be caused by the disruption of the particle wake, whereas the sharp decrease was believed to be caused by the premature transition of the laminar boundary layer into a turbulent boundary layer and its consequent reattachment to the particle, thereby reducing the form drag, which constitutes the main portion of the total drag force under these conditions. The value of the critical Reynolds number, based on relative velocity between the air stream and the particle, at which this transition took place varied with the intensity of free-stream turbulence, I_t. Torobin and Gauvin found that the criterion for transition was adequately described by the relationship

$$Re_c \, I_t^2 = 45 \qquad (2.53)$$

where

$$Re_c = \frac{d_p \, v_{23} \, \rho_2}{\mu_2}$$

If the free-stream Reynolds number was now increased beyond Re_c, for a fixed intensity of free-stream turbulence, the drag coefficient of the particle decreased to a definite minimum after which it increased again quite noticeably [94].

In fluidization, the particles are maintained in a suspended state because their weight, modified by buoyancy, is balanced exactly by the drag forces due to the relative motion of the liquid with respect to the particles. Should the fluidizing stream be turbulent and the criterion established by equation 2.53 be satisfied on increasing the flow rate, the drag coefficient as well as the total drag force experienced by the particles would then be reduced. This would result in contraction of the bed, that is, reduction of bed voidage. For all other ranges of Reynolds number, any increase of turbulence in the fluidizing liquid stream on increasing the flow rate would give rise to an increase in the drag coefficient over and above that caused by the increased flow itself, thereby causing further expansion of the liquid-solid fluidized bed.

No detailed study has been conducted to elucidate the effects of turbulence on the expansion characteristics

of a liquid-solid fluidized bed. However, a limited study involving water fluidization of very large and very heavy spheres, carried out by Trupp [87], revealed that such fluidized beds expanded more than predictable by the Richardson - Zaki correlations. It is known that a fluidized bed of randomly spaced and randomly moving solid particles generates fluid-phase turbulence [97]. The quantitative characteristics of this induced turbulence, viz., the intensity and the scale, have not, however, been measured. Therefore at this stage it can only be surmised that the turbulence of the fluidizing liquid stream significantly influences the behaviour of a liquid-solid fluidized bed. But for a better understanding of the importance of the turbulence phenomenon in fluidization, it is necessary to quantitatively study the characteristics of the turbulence and their influence on bed voidage of liquid-solid fluidized beds.

2.3 Holdup in gas-liquid-solid fluidized beds

The active academic interest in the study of three-phase fluidized beds originated from the preliminary investigations undertaken by Turner [6] and Adlington and Thompson [9], who reported that on slow addition of gas to a liquid-solid fluidized bed, the bed contracted. Volk [10], however, in an earlier and detailed study of three-phase fluidization, had observed that the liquid-solid fluidized bed expanded

smoothly on introduction of the gas phase. Based on these contrary observations, it was postulated [7,8,10] that in a three-phase fluidized bed the solid particles were entirely supported by the liquid whereas the gas travelled through the bed as discrete particle-free bubbles. This postulate forms the basis of various mathematical models formulated to describe the expansion behaviour of three-phase fluidized beds, three of which are considered in the following section.

2.3.1 Models for three-phase fluidized beds

The three mathematical models which have been or will be proposed to predict the volumetric fraction of the individual phases in a three-phase fluidized bed are: (A) the gas-free model, (B) the wake model and its modifications, and (C) the cell model.

A fourth model, whereby the gas and liquid are treated as a homogeneous fluidizing medium with appropriately averaged fluid properties and velocity, was considered by Volk [10]. This homogeneous model is rejected here on the grounds that it is unsuitable even for two-phase gas-liquid flow in most instances, especially for the slug flow regime.

(A) The gas-free model

Volk [10], who made an extensive study of the behaviour of three-phase fluidized beds using nitrogen as gas, heptane

as liquid and porous cylindrical catalyst pellets as solid particles, reported that the bed expanded smoothly on increasing the gas flow rate at a fixed liquid flow rate. He considered the three-phase fluidized bed to consist of a bubbling gas phase and a liquid-solid fluidized (particulate) phase, the liquid flow rate through which is modified due to the presence of the bubbles. The observed bed expansion was considered due to

(i) the increase in bed volume caused by the presence of the gas bubbles, and

(ii) the increase in interstitial liquid velocity caused by the reduction in area available for liquid flow.

These two factors are inter-dependent. The data processing scheme used by Volk was empirical in its nature and grossly in error. Therefore, by taking the two factors mentioned above into account, a simple mathematical model, along the lines suggested by Volk, is developed here. Figure 2.2 demonstrates the model schematically.

Let A be the cross-sectional area of the column and ε_i be the average volumetric fraction occupied by the i^{th} phase. Then

$$\sum_{i=1}^{3} \varepsilon_i = 1 \qquad (2.54)$$

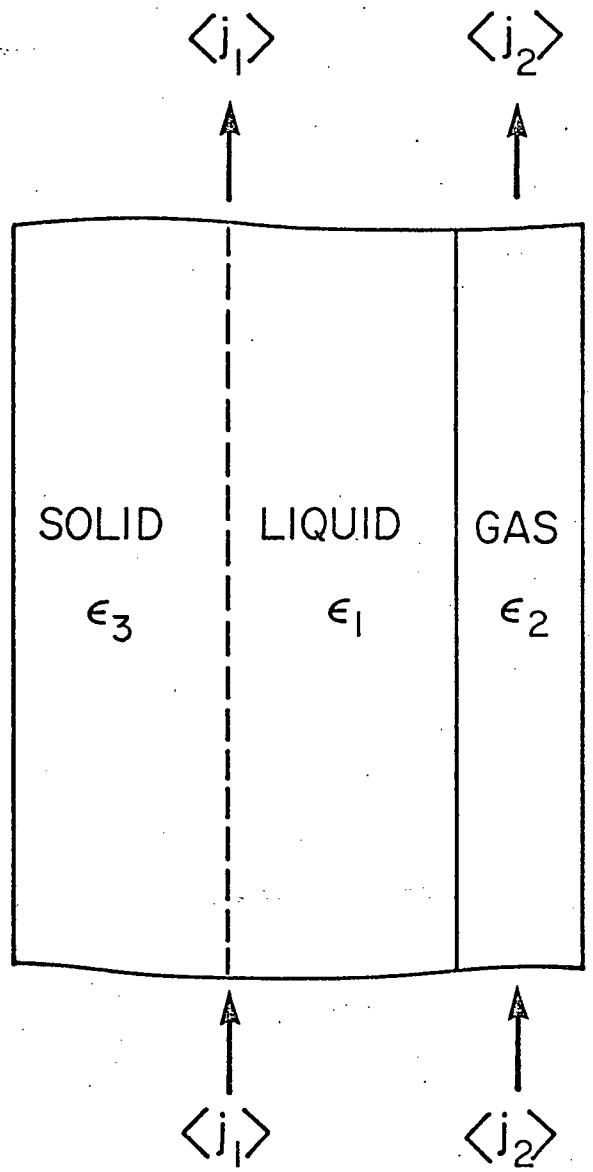

FIGURE 2.2 SCHEMATIC REPRESENTATION OF THE GAS-FREE MODEL

Let us assume that each phase is homogeneously distributed so that the area occupied by each phase is $\varepsilon_i A$. Then the

$$\text{Area occupied by the gas phase} = \varepsilon_2 A \tag{2.55}$$

and the

$$\text{Area occupied by the liquid-solid fluidized phase} = A(1-\varepsilon_2) \tag{2.56}$$

Since all the liquid is assumed to flow through the liquid-solid fluidized bed region, a material balance for the liquid gives

$$\text{Superficial liquid velocity through gas-free region} = \frac{A \langle j_1 \rangle}{A\ (1-\varepsilon_2)} = \frac{\langle j_1 \rangle}{(1-\varepsilon_2)} \tag{2.57}$$

Similarly a material balance of gas through the bed gives

$$\langle j_2 \rangle = \bar{v}_2\ \varepsilon_2 \tag{2.58}$$

where $\bar{v}_2$ is the average rise velocity of bubbles through the bed.

It has been assumed [8,16,79] that bed expansion of the liquid-solid fluidized phase can be well represented by the Richardson - Zaki correlation, using the modified super-

ficial liquid velocity through this region. Then the volume fraction of liquid in the particulate phase, ε''_{lf} is given by

$$\varepsilon''_{lf} = \left[\frac{\langle j_l \rangle}{V'_\infty (1-\varepsilon_2)}\right]^{1/n} \tag{2.59}$$

where the exponent n is a function of particle Reynolds number, Re_p, while ε''_{lf} is related to the overall volumetric fraction of liquid in the three-phase fluidized bed, ε_l, by

$$\varepsilon''_{lf} = \varepsilon_l/(1-\varepsilon_2) \tag{2.60}$$

Combining equations 2.59 and 2.60, ε_l is given by

$$\varepsilon_l = \left[\frac{\langle j_l \rangle}{V_\infty (1 - \varepsilon_2)}\right]^{1/n} (1-\varepsilon_2) \tag{2.61}$$

and the total bed voidage, ε, is given by

$$\varepsilon = (1-\varepsilon_3) = \varepsilon_l + \varepsilon_2 = \left[\frac{\langle j_l \rangle}{V_\infty (1-\varepsilon_2)}\right]^{1/n} (1-\varepsilon_2) + \varepsilon_2 \tag{2.62}$$

By rearranging equation 2.62, the solids holdup in the three-phase fluidized bed, ε_3, can be written as

$$\varepsilon_3 = (1-\varepsilon_2) \left\{1 - \left[\frac{\langle j_l \rangle}{V_\infty (1-\varepsilon_2)}\right]^{1/n}\right\} \tag{2.63}$$

Thus equation 2.62, in combination with equation 2.58, provides a simple scheme for describing the voidage and bubble velocity

in a three-phase fluidized bed. With the help of this model and a measurement or estimate of the volumetric fraction of one of the three phases at different gas and liquid flow rates, necessary information about the average volumetric fractions of the other individual phases in a three-phase fluidized bed can be obtained. The determination of solids holdup, by measuring the bed height, L_b, is probably the simplest procedure, as the solids holdup, ε_3, is related to the bed height, L_b, by the following relationship:

$$\varepsilon_3 = W/\rho_3 A L_b \qquad (2.64)$$

The average volumetric fraction of gas, ε_2, can then be obtained, by trial and error, from equation 2.63, and the average volumetric fraction of liquid, ε_1, from equation 2.54.

Thus a simple mathematical model can be obtained on the basis of the description of a three-phase fluidized bed given by Volk. However, it is important to note that this model has the inherent assumption that no liquid is associated with the gas phase. Such liquid, by definition, would not provide any effective force for fluidization of the solid particles and hence would not contribute to the expansion of the bed. It is therefore necessary to understand the distribution of the liquid phase between the gas phase and the particulate phase. The wake model derived originally by Østergaard [8], as described in section 1.3, considers

this distribution by assuming that the liquid associated with the gas phase is represented by the wake of the bubbles.

(B) The wake model

Stewart and Davidson [7] and Østergaard [8] each proposed a mechanism for the observed bed contraction in three-phase fluidization [6,9] by describing a three-phase fluidized bed as consisting of (i) a gas phase, (2), (ii) a wake phase, (k), and (iii) a liquid-solid fluidized (or particulate) phase, (f). The mechanisms proposed were similar in most respects; however, one difference was reported in the respective observations of these early investigators. Stewart and Davidson observed photographically that the bubble wake in a two-dimensional bed was essentially free of solid particles, whereas Østergaard's photographic observations of bubbles emerging from a three-phase fluidized bed showed them to be followed by a long trail containing solid particles. Østergaard, in proposing the mathematical model presented in section 1.3, therefore assumed that the volume fraction of solids in the wake was the same as in the particulate phase. The main weaknesses in the model proposed by Østergaard, as stated in section 1.3, are

(i) The assumption that the porosity of the wake phase is equal to that of the particulate phase.

(ii) The neglect of solids circulation induced by the motion of gas bubbles carrying wakes containing solid particles.

(iii) The quantitative representation of bubble rise velocity by equation 1.12 and of wake volume fraction by equation 1.13.

Modifications to remedy these shortcomings are proposed below.

In view of the controversy about the solids content of the wake, the wake model is rederived here for a wake solids content ranging from zero to the value prevailing in the particulate phase, in order to establish its effect on the bed characteristics. Figure 2.3 demonstrates the model schematically.

Consider the distribution of liquid between the wake phase, k, and the particulate phase, f. Let us assume that

$$\text{Volume of liquid in wake phase} = \Omega_{lk} \tag{2.65}$$

$$\text{Volume of liquid in particulate phase} = \Omega_{lf} \tag{2.66}$$

so that the total volume of liquid in the three-phase fluidized bed is given by

$$\Omega_l = \Omega_{lk} + \Omega_{lf} \tag{2.67}$$

and the average volumetric fraction of liquid in the three-phase fluidized bed is

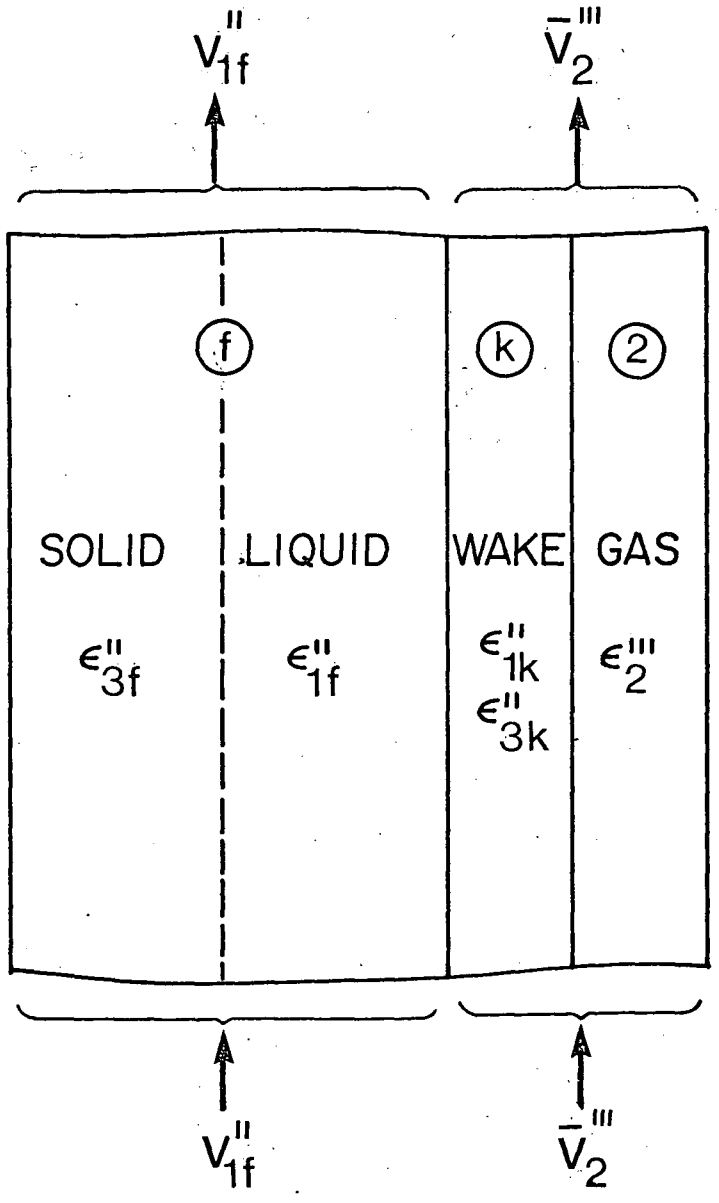

FIGURE 2.3 SCHEMATIC REPRESENTATION OF THE WAKE MODEL

$$\varepsilon_l = \Omega_l / AL_b \tag{2.68}$$

Let us now define the average volumetric fraction of wake liquid in the bed as

$$\varepsilon_{lk} = \frac{\Omega_{lk}}{AL_b} \tag{2.69}$$

and the average volumetric fraction of particulate phase liquid as

$$\varepsilon_{lf} = \frac{\Omega_{lf}}{AL_b} \tag{2.70}$$

Then it can easily be seen that

$$\varepsilon_l = \varepsilon_{lk} + \varepsilon_{lf} \tag{2.71}$$

Similarly let us consider the distribution of solids between the wake phase, k, and the particulate phase, f. Let us assume that W_k is the weight of solid particles in the wake phase and W_f the weight of solid particles in the particulate phase. Then the total weight of solid particles is given by

$$W = W_f + W_k \tag{2.72}$$

and the average volumetric fraction of solids in the three-phase fluidized bed is

$$\varepsilon_3 = W/\rho_3 \, AL_b \tag{2.64}$$

Let us define the average volumetric fraction of wake solids in the bed as

$$\varepsilon_{3k} = \frac{W_k}{\rho_3 \, AL_b} \tag{2.73}$$

and the average volumetric fraction of particulate phase solids as

$$\varepsilon_{3f} = \frac{W_f}{\rho_3 \, AL_b} \tag{2.74}$$

It can easily be seen that

$$\varepsilon_3 = \varepsilon_{3f} + \varepsilon_{3k} \tag{2.75}$$

Since all the gas passes through the bed as discrete bubbles, the average volumetric fraction of gas in the three-phase fluidized bed, ε_2, is indivisible. Then by material balance,

$$\varepsilon_1 + \varepsilon_2 + \varepsilon_3 = 1 \tag{2.76}$$

Combining equations 2.71, 2.75 and 2.76 we get

$$\varepsilon_{1k} + \varepsilon_{1f} + \varepsilon_2 + \varepsilon_{3k} + \varepsilon_{3f} = 1 \qquad (2.77)$$

Now the total volume occupied by the wake phase

= volume of solids in wake phase + volume of liguid in wake phase

$$= \frac{W_k}{\rho_3} + \Omega_{1k} = AL_b\,(\varepsilon_{3k} + \varepsilon_{1k})$$

and the average volumetric fraction of the wake phase in the three- phase fluidized bed, ε_k (= volume of wakes/bed volume), is therefore given by

$$\varepsilon_k = \varepsilon_{1k} + \varepsilon_{3k} \qquad (2.78)$$

Combining equations 2.77 and 2.78, and rearranging, we get

$$\varepsilon_{1f} + \varepsilon_{3f} = 1 - \varepsilon_2 - \varepsilon_k \qquad (2.79)$$

or

$$\frac{\varepsilon_{1f}}{1-\varepsilon_2-\varepsilon_k} + \frac{\varepsilon_{3f}}{1-\varepsilon_2-\varepsilon_k} = 1 \qquad (2.80)$$

In order to establish a relationship between the particulate (or liquid-solid fluidized bed) region and the liquid-solid wake region, let us first consider the particu-

late region. Let us define the average volumetric fraction of solids in this region, ε''_{3f}, as volume of solids in particulate phase/volume of particulate phase or

$$\varepsilon''_{3f} = \frac{W_f/\rho_3}{W_f/\rho_3 + \Omega_{1f}}$$

Dividing both numerator and denominator by the volume of the three-phase fluidized bed we get

$$\varepsilon''_{3f} = \frac{(W_f/\rho_3 AL_b)}{(N_f/\rho_3 AL_b) + (\Omega_{1f}/AL_b)} = \frac{\varepsilon_{3f}}{\varepsilon_{3f} + \varepsilon_{1f}} \qquad (2.81)$$

substituting equation 2.79 into equation 2.81 yields

$$\varepsilon''_{3f} = \frac{\varepsilon_{3f}}{(1-\varepsilon_2-\varepsilon_k)} \qquad (2.82)$$

Similarly it can be shown that the average volumetric fraction of liquid in the particulate phase is

$$\varepsilon''_{1f} = \frac{\varepsilon_{1f}}{(1-\varepsilon_2-\varepsilon_k)} \qquad (2.83)$$

Then from equations 2.80, 2.82 and 2.83, we can obtain that

$$\varepsilon''_{1f} + \varepsilon''_{3f} = 1 \qquad (2.84)$$

which also follows from the definitions of ε''_{1f} and ε''_{3f}.

For the liquid-solid wake region let us define the average volumetric fraction of solids in the wake as volume of solids in wake/total volume of wake or

$$\varepsilon''_{3k} = \frac{W_k/\rho_3}{W_k/\rho_3 + \Omega_{1k}}$$

Dividing both numerator and denominator by the volume of the three-phase fluidized bed we get

$$\varepsilon''_{3k} = \frac{W_k/\rho_3 AL_b}{(W_k/\rho_3 AL_b) + (\Omega_{1k}/AL_b)} = \frac{\varepsilon_{3k}}{\varepsilon_{1k} + \varepsilon_{3k}} \qquad (2.85)$$

Substituting equation 2.78 into equation 2.85 yields

$$\varepsilon''_{3k} = \frac{\varepsilon_{3k}}{\varepsilon_k} \qquad (2.86)$$

Similarly it can be shown that the average volumetric fraction of liquid in the wake is

$$\varepsilon''_{1k} = \frac{\varepsilon_{1k}}{\varepsilon_k} \qquad (2.87)$$

Then from equations 2.78, 2.86 and 2.87, we can obtain that

$$\varepsilon''_{1k} + \varepsilon''_{3k} = 1 \qquad (2.88)$$

which also follows from the definitions of ε''_{1k} and ε''_{3k}.

Now since the amount of solids in the wake of a bubble is not known a priori, it has been expedient to assume that ε''_{3k} is related to ε''_{3f} via

$$\varepsilon''_{3k} = x_k \varepsilon''_{3f} \tag{2.89}$$

where x_k is a coefficient of proportionality which can take any positive value between zero and unity. Then the case of $x_k = 0$ signifies that there are no solid particles in the wake (as observed by Stewart and Davidson), whereas the case of $x_k = 1$ signifies that the solids fraction in the wake is the same as that in the particulate phase (as postulated by Østergaard). It can easily be seen that

$$\varepsilon''_{1k} = 1-x_k\varepsilon''_{3f} = 1-x_k+x_k\varepsilon''_{1f} \tag{2.90}$$

and therefore the total bed voidage in a three-phase fluidized bed, from equations 2.71, 2.83, 2.87 and 2.90, is

$$\varepsilon = (1-\varepsilon_3) = \varepsilon_2 + \varepsilon_k(1-x_k) + \varepsilon''_{1f}(x_k\varepsilon_k + 1 - \varepsilon_2 - \varepsilon_k) \tag{2.91}$$

In order to find the velocity of liquid through the particulate phase, let us assume that the total volumetric flow rate of liquid through the column is Q_1 and the total

volumetric flow rate of gas through the column is Q_2. Then the average liquid flux through the column is

$$\langle j_1 \rangle = Q_1/A \tag{2.92}$$

and the average gas flux through the column is

$$\langle j_2 \rangle = Q_2/A \tag{2.93}$$

Now, since all the gas through the column travels as discrete bubbles, a simple material balance over any cross-section perpendicular to the flow path will give

$$\langle j_2 \rangle = \varepsilon_2 \bar{v}_2 \tag{2.94}$$

Let us now consider a similar material balance for the liquid over a cross-section perpendicular to the flow path. Then

$$\begin{bmatrix}\text{volumetric flow rate of liquid through the column}\end{bmatrix} = \left[\begin{pmatrix}\text{liquid flux through the particulate phase}\end{pmatrix} \times \begin{pmatrix}\text{cross-sectional area occupied by the particulate phase}\end{pmatrix}\right] + \left[\begin{pmatrix}\text{liquid flux through the wake phase}\end{pmatrix} \times \begin{pmatrix}\text{cross-sectional area occupied by the wake phase}\end{pmatrix}\right]$$

or

$$\langle j_1 \rangle A = [j_1'' A (1-\varepsilon_2-\varepsilon_k)]+[(\bar{v}_2 \varepsilon_{1k}'')(A \varepsilon_k)] \tag{2.95}$$

Substituting equation 2.90 into equation 2.95 and rearranging gives

$$j_1'' = \frac{\langle j_1 \rangle - \bar{v}_2 \, (1 - x_k + x_k \varepsilon_{1f}'') \, \varepsilon_k}{(1 - \varepsilon_2 - \varepsilon_k)} \tag{2.96}$$

The liquid flux through the particulate phase can be related to the average volumetric fraction of liquid in the particulate phase, ε_{1f}'', by the Richardson - Zaki correlation,

$$\varepsilon_{1f}'' = (j_1''/V_\infty)^{1/n} \tag{2.97}$$

where $n = f(Re_p)$ and the values of n for various Re_p are given by equations 2.47 to 2.50. Thus for a distribution of solid particles between the wake phase and the particulate phase as given by equation 2.89, equations 1.4 and 1.10 derived earlier for Østergaard's model have been modified to equations 2.91 and 2.96, respectively.

Another deficiency of the wake model, as postulated by Østergaard [8] and used subsequently by Efremov and Vakhrushev [16] as well as Rigby and Capes [80], has been the neglect of solids circulation in the particulate phase. Although the existence of solids circulation was not reported by these authors, the bubbles rising in a three-phase fluidized bed have been observed to carry sizeable wakes containing some particles. A simple consideration of continuity would then suggest a downward motion of solid particles in the

particulate phase as a result of their upward motion in the wakes of the bubbles. Based on this simple mechanism for solids circulation in a three-phase fluidized bed, a model will now be developed for it.

Let us assume that each bubble in a three-phase fluidized bed carries with it an attached wake containing solid particles. Then the rate at which solids reach the surface of the three-phase fluidized bed

$$= \begin{bmatrix}\text{Solids flux}\\ \text{through}\\ \text{wake}\end{bmatrix} \quad x \quad \begin{bmatrix}\text{cross-sectional area}\\ \text{occupied by wake}\\ \text{phase}\end{bmatrix}$$

or

$$\begin{bmatrix}\text{volumetric flow rate}\\ \text{of solids to bed}\\ \text{surface}\end{bmatrix} = \left[\bar{v}_2 \; \varepsilon''_{3k}\right] \; x \; \left[A\varepsilon_k\right] \qquad (2.98)$$

After a bubble emerges from the bed, solids carried in its wake will be washed out of it by continuous exchange with the surrounding liquid [80]. The distance for which the solids will be carried above the bed would then depend on the exchange rate between the surrounding liquid phase and the wake phase. The solid particles, after leaving the wake, would move downwards to the bed and downwards in the bed to compensate for the upward movement in the wake. Therefore the downward flow rate of solid particles in the par-

ticulate phase

$$= \begin{bmatrix} \text{Solids flux through} \\ \text{particulate phase} \end{bmatrix} \times \begin{bmatrix} \text{cross-sectional area} \\ \text{occupied by particulate} \\ \text{phase} \end{bmatrix}$$

$$= [-\bar{v}_3'' \quad \varepsilon_{3f}''] \quad \times \quad [A(1-\varepsilon_2-\varepsilon_k)] \tag{2.99}$$

Since there is no net flow of solid particles through the bed, the upward flow of solids in the wake must exactly equal the downward flow of solids in the particulate phase. Hence, equating equations 2.98 and 2.99 and rearranging, the linear velocity of solid particles in the particulate phase is given by

$$\bar{v}_3'' = - \frac{\bar{v}_2 \, \varepsilon_k \, \varepsilon_{3k}''}{\varepsilon_{3f}'' \, (1-\varepsilon_2-\varepsilon_k)} \tag{2.100}$$

and in combination with equation 2.89,

$$\bar{v}_3'' = - \frac{\bar{v}_2 \, \varepsilon_k \, x_k}{(1-\varepsilon_2-\varepsilon_k)} \tag{2.101}$$

From equation 2.101 it can be seen that if there are no solid particles in the wake ($x_k = 0$), the circulating velocity of solid particles in the fluidized bed is zero. Thus no circulation would exist by the mechanism postulated here.

The presence of other more complex modes of circulation is recommended for further investigations. For the present it will be assumed that equation 2.101 describes the solids circulation phenomenon adequately for $x_k > 0$.

As has been stated earlier in section 2.2, the relative velocity between the liquid and the solid particles controls the bed expansion [67]. The Richardson - Zaki correlation, equation 2.97, can be modified and represented in terms of the relative velocity:

$$\varepsilon''_{1f} = \left(\frac{\bar{v}''_{13}}{v_\infty} \right)^{1/(n-1)} \tag{2.102}$$

The liquid flux through the particulate phase is given by equation 2.96. Therefore the linear velocity of liquid through the particulate phase will be

$$\bar{v}''_1 = \frac{j''_1}{\varepsilon''_{1f}} = \frac{\langle j_1 \rangle - \bar{v}_2 (1 - x_k + \varepsilon''_{1f} x_k) \varepsilon_k}{\varepsilon''_{1f} (1 - \varepsilon_2 - \varepsilon_k)} \tag{2.103}$$

and the relative velocity between the liquid and the solid particles in the particulate phase will be

$$\bar{v}''_{13} = \bar{v}''_1 - \bar{v}''_3 = \frac{\langle j_1 \rangle - \bar{v}_2 (1 - x_k + \varepsilon''_{1f} x_k) \varepsilon_k}{\varepsilon''_{1f} (1 - \varepsilon_2 - \varepsilon_k)} + \frac{\bar{v}_2 \varepsilon_k x_k}{(1 - \varepsilon_2 - \varepsilon_k)} \tag{2.104}$$

By simplifying equation 2.104 we get

$$\bar{v}''_{13} = \frac{\langle j_1 \rangle - \bar{v}_2(1-x_k)\varepsilon_k}{\varepsilon''_{1f}\,(1-\varepsilon_2-\varepsilon_k)} \tag{2.105}$$

Then the volume fraction of liquid in the particulate phase, ε''_{1f}, will be given by the modified Richardson - Zaki correlation, equation 2.102, which when combined with equation 2.105 reduces to

$$\varepsilon''_{1f} = \left(\frac{\bar{v}''_{13}}{V_\infty}\right)^{\frac{1}{(n-1)}} = \left[\frac{\langle j_1 \rangle - \bar{v}_2(1-x_k)\varepsilon_k}{(1-\varepsilon_2-\varepsilon_k)\;V_\infty}\right]^{1/n} \tag{2.106}$$

Thus, in the presence of solids circulation in a three-phase fluidized bed, equations 2.97 and 2.96 are modified and replaced by equation 2.106 to predict the average volumetric fraction of liquid in the particulate phase, ε''_{1f}. The average volumetric fraction of gas, ε_2, and the total voidage, ε, in the bed are still given by equations 2.94 and 2.91 respectively.

In order to complete the model, independent relationships for the rise velocity of a bubble swarm and the volume fraction occupied by the wakes in a three-phase fluidized

bed have to be developed. For dispersed phase operations, Lapidus and Elgin [67] have demonstrated that the relative velocity between the phases determines the holdup of either phase. Thus if we postulate that the relative velocity between the gas and the liquid in a three-phase fluidized bed can be predicted by the same correlations as for two-phase gas-liquid flow, the problem then reduces to correctly formulating the relative velocity in two-phase gas-liquid flow, several competing models having been proposed (section 2.1.2). Towell et al. [59] have suggested rather arbitrarily that the relative velocity between the gas and the liquid in large diameter ($\geq$ 4 inch) columns, where systematic circulation of liquid is predominant, is given by

$$\bar{v}''_{21} = v_\infty + 2 \langle j_2 \rangle \qquad (2.107)$$

This empirical correlation was tested and confirmed by Reith et al. [68] for large diameter columns. However, for small diameter columns (< 4 in), in the absence of systematic liquid circulation, the relative velocity for the bubble flow regime can be obtained by combining equations 2.32 and 2.37 to give

$$\bar{v}''_{21} = \frac{v_\infty \sqrt{\tanh\left[0.25(1/\varepsilon''_2)^{1/3}\right]}}{\varepsilon''_1} \qquad (2.108)$$

It has been shown [76] that the model presented in section 2.1.2 satisfactorily represents a wide variety of data for bubble columns and for cocurrent gas-liquid flow. Equation 2.108, which is based on this model, is therefore recommended for predicting the relative velocity between gas and liquid in small columns (< 4 inch). In the absence of adequate understanding of the circulation phenomenon prevailing in larger columns, the description of bubble motion in such columns is incomplete and therefore modelling attempts have not been successful. Nevertheless, the empirical correlation developed by Towell et al. [59], equation 2.107, has been confirmed for large columns [68] and is therefore recommended.

The relative velocity in three-phase fluidization is defined as the difference in linear velocities between the gas and the liquid and is given by

$$\bar{v}_{21}''' = \bar{v}_2 - \bar{v}_1 = \frac{\langle j_2 \rangle}{\varepsilon_2} - \frac{j_1''}{\varepsilon_{1f}''} \qquad (2.109)$$

Substituting the value of j_1'' from equation 2.96 into equation 2.109 we get

$$\bar{v}_{21}''' = \frac{\langle j_2 \rangle}{\varepsilon_2} - \frac{\langle j_1 \rangle - \frac{\langle j_2 \rangle}{\varepsilon_2}\varepsilon_k(1-x_k+x_k\varepsilon_{1f}'')}{\varepsilon_{1f}''(1-\varepsilon_2-\varepsilon_k)} \qquad (2.110)$$

which after substitutions and rearrangements simplifies to

$$v''_{21} = \frac{\langle j_2\rangle \varepsilon_1 - \langle j_1\rangle \varepsilon_2}{\varepsilon_2\ \varepsilon''_{1f}(1-\varepsilon_2-\varepsilon_k)} \tag{2.111}$$

Substituting the value of ε_1 from equation 2.76 into equation 2.111 and rearranging gives

$$\frac{\langle j_2\rangle}{\varepsilon_2} = \frac{\langle j_1\rangle + \langle j_2\rangle}{(1-\varepsilon_3)} + \frac{\varepsilon''_{1f}\ (1-\varepsilon_2-\varepsilon_k)}{(1-\varepsilon_3)}\ \bar{v}'''_{21} \tag{2.112}$$

Bhaga [1], by a method very similar to the one employed by Zuber and Findlay [39] for gas-liquid flow, obtained for one-dimensional simultaneous flow of gas, liquid and solid in a vertical conduit

$$\frac{\langle(1-\alpha_3)j_2\rangle}{\langle\alpha_2\rangle} = C'''_o \langle j_1+j_2\rangle + \frac{\langle\alpha_1\alpha_2\ v_{21}\rangle}{\langle\alpha_2\rangle} \tag{2.113}$$

where C'''_o is the distribution parameter for cocurrent gas-liquid-solid flow and is given by

$$C'''_o = \frac{\langle\alpha_2(j_1+j_2)\rangle}{\langle\alpha_2\rangle\langle j_1+j_2\rangle} \tag{2.27d}$$

Comparing equation 2.113 with equation 2.26 it can be seen that the distribution parameter, C'''_o, represents the effect of radial distribution of both volumetric flux of the mixture

and in situ volume fraction of the gas (i.e. gas holdup) on the rise velocity of a bubble swarm. As was observed for gas-liquid flow, a value of C_o greater than unity indicates that neither the gas holdup nor the volumetric flux of the gas-liquid stream are constant over the cross-section. Therefore, for a three-phase fluidized bed, if both the gas holdup and the volumetric flux of the gas-liquid stream vary radially at a given vertical level in the bed, then equation 2.112 should be modified to include the distribution parameter, C_o'''. Thus

$$\frac{\langle j_2 \rangle}{\varepsilon_2} = \frac{C_o'''(\langle j_1 \rangle + \langle j_2 \rangle)}{(1-\varepsilon_3)} + \frac{\varepsilon_{1f}''' (1-\varepsilon_2-\varepsilon_k)}{(1-\varepsilon_3)} \bar{v}_{21}''' \qquad (2.114)$$

Since it has been assumed that the relative velocity in three-phase fluidization, $\bar{v}_{21}'''$, can be represented by the correlations developed for two-phase gas-liquid flow, v_{21}''' can be obtained from equation 2.107 for large diameter columns ($\geq$ 4 inch) and from equation 2.108 for small diameter columns ($<$ 4 inch). Both these correlations require a knowledge of V_∞, which can be estimated from the average diameter of bubbles in the swarm.

Since the structure and size of wakes behind gas bubbles has not been investigated systematically in either two-phase gas-liquid flow or three-phase fluidization, it is difficult

to develop a realistic model for the volume fraction of wakes in a three-phase fluidized bed. Letan and Kehat [36] have presented a limited set of data for the volume fraction of wake at various values of the dispersed phase holdup in a liquid-liquid system. In the absence of gas-liquid data, the Letan - Kehat results will be used in this thesis on the assumption that the wake behind a gas bubble has similar characteristics to the wake behind a liquid drop. To justify this assumption, a tentative model is suggested based on the wake structure postulated by de Nevers and Wu [61]. From the visual observation of large air bubbles ($d_e \simeq$ 1-2 cm), which were essentially hemispherical in shape, rising in either glycerine or water, these investigators inferred that the bubbles were each followed by a conical wake whose influence extended to a distance l_k behind the bubble. Thus, if the trailing bubble followed at a distance greater than l_k it would not be affected by the wake of the leading bubble. On the basis of such a structure for the bubble and the wake, de Nevers and Wu found that a dimensionless distance, l_k/R_s, of seven satisfied their data for bubbles rising and coalescencing in both the air-water and air-glycerine systems.

If we visualize a similar structure for the rise of a non-coalescing swarm of bubbles, we can therefore estimate that the vertical distance between any two bubbles in the swarm should be at least $(l_k + R_s)$. Then the volume of the

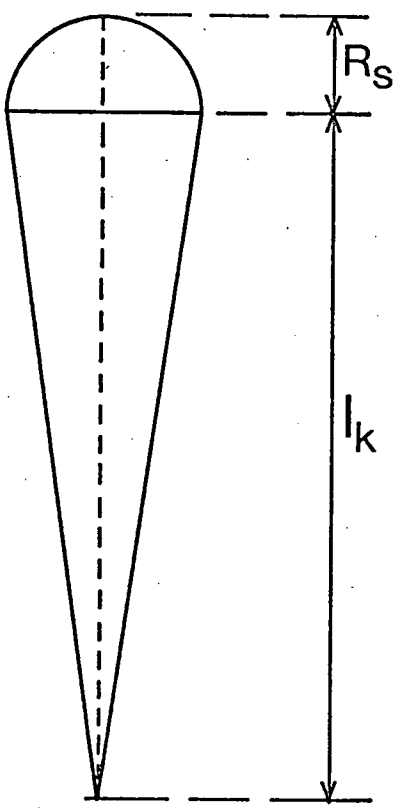

FIGURE 2.4 SCHEMATIC OF WAKE STRUCTURE SUGGESTED BY dE NEVERS AND WU [61]

wake as compared to the volume of the bubble is given by

$$\frac{\Omega_k}{\Omega_B} = \frac{1/3\pi R_s^2 l_k}{2/3\pi R_s^3} = \frac{l_k}{2R_s} \tag{2.115}$$

For a liquid-liquid system, both Letan and Kehat [36] and Hendrix et al. [99] have shown that the wake size is markedly affected by the presence of other drops. The effect of gas volume fraction on the wake size can be estimated if it is assumed for computational purposes that:

(a) the bubbles have an orderly distribution in the swarm, and

(b) the wake length is equal to the vertical distance between the bubbles, so that the wake of the leading bubble would just fall short of affecting the rise velocity of the trailing bubble.

Now, if we assume a simple cubic distribution for the bubbles in the swarm, with $(l_k + R_s)$ as the characteristic length of the cell, it can easily be shown that the ratio of wake size to bubble size is given by

$$\frac{\Omega_k}{\Omega_B} = \frac{1}{2}\left[\left(\frac{2}{3}\frac{\pi}{\varepsilon_2}\right)^{1/3} - 1\right] \tag{2.116}$$

In Table 2.1 are presented values of wake to bubble volume ratio for a cubic and two other systematic bubble distributions, as well as the values recommended by Letan and

TABLE 2.1

RATIO OF WAKE TO BUBBLE VOLUME FOR VARIOUS VALUES OF DISPERSED PHASE HOLDUP IN TWO-PHASE FLUID SYSTEMS

Dispersed phase holdup, ε_2	Ω_k/Ω_B (1)	Ω_k/Ω_B (2)	Ω_k/Ω_B (3)	Ω_k/Ω_B (*)
0.1	0.878	0.946	1.047	0.93
0.15	0.704	0.763	0.852	0.83
0.2	0.594	0.648	0.728	0.83
0.25	0.516	0.565	0.640	0.83
0.3	0.456	0.503	0.573	0.83
0.35	0.408	0.452	0.519	0.83
0.4	0.368	0.411	0.475	0.83
0.45	0.335	0.376	0.437	0.83
0.5	0.306	0.346	0.405	0.77
0.6	0.259	0.296	0.351	0.61

(1) Cubic Cell - $\Omega_k/\Omega_B = 1/2 \left[\left(\frac{2\pi}{3\varepsilon_2}\right)^{1/3} - 1\right]$

(2) Orthorhombic Cell - $\Omega_k/\Omega_B = 1/2 \left[\left(\frac{4\pi}{3\sqrt{3}\,\varepsilon_2}\right)^{1/3} - 1\right]$

(3) Rhombohedral Cell - $\Omega_k/\Omega_B = 1/2 \left[\left(\frac{2\pi\sqrt{2}}{3\varepsilon_2}\right)^{1/3} - 1\right]$

(*) From Figure 6 of Letan and Kehat [36]

Continuous phase: distilled water

Dispersed phase: kerosene

Kehat [36] for wakes behind liquid drops. As can be seen from Table 2.1, the model improvised here for estimation of the volume fraction of wakes in gas-liquid systems, though undoubtedly oversimplified, are matched by the trend of the liquid-liquid data closely enough to justify the use of these data for gas-liquid systems as a first approximation. A more complicated model based on the exponential wake structure recommended by de Nevers and Wu [61] and by Crabtree and Bridgwater [78] can be developed similarly, but lack of detailed data for wake sizes in gas-liquid systems does not warrant such complicated models at this stage.

The presence of solid particles in three-phase fluidization would affect the wake size, as inferred by Østergaard [8] and clearly demonstrated by Rigby and Capes [80] and by Efremov and Vakhrushev [16]. Thus, following the latter's recommendations, it is postulated that the volume fraction of wakes in three-phase fluidization will be represented by

$$(\Omega_k/\Omega_B)''' = (\Omega_k/\Omega_B)'' \; f(\varepsilon) \qquad (2.117)$$

The exact form of the function f can only be developed from experimentally observed values of wake sizes in two-phase gas-liquid flow and in three-phase fluidization.

Thus the model proposed here is similar in principle to the wake model proposed by Østergaard, the main difference

being the inclusion of solids circulation and its effect on bed expansion in the former. A possible mechanism for solids circulation, based on the rise of solid particles in the wake of rising bubbles, is suggested, along with relationships for both the rise velocity of a bubble swarm and the volume fraction of wakes in a three-phase fluidized bed.

(C) The cell model

As stated earlier, the cell model technique has been successfully used to describe various dispersed phase operations [49,90,86]. This technique consists of representing an assemblage of particles by a spherical (or sometimes a cylindrical) cell containing a single particle and liquid in such a proportion that the voidage in the cell is equal to the voidage of the entire assemblage. The Navier-Stokes equations of motion are then solved for the closed cell, with adequate and consistent boundary conditions, to obtain the relative velocity of the particle with respect to the liquid in the cell.

The proposed cell model for three-phase fluidization consists of representing a bubble and a solid particle individually by two separate spherical cells. Smith [91] used such a model to analyse the rate of sedimentation of particles of two different species. In order to form a consistent set, Smith matched the two spherical cells each

representing an individual species, by using the boundary conditions of (a) equal tangential velocities at the equator of both envelopes and (b) equal pressure gradients at all surfaces of both envelopes. The proposed model, which is presented in its entirety in Appendix 8.1, uses similar but slightly modified boundary conditions to match the two spherical cells viz. (a) equality of tangential velocities at the equatorial surface of both envelopes and (b) equality of drag per unit volume in each cell such that the overall pressure gradient ($-\Delta p/L$) is the same for both the cells and throughout the bed.

The solution obtained for the cell model, using the creeping flow equations with the above boundary conditions to match the two spherical cells, and Happel's [49] boundary conditions for each individual cell (it is realized that these may not be the unique set of boundary conditions) shows the liquid-solid fluidized bed to expand smoothly on introduction of gas. Since the wake behind a gas bubble is non-existent in creeping flow, this result is not surprising because, as explained by Østergaard [8] and by Stewart and Davidson [7], it is the wake behind the gas bubble that is responsible for the observed contraction in three-phase fluidization. It is therefore recommended that the full Navier-Stokes equations be solved by existing numerical techniques [82, 90], for a critical evaluation of the proposed cell model.

2.3.2 Gas holdup in three-phase fluidized beds

The behaviour of bubbles in a three-phase fluidized bed has been the subject of limited study [15,79], although many investigators [14,18,100] have observed that in well expanded beds of small solid particles bubble coalescence predominates, whereas in slightly expanded (close to packed bed voidage) beds of large particles bubble breakup generally occurs. A number of attempts [14,16,17,79] have been made to study the gas holdup in three-phase fluidization, but as yet no realistic model has been formulated to incorporate the qualitative observations and to point out the areas required for further study, in order to complete the understanding of gas bubble behaviour. Nevertheless, empirical correlations have been suggested by various investigators. Thus Vail et al. [17], who measured the gas holdup in a 146 mm diameter column by quickly shutting off the gas and liquid flow rates simultaneously, thus isolating the experimental section, recommended the following correlation for a bed of 0.77 mm glass beads fluidized by air and water:

$$\varepsilon_2''' = 0.1026\ (1-\varepsilon_3)^{2.09} (\langle j_2\rangle/\langle j_1\rangle)^{0.78} \qquad (2.118)^*$$

for $1.5 < \langle j_1 \rangle < 9.0,\ 4.0 < \langle j_2 \rangle < 20$

---

*The exponents 2.09 and 0.78 were erroneously interchanged in the original paper [17].

They further suggested that when $\varepsilon_3=0$, the above correlation satisfactorily predicted the gas holdup in two-phase gas-liquid flow. Therefore

$$\varepsilon_2'' = 0.1026 \left(\langle j_2\rangle/\langle j_1\rangle\right)^{0.78} \tag{2.119}$$

and combining the above two equations we see that

$$\varepsilon_2''' = \varepsilon_2'' (1 - \varepsilon_3)^{2.09} \tag{2.120}$$

Equation 2.120 thus shows the importance of bed expansion, which had been implied by other investigators but not formulated logically. However, equation 2.120 is only an empirical correlation and cannot be extrapolated beyond the range of its supporting data without the risk of serious error.

Michelsen and Østergaard [14] measured gas holdups by measuring the static pressure drop across the length of the bed and also by employing a tracer injection technique. They proposed the following correlation for a bed of 1 mm glass beads fluidized by air and water in a 216 mm diameter column:

$$\varepsilon_2''' = 0.011 \langle j_1\rangle^{0.37} \langle j_2\rangle^{0.78} \tag{2.121}$$

for $2 < \langle j_1 < 7.5$ and $0.35 < \langle j_2 < 2.2$

and for two-phase gas-liquid flow of the air-water system,

$$\varepsilon_2'' = 0.0394 \langle j_1 \rangle^{-0.16} \langle j_2 \rangle^{1.05} \qquad (2.122)$$

for $0.7 < \langle j_1 < 17.0$ and $0.35 < \langle j_2 < 2.2$

The format of equation 2.121 contributes little to the understanding of bubble behaviour in three-phase fluidized beds, but the equation itself is found to be in quantitative agreement with equation 2.118 within the limits of applicability of equation 2.121.

Capes et al. [79] studied the local properties of gas bubbles in three-phase (air-water-glass beads) fluidized beds by locating two electro-resistivity probes, separated vertically by a short distance, inside the bed. The measured bubble rise velocities were correlated with the measured voidage in the bed and the average length, l, of bubbles in the swarm, by means of the following relationship:

$$\bar{v}_2 - (\langle j_1 + j_2 \rangle) = 32.5\, l^{1.53} \left(\frac{\varepsilon}{1-\varepsilon}\right)^2 \qquad (2.123)$$

for $0.03 < \langle j_1 < 2.61$ and $0.5 < \langle j_2 < 2.0$

They also suggested that if a spherical cap bubble with a flat base is assumed to have an included wake angle of 135°, then the average length and the equivalent radius of the

bubble can be correlated by

$$l = 1.14\ r_e \qquad (2.124)$$

It has been found, however, by the present author that for an included wake angle of 135° the above relationship is incorrect and should read

$$l = 1.02\ r_e \qquad (2.125)$$

while only for an included wake angle of 158° does equation 2.124 give the correct relationship between l and r_e.

Equation 2.123 in combination with equation 2.125 shows the influence of bubble diameter and the important effect of bed voidage on bubble velocity. Equation 2.123 is found to be in quantitative agreement with equation 2.118 on assuming a realistic bubble diameter, no measurements of bubble diameter having been reported by Vail et al. Thus all these empirical correlations are quantitatively compatible and demonstrate the importance of bed voidage and average bubble diameter in determining the rise velocity of a bubble swarm, and thereby also the gas holdup, in three-phase fluidization.

From the generalized wake model for a three-phase fluidized bed, presented in section 2.3.1, the rise velocity of bubbles is given by

$$\bar{v}_2 = \frac{C_o''' \langle j_1+j_2 \rangle}{\varepsilon} + \frac{\varepsilon_{1f}'' (1-\varepsilon_2-\varepsilon_k)}{\varepsilon} \bar{v}_{21}''' \qquad (2.114)$$

where

$$\bar{v}_{21}''' = (V_\infty)_B + 2 \langle j_2 \rangle \qquad (2.107)$$

for $D \geq 4$ inch and

$$\bar{v}_{21}''' = \frac{(V_\infty)_B \sqrt{\tanh [0.25 (1/\varepsilon_2''')^{1/3}]}}{\varepsilon_1'''} = \frac{v_{2j}}{\varepsilon_1'''} \qquad (2.108)$$

for $D < 4$ inch, where $(V_\infty)_B$ is the rise velocity of a single bubble in a three-phase fluidized bed and depends mainly on the average bubble diameter. The gas holdup is then obtained from

$$\varepsilon_2 = \langle j_2 \rangle / \bar{v}_2 \qquad (2.94)$$

Thus equation 2.114 in combination with equation 2.108 (or equation 2.107) and equation 2.94 provides a general model for describing the gas bubble behaviour in three-phase fluidized beds. Qualitatively this model is better than any of the empirical correlations, as it not only takes into account the effect of bed voidage and bubble diameter on the rise velocity of bubbles, but also illustrates the necessity of investigating the radial profiles of gas holdup and gas-liquid flux through the bed (to determine the distribution

parameter C_o''') and the phenomenon of wake formation (to determine ε_k), in order to better the understanding of gas bubble behaviour in three-phase fluidization.

2.3.3 Voidage in three-phase fluidized beds

The number of independent models postulated for overall voidage $(1-\varepsilon_3)$ in three-phase fluidized beds is limited. Østergaard [8] derived a wake model, which has subsequently been used and modified by various investigators without significantly enhancing the understanding of bed expansion behaviour in three-phase fluidization. Thus Efremov and Vakhrushev [16], who used the wake model on the assumption that no particles are present in the wake [7], postulated that the bed voidage is given by

$$\varepsilon = \frac{\langle j_1 \rangle - (\Omega_k/\Omega_B)\ \langle j_2 \rangle}{V_\infty} (1-\varepsilon_2-\varepsilon_k)^{1-n'} + \varepsilon_2 + \varepsilon_k \qquad (2.126)$$

where

$$\varepsilon_k = \varepsilon_2 \left(\frac{\Omega_k}{\Omega_B}\right) \qquad (2.127)$$

and n' $(=Re^{0.1}/4.45)$ is the improvised Richardson - Zaki exponent evaluated by using the Reynolds number, Re, based on the liquid flux through the particulate phase instead of the free settling Reynolds number, Re_p, as suggested by Richardson and Zaki [2]. The ratio of wake volume to bubble

volume, Ω_k/Ω_B, as determined from the measured values of ε and ε_2 using equations 2.126 and 2.127, was then empirically correlated to fit the observed bed voidage data by the following relation:

$$\Omega_k/\Omega_B = 5.1(\varepsilon_1'')^{4.85}[1 - \tanh\{40 \frac{\langle j_1 \rangle}{\langle j_2 \rangle} (\varepsilon_1'')^{10} - 3.2(\varepsilon_1'')^{5.45}\}] \quad (2.128)$$

where ε_1'' is the voidage in the liquid-solid fluidized bed before the introduction of the gas.

The other noteworthy attempt to improve the wake model is due to Rigby and Capes [80]. They tested this model to find out the effect of assumed particle content of the wake by considering the two extremes suggested by Stewart and Davidson [7] and Østergaard [8]. They concluded that the presence of particles in the wake had a marked influence on the wake volume, which was also found to be affected by the bed voidage and to a lesser degree by the particle size. No phenomenological equation was presented to correlate the wake volume with various bed parameters.

Other empirical correlations for the voidage in three-phase fluidized beds are either unnecessarily complicated [10] or outrightly misleading [11], and will therefore not be included in further discussions.

From the generalized wake model for three-phase fluidized beds presented in section 2.3.1, the bed voidage is given by

$$\varepsilon = \varepsilon_2 + \varepsilon_k(1-x_k) + \varepsilon''_{lf}(x_k\varepsilon_k + 1 - \varepsilon_2 - \varepsilon_k) \qquad (2.91)$$

where ε''_{lf} is given by equation 2.106. The terms x_k and ε_k are the two quantities for which estimates have to be obtained experimentally, since no reliable information concerning them exist in the three-phase fluidization literature. As has already been pointed out in section 2.3.1, the improvised wake model takes into consideration not only wake formation behind the bubbles and the particle content of the wake, but also particle circulation and its effect on the contraction-expansion characteristics of a three-phase fluidized bed.

CHAPTER 3

EXPERIMENTAL

The main aim of this work was to establish the effect of liquid and solid phase properties on holdups of gas, liquid and solid in a three-phase fluidized bed. The solids holdup, or the volume fraction of solids inside the bed, ε_3, can be directly calculated if the weight of solid particles present in the bed, W, is known and if the expanded bed height, L_b, can be measured. Thus

$$\varepsilon_3 = W/\rho_3 A L_b \qquad (3.1)$$

However, the expanded bed height, L_b, cannot always be measured directly. At low gas flow rates, especially in a bed of large or heavy particles, the upper boundary of the bed is very well defined and can be measured easily by visual observation through transparent column walls. But at large gas flow rates, the upper bed level is not so clearly delineated and it becomes difficult to establish the expanded bed height visually. It is therefore necessary to develop a criterion to define the expanded bed height consistently under all conditions of gas and liquid flow rates. Such a criterion was developed and is discussed in detail in

Appendix 8.2. Thus with the knowledge of W and L_b, ε_3 can be calculated from equation 3.1.

Since

$$\varepsilon_1 + \varepsilon_2 + \varepsilon_3 = 1.0 \qquad (3.2)$$

ε_1 becomes known if the gas holdup inside the bed, ε_2, could be measured. Of the various techniques available for measurement of gas holdup, the following two were chosen for this work:

1. direct volumetric measurements using quick closing valves,
2. the measurement of static pressure drop gradient.

A third technique, that of measuring the local gas fraction by an electro-resistivity probe, was later developed and used in part of the work.

The experimental equipment used was designed to incorporate these techniques for measuring the expanded bed height and gas holdup into this study.

3.1 Apparatus

The three-phase fluidization studies were carried out in two columns: (i) a 20 mm i.d. glass column and (ii) a 2 inch i.d. perspex column. The two experimental set ups are discussed separately in the following sections.

3.1.1 The 20 mm bench top glass column

The design of the 20 mm glass column was based on the apparatus used for liquid-solid fluidization studies by Andersson [56], with suitable modifications for three-phase fluidized bed operation. The overall layout of the equipment is shown schematically in Figure 3.1. The main experimental column consisted of a 660 mm long, 20 mm i.d. glass column with a straight 168 mm long entrance section. A 60 mesh copper screen, S, was push-fitted to separate the calming section D from the experimental section E and also to act as a bed support. Two pressure taps, 49.3 cm apart, were provided with a 6 mm U-tube manometer, M_1, to measure the static pressure drop across the bed.

The test liquid from the feed tank was circulated by a centrifugal pump driven by a 1/15 horsepower motor. A bypass was provided to regulate the flow and a needle valve to control the flow rate to the experimental column. The liquid flow rate was measured by a calibrated rotameter, R_1. The liquid from the experimental column was allowed to overflow into an exit section, X, from which it was returned to the feed tank, thus completing the liquid cycle. The temperature of the liquid was measured by a thermometer, T, and kept close to the room temperature by adding some fresh tap water occasionally. However, when the water glycerol solution was used as the test liquid, an immersion cooler was used to keep the liquid temperature within ± 1°F of the

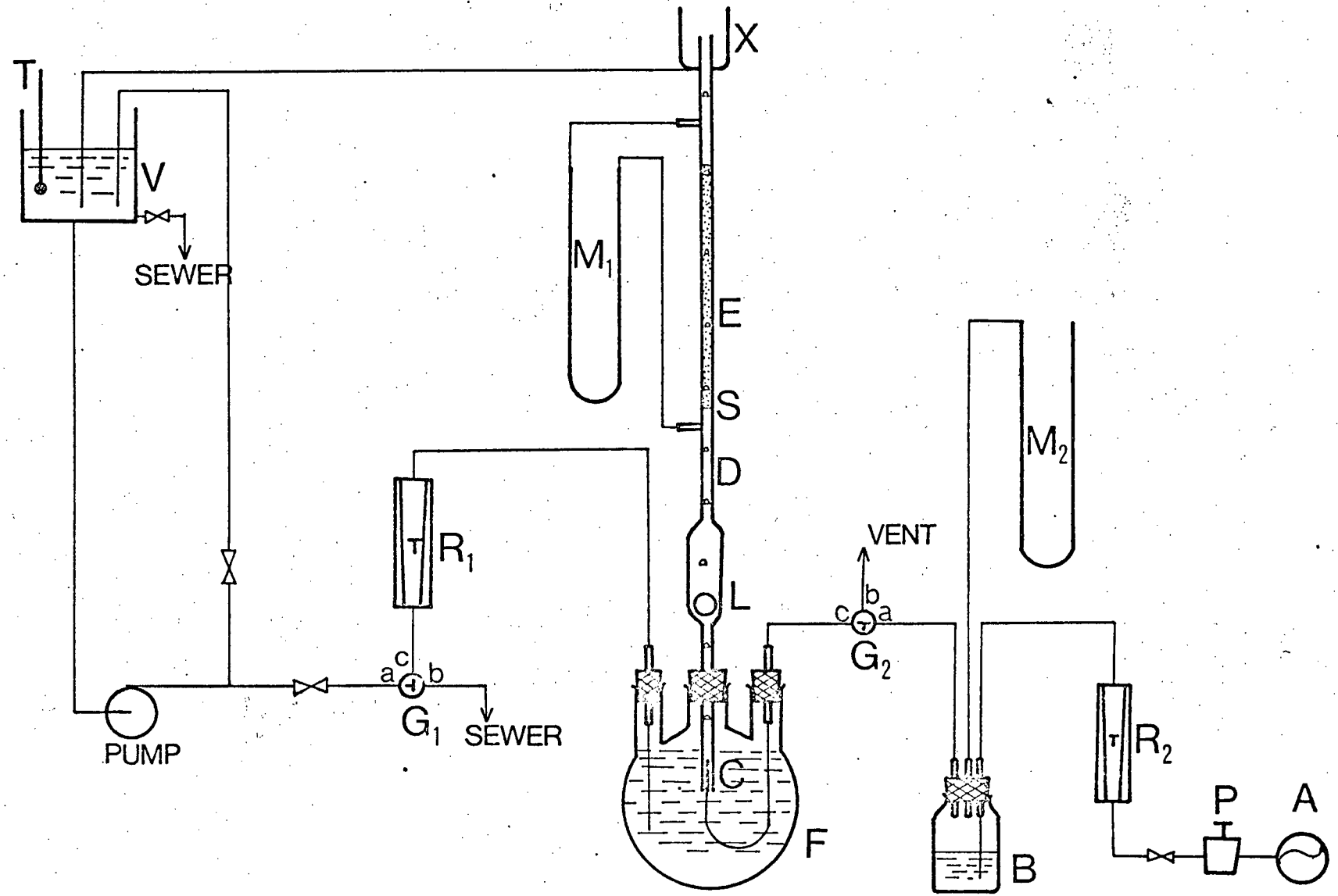

FIGURE 3.1 SCHEMATIC DIAGRAM OF 20 MM GLASS COLUMN APPARATUS

LEGEND FOR FIGURE 3.1

A - air source (85 psig)

B - buffer bottle

C - 1 mm glass capillary gas distributor

D - calming section

E - experimental section

F - triple-necked 2 liter flask

G_1, G_2 - three-way glass stop-cocks

L - ground perspex ball

M_1 - carbon tetrachloride U-tube manometer

M_2 - open mercury manometer

P - pressure regulator

R_1, R_2 - rotameters

S - 60 mesh copper screen bed support

T - thermometer

V - liquid reservoir

X - exit section

room temperature. The three-way stopcock G_1 was used to turn off the liquid flow.

The air supply was obtained from the laboratory outlet through a filter-reducer valve assembly, P. The air flow rate to the column was carefully controlled by a needle value and measured by the calibrated rotameter, R_2. The air entered at the base of the glass column through a 5 cm long, 1 mm glass capillary, held in a vertical position close to the column axis by a spacer fixed to the column wall. A 5 cm long, 1/2 mm glass capillary was also used especially for the low air flow rates studied. To damp out the fluctuations in the air line a damper bottle, B, was used. The pressure at which the air was supplied to the column was measured by the open mercury manometer, M_2. The three-way stop-cock, G_2, was used to instantly shut off the gas flow to the column.

A carefully ground perspex ball, L, which fitted quite snugly into a ground glass joint, was used as a stop-valve to isolate the experimental section, once the gas and the liquid flows had been cut off. The gas in section D collected below the screen S and the gas in the experimental section collected near the top of the glass column. Only the latter reading was recorded. The details of the 20 mm glass column are given in Figure 3.2.

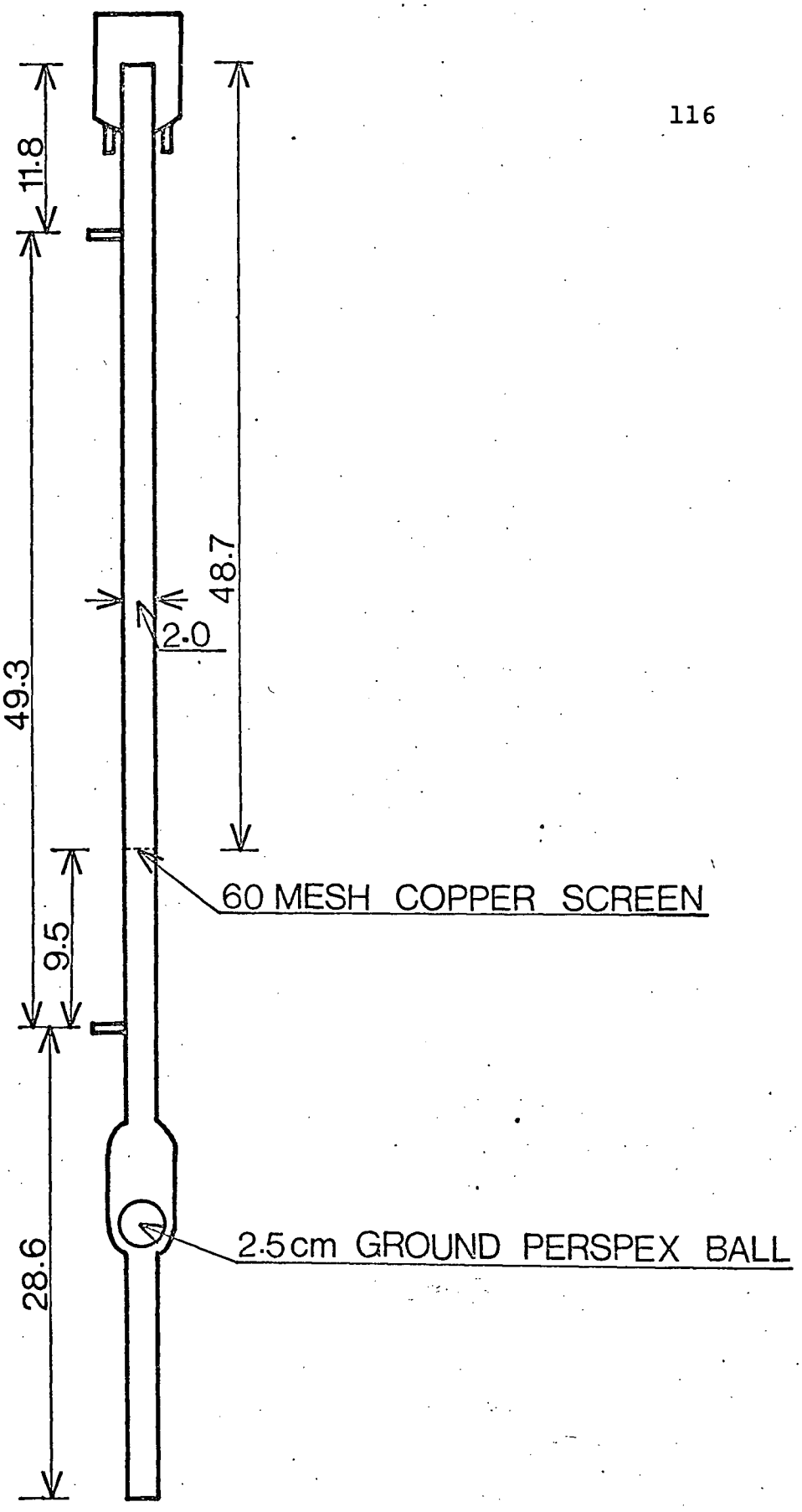

FIGURE 3.2 THE 20 MM GLASS COLUMN

3.1.2 The 2 inch perspex column

The main bulk of the three-phase fluidization study was carried out in a 2 inch perspex column, the schematic drawing of which is given in Figure 3.3.

3.1.2.1 Liquid cycle and test section

The details of the bulk of the equipment have been given by LeClair [101], who designed and used most of the same apparatus for an earlier study. Therefore only the main features of the equipment are discussed here. The liquid circulation loop is made from seamless copper tubing. A 152 inch long straight run of the 2 inch copper tubing preceding the experimental section acts as the calming section. The test liquid is circulated by a centrifugal pump driven by a 3 horse-power motor. A bypass is provided to regulate the pressure at which the liquid is pumped. With water as the test liquid, the setting of the bypass valve is not important, but when polyethylene-glycol solution is used, the setting is found to be critical since an excessive circulation of the liquid in the bypass loop makes it quite frothy. Therefore the opening of the bypass valve was so regulated as to maintain a pump delivery pressure of over 40 psig when using polyethylene-glycol solution as the test liquid. The liquid from the pump flows through a heat exchanger where it is cooled to maintain a steady temperature

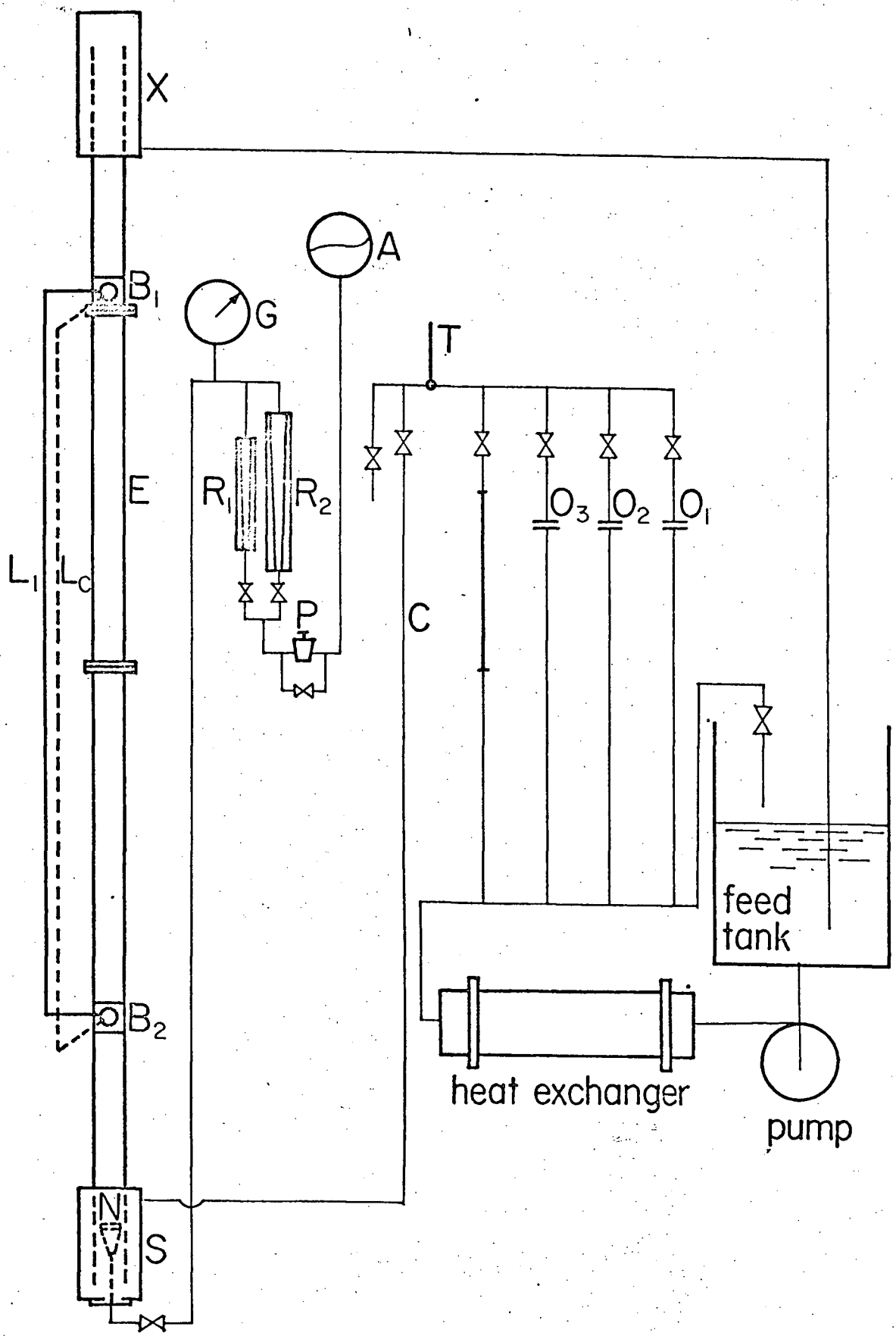

FIGURE 3.3 SCHEMATIC DIAGRAM OF 2 INCH PERSPEX COLUMN APPARATUS

LEGEND FOR FIGURE 3.3

A - Air source (35 psig)

B_1, B_2 - 2 inch full-bore ball valves

C - Capillary flow meter

E - Experimental perspex test section

G - Pressure gauge

I - Glass tube level indicator

N - Air inlet cone

O_1, O_2, O_3 - Orifice meters

P - Air filter and pressure regulator

R_1, R_2 - Rotameters

S - Entry section

T - Thermometer

X - Exit section

L_I - Lever arm position when ball valves are fully open

L_C - Lever arm position when ball valves are fully closed

in the liquid cycle. The temperature of the liquid is measured at a location downstream from the measuring station by a thermometer, T. The liquid then enters the main experimental column through an annular entry section, S. The liquid from the experimental column overflows into the exit section, X, whence it is returned to the feed tank, thus completing the liquid cycle.*

The liquid flow rate to the column is measured at the measuring station, either by one of the three orifice-meters O_1, O_2 or O_3, or by the capillary-tube meter, C. The calibration curves for these flow meters are given in Appendix 8.4.

The test section consists of a 5 ft long 2 in. inside diameter perspex tube. All along the test section carefully drilled pressure taps are provided, each of which houses a carefully shaped 1/4 inch copper tube with a 1/16 inch opening into the column, to fit flush with the inside of the test section. The pressure taps are connected to a 100 cm long, 8 mm i.d. U-tube manometer through a pressure manifold system (Figure 3.4) which permits the pressure drop to be measured between any two taps. Carbon tetrachloride dyed with a crystal of potassium permanganate was used as the manometric fluid for most of the study, while tetra-bromo-ethane was used for the rest. An open mercury manometer was also located in the test section to measure the absolute pressure in the column.

*A screen trap is clamped on to the opening of the liquid return line into the feed tank, to catch any particles elutriated out of the experimental column.

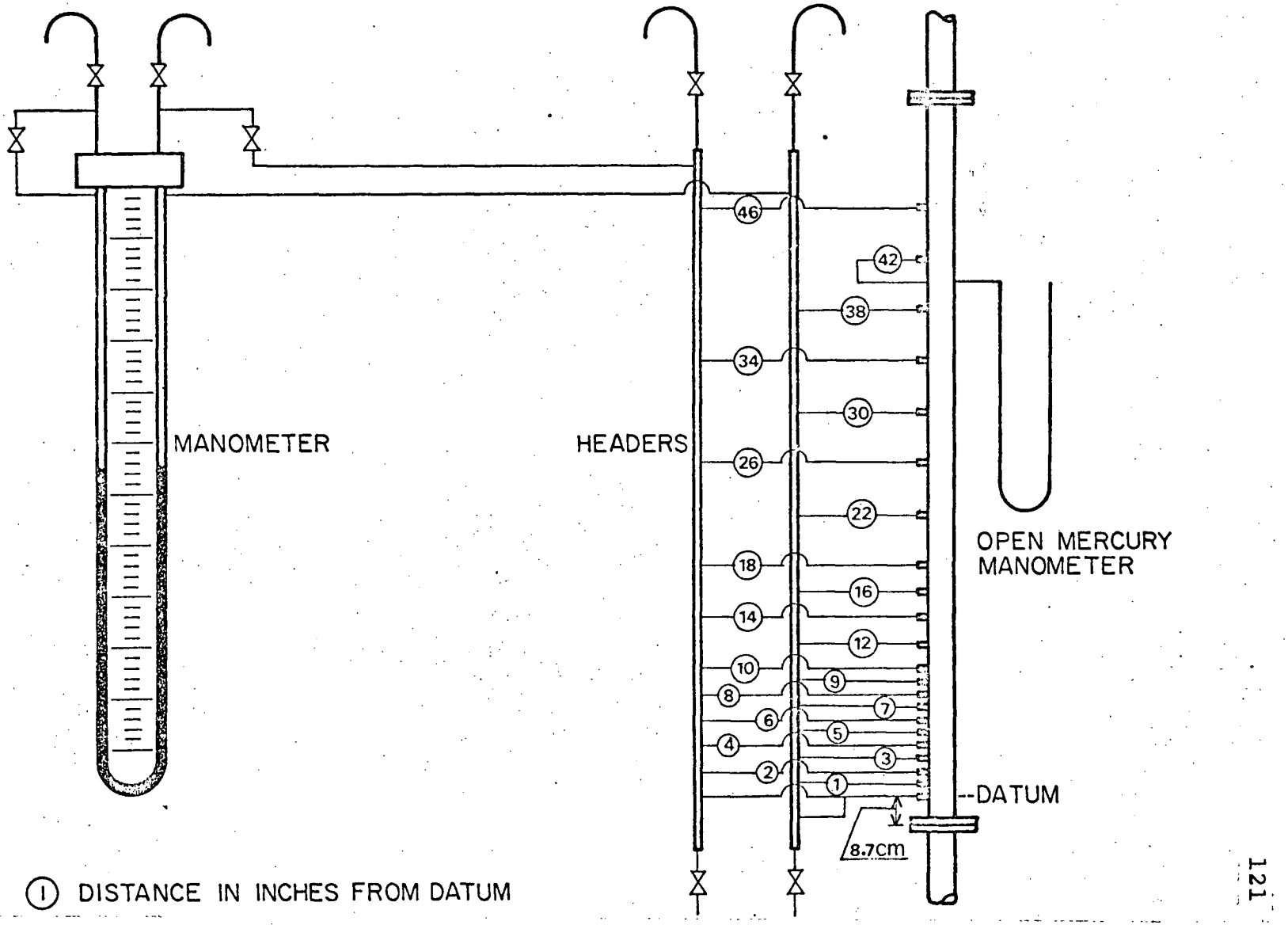

FIGURE 3.4 PRESSURE DROP APPARATUS FOR MEASURING LONGITUDINAL PRESSURE DROP PROFILE IN THE EXPERIMENTAL SECTION

The test section is separated from the calming section by a 60 mesh copper screen held in the recess of a rubber gasket, which in turn is held between two flanges. Since this screen also acted as the bed support, for fluidizing 0.25 mm glass beads another finer screen (100 mesh) was used on top of the 60 mesh screen to prevent the small particles from falling through. Two 2 inch full bore ball valves were used to trap the flowing mixture in the test section by closing them simultaneously. One valve was located 5 feet below the test section and the other at the top of the test section. The two valves were connected through lever arms by a link rod and could be shut completely and simultaneously by quickly rotating the balls through 90° via the link rod. Carefully drilled taps were provided in the section below the test section for liquid level indication, and both below and above the test section for static pressure drop measurements. Figure 3.5 shows the location of these pressure taps. Again carbon tetra-chloride dyed with potassium permanganate was used as the manometric fluid.

3.1.2.2 Gas cycle and bubble nozzle

Air was taken from the laboratory supply at 35 psig through a 1/2 inch copper line and reduced to a pressure of 12-16 psig by a pressure regulator and filter assembly, P, which maintained the reduced supply pressure constant at any desired level. This pressure was read downstream from the

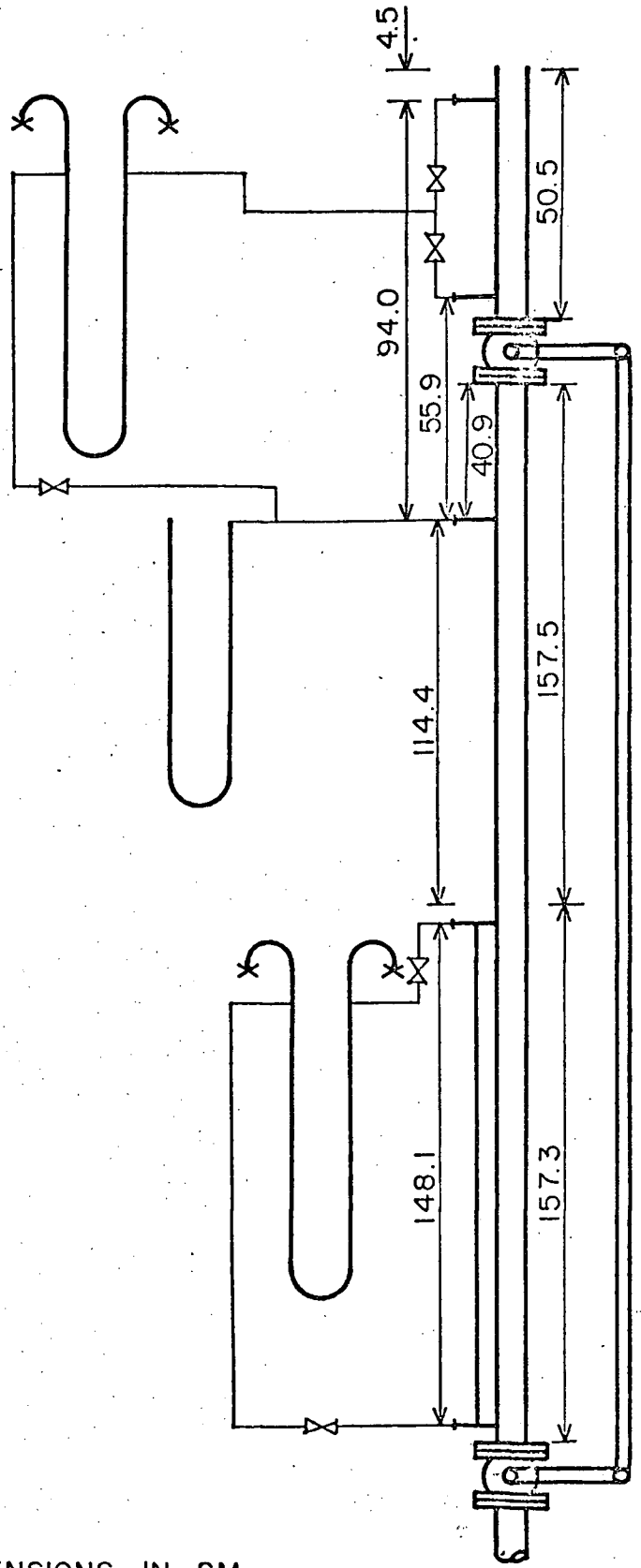

ALL DIMENSIONS IN CM.

FIGURE 3.5 LOCATION OF PRESSURE TAPS AND BALL VALVES FOR GAS HOLDUP MEASUREMENTS

measuring station on a Bourdon tube type pressure gauge, G. Air was then brought to the bottom of the main experimental column through a 1/2 inch copper line and admitted through the gas distributor, N. The air leaving the experimental column at the top was vented to the atmosphere.

The air flow rate to the experimental column was measured by either of the two calibrated rotameters, R_1 and R_2. Yet another rotameter was used for part of this study to measure very small gas flow rates. The calibration curves for these rotameters are given in Appendix 8.5.

The gas entered the column through a gas distributor, the details of which are given in Figure 3.6. The main bubble nozzle, N, was turned from a brass block to house various gas distributors that can be screwed on to it. In order to distribute the gas uniformly, a perforated 1/4 inch thick perspex plate distributor with 1 hole per square cm [4] was designed. Similar perforated plate distributors with fewer holes were also designed in order to check any effect of the gas distributor design on the gas holdup in two-phase gas-liquid flow. Preliminary investigations revealed little or no effect of the gas distributor geometry, and therefore a perforated 1/4 inch thick perspex plate distributor with four 1/16 inch holes was used in most of the studies.

The gas distributor was located 12 feet below the bed support screen with the hope that the flow and gas distribution

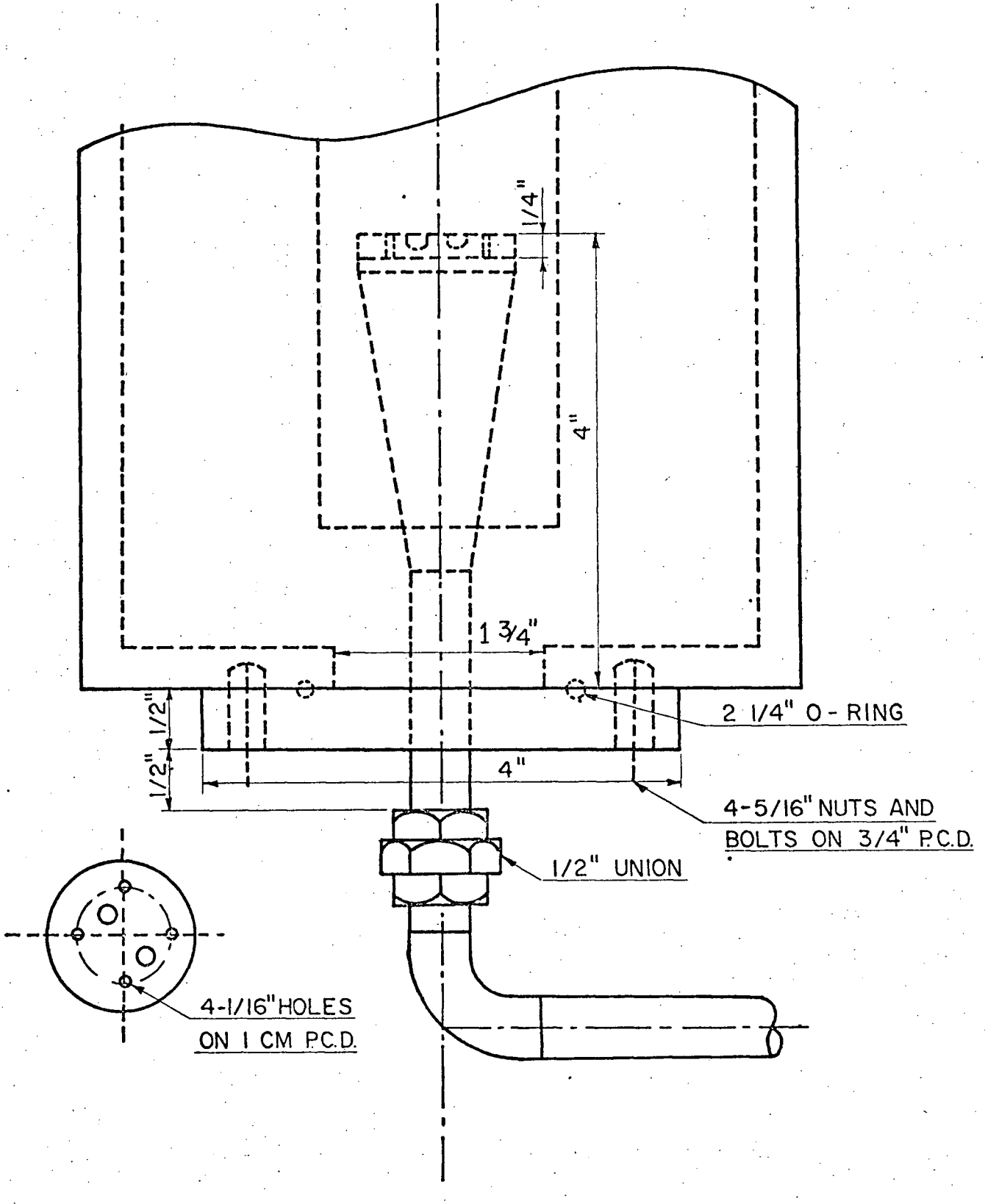

FIGURE 3.6 DESIGN OF GAS INLET AND DISTRIBUTOR

profiles would be fully developed in the test section. Visual observation of the test section, however, showed bubble coalescence occurring at different gas flow rates. It was therefore considered doubtful that the gas distribution profiles were fully developed. Nevertheless the gas distributor was left at the foot of the column throughout the entire study since it provided a two-phase gas-liquid region preceding the three-phase fluidized bed region; since a gas-liquid zone also followed the fluidized bed, the effect of the presence of solid particles in the test section on the gas holdup in the two-phase region above it could therefore be determined.

3.1.3 Electro-resistivity probe

An electro-resistivity probe was originally developed by Neal and Bankoff [103] for measuring the local volumetric gas fraction in mercury-nitrogen flow. The sensing element of their probe consisted of an insulated sewing needle with its exposed tip pointing into the flow. The probe was supplied with a D.C. potential and grounded through the continuous phase to complete the circuit, which is shown schematically in Figure 3.7. When an individual bubble passed over the probe, it served to open the circuit, which resulted in a nearly square wave output. Nassos and Bankoff [104] tested the applicability of the same probe in air-

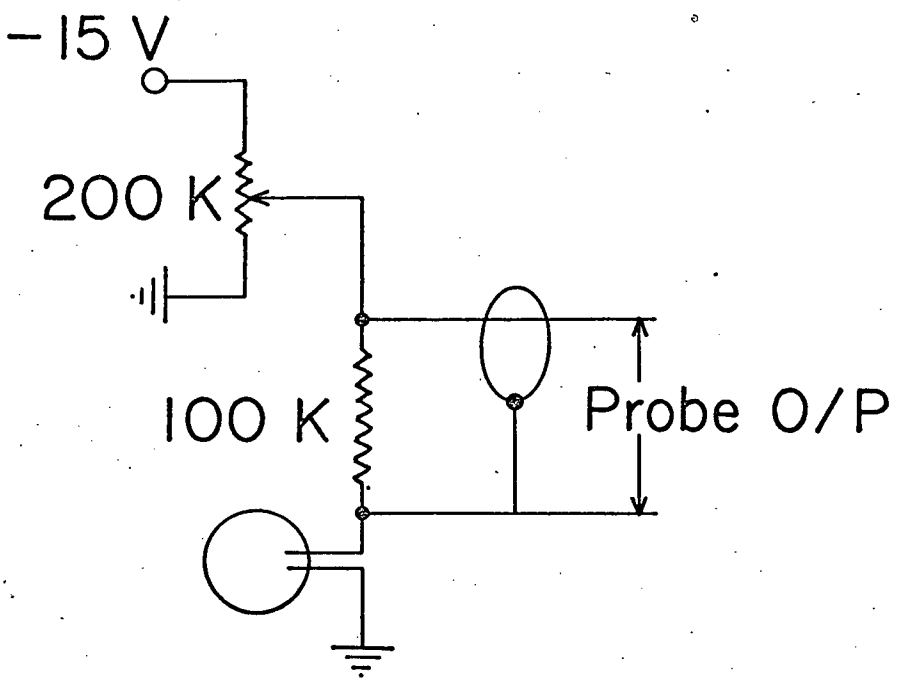

FIGURE 3.7 CIRCUIT DIAGRAM FOR ELECTRO-RESISTIVITY PROBE

water flow and found that, due to deflection of bubbles away from the probe, the average gas fraction obtained by integrating the local gas fraction profile was smaller than the value obtained by static pressure drop measurements. Some modifications were suggested to improve the agreement [104], but since the deflection of a bubble from a pointed sensing element remained as a basic problem, it was decided to change the design of the probe slightly for the present study.

The electro-resistivity probe used in this study consisted of two electrodes held at a small but fixed distance apart. The arrival of an individual bubble is sensed by the passage of the bubble through the gap. Although the probe supports could deflect a bubble into or away from the gap, it was nevertheless believed that the probability of registering an impinging bubble would be increased over that of the original needle probe. Since the diameter of the bubbles encountered in the gas-liquid flow study was always larger than the overall probe dimension (1.7 mm), the spatial resolution of the probe could be considered good. However, it is believed that a quick penetration of the bubble on impingement remains a problem and would become a major source of error when the probe is used in more viscous liquids.

The probe used was originally a miniature hot-film probe (1270-20W-6) supplied by Thermo Systems Inc., from which the hot-film filament was carefully cut off so as to

expose the two electrodes, leaving a gap of 1 mm. The details of the probe are given in Figure 3.8. The support needles are epoxy coated to insulate them from the continuous phase. The probe was mounted in the experimental section E through a traversing mechanism to allow for a radial traverse of the column to positions very close to the column walls. The details of the mounting mechanism are shown in Figure 3.8. One of the electrodes was maintained at a constant D.C. potential with respect to the other electrode, which was grounded through a 5 meter coaxial cable. The potential applied (2-3 volts) was so adjusted as to produce pulses of an amplitude of about 0.22 volts across a 100,000 ohm resistor connected in series. The electronic circuit used to analyse the probe signal is described in the next section.

3.1.4 Description of auxiliary circuits for measurement of local gas holdup and bubble frequency

Before discussing the circuits used, it is important to clearly define the variables being measured.

Quantities measured

(a) local gas fraction

The local volumetric gas fraction is defined as the probability that gas will exist at a point under consideration. For flow with stationary time-averaged properties (quasi-steady flow) this probability is the fraction of time the gas exists at that point [103]. Thus

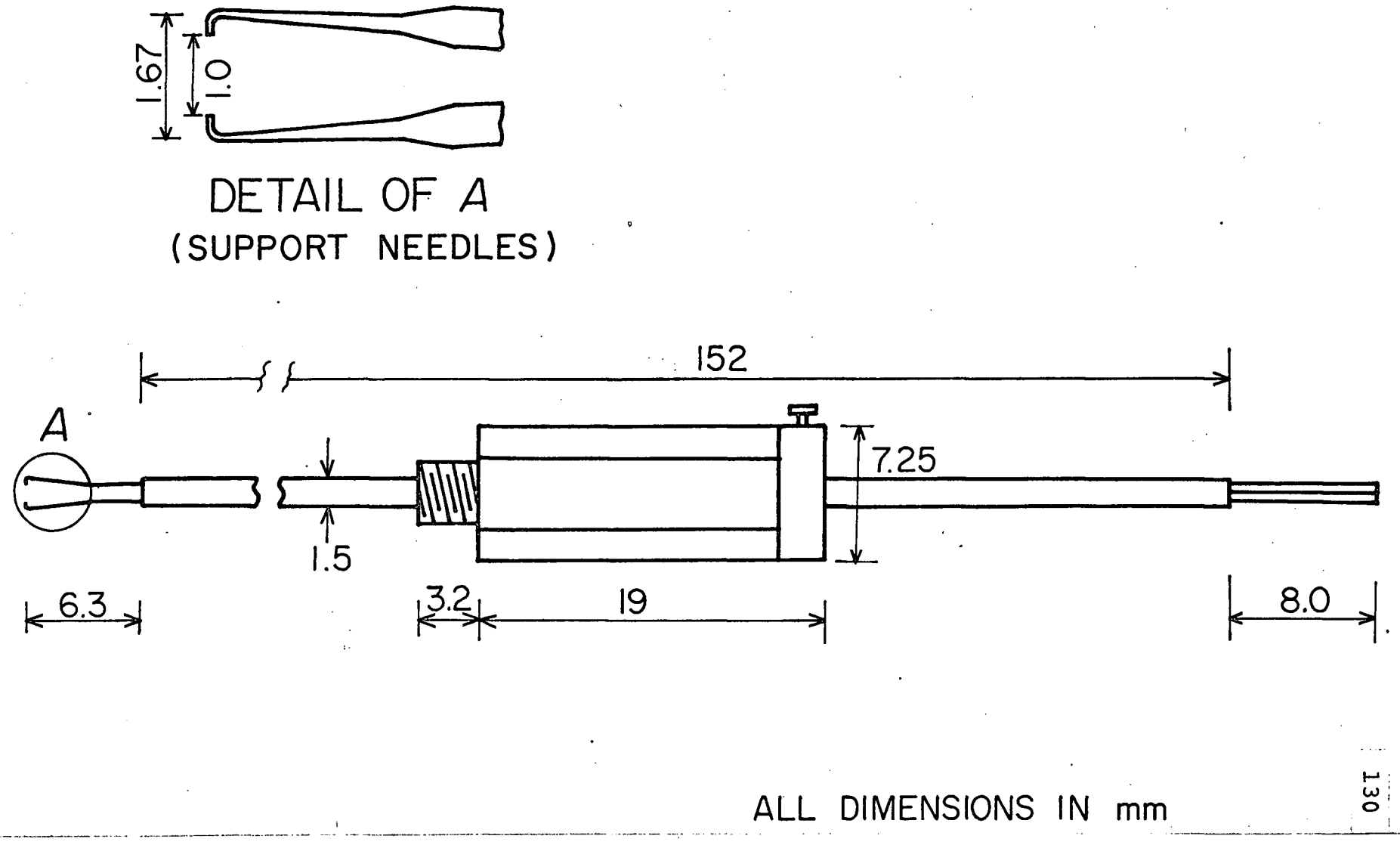

FIGURE 3.8 ELECTRO-RESISTIVITY PROBE AND MOUNT FOR TRAVERSING MECHANISM

$$\alpha_{2r} = t_2/T \tag{3.3}$$

where t_2 is the time the probe is exposed to the gas phase and T is the total sample interval. In order to obtain a true statistical average, the sample interval must be large compared to the time scale of flow oscillations, $1/n'$, where n' is the local bubble frequency. Thus, for a quasi-steady flow, the local gas fraction can be expressed as

$$\alpha_{2r} = \frac{1}{T} \sum_{i=1}^{N} t_i \tag{3.4}$$

In order that the gas fraction measured locally by this technique could be compared with the overall gas fraction measured by static pressure drop gradient, a traverse of the probe was made to obtain a radial profile of the local gas fraction. These profiles were then integrated over the cross-section to provide the overall average gas fraction, as given by

$$\langle \alpha_2 \rangle = \varepsilon_2 = 2 \int_0^1 \alpha_{2r} R^* \, dR^* \tag{3.5}$$

where R^* is the dimensionless distance from the center of the pipe.

(b) bubble frequency

The bubble frequency at a point, n_r', is defined as the number of bubbles passing through that point per unit time:

$$n_r' = N/T \qquad (3.6)$$

where N is the total number of bubbles that pass through the point in time T. The time T must be long enough to obtain a representative sample, which implies that N>>1. Normally 100 - 1000 bubbles, depending on the radial location of the probe, were counted in order to obtain the bubble frequency.

Analysis of the probe signal

A simple electronic analogue logic circuit was designed to obtain these quantities from the probe signal and is shown schematically in Figure 3.9. The principal component of the circuit was the logic differential comparator, which was used to trigger pulses of width equal to the residence time of an individual bubble, utilizing the following characteristic of the comparator:

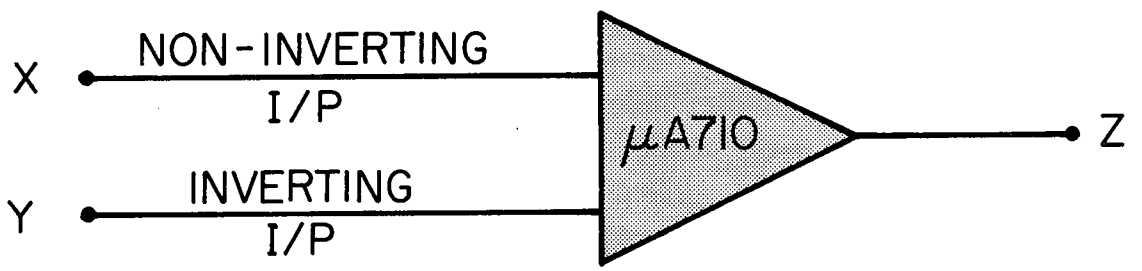

IF $X+Y > 0$, $Z = 1$
IF $X+Y < 0$, $Z = 0$

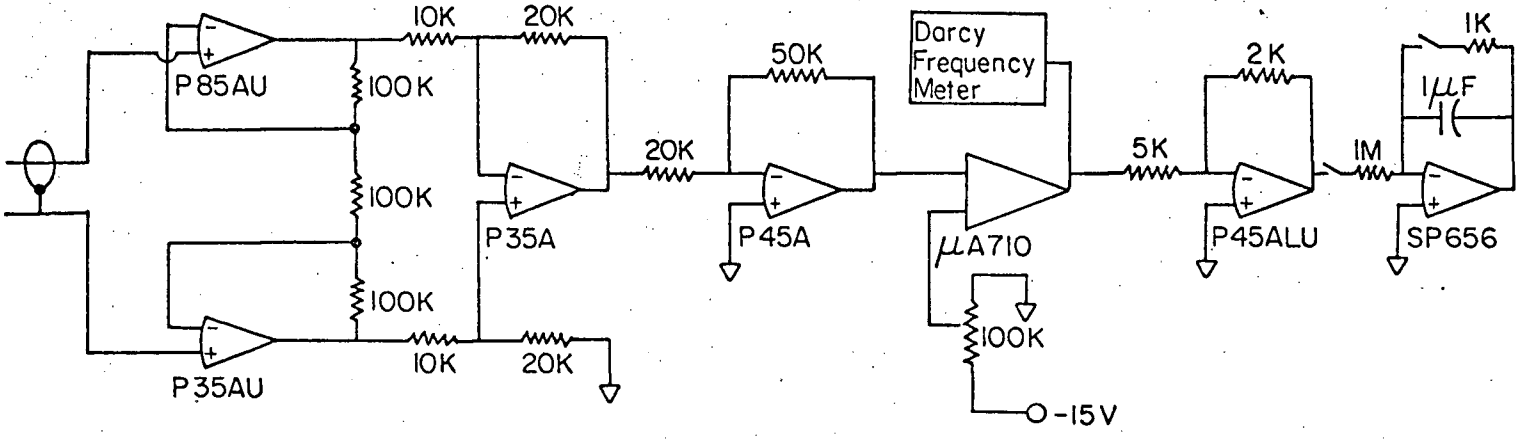

P35A — Philbrick solid state amplifier
P35AU — Philbrick solid state amplifier
P85AU — Philbrick solid state amplifier
P45A — Philbrick solid state amplifier
P45ALU — Philbrick solid state amplifier
SP656 — Philbrick photochopper stabilized solid state amplifier

μA710 — Fairchild logic differential comparator
↓ — To high quality ground
⏚ — To power common

FIGURE 3.9 SCHEMATIC DIAGRAM OF THE ANALOGUE-LOGIC CIRCUIT FOR MEASURING LOCAL BUBBLE-FREQUENCY AND GAS FRACTION

The pulses of uniform amplitude thus triggered by the comparator were then integrated to obtain the total time the probe is exposed to the gas phase, from which the local gas fraction was calculated by means of equation 3.4. The circuit preceding the comparator was designed to amplify the probe signal, but most importantly to isolate the measuring circuit from the probe, so as not to create any feedbacks [105].

The bubble frequency was obtained by counting the number of pulses triggered by the comparator on a Darcy frequency counter for a fixed time of 10 seconds. The total number of pulses counted were then read from the electronic display of the counter. Alternatively, a strip chart recorder was used to record the comparator output. The number of pulses were then counted from the recording of over a minute. Either method of obtaining the bubble frequency was found to be satisfactory and used interchangeably, depending on the availability of the equipment. The bubble frequency measurements were used to obtain an estimate of average bubble size in the test section by the method presented in Appendix 8.3.

3.2 Range of variables studied

The experimental programme for collecting the data was divided into two parts:

(A) The study of gas holdup in two-phase gas-liquid flow, and

(B) The study of solids and gas holdup in a three-phase fluidized bed.

The main experimental programme was carried out in the 2 inch i.d. perspex column located in a 2 inch diameter forced circulation loop. However, the 20 mm i.d. glass column was used to carry out a preliminary study to establish the relevance of various parameters involved. Although only a limited amount of data was obtained in the latter, an appreciable range was investigated and therefore the results obtained are included.

(A) Gas holdup in two-phase gas-liquid flow

The need to study two-phase gas-liquid flow arose from the lack of established and reliable methods to predict the gas holdup for such flow. The purpose of this study was two-fold:

(i) to check the applicability of the mathematical model proposed in section 2.1.2, and

(ii) to obtain data that could be used later for comparing with the data on gas holdup in three-phase fluidization, in order to establish the role of solid particles in promoting either the coalescence or breakup of bubbles in three-phase fluidized beds.

Therefore the scope of this study was limited, Tables 3.1 and 3.2 summarizing the range of variables studied.

(B) Solids and gas holdup in a three-phase fluidized bed

As has been outlined above, the main aim of this work was to establish the effect of liquid- and solid-phase properties on the individual gas, liquid and solid holdups in a three-phase fluidized bed, for a wide range of conditions. The choice of fluids selected for this study was guided by the findings in corresponding two-phase gas-liquid studies. Thus, air was conveniently chosen as the gas phase and used throughout the study, since it has been shown [108] that the properties of the gas phase had little or no effect under normal atmospheric conditions. Ordinary tap water was used as the liquid phase for the most part, so that the data collected in this study could be compared with earlier investigations. In the later part of the work, an aqueous polyethylene-glycol solution was used to investigate the effect of liquid viscosity. The polyethylene-glycol solution was chosen because it is a very viscous liquid, the Newtonian behaviour of which has been verified [101], and because its density and surface tension are only a little different from that of water. For the solid phase, equi-sized spherical glass beads, lead shot and steel ball bearings were chosen to give a broad range of particle size and density.

TABLE 3.1

EXPERIMENTAL CONDITIONS FOR TWO-PHASE GAS-LIQUID FLOW IN 20 MM GLASS COLUMN

Liquid Velocity, j_1 (cm/sec)	Gas Velocity, j_2 (cm/sec)	Liquid Viscosity, μ_1 (cp)	Gas Holdup, ε_2 (-)
0.0 - 18.0	5.0 - 18.0	1.0	0.20 - 0.39

TABLE 3.2

EXPERIMENTAL CONDITIONS FOR TWO-PHASE GAS-LIQUID FLOW IN 2 INCH PERSPEX COLUMN

Liquid Velocity, j_1 (cm/sec)	Gas Velocity, j_2 (cm/sec)	Liquid Viscosity, μ_1 (c_p)	Gas Holdup, ε_2 (-)	Flow Regime
0.0 - 19.0	1.5 - 13.0	1.0 & 69.0	0.05 - 0.28	bubble-slug

Tables 3.3 and 3.4 list the range of variables studied in both the 20 mm glass column and the 2 inch perspex column.

3.3 Experimental procedure

The experimental procedure used to obtain data in the 20 mm glass column and the 2 inch perspex column were essentially similar. The salient features of the procedure adopted are described in the following sections.

3.3.1 Physical properties of the liquids used

For the major part of this work water was used as the test liquid. Ordinary tap water containing 0.2% by weight sodium dichromate and 0.05% by weight sodium hydroxide as corrosion inhibitors [101] was tried for the early runs in the 2 inch perspex column. Since the additives did not inhibit corrosion as effectively as had been hoped for, ordinary tap water without additives was used thereafter. This required frequent cleaning of the mercury manometer traps and the copper bed support screen. For the studies in the 20 mm glass column ordinary tap water was used without any problems. The density of the water was checked occasionally, but in the final processing of the data collected, both the density and viscosity of water were obtained from Perry [106]. Surface tension too was measured for the early runs and found to remain essentially unchanged.

TABLE 3.3

EXPERIMENTAL CONDITIONS FOR THREE-PHASE FLUIDIZATION

IN 20 mm GLASS COLUMN

Liquid Velocity, j_1 (cm/sec)	Gas Velocity, j_2 (cm/sec)	Liquid Viscosity, μ_1 (cp)	Particle Diameter, d_p (mm)	Solids Density, ρ_3 (gm/cc)	Solids Holdup, ε_3 (-)	Gas Holdup, ε_2 (-)
1.7 - 8.1	0.2 - 8.2	1.0 & 2.1	0.5 - 1.0	2.5 - 3.0	0.5 - 0.2	0.05 - 0.15

TABLE 3.4

EXPERIMENTAL CONDITIONS FOR THREE-PHASE FLUIDIZATION

IN 2 INCH PERSPEX COLUMN

Liquid Velocity, j_1 (cm/sec)	Gas Velocity, j_2 (cm/sec)	Liquid Viscosity, μ_1 (cp)	Particle Diameter, d_p (mm)	Solids Density, ρ_3 (gm/cc)	Solids Holdup, ε_3 (-)	Gas Holdup, ε_2 (-)	Flow Regime
0.4 - 39.0	0.4 - 21.0	1.0 & 63.3	0.25 - 3.2	2.9 - 11.1	0.5 - 0.1	0.05 - 0.25	bubble-slug

The viscosity of the polyethylene glycol solution was measured by a Cannon Viscometer (H-304) which was calibrated with ASTM Standard Oil No. S-20 and No. S-60, according to the procedure recommended in the ASTM manual (D445-53T). The viscosity of the solution was then measured by the calibrated viscometer, following the procedure recommended, and these measurements too are reported in Appendix 8.6. A plot of dynamic viscosity against the inverse of the absolute temperature is presented as Figure 8.6.1 of Appendix 8.6. This plot was used to obtain the viscosity of the solution at the measured temperature in the final analysis of the data.

The surface tension of polyethylene glycol solution was also checked and was found to be 63 dynes/cm. Since it is not very different from that of pure water (70 dynes/cm) no further measurements of the surface tension were made or reported.

3.3.2 Physical properties of the solids used

Glass beads of three different sizes, 0.25, 0.5 and 1.0 mm, lead shot, and steel ball bearings were used for studies in the 2 inch perspex column; washed granular sand and 1.0 mm glass beads were used for studies in the 20 mm glass column. For all the glass beads, lead shot and washed sand, a carefully screened cut was selected from the screen analysis and the average particle size was taken

as the arithmetic mean of the two consecutive sieve sizes. The diameter of lead shot was also checked by measuring the diameter of some 50 randomly chosen particles by a micrometer. The chrome-plated steel ball bearings were of precisely ground grade; therefore the quoted diameter was taken as the size of the particles. A random check on the diameter of a few steel balls with a micrometer showed no difference in size from the quoted diameter.

The density of glass beads and sand was measured by the specific gravity bottle method. Ten to fifteen grams of particles were placed in a 10 ml specific gravity bottle and weighed carefully on a balance. The bottle was then carefully filled with distilled water to the mark and weighed again. The density of the distilled water was measured separately in another 10 ml specific gravity bottle. The density of the particles was then calculated from these measurements and is reported in Appendix 8.6.

The density of the lead shot and the steel balls was measured by weighing some 50 randomly selected particles both individually and collectively on a carefully adjusted balance, and in the case of the lead shot by measuring the particle size in two perpendicular directions with a micrometer. The densities calculated from these measurements are reported in Appendix 8.6.

The density of the 25-75 glycerol-water solution used in the 20 mm glass column was measured both before and after each run. Since the measured densities agreed with the published values, the density of the solution used was subsequently obtained from Perry [106]. The viscosity of the 25-75 glycerol water solution was taken from Mathur [107] and is reported in Appendix 8.6.

A 33% by weight solution of polyethylene glycol in water was used for the measurements in the 2 inch perspex column. The solution was found to be quite acidic and it corroded the mechanical seals of the centrifugal pump. It was then decided to neutralize the solution with a dilute solution of sodium hydroxide; 0.2% by weight of sodium dichromate was also added to inhibit corrosion. It was also found that for restarting the pump after a long shut-down, the mechanical seals should be thoroughly washed with fresh water so as to remove from them any deposits of solidified polyethylene glycol. The clear orange-yellow solution turned dark brown with usage and was replaced with fresh solution. It was found that the deterioration in colour of the clear solution was due to the suspended corrosion products. If the solution was allowed to stand undisturbed, it became clear once again as the corrosion products settled out.

The density of the polyethylene glycol solution was measured by a specific gravity bottle, and the measurements are reported in Appendix 8.6.

3.3.3 Measurement of gas holdup in gas-liquid flow

For starting a run, the liquid was circulated in the column until a constant temperature was achieved and noted. All the runs were conducted at about the room temperature. All the manometer taps in the experimental section, and above and below the experimental section, were carefully flushed to remove any air bubbles in the connecting lines. The liquid flow rate was then adjusted to obtain the desired velocity through the column. When polyethylene glycol solution was used as the test liquid, static pressure drop readings were taken on all the manometers in order to determine the frictional pressure drop in single phase flow.

The air was then introduced by pressurizing the air line, and the back-pressure was so adjusted that no fluctuations in the rotameter reading were observable. This back-pressure in the air line was recorded. The liquid flow rate was once again adjusted to the desired flow rate and the static pressure drop measurements along the experimental section, as well as above and below it, were recorded. The absolute pressure near the top of the experimental section was recorded with the help of the open mercury manometer. The visual observations of bubble size distribution and flow regime encountered were also recorded.

The two ball valves were then shut off by manually actuating the link rod connecting them. The gas flow was

cut off by venting the air to the atmosphere and the liquid flow by switching off the motor. The settled liquid height in the experimental section was measured directly, that in the section below it by noting the liquid level in the glass tube indicator (see Figure 3.3) and that above the experimental section by a direct dip-rod measurement. The absolute pressure near the top of the experimental section was once again recorded with the help of the open mercury manometer. The ball valve at the top of experimental section was then opened and the settled liquid height below the experimental section was checked again to ensure that the copper screen allowed no liquid to leak through.

From these measurements the gas holdup was calculated as described subsequently under Data Processing.

During the later part of the work an electro-resistivity probe was developed mainly to study the gas holdup in the three-phase fluidized bed region. However, a few runs were conducted to check the applicability of the probe for measurements of local gas fractions in air-water and air-polyethylene glycol solution flow.

In order to use the electronic circuit described above, the amplifiers were warmed for 20 minutes under zero load conditions and then checked for any offset by the circuit described in the manual [105]. The probe was located in the experimental section so that the gap between the electrodes was nearly horizontal and perpendicular to the

flow direction. This adjustment was not found to be critical in these measurements. The probe was then supplied a D.C. potential from a constant D.C. source, through a potential divider. The applied voltage was so regulated as to produce pulses of approximately 0.22 volts amplitude across a 100,000 ohm resistor in series.

As has been stated earlier, the logic differential comparator was the central component of the measuring circuit. The output of the probe was carefully amplified to produce pulses of approximately 3.2 volts amplitude, which were then fed as the non-inverting input to the comparator. The inverting input to the comparator was a reference D.C. potential of approximately -3.0 volts amplitude, taken from a constant D.C. source through a potential divider. The reference voltage was adjusted in such a manner that the cutting off level of the pulses was at approximately 0.2 volts above the datum. Both the input and the output of the comparator were monitored continuously on a dual beam oscilloscope to ensure that the cut-off level in the comparator was such that no pulses were triggered from the input signal corresponding to the liquid phase.

The comparator output was integrated by the integrating circuit with a time constant of nearly one second. The time required to integrate the comparator output to 8 volts was noted. The gain of the amplifier following the comparator

was so adjusted that this time was about 2 minutes. The non-inverting input terminal of the comparator was then grounded, rendering the comparator output constant and equal to its peak value. The time required to integrate the comparator output to 8 volts through the same amplifier was again noted. The local gas fraction was then obtained from the ratio of these two times.

The bubble frequency was obtained, as mentioned earlier, by counting the pulses in the comparator output either electronically by a Darcy frequency counter or manually from the recording of the output.

3.3.4 Holdup studies in three-phase fluidized beds

A typical run was conducted by feeding a carefully weighed amount of well screened particles into the test section. Depending on the desired velocity of liquid through the column, the liquid flow rate was measured by either of the flow meters. The liquid was circulated in the column until a constant temperature was achieved and noted. All the manometer taps were carefully flushed to remove any air bubbles remaining in the connecting lines.

Once the temperature and liquid flow rates were stabilized, the expanded bed height was recorded. To determine the static pressure profile along the fluidized bed, static pressure drop readings were taken between tap 1 and other

taps above it (see Figure 3.4). The open mercury manometer measured the absolute pressure near the top of the experimental section.

The air was introduced by pressurizing the air line and making liquid flow rate adjustments to ensure that no solid particles were ejected out of the column during the introduction of the air stream. The back pressure in the air line was then so adjusted as to obtain the desired gas flow rate without any fluctuations in the rotameter reading. The liquid flow rate was then readjusted, so as to give a stable operation of the fluidized bed. In order to determine the complete static pressure profile in the test section, static pressure drop readings were taken between tap 1 and all other taps above it. The measurements of static pressure drop gradient below and above the test section were recorded by separate U-tube manometers. A record was kept of the observed bed behaviour and the flow regime encountered in the test section. The open mercury manometer was used to measure the absolute pressure near the top of the experimental section.

The two ball valves were then closed by actuating the link rod manually. The gas flow rate was cut off by venting the air and the liquid flow rate by switching off the motor. The settled liquid height in various sections was measured (see Figure 8.2.3), and the absolute pressure near the top of the test section was read from the open mercury manometer. A check of fixed bed height before and

after the run revealed if any of the particles were elutriated from the experimental column. If the proportion of particles carried out of the experimental section during a run was large, the run was discarded.

From these measurements the expanded bed height, the solids and gas holdup inside the three-phase fluidized bed, and the gas holdup above and below the fluidized bed were calculated as described under Data processing.

The electro-resistivity probe was used to obtain the radial profile of local gas fraction inside the bed and was located 8 inches above tap 1 (29.0 cm above the bed support screen). The same procedure as used for measuring the gas holdup in gas-liquid flow was followed.

3.4 Data processing

From the data obtained in the 2 inch perspex column, the expanded bed height, L_b, and the solids holdup in the fluidized bed, as well as the gas holdup in the gas-liquid and gas-liquid-solid regions, were calculated as outlined in the following sections.

3.4.1 Expanded bed height and solids holdup

The longitudinal pressure drop profiles for all the two-phase liquid-solid and the three-phase gas-liquid-solid fluidization studies were measured up to a height of 46 inches

above tap 1 (Figure 3.4). The method of obtaining the expanded bed height, and thereby the solids holdup, from these measurements is discussed in Appendix 8.2. Accordingly, the observed pressure drop, as represented by the U-tube manometer reading, is plotted against the distance from tap 1. Then for a two-phase liquid-solid fluidized bed, as shown in Appendix 8.2, the following straight line represents the pressure drop for $Z \leq Z_{max}$:

$$H\ (\rho_M - \rho_1) = Z\ \varepsilon_3\ (\rho_3 - \rho_1) \qquad (8.2.18)$$

and the point of intersection of this straight line with $H = H_{max}$ satisfies

$$H_{max}\ (\rho_M - \rho_1) = Z_{max}\ \varepsilon_3\ (\rho_3 - \rho_1) \qquad (8.2.19)$$

The measured longitudinal pressure drop profile for a typical liquid-solid fluidization experiment is shown in Figure 3.10. The straight line for the fluidized bed region is obtained by fitting the best line through the pressure drop data for $Z \ll Z_{max}$ by the method of least squares. The intercept of this straight line with the averaged value of $H = H_{max}$ gives the value of Z_{max}, from which the expanded bed height is calculated as

$$L_b = Z_{max} + 8.7 \qquad (3.6)$$

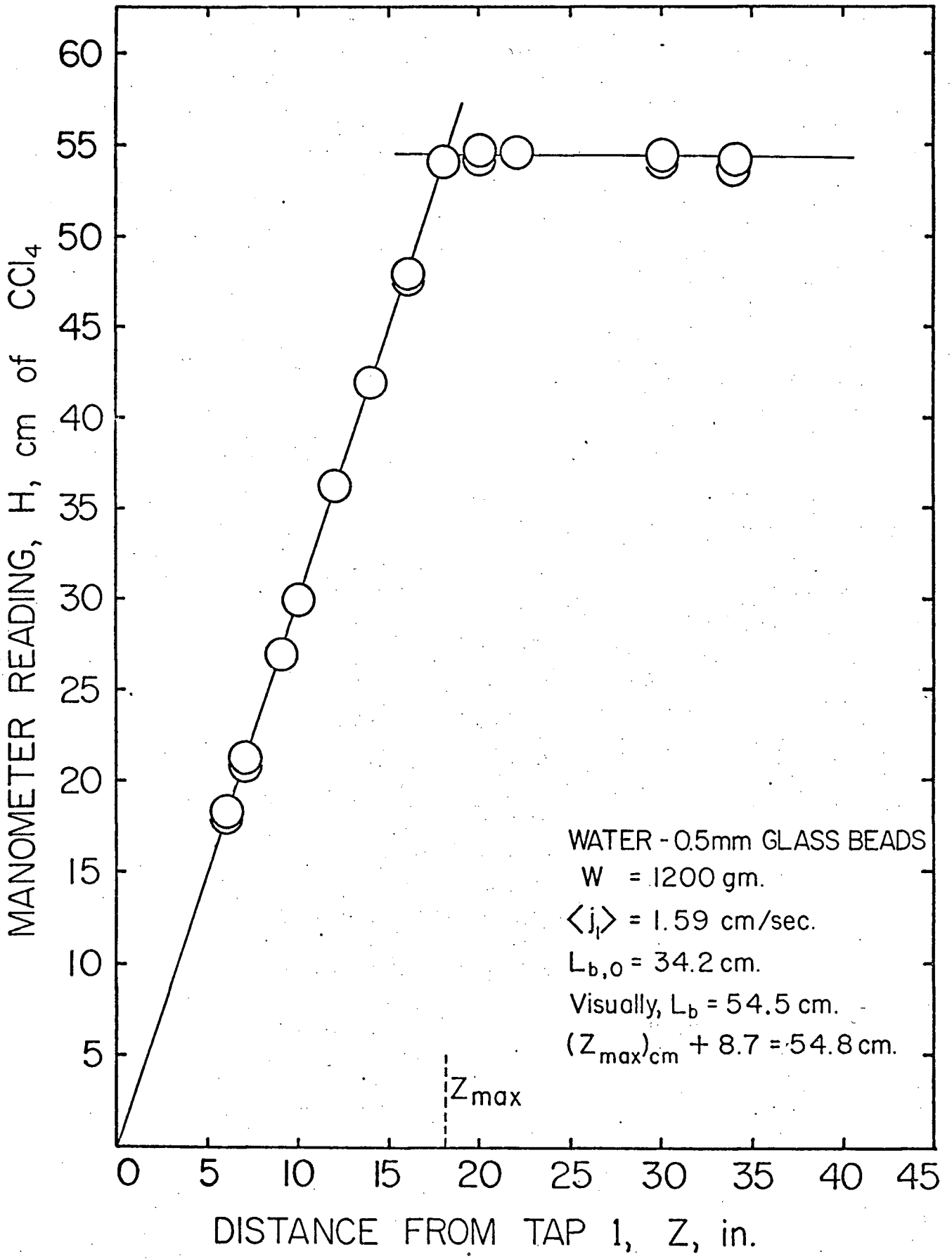

FIGURE 3.10 TYPICAL PRESSURE DROP PROFILE IN LIQUID-SOLID FLUIDIZATION

The expanded bed height so calculated was found generally to be in good agreement with the bed height measured by direct observation of the bed boundary. However, for the particular case of small glass beads at a large degree of bed expansion, the observed pressure drop data near $Z = Z_{max}$ deviated considerably from the initial straight line. This deviation is believed to be caused by the non-uniformity of longitudinal solids distribution arising from stratification by size of the imperfectly sized solids. In such cases the expanded bed height calculated by the straight line intersection method was found to be smaller than the measured bed height by visual estimation of the bed boundary; nevertheless the former was used to calculate the solids holdup in the fluidized bed.

The solids holdup was then determined from the equation

$$\varepsilon_3 = W/\rho_3 A L_b \qquad (3.1)$$

and also from the slope, S_I, of the best straight line through the pressure drop data. Then from equation 8.2.13, since $\varepsilon_2 = 0$,

$$\varepsilon_3 = S_I (\rho_M - \rho_1)/(\rho_3 - \rho_1) \qquad (3.7)$$

The values of solids holdup obtained from equations 3.1 and 3.7, respectively, were found to be in good agreement, and an arithmetic mean of these two values is reported as the solids holdup.

The procedure for obtaining the expanded bed height of a three-phase fluidized bed, is essentially the same as described above. The observed pressure drop, as represented by the manometer reading, is plotted against the distance from tap 1. As shown in Appendix 8.2.1, the following straight line represents the pressure drop data for $Z \ll Z_{max}$:

$$H\ (\rho_M-\rho_1) = Z\ [\varepsilon_3(\rho_3-\rho_1) - \varepsilon_2'''\ (\rho_1-\rho_2)] \qquad (8.2.12)$$

while for $Z \geq Z_{max}$,

$$H\ (\rho_M-\rho_1) = Z_{max}[\varepsilon_3(\rho_3-\rho_1)-(\varepsilon_2'''-\varepsilon_2'')(\rho_1-\rho_2)]$$

$$- Z\ \varepsilon_2''\ (\rho_1-\rho_2) \qquad (8.2.10)$$

The intersection of these two lines satisfied

$$H_{max}(\rho_M-\rho_1) = Z_{max}[\varepsilon_3(\rho_3-\rho_1) - \varepsilon_2'''(\rho_1-\rho_2)] \qquad (8.2.11)$$

The measured longitudinal pressure drop profile for a typical gas-liquid-solid fluidization experiment is shown in Figure 3.11. The line for the fluidized bed region is obtained by fitting the best straight line through the pressure drop data for $Z \ll Z_{max}$ by the method of least squares. Similarly the line for the region above the bed is obtained by fitting the best straight line through the pressure drop data for

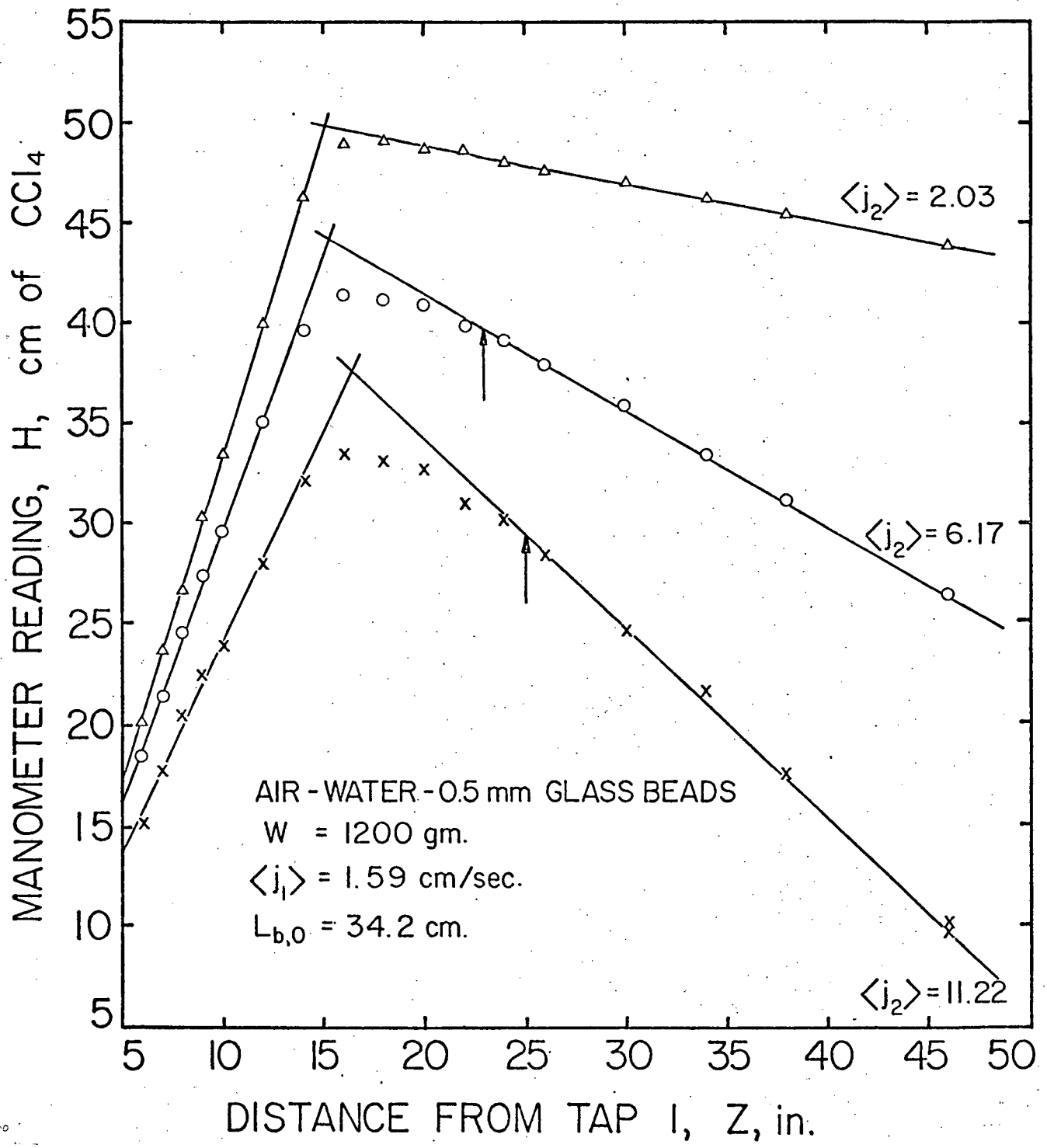

FIGURE 3.11 TYPICAL PRESSURE DROP PROFILE IN THREE-PHASE FLUIDIZATION (arrows indicate upper limit of bed level as visually observed)

$Z \gg Z_{max}$ by least squares. The point of intersection of these two straight lines determines Z_{max}, from which the expanded bed height is calculated:

$$L_b = Z_{max} + 8.7 \qquad (3.6)$$

The expanded bed height from equation 3.6 was found to be in good agreement with the bed height measured by direct visual observation of the bed boundary at small gas flow rates, when this boundary could be clearly defined. However, for higher gas flow rates (> 4 cm/sec), the bed boundary was quite diffuse and could no longer be located visually with any confidence and consistency. Under these circumstances the method outlined above provides a meaningful definition to the expanded bed height, and was used throughout this study to obtain expanded bed heights with a high degree of reproducibility and confidence.

The solids holdup in the three-phase fluidized bed was then obtained from

$$\varepsilon_3''' = W/\rho_3 A L_b \qquad (3.1)$$

Care was exercised in all experiments to prevent elutriation or ejection of solid particles from the experimental column. Nevertheless some elutriation, depending on the gas and the liquid flow rates and the size of the particles present in

the column, did occur, as evidenced by the presence of particles in the screen catch-all and by the reduction in static bed height. If the weight of particles lost from the column during a particular run was disproportionately large (>5%), that run was discarded; otherwise the weight of particles in the system was taken as the mean of the weights of particles in the system before and after the run. No such problem was encountered for the large and heavy particles.

It is also important to point out that no measurable frictional pressure drop was observed when operating without solids in the column with water as the test liquid, at all the water flow rates investigated (2-39 cm/sec). However, with polyethylene glycol-water solution as the test liquid, frictional pressure drop in the column without solids was measurable for two of the flow rates studied (13.82 and 18.84 cm/sec). In such instances, the measured pressure drops for the longitudinal profiles were corrected by subtracting the appropriate frictional pressure drop from each of the measured values. The corrected pressure drop readings were than used to obtain the expanded bed height for determining the solids holdup.

In the 20 mm glass-column the expanded bed height was measured by locating the bed boundary visually. The small cross-section of the tube employed facilitated observation of the bed boundary; nevertheless, the upper range of gas flow rate investigated was restricted due to the difficulty

of defining the bed boundary at higher gas flow rates. The solids holdup was calculated from equation 3.1 as before.

3.4.2 Gas holdup

The two main methods used to study the average gas holdup in the two-and three-phase systems viz. the measurement of static pressure drop gradient and the measurement of liquid level after isolating the sections by shutting off the valves, are described in Appendix 8.2. It is shown there that due to changes in kinetic energy of the stream and frictional pressure losses, which Neal and Bankoff [103] estimated to be only about 2.5% of the total static pressure drop in their own gas-liquid system, the gas holdup obtained by static pressure drop measurements is subject to some error. However, if these losses are properly accounted for, the pressure drop per unit length in gas-liquid flow is very nearly equal to the mean density of the two-phase flow stream. In such instances, the gas holdup is given by

$$\varepsilon_2'' = -H\ (\rho_M-\rho_1)/(\rho_1-\rho_2)\ Z \qquad (8.2.17)$$

The gas holdups above and below the experimental section are thus obtained by measuring the pressure drop with the U-tube manometer provided in each of these sections. These measured gas holdups are then suitably corrected from the

midpoint pressure of the measuring section to a standard pressure of 760 mm of mercury. All gas holdups are reported at this pressure.

For the estimation of gas holdup in a three-phase fluidized bed, a complete longitudinal pressure drop profile is required. As shown in Appendix 8.2, the slope of the straight line for the three-phase region is given by

$$S_I = [\varepsilon_3 (\rho_3-\rho_1) - \varepsilon_2''' (\rho_1-\rho_2)] \frac{1}{(\rho_M-\rho_1)} \qquad (8.2.13)$$

from which, on rearrangement,

$$\varepsilon_2''' = [\varepsilon_3(\rho_3-\rho_1) - S_I(\rho_M-\rho_1)] \frac{1}{(\rho_1-\rho_2)} \qquad (3.8)$$

where ε_3 is obtained from equation 3.1 as discussed in the preceding section, and S_I is obtained from the slope of the best straight line through the pressure drop data for $Z \ll Z_{max}$ by the method of least squares.

Alternately, in fluidization one can utilize the fact that pressure drop across the bed is equal to the weight of the bed per unit area [98]. In three-phase fluidization H_{max} is a measure of the pressure drop across the bed of height Z_{max} and satisfies equation 8.2.11. Then by rearranging equation 8.2.11, the gas holdup in the three-phase fluidized bed is given by

$$\varepsilon_2''' = \frac{\varepsilon_3(\rho_3-\rho_1)\ Z_{max} - H_{max}\ (\rho_M-\rho_1)}{(\rho_1-\rho_2)\ Z_{max}} \qquad (3.9)$$

The method of measuring gas holdup by quickly shutting off the valves and recording the subsequent liquid level in each isolated section is described in Appendix 8.2.2. As discussed there, the gas collected in each section is at a different pressure depending on the hydrostatic head above that section. Therefore suitable pressure corrections given by equations 8.2.29 and 8.2.30 were applied respectively to the gas collected in and below the experimental section, so as to obtain gas holdups in these sections at a standard pressure of 760 mm of mercury. For the gas holdup above the experimental section, no such correction factor is necessary. The quick valve shut-off measurements of gas holdups in this section under slug flow conditions were found to be unreliable due to the short length of the section, and were therefore discarded.

As shown in Appendix 8.2, the gas holdup in the three-phase fluidized bed region by the quick valve shut-off method is obtained from

$$\varepsilon_2''' = \varepsilon_2'' + [\varepsilon_{2EC} - \varepsilon_2'']\ L_E/L_b \qquad (8.2.33)$$

where ε_2'' is the gas holdup in the two-phase gas-liquid region

above the bed and is measured independently by a U-tube manometer located near the top of the experimental section. For low gas flow rates it was not possible to measure the liquid level in the transparent experimental section. In such instances a mean of gas holdups obtained from equations 3.8 and 3.9 is reported; otherwise, in all other cases, a mean of gas holdups by the two pressure drop methods and by the quick valve shut-off method is reported.

The gas holdup in the 20 mm glass column was measured mainly by observing the pressure drop across the bed on a U-tube manometer. Then the reduction in manometer reading on introduction of the gas corresponds to the gas fraction between the taps. No attempt was made to specifically calculate the gas fraction inside the three-phase region; nevertheless the gas holdup measured in this manner could reveal whether the presence of solid particles modified the two-phase gas-liquid holdup significantly.

CHAPTER 4

RESULTS AND DISCUSSION

In this chapter, the mathematical models derived in Chapter 2 are first compared with existing models and data from the literature, and then the experimental data obtained in this study are used to evaluate the proposed models.

4.1 Comparison of proposed mathematical models with previous work

4.1.1 Gas holdup in gas-liquid flow

Zuber and Findlay [39] derived equation 2.26, presented in Section 2.1.2, for two-phase gas-liquid flow; in combination with equation 2.24 it can be written as

$$\bar{v}_2 = \frac{\langle j_2 \rangle}{\langle \alpha_2 \rangle} = C_0(\langle j_1 + j_2 \rangle) + \frac{\langle \alpha_2 v_{2j} \rangle}{\langle \alpha_2 \rangle} \qquad (4.1)$$

Equation 4.1 is quite general and is applicable to all the gas-liquid flow regimes if the distribution parameter and the weighted mean drift velocity can be obtained independently.

The distribution parameter, C_0, was shown theoretically, with the help of equations 2.27a-c, to vary between 1.0 and

1.5 for most cases of gas-liquid flow. Using the data of Smissaert [113] for air-water flow in a 2 inch vertical pipe, Zuber and Findlay were also able to show empirically that for the churn-turbulent bubbly and slug flow regimes, C_0 was equal to 1.2. Nicklin et al. [114] used a different line of argument and also found a value of 1.2 for C_0 to satisfy a wide range of data for gas-liquid flow, if the Reynolds number based on the gas-liquid flux through the conduit exceeded 8,000.

For drift velocity, Zuber and Findlay proposed

$$v_{2j} = V_\infty (1 - \alpha_2)^m \tag{2.31}$$

where the exponent m was found to vary between 0 and 3, depending on the bubble size. It was further noticed that the local drift velocity was constant for both slug flow and bubbly flow in a turbulent stream (i.e., m = 0); then the weighted mean drift velocity is simply

$$\frac{\langle \alpha_2 v_{2j} \rangle}{\langle \alpha_2 \rangle} = 0.35 \sqrt{gD} \tag{4.2}$$

for the slug flow regime and

$$\frac{\langle \alpha_2 v_{2j} \rangle}{\langle \alpha_2 \rangle} = 1.53 \left[\frac{\sigma g}{\rho_1}\right]^{0.25} \tag{4.3}$$

for the churn-turbulent bubbly flow regime.

The present author has proposed a model for drift velocity in the bubble flow regime [76] which, as shown earlier, yields the equation

$$v_{2j} = V_\infty \sqrt{\tanh\ [0.25\ (1/\alpha_2)^{1/3}} \tag{2.37}$$

and which for the slug flow regime ($r_e = R$), applying equation 2.10 for large Eötvös number, simplifies to

$$v_{2j} = 0.35\ \sqrt{gD} \tag{2.39}$$

Thus for the slug flow regime the two models for drift velocity (equations 2.39 and 4.2) are identical, so that equation 4.1, with $C_0 = 1.2$, reduces to the slug flow relationship proposed by Nicklin [19]:

$$\frac{\langle j_2 \rangle}{\langle \alpha_2 \rangle} = 1.2\ (\langle j_1 + j_2 \rangle) + 0.35\ \sqrt{gD} \tag{4.4}$$

Various models for predicting the drift velocity in the bubble flow regime are shown in Figure 4.1, along with Happel's [49] equation for sedimentation of solid spheres. The following remarks are based on Figure 4.1:

(a) The discrepancy between the curves for bubble swarms and solid particles arises from the fact that the tangential liquid velocity is zero at the surface of

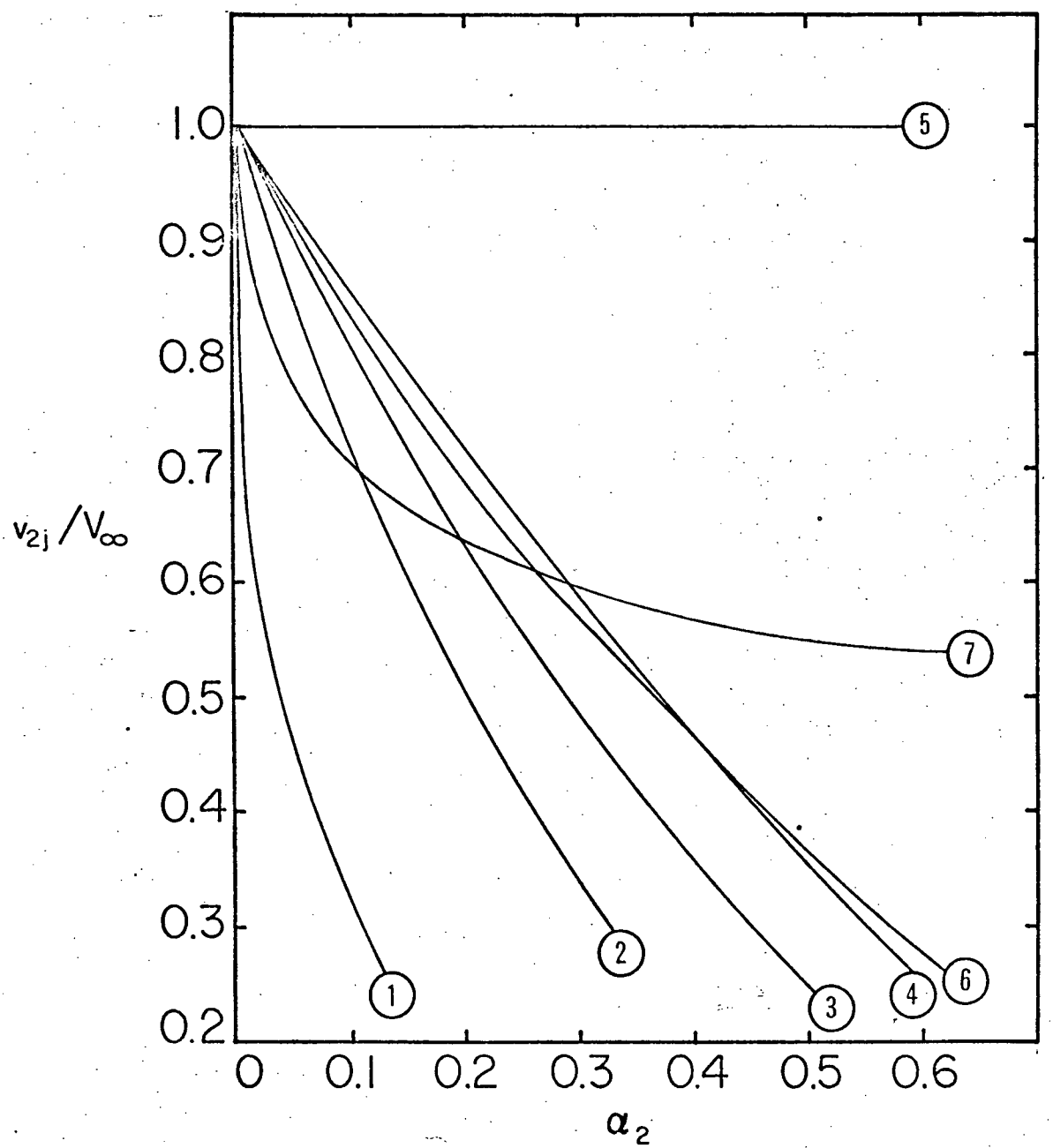

FIGURE 4.1 PROPOSED MODELS FOR DRIFT VELOCITY OF BUBBLE SWARMS

LEGEND FOR FIGURE 4.1

1. Sedimentation of solid particles by Happel's model.
2. Equation 2.31 with m = 3 for small bubbles (d_b < 0.5 mm) obeying Stokes law [74].
3. Equation 2.31 with m = 2 recommended for bubble flow regime by Bhaga [1].
4. Equation 2.31 with m = 1.5 for larger bubbles (1 < d_b < 20 mm) [74].
5. Equation 2.31 with m = 0 for churn turbulent-bubbly flow and slug flow regimes [39].
6. Equation 2.34 proposed for bubble flow regime by Marrucci [75].
7. Equation 2.37 proposed for bubble flow regime by Bhatia [76].

a solid particle but is not zero at the surface of a bubble. Consequently the energy dissipation is smaller and the drift velocity is higher for the bubble swarm.

(b) The model proposed by Marrucci [75] based on potential flow shows a dependence of drift velocity on volumetric gas fraction which is very similar to that of the Zuber-Findlay model with the exponent m equal to 1.5.

(c) The exponent m in the Zuber-Findlay model (equation 2.31) was reported to vary between 0 and 3, depending on the bubble size, the larger values corresponding to the smaller bubble sizes. The slope of the curve representing equation 2.37 shows a gradual reduction with increasing gas holdup. Since the stable bubble size and the gas holdup are interrelated, increases in the latter accompanying increases in the former, it can be argued at least qualitatively that the present model has the virtue of predicting the correct trend in drift velocity of a bubble swarm over a wide range of operating variables.

In order to test the quantitative applicability of the present model, a comparison of the predictions with some of the available literature data for bubble columns and for cocurrent gas-liquid flow in vertical pipes has been published by the present author [76] and is presented

in Appendix 8.8. It was found that:

(a) The model is applicable to low viscosity and comparatively pure gas-liquid systems.

(b) For bubble columns, the model satisfied the data obtained in small columns ($D \leq 2$ inch), systematic bulk circulation not being important in such columns [59, 60]. The systematic circulation found in columns with $D \geq 4$ inch [59, 60] would increase the bubble concentration in the upward moving central core, thereby reducing the average gas holdup and increasing the value of the distribution parameter, C_0, by making the flow and gas holdup profiles more pointed (as opposed to flat).

(c) For cocurrent flow the present model in conjunction with equation 2.20 for bubble diameter [69] agrees well with Hughmark's empirical correlation [52], which has been corroborated against experimental data by Dukler et al. [72].

In order to check the general validity of the above model for determining the drift velocity of a bubble swarm, systematic data for average bubble diameter and gas-holdup as a function of gas and liquid velocities are needed. The model, which strictly speaking applies only locally, should be supplemented by equation 4.1 to account for any radial non-uniformities in velocities and holdups.

4.1.2 Gas holdup in three-phase fluidized beds

Before a comparison of the general model for describing the rise velocity of bubble swarms in three-phase fluidized beds with the empirical correlations based on data of various investigators [14, 17, 79] can be attempted, it is necessary that a mathematical expression be obtained to predict the wake volume fraction. As defined earlier, the wake fraction in a three-phase fluidized bed is given by

$$\varepsilon_k = \varepsilon_2''' \left(\frac{\Omega_k}{\Omega_B}\right)''' \tag{4.5}$$

where the ratio of wake volume to bubble volume in the three-phase fluidized bed may be represented by

$$\left(\frac{\Omega_k}{\Omega_B}\right)''' = \left(\frac{\Omega_k}{\Omega_B}\right)'' f(\varepsilon) \tag{2.117}$$

f being a continuous function of bed voidage which approaches unity as the solids fraction, ε_3, in the three-phase fluidized bed approaches zero. The simplest such function is

$$f(\varepsilon) = (1-\varepsilon_3)^p \tag{4.6}$$

Combining equations 4.5, 2.117 and 4.6, the necessary mathematical expression for the wake fraction in a three-phase fluidized bed is given by

$$\varepsilon_k = \varepsilon_2''' \left(\frac{\Omega_k}{\Omega_B}\right)'' (1-\varepsilon_3)^p \qquad (4.7)$$

where $\left(\frac{\Omega_k}{\Omega_B}\right)''$ may be estimated from the data of Letan and Kehat [61] for a liquid-liquid system, as shown previously.

In order to evaluate the exponent p, simultaneous measurements of ε_k, ε_2''' and ε_3 are needed. Such measurements are scarce. Nevertheless Efremov and Vakhrushev [16] presented an equation for ε_k, based on measurements of ε_2''' and ε_3 in beds of glass beads (0.32 - 2.15 mm) fluidized by a cocurrent stream of air and water:

$$\left(\frac{\Omega_k}{\Omega_B}\right)''' = 5.1\ (\varepsilon_1'')^{4.85}\ [1-\tanh\ \{40\ \frac{\langle j_1\rangle}{\langle j_2\rangle}\ (\varepsilon_1'')^{10} - 3.32\ (\varepsilon_1'')^{5.45}\}\ ] \qquad (2.128)$$

where ε_1'' is the voidage in the liquid-solid fluidized bed before the introduction of gas and can be computed from equation 2.46. Tables 4.1 and 4.2 present the ratio of wake to bubble volume for two sizes of glass beads, fluidized by a cocurrent stream of air and water, as predicted by equations 4.7 (for p=3), 2.128 and 1.13, respectively, along with some limited data of Rigby and

TABLE 4.1

RATIO OF WAKE TO BUBBLE VOLUME IN

THREE-PHASE FLUIDIZED BED

PARTICLES - Glass beads (d_p=0.775 mm) ρ_3=2.67 gm/cm^3

D $\geq$ 4 inches

Liquid Flux, $\langle j_1 \rangle$ (cm/sec)	Gas Flux, $\langle j_2 \rangle$ (cm/sec)	(1) Ω_k/Ω_B [x_k=0.0]	(2) Ω_k/Ω_B [x_k=0.0]	(3) Ω_k/Ω_B [x_k=1.0]	(4) Ω_k/Ω_B [x_k=0.0]
2.61	0.5	0.689	0.541	2.26	0.72(1.80)*
	1.0	0.607	0.516	1.50	(1.08)*
	2.0	0.486	0.466	0.99	(0.73)*
	3.0	0.401	0.412	0.77	-
	4.0	0.337	0.367	0.65	-
4.35	0.5	1.127	1.483	4.19	-
	1.0	0.968	1.298	2.80	-
	2.0	0.745	0.899	1.85	-
	3.0	0.594	0.545	1.45	-
	4.0	0.483	0.298	1.22	-

(1) From generalized wake model, using equation 4.7 with p = 3

(2) Equation 2.128 by Efremov and Vakhrushev [16]

(3) Equations 1.12 and 1.13 by Østergaard [8]

(4) From Figure 2 of Rigby and Capes [80]

(*) Values in brackets are for x_k = 1.0

TABLE 4.2

RATIO OF WAKE TO BUBBLE VOLUME IN

THREE-PHASE FLUIDIZED BED

PARTICLES - Glass beads (d_p=2.0 mm) ρ_3 = 2.88 gm/cm^3

D = 2.0 inches

Liquid Flux, $\langle j_1 \rangle$ (cm/sec)	Gas Flux, $\langle j_2 \rangle$ (cm/sec)	(1) Ω_k/Ω_B [x_k=0.0]	(2) Ω_k/Ω_B [x_k=0.0]	(3) Ω_k/Ω_B [x_k=1.0]
3.38	0.5	0.364	0.154	0.827
	1.0	0.342	0.154	0.551
	2.0	0.301	0.152	0.364
	3.0	0.265	0.151	0.284
	4.0	0.231	0.150	0.238
	5.0	0.199	0.149	0.207
	6.0	0.166	0.148	0.184
	7.0	0.131	0.147	0.167
	8.0	0.129	0.146	0.153
	9.0	0.128	0.145	0.142
8.51	0.5	0.99	1.02	6.77
	1.0	0.91	0.99	4.55
	2.0	0.76	0.92	3.04
	3.0	0.63	0.85	2.40
	4.0	0.52	0.78	2.02
	5.0	0.41	0.71	1.77
	6.0	0.31	0.64	1.59
	7.0	0.31	0.57	1.44
	8.0	0.30	0.50	1.33
	9.0	0.29	0.44	1.24

(1) From generalized wake model, using equation 4.7 with p=3.

(2) Equation 2.128 by Efremov and Vakhrushev [16].

(3) Equation 1.13 by Østergaard [8].

Capes [80]. A comparison of these values reveal that:

(a) The values predicted by equation 4.7 with p=3 show moderate agreement with the equation of Efremov and Vakhrushev [16] and the data of Rigby and Capes [80]. The wake was assumed to be free of solids in the generalized wake model in order to match the assumption inherent in the equation of Efremov and Vakhrushev.

(b) The values predicted by Østergaard's [8] equation are generally higher than those by the other two equations; this discrepancy is partially due to Østergaard's assumption that the concentration of solid particles in the wake is equal to the concentration in the particulate phase.

The agreement of predictions by equations 4.7 with those by equation 2.128 was found to improve by assuming different values of the exponent p for different operating conditions. However, a value of 3 for the exponent gave a rough agreement with all available information, but is not to be interpreted as either the best or the universally recommended value. Only a systematic investigation of wakes behind bubbles in three-phase fluidized beds, with simultaneous measurements of gas and solids holdups, could provide a justifiable correlation. Nevertheless, in the absence of suitable data for wake volume fraction, equation 4.7, with p=3, will be used in the generalized wake model of Section

2.32 for the purpose of comparing its predictions of gas and solids holdups with experimental data. It will be seen that in many instances the predictions are insensitive to the wake fraction and hence to the function $f(\varepsilon)$ in equation 2.117. The more complex equation 2.128 will be used simultaneously to provide guidelines within its range of applicability.

Now, according to the model proposed in Section 2.3.2, the rise velocity of a bubble swarm in a three-phase fluidized bed is given by

$$\bar{v}_2 = \frac{C_0''' \langle j_1+j_2 \rangle}{\varepsilon} + \frac{\varepsilon_{1f}''(1-\varepsilon_2-\varepsilon_k)}{\varepsilon} \bar{v}_{21}''' \qquad (2.114)$$

where $\bar{v}_{21}'''$ is calculated from equation 2.107 for $D \geq 4$ inches and from equation 2.108a for $D < 4$ inches. Since the value of the distribution parameter in three-phase fluidized beds, C_0''', cannot be estimated at present, therefore, in all the calculations and discussions which follow, it will be tacitly assumed that $C_0''' = 1.0$ and that the effects of non-uniform radial profiles can be lumped into the relative velocity term, as has been done in the past for gas-liquid flow [19]. The gas holdup is then obtained from

$$\varepsilon_2 = \langle j_2 \rangle / \bar{v}_2 \qquad (2.94)$$

Tables 4.3-A and 4.3-B present the values of $\varepsilon_2'''/\varepsilon_2''$ and $\bar{v}_2$, respectively, predicted by the present generalized wake model [equations 2.114, 2.107 and 2.94] for 0.775 mm glass beads fluidized by a cocurrent stream of air and water [80], along with the values calculated from the empirical correlations presented in Section 2.3.2. An estimate of bubble length was obtained from the data of Rigby et al. [79] ($l \simeq 0.61$ cm; then from equation 2.125, $r_e \simeq 0.6$ cm) and was used for calculations in the present model as well as in the correlation proposed by Rigby and Capes [80]. Equation 2.107 was used for calculating the relative velocity of a bubble swarm in the model because the empirical correlations presented in Tables 4.3-A and -B were all based on data obtained in columns of $D \geq 4$ inch. On comparing the predictions from the model with those from the correlations in Table 4.3-A, it can be seen that:

(a) The predictions from the model are in reasonable agreement with the results of Efremov and Vakhrushev [16], who were forced to limit their measurements to low gas velocities because of the uncertainty of locating the three-phase boundary at high-gas flow rates, especially for large bed expansions.

(b) Although the correlation reported by Michelsen and Østergaard is also based on data for low gas velocities, it too is found to give results which are in fairly good agreement with the predictions of the model.

TABLE 4.3-A

RATIO OF GAS HOLDUP IN THREE-PHASE FLUIDIZED BED TO GAS HOLDUP IN TWO-PHASE GAS-LIQUID FLOW (D $\geq$ 4 INCHES)

PARTICLES - Glass beads (d_p = 0.775 mm) ρ_3 = 2.67 gm/cm^3

Liquid Flux, $\langle j_1 \rangle$ (cm/sec)	Gas Flux $\langle j_2 \rangle$ (cm/sec)	(1) $\varepsilon_2'''/\varepsilon_2''$	(2) $\varepsilon_2'''/\varepsilon_2''$	(3) $\varepsilon_2'''/\varepsilon_2''$	(4) $\varepsilon_2'''/\varepsilon_2''$
2.61	0.5	0.602	0.542	0.556	0.340
	1.0	0.596	0.542	0.576	0.327
	2.0	0.587	0.542	0.567	0.311
	3.0	0.581	0.542	0.533	0.302
	4.0	0.579	0.542	0.546	0.299
4.35	0.5	0.716	0.632	0.734	0.482
	1.0	0.716	0.632	0.734	0.482
	2.0	0.696	0.632	0.505	0.432
	3.0	0.689	0.632	0.452	0.418
	4.0	0.687	0.632	0.419	0.414

(1) From generalized wake model with $x_k = 0$

(2) From equation of Efremov and Vakhrushev [16]

(3) From equations 2.121 and 2.122, Michelsen and Østergaard [14]

(4) From equation 2.120, Vail et al. [17]

TABLE 4.3-B

RISE VELOCITY OF BUBBLE SWARMS IN THREE-PHASE FLUIDIZED BED (D $\geq$ 4 INCHES)

PARTICLES - Glass beads (d_p = 0.775 mm) ρ_3 = 2.67 gm/cm^3

Liquid Flux, $\langle j_1 \rangle$ (cm/sec)	Gas Flux, $\langle j_2 \rangle$ (cm/sec)	(1) $\bar{v}_2$, cm/sec [r_e=0.6 cm]	(2) $\bar{v}_2$	(3) $\bar{v}_2$	(4) $\bar{v}_2$	(5) $\bar{v}_2$ [l=0.612 cm]
2.61	0.5	50.24	27.50	50.00	52.05	36.65
	1.0	52.51	24.31	52.63	62.85	34.43
	2.0	56.90	21.12	58.82	77.05	32.04
	3.0	61.04	19.26	61.22	86.82	31.28
	4.0	64.88	17.93	66.67	93.71	31.55
4.35	0.5	44.72	29.24	45.30	54.65	92.67
	1.0	46.74	26.05	52.77	66.70	81.09
	2.0	50.62	22.86	61.46	82.72	73.78
	3.0	54.20	21.00	67.19	93.47	64.61
	4.0	57.40	19.67	71.59	100.54	64.11

(1) From generalized wake model with x_k = 0

(2) From equation 1.12, Østergaard [8]

(3) From equations 2.121 and 2.94, Michelsen and Østergaard [14]

(4) From equations 2.118 and 2.94, Vail et al. [17]

(5) From equation 2.123, Capes et al. [79]

(c) The predictions from the model are consistently higher than the results of Vail et al. [17]. This discrepancy could be partially due to the approximate method used by Vail et al. to measure the solids holdup and partially due to their method for measuring the gas holdup itself (see Appendix 8.2).

Table 4.3-B presents the rise velocities of bubble swarms calculated from various empirical correlations. A comparison of these values with the predictions from the generalized wake model reveals that:

(a) The original Østergaard correlation for estimating the rise velocity of a bubble swarm, equation 1.12, gives values which are far out of line from those given by the other correlations as well as from the model. The correlation proposed later by Michelsen and Østergaard [14], on the other hand, gives values which are in good agreement with the predictions from the model.

(b) The bubble rise velocities calculated from the correlation proposed by Vail et al. [17] are found to be larger than those predicted by the model, though the two exhibit similar trends with respect to increase in gas velocity.

(c) The values calculated from the correlation proposed by Rigby and co-workers [79] show no similarities with those of the model. At the smaller liquid flux the bubble velocities are smaller, whereas at the larger

liquid flux the bubble velocities are much larger, than predicted by the model. However, it is important to notice that the correlation of Rigby et al. (equation 2.123) is quite sensitive to the length of bubbles in the swarm. Since only limited data for bubble lengths are available [79], a fair comparison of equation 2.123 with the other correlations as well as with the model is not possible at present.

Since the model proposed here is used later to test the 2 inch diameter column data obtained in the present study, an attempt is first made to compare the predictions of the model with data obtained from 2 inch diameter columns by earlier investigators. Although the bed voidage data for the 2 inch columns are available, no such data for gas hold-up are reported. Therefore the bed voidage data of Østergaard and Theisen [18], for 2 mm glass beads fluidized by a cocurrent stream of air and water in a 2 inch column, are used as a basis for obtaining the values of $\varepsilon_2'''/\varepsilon_2''$ and $\bar{v}_2$ from empirical correlations. For the model the relative velocity is obtained from equation 2.108a, where the drift velocity for the slug flow regime is obtained by modifying equation 2.39 to account for non-uniformities in radial profiles, following the recommendation of Nicklin [19]:

$$v_{2j} = 0.2 \langle j_1 + j_2 \rangle + 0.35 \sqrt{gD} \qquad (4.8)$$

The calculated values are presented in Tables 4.4-A and 4.4-B.

A comparison of various values of $\varepsilon_2'''/\varepsilon_2''$ in Table 4.4-A reveals that:

(a) The predictions from the model are in fairly good agreement with the results of Efremov and Vakhrushev [16] for small liquid velocity, becoming poorer as the liquid velocity is increased.

(b) The predictions from the model agree with the results of Vail et al. [17] only in their respective trends, but not in absolute values.

(c) The predictions from the model do not agree with the values calculated from the Michelsen-Østergaard [14] correlation, either absolutely or in trends displayed.

Similarly a comparison of rise velocities of bubble swarms in three-phase fluidized beds (Table 4.4-B) reveals that:

(a) The correlation proposed by Østergaard [8], equation 1.12, provides a poor estimate for the bubble rise velocity, if one gives any credence at all to the empirical correlations of references [14] and [17]. The correlation proposed later by Michelsen and Østergaard [14] gives moderate agreement with the predictions from the model.

(b) The bubble rise velocities calculated from the correlation proposed by Vail et al. [17] do not agree with the predictions from the model.

TABLE 4.4-A

RATIO OF GAS HOLDUP IN THREE-PHASE FLUIDIZED BED TO GAS HOLDUP IN TWO-PHASE GAS-LIQUID FLOW (D = 2 INCHES)

PARTICLES - Glass beads (d_p = 2.0 mm) ρ_3 = 2.88 gm/cc

Liquid Flux, $\langle j_1 \rangle$ (cm/sec)	Gas Flux, $\langle j_2 \rangle$ (cm/sec)	(1) $\varepsilon_2'''/\varepsilon_2''$	(2) $\varepsilon_2'''/\varepsilon_2''$	(3) $\varepsilon_2'''/\varepsilon_2''$	(4) $\varepsilon_2'''/\varepsilon_2''$
3.38	0.5	0.471	0.436	0.216	0.645
	1.0	0.485	0.436	0.216	0.532
	2.0	0.484	0.436	0.218	0.442
	3.0	0.495	0.436	0.220	0.396
	4.0	0.504	0.436	0.225	0.366
	5.0	0.507	0.436	0.232	0.345
	6.0	0.515	0.436	0.241	0.328
	7.0	0.532	0.436	0.253	0.315
	8.0	0.531	0.436	0.257	0.304
	9.0	0.535	0.436	0.260	0.294
8.51	0.5	0.714	0.560	0.436	1.044
	1.0	0.679	0.560	0.433	0.868
	2.0	0.685	0.560	0.430	0.720
	3.0	0.705	0.560	0.433	0.650
	4.0	0.703	0.560	0.440	0.597
	5.0	0.713	0.560	0.455	0.562
	6.0	0.720	0.560	0.472	0.535
	7.0	0.728	0.560	0.475	0.514
	8.0	0.733	0.560	0.479	0.495
	9.0	0.741	0.560	0.482	0.480

(1) From generalized wake model with $x_k = 0$

(2) From empirical equation of Efremov and Vakhrushev [16]

(3) From equation 2.120, Vail et al. [17]

(4) From equations 2.121 and 2.122, Michelsen and Østergaard [14]

TABLE 4.4-B

RISE VELOCITY OF BUBBLE SWARMS IN THREE-PHASE FLUIDIZED BED (D = 2 INCHES)

PARTICLES - Glass beads (d_p = 2.0 mm) ρ_3 = 2.88 gm/cc

Liquid Flux, $\langle j_1 \rangle$ (cm/sec	Gas Flux, $\langle j_2 \rangle$ (cm/sec)	(1) $\bar{v}_2$ (cm/sec)	(2) $\bar{v}_2$	(3) $\bar{v}_2$	(4) $\bar{v}_2$
3.38	0.5	60.84	28.27	49.74	100.2
	1.0	61.80	25.08	57.93	116.7
	2.0	63.66	21.89	67.47	134.6
	3.0	65.40	20.03	73.77	146.0
	4.0	67.00	18.70	78.59	152.0
	5.0	68.36	17.68	82.54	154.8
	6.0	69.48	16.84	85.92	155.1
	7.0	70.26	16.13	88.89	152.8
	8.0	71.87	15.52	91.54	155.0
	9.0	73.54	14.97	93.94	157.1
8.51	0.5	52.26	33.40	35.46	106.1
	1.0	52.88	30.21	41.17	119.6
	2.0	54.11	27.02	47.95	140.3
	3.0	55.28	25.16	52.42	152.3
	4.0	56.36	23.83	55.85	160.0
	5.0	57.32	22.81	58.66	162.2
	6.0	58.21	21.97	61.06	162.7
	7.0	59.38	21.26	63.16	167.3
	8.0	60.57	20.65	65.05	170.8
	9.0	61.79	20.10	66.75	174.2

(1) From generalized wake model with $x_k = 0$

(2) From equation 1.12, Østergaard [8]

(3) From equations 2.121 and 2.94, Michelsen and Østergaard [14]

(4) From equations 2.118 and 2.94, Vail et al [17]

Thus it can now be tentatively concluded that the present model, when used with a suitable correlation for the relative velocity of bubble swarms in three-phase fluidized beds, provides an effective method for estimating the gas holdups and bubble rise velocities in three-phase fluidization, since the predictions from the model generally agree with the available correlations of data from columns of $D \geq 4$ inches [14, 16]. Since the bubble dynamics for gas-liquid flow in small columns ($D < 4$ inch) differ markedly from those in larger ones [59, 60, 68], no single correlation can be successfully used for all column sizes unless these dynamics are properly accounted for. The present model does so by allowing a separate correlation for the relative velocity of bubble swarms to be used for small diameter columns than for large columns.

4.1.3 Voidage in three-phase fluidized beds

The measurement of voidage in three-phase fluidized beds has been carried out by various investigators, of whom Østergaard and co-workers [8, 14, 18, 54] and Efremov and Vakhrushev [16] are most noteworthy because of the wide range of particle sizes which they investigated. Most of these measurements were obtained in columns with diameter $D \geq 4$ inches; we note, however, that Østergaard and Theisen [18] reported on limited data obtained in a 2 inch diameter column.

The number of theoretical analyses attempted for predicting the voidage in a three-phase fluidized bed has been limited. The wake model proposed by Østergaard [18] and presented in Chapter 1 was the first successful analysis to satisfy the reported paradox [6, 9] of bed contraction in three-phase fluidization. However this model failed to satisfy the extensive data of Østergaard and Theisen [18] quantitatively. Efremov and Vakhrushev [16] then proposed and derived a model quite similar to the wake model but with the assumption that the particle content of bubble wakes was zero. From simultaneous measurements of gas and solid holdups, the wake fraction in a three-phase fluidized bed was calculated from equations 2.126 - 2.127. The wake fractions so calculated were found to be adequately represented by equation 2.128.

Efremov and Vakhrushev then tested the applicability of equations 2.126 - 2.128 for predicting the data of Østergaard and Theisen [18], and reported a satisfactory agreement. Michelsen and Østergaard [14], in a later study of three-phase fluidization of 1, 3 and 6 mm glass beads in a 6 inch diameter column, reported data on bed voidage and gas holdup for a wider range of operating variables ($<j_1>$ up to 26.0 cm/sec and $<j_2>$ up to 15.0 cm/sec). These data have not been tested hitherto by any of the theoretical analyses. Therefore the generalized wake model derived in Section 2.3, which assumes various possible solids contents of the wake with consequent circulation of solids in the particulate phase, will now be compared with the data of Michelsen and Østergaard [14] and the model of Efremov and Vakhrushev [16].

It is important to note at the outset that the generalized wake model with $x_k = 0.0$ is, in essence, identical to the model formulated by Efremov and Vakhrushev [16], differing only in the exact expressions used to calculate the rise velocity of a bubble swarm and the wake fraction in a three-phase fluidized bed. From a comparison of the models with respect to these two quantities in the preceding section, it was found that

(i) the rise velocity of a bubble swarm calculated from the generalized wake model is in general smaller than predicted by the Efremov-Vakhrushev equations, and

(ii) the ratio of wake fraction to gas fraction predicted by the generalized wake model with $x_k = 0$ shows a scattered agreement with equation 2.128 of Efremov and Vakhrushev. The full comparison is summarized in Table 4.5.

Michelsen and Østergaard [14], who used two independent techniques (residence time distribution by tracer studies and pressure drop measurement) to measure the gas holdup in a three-phase fluidized bed, found the techniques to give results that differed widely, especially for beds of large particles. Hence, since no agreement is found for the predicted values of rise velocities of bubble swarms from the generalized wake model with those from the Efremov-Vakhrushev equations, and since the measurements of gas holdup by Michelsen and Østergaard are uncertain, a comparison between measured and predicted values is made for liquid fraction, ε_1, rather than for bed voidage, $\varepsilon(=\varepsilon_1+\varepsilon_2)$. Predictions by the generalized wake model are compared here with those by the Efremov-Vakhrushev equations, as well as with the experimental data of Michelsen and Østergaard.

Another special case of the generalized wake model is realized by assuming the wake volume fraction, ε_k, to be insignificant and negligible. In that case equation 2.106 simplifies to

TABLE 4.5

DEGREE OF AGREEMENT BETWEEN EQUATIONS 4.7 AND 2.128 FOR PREDICTING RATIO OF WAKE FRACTION TO GAS FRACTION IN A THREE-PHASE FLUIDIZED BED

Particle Size / Bed Expansion	Large (d_p>3mm)	Medium (1<d_p<3mm)	Small (d_p<1mm)
High ($\varepsilon > 0.8$)	adequate agreement at all gas flow rates	poor agreement at all gas flow rates	worst agreement at all gas flow rates
Medium (0.6<ε<0.8)	excellent agreement at all gas flow rates	adequate agreement up to $j_2 \simeq 10$ cm/sec	poor agreement at all gas flow rates
Low (0.4<ε<0.6)	favorable agreement at all gas flow rates	favorable agreement at all gas flow rates	adequate agreement up to $j_2 \simeq 10$ cm/sec

$$\varepsilon''_{lf} = \left[\frac{\langle j_l \rangle}{V_\infty (1-\varepsilon'''_2)} \right]^{1/n}$$

which, when substituted into equation 2.91, gives the bed voidage as

$$\varepsilon = (1-\varepsilon'''_2) \left[\frac{\langle j_l \rangle}{V_\infty (1-\varepsilon'''_2)} \right]^{1/n} + \varepsilon'''_2 \qquad (4.9)$$

Equation 4.9 is identical to equation 2.62 derived in Section 2.3.1 for the gas-free model. Thus for a three-phase fluidized bed, if ε_k is small, the generalized wake model approaches the gas-free model.

Before any comparisons could be attempted it was necessary to find a correlation which could satisfactorily represent the bed voidage for liquid-solid fluidization. As shown in Table 4.6, the Neuzil-Hrdina correlation (equation 2.51)predicts the data much more satisfactorily than does the Richardson-Zaki correlation (equation 2.46), even though the data of Michelsen and Østergaard are outside the recommended range of applicability of the former. It is of interest to point out too that the bed expansion data for 3 and 6 mm glass beads ($Re_p > 1000$) also agree well with the predictions of Trupp [87], thereby supporting the hypothesis that turbulence may affect the bed expansion behaviour of a liquid-solid fluidized bed. The empirical correlation (equation 2.51) recommended by Neuzil and Hrdina

TABLE 4.6

COMPARISON OF MEASURED AND PREDICTED BED VOIDAGES FOR LIQUID-SOLID FLUIDIZATION

Particle Diameter (mm)	Liquid Flux $\langle j_l \rangle$ (cm/sec)	(1) ε	(2) ε	(3) ε	(4) ε
1.25 (ρ_3=2.67 $\frac{gm}{cm^3}$)	3.0	0.575	0.487	0.552	-
	4.2	0.645	0.555	0.625	-
	5.4	0.705	0.612	0.685	-
	6.6	0.750	0.662	0.739	-
	7.8	0.810	0.706	0.786	-
	9.0	0.850	0.747	0.829	-
2.95 (ρ_3=2.45 $\frac{gm}{cm^3}$)	6.6	0.570	0.494	0.579	0.563
	8.4	0.630	0.546	0.633	0.626
	11.0	0.700	0.611	0.699	0.704
	14.0	0.770	0.676	0.764	0.783
	16.0	0.805	0.715	0.803	0.830
5.93 (ρ_3=2.63 $\frac{gm}{cm^3}$)	10.0	0.580	0.495	0.577	0.547
	14.0	0.646	0.570	0.653	0.634
	20.0	0.776	0.662	0.746	0.741
	26.0	0.833	0.739	0.822	0.832

(1) Measurements by Michelsen and Østergaard [14]
(2) Equation 2.46 by Richardson and Zaki [2]
(3) Equation 2.51 by Neuzil and Hrdina [47]
(4) Dimensional correlation proposed by Trupp [87]

[47] will, nevertheless, be used to describe the bed expansion characteristics of all particle sizes in the particulate phase of a three-phase fluidized bed. Thus for calculations of ε_l''' from the generalized wake model it is assumed that

(a) the relative velocity of bubble swarms is represented by equation 2.107 (since all the data reported in references 14 and 16 were obtained in columns of $D \geq 4$ in), and

(b) the voidage in the particulate phase is represented by the Neuzil-Hrdina correlation (equation 2.51).

It is worth noting that since the voidage in the particulate phase, for $x_k = 0.0$, is given by

$$\varepsilon_{lf}'' = \left[\frac{\langle j_l \rangle - \bar{v}_2 \, \varepsilon_k}{V_\infty (1-\varepsilon_2-\varepsilon_k)} \right]^{1/2} \qquad (2.106\text{-a})$$

and since the liquid fraction in a three-phase fluidized bed is given by

$$\varepsilon_l''' = \varepsilon_{lf}'' \, (1-\varepsilon_2-\varepsilon_k) + \varepsilon_k \qquad (2.91\text{-a})$$

then for determining ε_l''' accurately, ε_{lf}'' should be calculable accurately (as normally $\varepsilon_{lf}'' > \varepsilon_k$, and both ε_2 and ε_k are very much smaller than unity), and for determining ε_{lf}''

accurately, the product $\bar{v}_2\ \varepsilon_k$ need be known accurately. An overestimate of ε_k would result from an underestimate of $\bar{v}_2$ (as in Østergaard's equations), while an underestimate of ε_k would conversely result from an overestimate of $\bar{v}_2$ (as in the Efremov-Vakhrushev equations).

The predicted values of liquid fraction in a three-phase fluidized bed calculated from the generalized wake model for $x_k = 0.0$ and from the gas-free model for the larger particles, are shown in Figures 4.2-4.4, along with the data of Michelsen and Østergaard [14] and the predicted values from the equations of Efremov and Vakhrushev [16] and of Østergaard [8]. Some results are also presented in Tables 4.7 and 4.8.

Beds of 6 mm particles (Figures 4.2a, b and Table 4.7)

The data of Michelsen and Østergaard show that the liquid holdup reduces gradually as the gas velocity is increased. The predictions from the model for $\langle j_1 \rangle = 20$ cm/sec show excellent agreement with the data up to $\langle j_2 \rangle \simeq 6$ cm/sec, and then only an agreement in trend for $j_2 > 8$ cm/sec, whereas the predictions from the Efremov-Vakhrushev equations show only an agreement in trend with the data up to $\langle j_2 \rangle = 7$ cm/sec, and no agreement for $j_2 > 8$ cm/sec. The predictions from Østergaard's model are at best qualitative up to $\langle j_2 \rangle = 3$ cm/sec. The discrepancy between the predictions of the

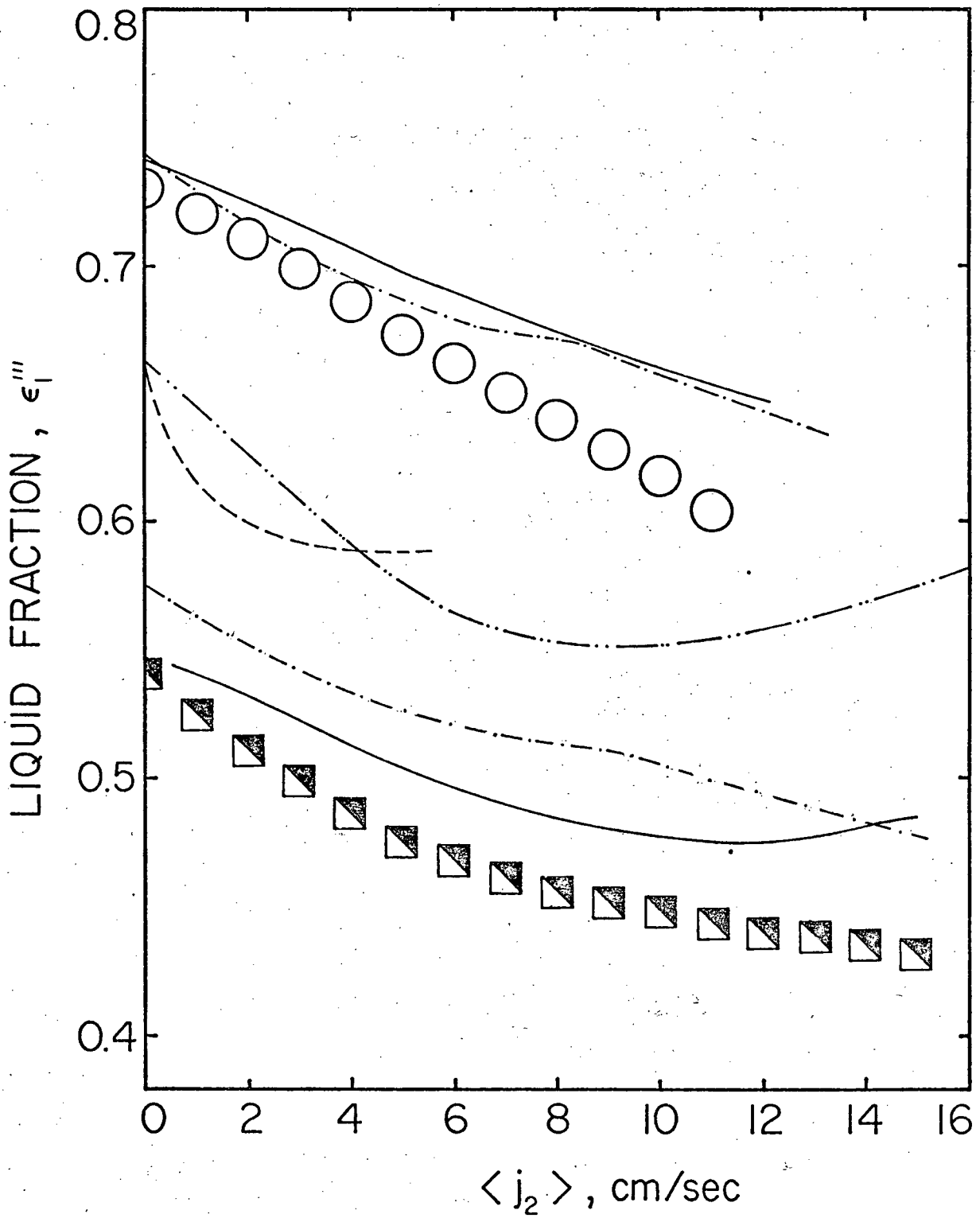

FIGURE 4.2a LIQUID FRACTION DATA OF MICHELSEN AND ØSTERGAARD [14] FOR 6 MM GLASS BEADS (○ -j_1=20.0; ◪ -j_1= 10.0; —·—·— generalized wake model with x_k = 0; —··—··—Efremov-Vakhrushev equations 2.126 - 2.128, for j_1 = 20.0; – – – – Østergaard's equations, for j_1 = 20.0; ——— gas-free model)

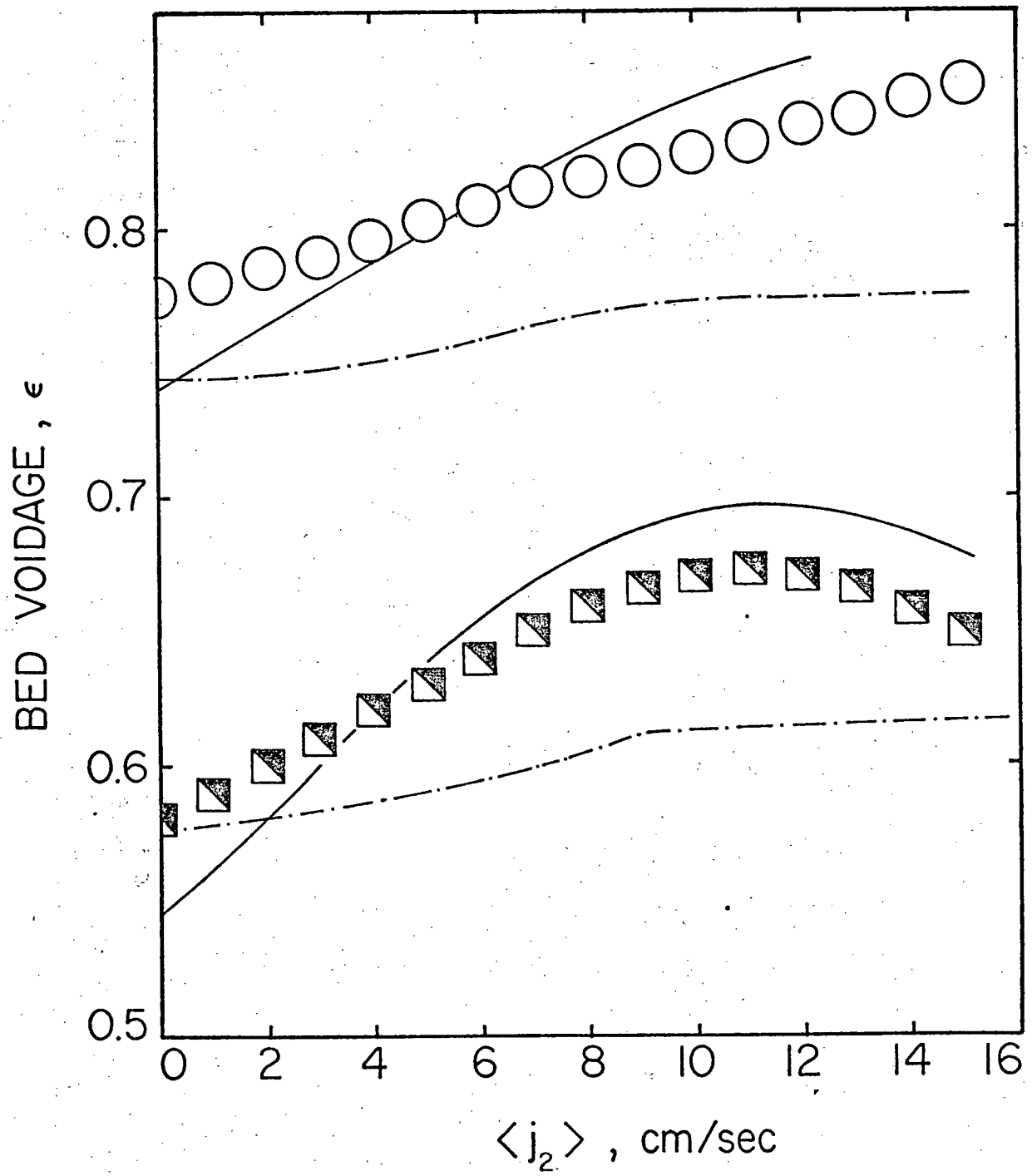

FIGURE 4.2b BED VOIDAGE DATA OF MICHELSEN AND ØSTERGAARD [14] FOR 6 MM GLASS BEADS (▨ -j_1=20.0; ○ -j_1= 10.0; —·—·— generalized wake model with x_k=0; ——— gas-free model)

TABLE 4.7

COMPARISON OF MEASURED AND PREDICTED GAS AND LIQUID FRACTIONS IN THREE-PHASE FLUIDIZED BEDS

d_p = 5.93 mm, ρ_3 = 2.63 gm/cc, $\langle j_1 \rangle$ = 20.0 cm/sec, D = 6.0 inch

Gas Flux, $\langle j_2 \rangle$ (cm/sec)	Measured (1)		Predicted (2)			Predicted (3)			Predicted (4)			Predicted (5)	
	ε_1'''	ε_2'''	$\varepsilon_k/\varepsilon_2'''$	ε_1'''	ε_2'''	$\varepsilon_k/\varepsilon_2'''$	ε_1'''	ε_2'''	$\varepsilon_k/\varepsilon_2'''$	ε_1'''	ε_2'''	ε_1'''	$\varepsilon = \varepsilon_1'' + \varepsilon_2''$
0.0	0.730	-	-	0.662	-	-	0.744	-	-	0.662	-	0.741	0.741
1.0	0.720	0.018	1.827	0.644	0.011	1.282	0.730	0.015	12.95	0.615	0.024	0.734	0.752
2.0	0.710	0.040	1.729	0.625	0.018	1.135	0.716	0.030	8.80	0.601	0.052	0.725	0.765
3.0	0.698	0.060	1.622	0.607	0.025	1.000	0.705	0.043	7.01	0.592	0.082	0.716	0.776
4.0	0.685	0.080	1.507	0.590	0.030	0.875	0.695	0.056	5.96	0.587	0.113	0.707	0.787
5.0	0.673	0.100	1.386	0.576	0.036	0.758	0.687	0.067	5.25	0.588	0.146	0.699	0.799
6.0	0.662	0.120	1.262	0.564	0.041	0.650	0.680	0.078	-	-	-	0.690	0.810
7.0	0.650	0.138	1.136	0.556	0.045	0.547	0.675	0.088	-	-	-	0.682	0.820
8.0	0.639	0.156	1.012	0.551	0.050	0.450	0.672	0.098	-	-	-	0.674	0.830
9.0	0.628	0.172	0.893	0.550	0.054	0.422	0.665	0.107	-	-	-	0.667	0.839
10.0	0.617	0.190	0.779	0.551	0.058	0.416	0.658	0.115	-	-	-	0.659	0.849
11.0	0.604	0.200	0.674	0.554	0.062	0.409	0.651	0.123	-	-	-	0.654	0.854
12.0	-	0.214	0.578	0.558	0.066	0.403	0.644	0.131	-	-	-	0.648	0.862
13.0	-	-	0.492	0.563	0.070	0.397	0.637	0.138	-	-	-	-	-
14.0	-	-	0.416	0.568	0.073	0.391	0.630	0.145	-	-	-	-	-
15.0	-	-	0.349	0.574	0.077	0.386	0.624	0.151	-	-	-	-	-

(1) Measurements by Michelsen and Østergaard [14]

(2) From equations 2.126 and 2.128, Efremov and Vakhrushev [16]

(3) From generalized wake model

(4) From equations 1.10 - 1.13, Østergaard [8]

(5) From gas-free model, equation 4.11, using the values of ε_2''' measured by Michelsen and Østergaard

generalized wake model and the Efremov-Vakhrushev equations arises, in part, from overestimation of $\bar{v}_2$ (due to underestimation of ε_2) by the latter, the estimates of ε_k by these two methods being in reasonable agreement with each other.

However, if it is assumed that the role of bubble wakes is insignificant, the gas-free model can be used for calculating the liquid fraction by substituting Trupp's dimensional equation for ε''_{1f} into equation 2.60:

$$\varepsilon'''_1 = (1-\varepsilon'''_2) \left[\frac{\langle j_1 \rangle}{0.36\ V_\infty^{1.18} (1-\varepsilon'''_2)} \right]^{1/2.28} \qquad (4.11)$$

and the bed voidage from

$$\varepsilon = \varepsilon'''_1 + \varepsilon'''_2 \qquad (1.3)$$

The liquid fractions calculated from equation 4.11, using the gas holdup data as reported by Michelsen and Østergaard [14], are presented in Table 4.7 and also shown in Figure 4.2a. These values of liquid fraction appear to be in as good agreement with the experimental values as those calculated from the generalized wake model. The values of bed voidage calculated from the gas-free model (equations 4.11 and 2.91) are presented in Figure 4.2b and also show only small percentage deviations from the experimental values [14].

Thus for fluidized beds of 6 mm particles the role of bubble wakes appears to be insignificant and the bed voidage can be well represented by the simple gas-free model.

Beds of 3 mm particles (Figures 4.3a,b)

The data of Michelsen and Østergaard [14] for liquid fraction in three-phase fluidized beds show excellent agreement with the predicted values from the generalized wake model, particularly if the parameter x_k is suitably adjusted. On the other hand, the overall void fraction, especially at $\langle j_l \rangle$ = 14.0 cm/sec, shows poor agreement with the predictions from the model. This discrepancy is caused by the predicted gas holdup being considerably smaller at the higher liquid flux and considerably larger at the lower liquid flux than the measured values reported by Michelsen and Østergaard. They observed the bubble behaviour for liquid flux below 7 cm/sec to be markedly different than that for higher liquid fluxes. Since in calculating the liquid fraction from the generalized wake model it was assumed that the relative velocity for all gas fluxes is well represented by equation 2.107 with r_e = 6 mm [79], the discrepancy from the measured values is not entirely unexpected. To improve the predictions it would be necessary to obtain a relationship for describing the average diameter of bubbles in the swarm as a function of

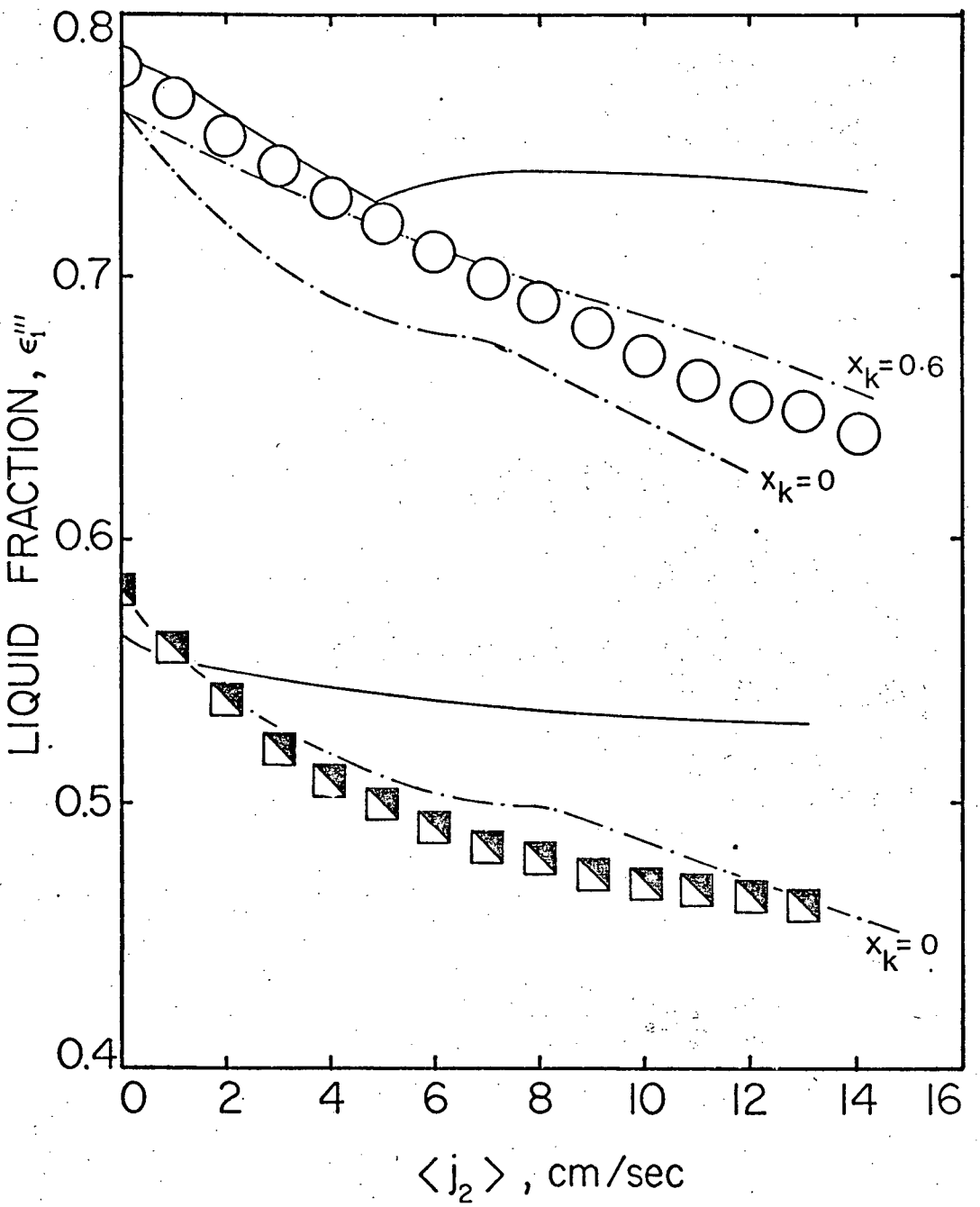

FIGURE 4.3a LIQUID FRACTION DATA OF MICHELSEN AND ØSTERGAARD [14] FOR 3 MM GLASS BEADS (o -j_1=14.0; ◙ -j_1=6.6; -·-·- generalized wake model; ——— gas-free model)

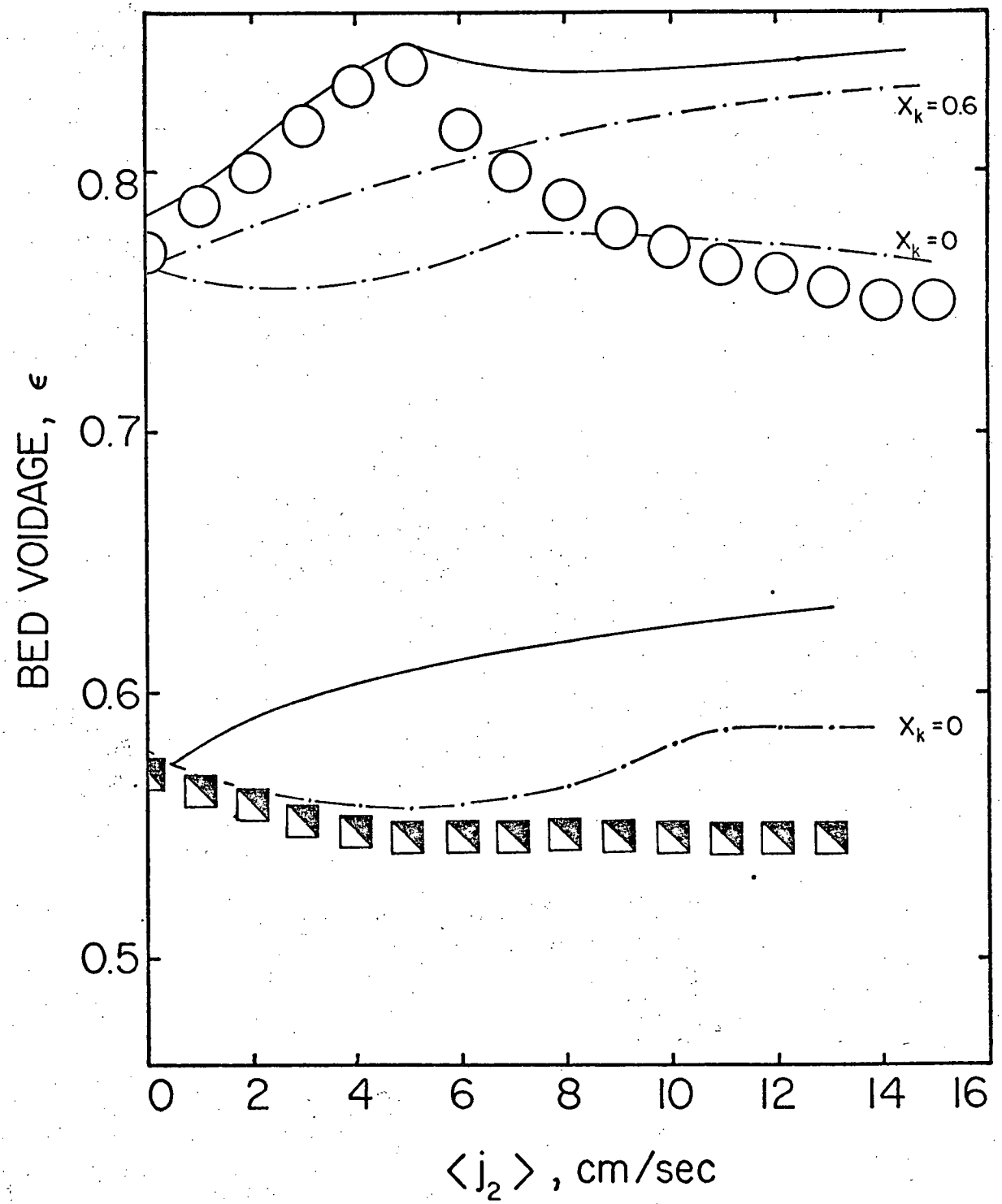

FIGURE 4.3b BED VOIDAGE DATA OF MICHELSEN AND ØSTERGAARD [14] FOR 3 MM GLASS BEADS (○ -j_1=14.0; ◪ -j_1=6.6; ←·—·— generalized wake model; ——— gas-free model)

gas and liquid fluxes and particle properties.

However, if it is assumed again that the role of bubble wakes is insignificant, the gas-free model can be used for describing the bed behaviour. Thus for the liquid flow rate of 14.0 cm/sec, the liquid fractions calculated from equation 4.11, using the measured values of gas holdup [14], are shown in Figure 4.3a. These values are found to be in good agreement with the experimental values up to a gas flow rate of 5.0 cm/sec, the agreement becoming poorer for larger gas flow rates. The values of bed voidage, calculated from equation 2.91 and presented in Figure 4.3b, exhibit a similar range of agreement with the measured values. However, for the liquid flow rate of 6.6 cm/sec, the agreement of calculated values of liquid fraction and bed voidage with the corresponding experimental values was poor at almost all gas flow rates. Therefore for fluidized beds of 3 mm glass beads, the role of bubble wakes cannot be considered totally insignificant. Nevertheless, the bed voidage predicted by the gas-free model can be used as a first approximation.

Beds of 1 mm particles (Table 4.8 and Figure 4.4)

The data of Michelsen and Østergaard show a gradual reduction in liquid fraction as the gas flux through the bed is increased. For a volumetric liquid flux of 7.8 cm/sec,

TABLE 4.8

COMPARISON OF MEASURED AND PREDICTED GAS AND LIQUID FRACTIONS FOR THREE-PHASE FLUIDIZED BEDS

d_p = 1.25 mm, ρ_3 = 2.67 gm/cc, Liquid Flux, $\langle j_1 \rangle$ = 7.8 cm/sec, D = 6.0 inch

Gas Flux, $\langle j_2 \rangle$ (cm/sec)	Measured (1)		Predicted (2)			Predicted (3)			Predicted (4)		
	ε_1'''	ε_2'''	$\varepsilon_k/\varepsilon_2'''$	ε_1'''	ε_2'''	$\varepsilon_k/\varepsilon_2'''$	ε_1'''	ε_2'''	$\varepsilon_k/\varepsilon_2'''$	ε_1'''	ε_2'''
0.0	0.780	-	-	0.728	-	-	0.786	-	-	0.706	-
1.0	0.710	0.027	2.225	0.667	0.021	1.298	0.739	0.021	4.974	0.610	0.034
2.0	0.680	0.045	1.539	0.635	0.034	1.026	0.706	.040	3.322	0.570	0.076
3.0	0.663	0.060	0.869	0.644	0.045	0.826	0.683	.057	2.615	0.537	0.123
4.0	0.650	0.070	0.416	0.667	0.054	0.667	0.669	.072	2.202	0.506	0.173
5.0	0.640	0.079	0.181	0.684	0.063	0.532	0.662	.087	1.926	0.477	0.226
6.0	0.630	0.088	0.075	0.693	0.072	0.411	0.661	.101	-	-	-
7.0	0.625	0.094	0.030	0.696	0.080	0.393	0.645	.112	-	-	-
8.0	0.620	0.100	0.012	0.700	0.087	0.377	0.630	.122	-	-	-
9.0	0.615	0.107	0.005	0.697	0.094	0.362	0.616	.132	-	-	-
10.0	0.612	0.112	0.002	0.695	0.101	0.348	0.602	.140	-	-	-
11.0	0.609	0.118	0.001	0.693	0.108	0.335	0.590	.148	-	-	-
12.0	0.608	0.124	0.000	0.690	0.114	0.324	0.577	.154	-	-	-
13.0	0.605	0.128	0.000	0.688	0.120	0.315	0.564	.160	-	-	-
14.0	0.600	-	0.000	0.686	0.126	0.307	0.552	.166	-	-	-
15.0	-	-	0.000	0.684	0.132	0.298	0.540	.171	-	-	-

(1) Measurements by Michelsen and Østergaard [14]

(2) Predicted values from correlations (equations 2.126 - 2.128) by Efremov and Vakhrushev [16]

(3) Predicted values from generalized wake model with $x_k = 0$

(4) Predicted values from wake model by Østergaard [8]

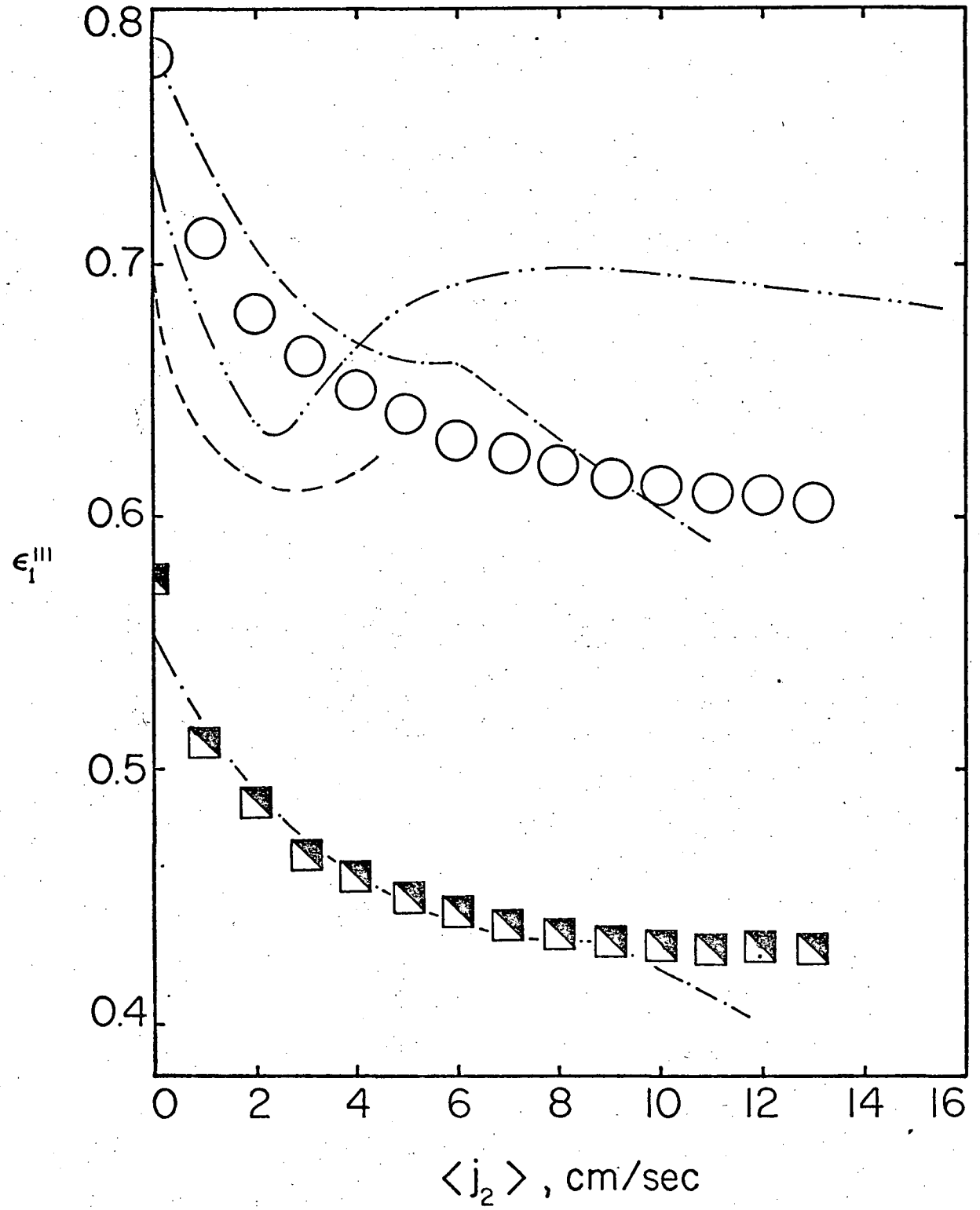

FIGURE 4.4 LIQUID FRACTION DATA OF MICHELSEN AND ØSTERGAARD [14] FOR 1 MM GLASS BEADS (▪ -j_1=3.0; o -j_1=7.8; —·—·— generalized wake model with x_k=0; —··—··— Efremov-Vakhrushev equations, 2.126-2.128, for j_1=7.8; - - - - Østergaard's equation, for j_1=7.8)

there is considerable disagreement between the predicted values from both the generalized wake model and the Efremov-Vakhrushev equations, and the measured values, for $j_2 > 9$ cm/sec. However the predictions from the model are in good quantitative agreement with the measured values up to $\langle j_2 \rangle = 6.0$ cm/sec, whereas the predictions from the equations of Efremov and Vakhrushev show better qualitative agreement with the measured values for $j_2 > 8$ cm/sec. As can be noted from Table 4.5, for highly expanded beds of 1 mm particles, the wake fractions estimated by the model show poor agreement with the values calculated from equation 2.128, the wake fraction predicted by the model being smaller at lower gas fluxes and considerably larger at higher gas fluxes ($j_2 > 6$ cm/sec). This inequality of wake fractions overshadows the inequality of bubble rise velocities in this case and is probably the principal source of discrepancy between the two predictions. It therefore appears that the generalized wake model overestimates the wake fraction whereas equation 2.128 underestimates it for the larger gas velocities.

For the smaller liquid flow rate of 3 cm/sec, the predictions from the model are in excellent agreement with the measured values [14] up to $\langle j_2 \rangle = 9$ cm/sec, where, due to the apparent overestimation of wake fraction by the model, the predictions from it start to deviate from the measured values. Since the gas holdups predicted by the model were

also found to be in excellent agreement with the measured values up to $\langle j_2 \rangle$ = 9 cm/sec, it can be stated that the wake fractions predicted by the model are at least as realistic as those given by equation 2.128, with which they were found to be in reasonable agreement (Table 4.5).

Since the generalized wake model developed in Section 2.3 will subsequently be used to analyse the data obtained in the 2 inch diameter column of this study, its predictions are now compared with the limited data of Østergaard and Theisen [18] for 2 mm glass beads in a 2 inch diameter column and with the predictions of the Efremov-Vakhrushev equations, good agreement of the latter equations with the Østergaard-Theisen data having been reported [16]. For calculating the bed voidage from the generalized wake model it is assumed that

(a) the relative velocity is represented by equation 2.108a, the local drift velocity being obtained from equation 4.8 for the slug flow regime, and that
(b) the voidage in the particulate phase is represented by the Neuzil-Hrdina correlation, equation 2.51.

The bed voidages calculated from the generalized wake model for 2 mm glass beads fluidized by a cocurrent stream of air and water are shown in Figure 4.5a, along with the data of Østergaard and Theisen [18] and the predicted values from the Efremov-Vakhrushev equations. For a volumetric liquid flux of 11.0 cm/sec, the predicted values of bed

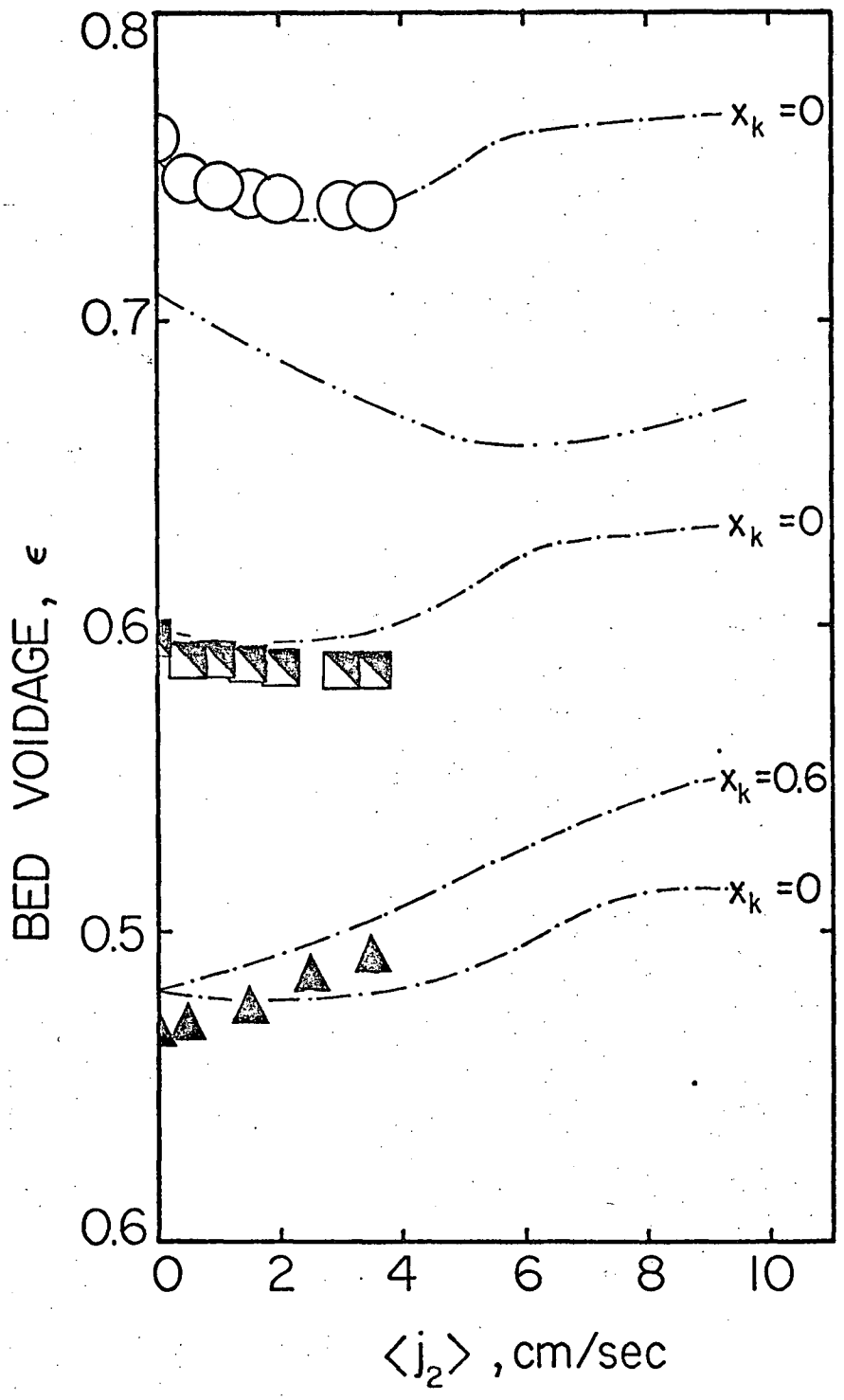

FIGURE 4.5a BED VOIDAGE DATA OF ØSTERGAARD AND THEISEN [18] FOR 2 MM GLASS BEADS (▲ -j_1=3.38; ◪ -j_1=6.17; ○ -j_1=11.0; —·—·— generalized wake model; —··—··—Efremov-Vakhrushev equations, 2.126-2.128, for j_1=11.0)

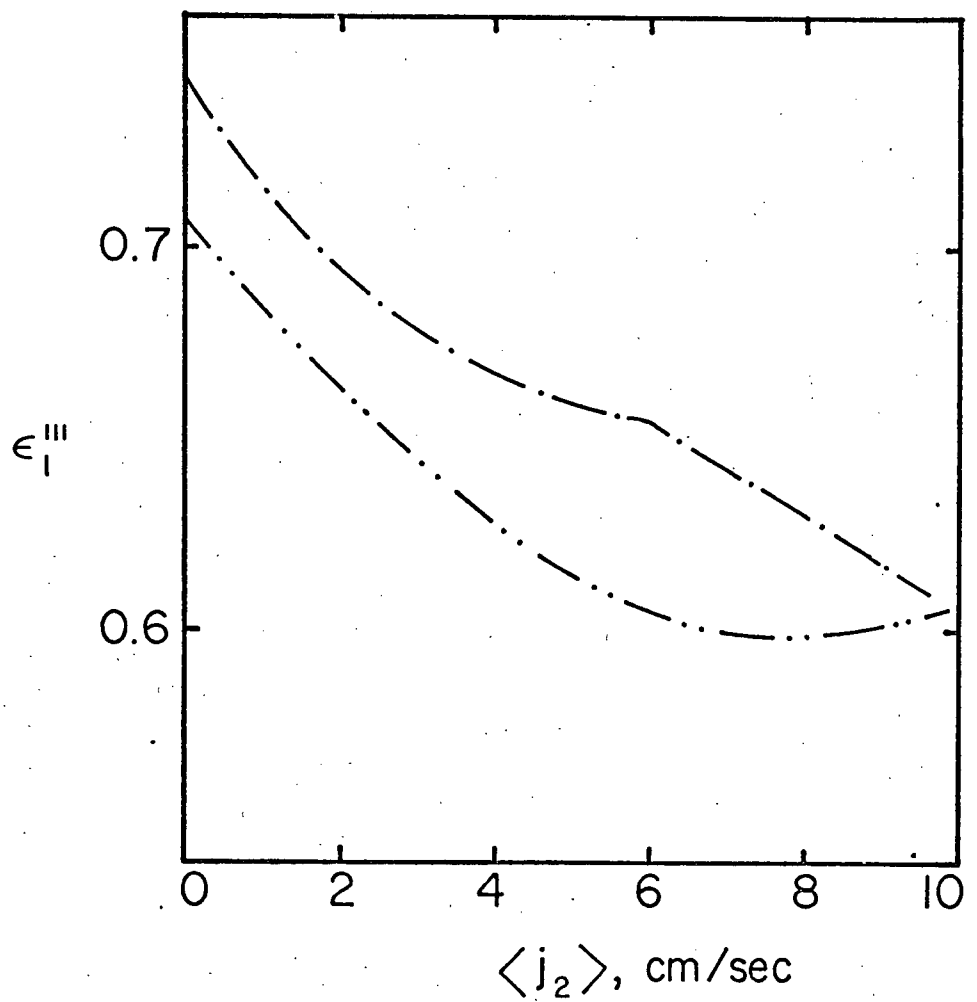

FIGURE 4.5b COMPARISON OF ε_1''' BY GENERALIZED WAKE MODEL WITH ε_1''' BY EFREMOV-VAKHRUSHEV EQUATIONS FOR 2 MM GLASS BEADS AT $\langle j_1 \rangle$=11.0 cm/sec (—·—·— generalized wake model with x_k=0; —··—··—Efremov-Vakhrushev equations, 2.126-2.128)

TABLE 4.9

COMPARISON OF MEASURED AND PREDICTED GAS AND LIQUID FRACTIONS FOR THREE-PHASE FLUIDIZED BEDS

d_p = 2.0 mm, ρ_3 = 2.88 gm/cc, $\langle j_1 \rangle$ = 11.0 cm/sec, D = 2.0 inch

Gas Flux $\langle j_2 \rangle$ (cm/sec)	Measured (1)	Predicted (2)			Predicted (3)			Predicted (4)		
	$\varepsilon = \varepsilon_1'' + \varepsilon_2''$	$\varepsilon_k/\varepsilon_2''$	ε_1''	ε_2''	$\varepsilon_k/\varepsilon_2''$	ε_1''	ε_2''	$\varepsilon_k/\varepsilon_2''$	ε_1''	ε_2''
0.0	0.76	-	0.708	-	-	0.744	-	-	0.708	-
1.0	0.744	1.306	0.685	0.014	1.197	0.717	0.019	6.73	0.633	0.031
2.0	0.740	1.208	0.664	0.024	0.995	0.695	0.038	4.52	0.600	0.068
3.0	0.738	1.104	0.644	0.032	0.820	0.679	0.056	3.57	0.572	0.109
4.0	0.737	0.997	0.628	0.039	0.661	0.667	0.073	3.02	0.546	0.152
5.0	-	0.888	0.616	0.046	0.509	0.661	0.089	2.65	0.522	0.1980
6.0	-	0.781	0.607	0.052	0.405	0.656	0.106	-	-	-
7.0	-	0.678	0.602	0.058	0.395	0.642	0.121	-	-	-
8.0	-	0.582	0.601	0.063	0.385	0.630	0.136	-	-	-
9.0	-	0.494	0.602	0.069	0.375	0.618	0.150	-	-	-

(1) Measurements by Østergaard and Theisen [18]

(2) Predicted values from equations 2.126 - 2.128 of Efremov and Vakhrushev [16]

(3) Predicted values from generalized wake model

(4) Predicted values from wake model of Østergaard [8]

voidage from the generalized wake model are found to be in excellent agreement with the measured values, whereas the predicted values from the equations of Efremov and Vakhrushev exhibit only a qualitative agreement even though a quantitative agreement was claimed in their publication [16]. Since the ratios of wake fraction to gas fraction predicted by these two methods are in relatively good agreement with each other (Table 4.9), the discrepancy in voidage between them shown in Figure 4.5a can be ascribed to the differences in the respective values of gas holdup predicted. This is further illustrated in Figure 4.5b, where the values of liquid fraction in a three-phase fluidized bed of 2 mm glass beads predicted by the two methods are compared directly (no estimate of liquid fraction could be obtained from the data of Østergaard and Theisen, since the gas holdup inside the bed was not measured). The respective values show adequate agreement with each other, although the values predicted by the Efremov-Vakhrushev equations are consistently lower than those by the generalized wake model.

The values for the bed voidage of 2 mm glass beads predicted by the generalized wake model at other liquid flow rates are also found to be in excellent agreement with the measured values, as shown in Figure 4.5a.

Thus the above comparison of predictions from the Efremov-Vakhrushev equations and with the measurements of Michelsen and Østergaard shows that:

(1) The agreement of the simple equation proposed here for the wake fraction in a three-phase fluidized bed with equation 2.128 (cf. Table 4.5) suggests the former to be a realistic approach to correlating wake fractions which warrants further investigation. Equation 4.7 with p = 3 has been corroborated, at least as a first approximation.

(2) Since the reported values of gas holdup in three-phase fluidized beds exhibit a wide variation for similar conditions, the authenticity of the model proposed here for the rise velocity of a bubble swarm cannot be ascertained from the literature data. Nevertheless, since the proposed model is based on the available information concerning the fluid dynamics of multi-phase flow, it provides a better and simpler method for analysis of experimental data than hitherto available.

(3) The reasonable agreement of the predicted values of liquid fraction from the generalized wake model with both the measured values [14] and the predicted values from the Efremov-Vakhrushev equations [16] ascertains the basic correctness of the present fluid-dynamic description of a three-phase fluidized bed. In most instances, $x_k = 0.0$ (equivalent to no particles in the wake, as originally postulated by Stewart and Davidson [7]) gives adequate agreement with the reported data. However, for beds of large particles, for example 6 mm

glass beads, the voidage is found to be as well represented by the simple gas-free model. What discrepancies were observed between the predicted and the measured values of bed voidages could be due partly to the inaccuracies and uncertainties in the measurement of gas holdup, thus necessitating the development of better techniques for the measurement of local and overall gas holdup. This task was undertaken in the present investigation.

4.2 Discussion of experimental results and comparison with theoretical predictions

4.2.1 Evaluation of experimental techniques

The typical experimental errors involved in various measured quantities are estimated in Appendix 8.9. The two techniques used for measuring the gas holdup in gas-liquid flow, viz. the pressure drop gradient method and the valve shut-off technique, gave satisfactory results. Thus, for measuring gas holdups greater than 0.1, either of the two techniques could be used with equal accuracy. However, for measurements concerning the local structure in gas-liquid flow other suitable methods have to be adopted [115]. One such method, the electro-resistivity probe, was developed and used successfully in this study and will be discussed later in detail. For measuring the gas holdups in three-phase fluidized beds, the first two methods above were found to be somewhat more erroneous than for gas-liquid flow, especially for measurements of small gas holdups ($\varepsilon_2''' < 0.1$), but were nevertheless considered adequate for present purposes. A complete and more accurate technique of measurement is needed for better understanding of the local structure of gas flow in three-phase fluidized beds. The electro-resistivity probe developed and tested in this work was used for measuring local quantities, but the processing of the probe output with the available electronic equipment, especially for measuring the local gas fraction, was cumber-

some and subject to errors; other local quantities, e.g. bubble frequency and film thickness at the wall, could be measured quite accurately. It is therefore not yet possible to critically appraise the suitability of the electro-resistivity probe for measurements concerning the local structure of gas flow in three-phase fluidized beds.

The measurement of solids holdup in liquid-solid fluidized beds was straightforward, and either of the two methods, viz. by the expanded bed height and by the slope of the longitudinal pressure drop profile, could be used with equal accuracy. However, for determining the solids holdup in three-phase fluidized beds, the knowledge of, as well the manner of defining, the expanded bed height was critical. The method for measuring the bed height developed and used in this work not only provided accurate and reproducible measurements, but also a meaningful definition.

4.2.2 Gas holdup results

4.2.2.1 Gas holdup in gas-liquid flow

The purpose of obtaining gas holdup data in cocurrent gas-liquid flow was two-fold:

1. To have reliable data available for comparing later with gas holdup measurements in three-phase fluidized beds under similar flow conditions. Thus efforts were

made to obtain gas holdup data for all possible combinations of gas and liquid flow rates that were used later in the three-phase fluidization studies.

2. To check the applicability of the two-phase gas holdup model (equation 2.37 for bubbly flow and equation 2.39 for slug flow) to the 20 mm and 2 inch column data obtained in this study.

The data from the 20 mm and 2 inch i.d. columns, respectively, are presented and discussed separately. The graphs and tables in this section are obtained from data presented in Appendix 8.7.

(A) 20 mm glass column

The visual observation of the column revealed that slug flow prevailed at all the gas and liquid flow rates studied. The slugs appeared to travel independently of each other as no coalescence could be detected.

The simplest scheme for analyzing the data is to use equation 4.1 in combination with equation 2.37 in the bubbly flow regime and with equation 2.39 in the slug flow regime. Thus, combining equations 4.1 and 2.39 for the slug flow regime,

$$\bar{v}_2 = \frac{\langle j_2 \rangle}{\varepsilon_2} = C_0 \langle j \rangle + 0.35 \sqrt{gD} \qquad (4.12)$$

Then assuming C_0 to be 1.2 [19, 39], equation 4.12 for the

20 mm glass column becomes

$$\bar{v}_2 = \frac{\langle j_2 \rangle}{\varepsilon_2} = 1.2 \langle j \rangle + 15.50 \qquad (4.13)$$

The predictions from equation 4.13 are compared with experimental data in Figure 4.6, and exhibit sufficient agreement with the data to justify the assumed value for C_0. Thus the model for the slug flow regime, represented by equation 4.13, can be successfully used to predict the gas holdup for air-water flow in 20 mm columns.

(B) 2 inch perspex column

The gas holdups in the 2 inch i.d. perspex column were measured both by the pressure drop gradient method and by the valve shut-off technique, and supplemented in part by the electro-resistivity probe. Data were obtained for a bubble column ($\langle j_1 \rangle = 0.0$) as well as for cocurrent gas-liquid flow.

(i) Bubble column

The flow regime in bubble columns at low gas flow rates ($j_2 < 3$ cm/sec) was mainly bubbly with little or no evidence of coalescence. However, bubble clusters began to appear at a gas flow rate of about 5 cm/sec, after which coalescence increased progressively. Fully developed slugs were not observed until the gas flow rate was 7.8 cm/sec, but bubble conglomerates leading to slugs near the top of

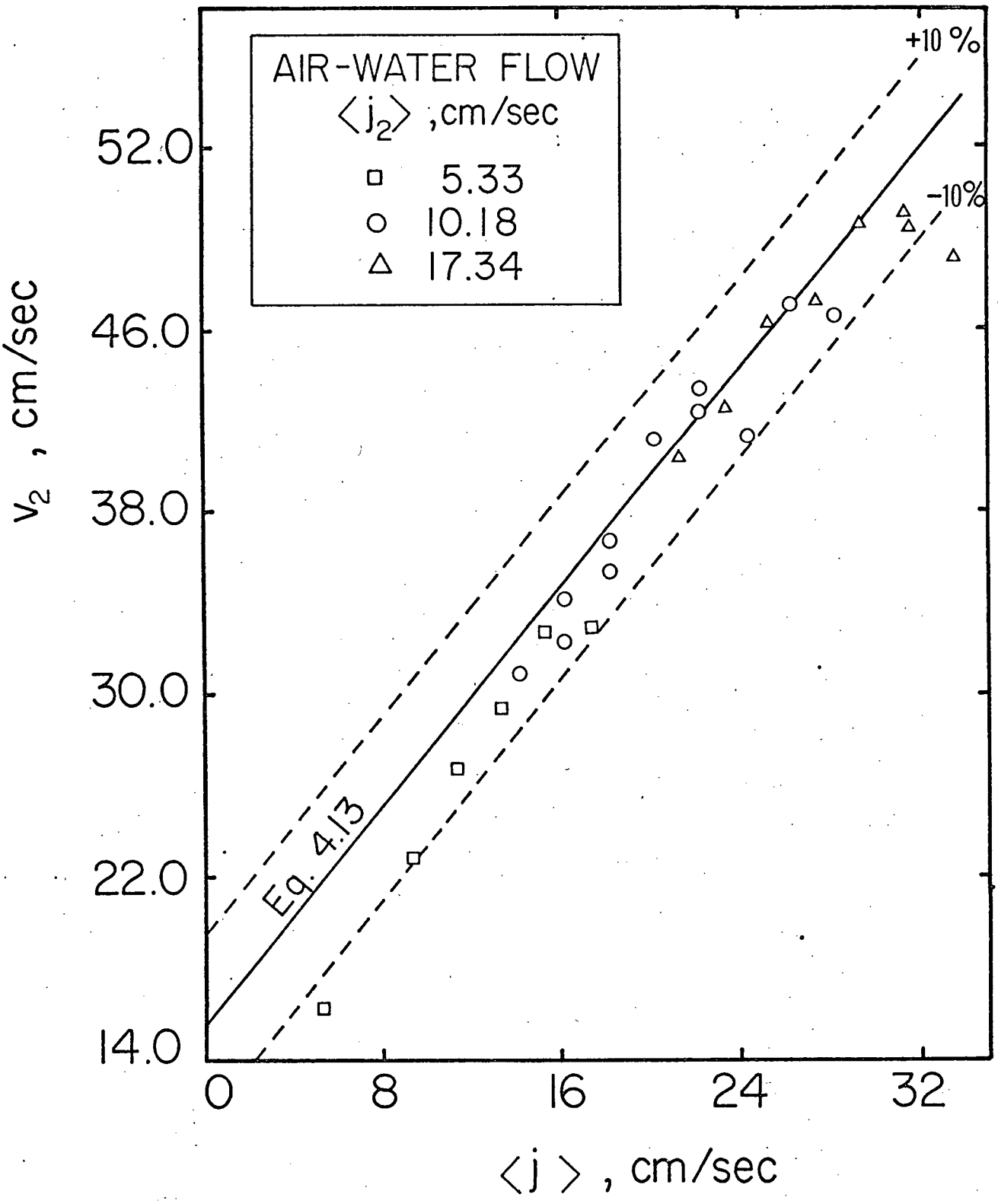

FIGURE 4.6 COMPARISON OF AVERAGE BUBBLE RISE VELOCITIES PREDICTED BY EQUATION 4.13 WITH EXPERIMENTAL DATA IN 20 MM GLASS COLUMN

the test section were noticeable.

As discussed in Appendix 8.2, the hydrostatic pressure on a bubble decreases continuously during its ascent. This change in hydrostatic head would cause the bubble size to change, thereby affecting the bubble rise velocity, and both effects together could change the gas holdup along the column. Yet for simplification it was assumed in Appendix 8.2 that gas holdup along the column axis remained constant.

The gas holdup at a given vertical level of the experimental section could be calculated from the longitudinal pressure drop profile along the column wall. Figure 4.7 shows such longitudinal gas holdup profiles, calculated from unsmoothed data. It is seen in Figure 4.7 that the gas holdup for all gas flow rates greater than 2 cm/sec increases along the column axis, the increase, however, being almost insignificant for all but the highest gas flow rates. Therefore in each case an average of all the gas holdups was taken, and this value was assumed to exist at the mid-point of the column. The gas holdup was then corrected to a pressure of 760 mm of mercury. The gas holdups from the valve shut-off technique were similarly corrected to a pressure of 760 mm of mercury and are presented in Appendix 8.7.

As shown earlier, the simplest and most comprehensive scheme for analyzing the data is provided by

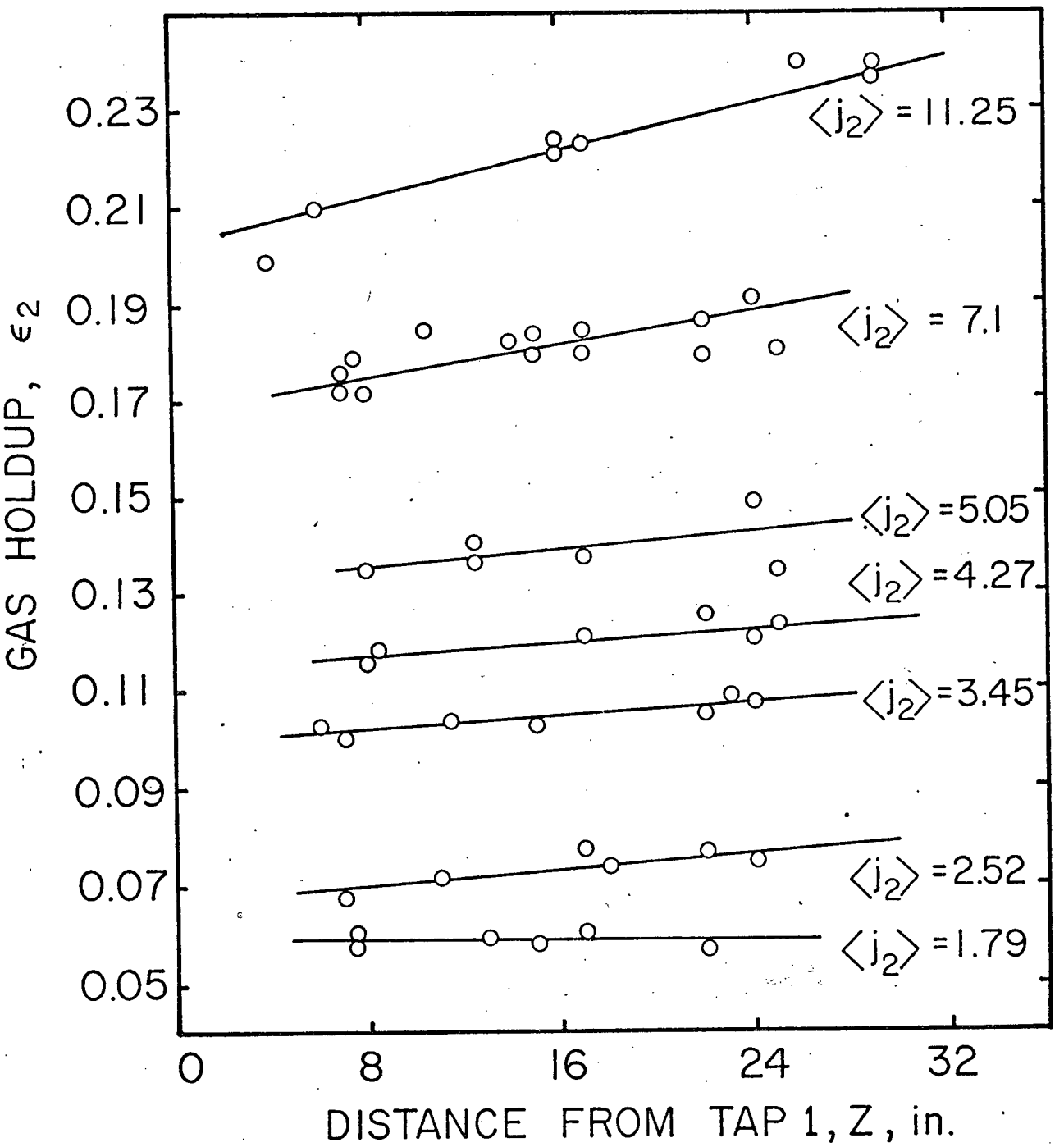

FIGURE 4.7 AXIAL VARIATION OF GAS HOLDUP IN BUBBLE COLUMN ($\langle j_1 \rangle$=0.0)

$$\bar{v}_2 = \frac{\langle j_2 \rangle}{\langle \alpha_2 \rangle} = C_0(\langle j_1+j_2 \rangle) + \frac{\langle \alpha_2 v_{2j} \rangle}{\langle \alpha_2 \rangle} \qquad (4.1)$$

The second term on the right-hand side of equation 4.1 represents the "weighted mean drift velocity" of the two-phase mixture. Several competing models for the drift velocity have been proposed [1, 39, 75, 76], but in general

$$\frac{\langle \alpha_2 v_{2j} \rangle}{\langle \alpha_2 \rangle} = f(\langle \alpha_2 \rangle)(V_\infty)_B \qquad (4.14)$$

where $f(\langle \alpha_2 \rangle)$ is normally a monotonic function of $\langle \alpha_2 \rangle$ that approaches unity as $\langle \alpha_2 \rangle$ approaches zero. Then combining equations 4.1 and 4.14, we get

$$\frac{\langle j_2 \rangle}{\langle \alpha_2 \rangle} = C_0(\langle j_1+j_2 \rangle) + f(\langle \alpha_2 \rangle)(V_\infty)_B \qquad (4.15)$$

Now differentiating equation 4.15 with respect to $\langle \alpha_2 \rangle$, the slope of the $\langle j_2 \rangle$ versus $\langle \alpha_2 \rangle$ curve at the origin, that is as $\langle j_2 \rangle$ and hence $\langle \alpha_2 \rangle$ approaches zero, would be given by

$$\left.\frac{d\langle j_2 \rangle}{d\langle \alpha_2 \rangle}\right|_{\langle j_2 \rangle = 0} = C_0 \langle j_1 \rangle + (V_\infty)_B \qquad (4.16)$$

and since for bubble columns $\langle j_1 \rangle = 0$, equation 4.16 simplifies to

$$\left.\frac{d\langle j_2\rangle}{d\langle \alpha_2\rangle}\right|_{\langle j_2\rangle = 0} = (V_\infty)_B \qquad (4.17)$$

which was also derived by Bhaga [1] in a different manner.

The measured gas holdups for the bubble column are shown on the $\langle j_2\rangle - \varepsilon_2$ plane in Figure 4.8a, and from the slope of the curve at the origin, the rise velocity of a bubble is found to be $(V_\infty)_B = 24.7$, which corresponds from equation 2.10 to a bubble diameter of 9.4 mm. The observed bubble size in the bubble column was between 5 and 10 mm.

Zuber and Findlay [39] reported that for both churn-turbulent bubbly flow and slug flow, the weighted mean drift velocities were constant and given by equations 4.3 and 4.2 respectively. The above rise velocity of 24.7 cm/sec compares favorably with the value of 24.91 cm/sec from equation 4.3 and 24.71 from equation 4.2. Since for the 2 inch i.d. column the drift velocities for the churn-turbulent bubbly flow and the slug flow regimes are practically the same, equation 4.1 with $C_0 = 1.2$ [39] becomes

$$\bar{v}_2 = \frac{\langle j_2\rangle}{\varepsilon_2} = 1.2\ (\langle j_1+j_2\rangle) + 24.7 \qquad (4.18)$$

Equation 4.18 is equivalent to equation 4.4 proposed by Nicklin [19] from a totally different approach. Now, since for bubble columns $\langle j_1\rangle = 0$, equation 4.18 further simplifies to

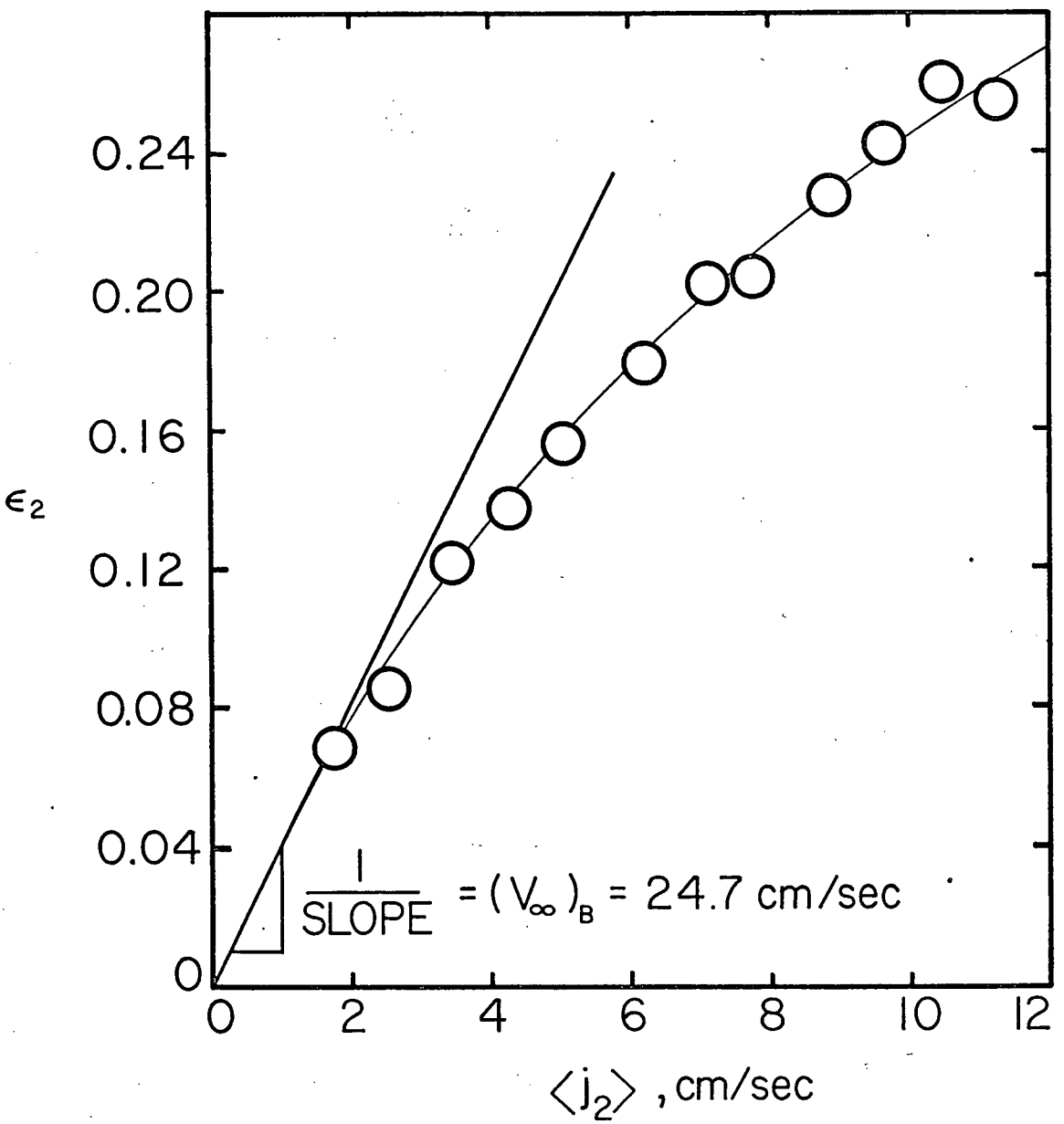

FIGURE 4.8a GAS HOLDUP IN BUBBLE COLUMN

$$\bar{v}_2 = \frac{\langle j_2 \rangle}{\varepsilon_2} = 1.2 \langle j_2 \rangle + 24.7 \qquad (4.19)$$

The gas holdups predicted by equation 4.19 are compared in Figure 4.8b with the experimental data and exhibit good agreement. Also shown in Figure 4.8b is the curve representing the data obtained by Ellis and Jones [60] in a 2 inch i.d. column. The agreement of this curve with the present data is strong support for the data, whereas the curve representing the Efremov-Vakhrushev correlation [66] undoubtedly underestimates the gas holdup. The present model for the bubbly flow regime (represented by equation 4.20, which is based on equation 2.37) and that recommended by Bhaga [1], although in good agreement with each other, considerably overestimate the gas holdups at the gas velocities of the present experiments. It can then be concluded that the model for the slug flow regime, represented by equation 4.19, can be successfully used to predict the gas holdup in 2 inch diameter bubble columns.

(ii) Cocurrent flow

The flow regimes encountered in cocurrent gas-liquid flow were bubbly and slug flow. The gas flow rates when the slugs were first observed in the column for air-water flow are presented in Table 4.10 for the various liquid flow rates studied. It can generally be stated that in the present 2 inch diameter column, the slug flow regime occurred

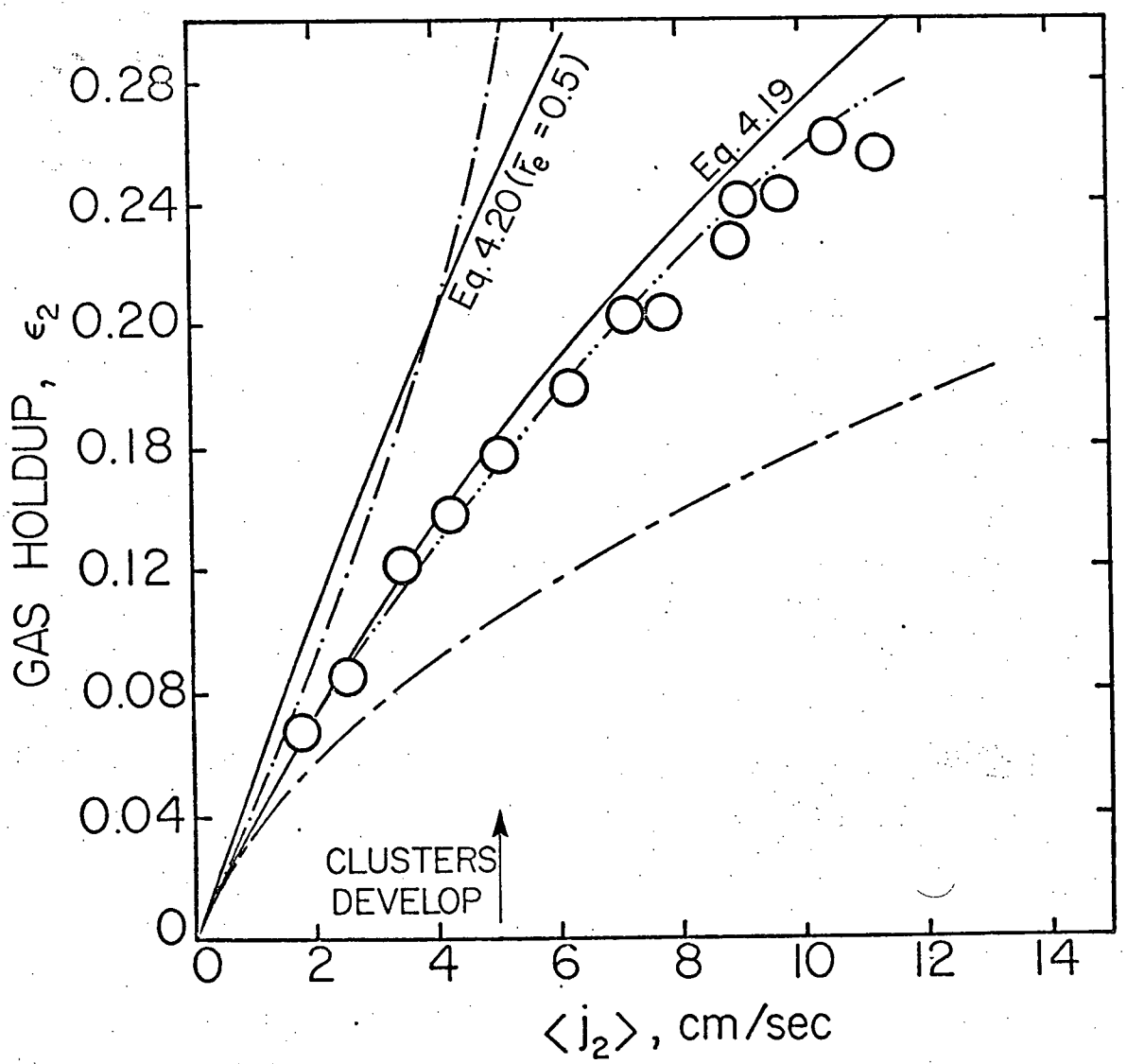

FIGURE 4.8b COMPARISON OF MEASURED AND PREDICTED GAS HOLDUPS IN 2 INCH BUBBLE COLUMNS (—·—·— Bhaga [1], —··—··— Ellis and Jones [60], —·—·—·— Efremov and Vakhrushev [66])

TABLE 4.10

TRANSITION FROM BUBBLY TO SLUG FLOW IN AIR-WATER FLOW

Liquid Flux $\langle j_1 \rangle$ (cm/sec)	Gas Flux, $\langle j_2 \rangle$, at Transition	
	From visual Observation	From Equation 2.21
0.0	4.3 - 5.1	3.1
1.25	4.8 - 5.3	3.3
6.25	4.4 - 4.9	4.3
7.00	4.0 - 4.5	4.5
7.65	4.3 - 5.0	4.6
17.75	4.3 - 5.4	6.6

for all gas flow rates greater than 5 cm/sec irrespective of the liquid flow rate, as was also noted by Reith et al. [68]. Also presented in Table 4.10 are the gas flow rates predicted for transition from bubbly to slug flow by equation 2.21 [60]. These correspond only roughly to the observed transition points. In air-polyethylene glycol solution flow, the slug flow regime was encountered at all the gas and liquid flow rates studied and therefore no data for the transition point were recorded. However it was observed that at low liquid flow rates coalescence was quite prominent, whereas at high liquid flow rates the large spherical capped bubbles rose at regular intervals without much coalescence.

The flow of air-water mixture at very low water flow rates differed visibly from that at all other water flow rates studied. Thus for a water rate of 1.25 cm/sec, the air-water flow was predominantly bubbly for all the gas flow rates studied, although for gas rates greater than 5 cm/sec coalescence in the system became so much more active that bubble conglomerates were observed to rise through the column with a rolling action. No fully developed slugs were observed even at the highest gas flow rate studied ($\langle j_2 \rangle$ = 8.44 cm/sec), but the presence of bubble conglomerates was taken to mean a change in flow regime and the corresponding gas flow rate was recorded as a transition point in Table 4.10. For the next higher liquid flow rate

($\langle j_l \rangle$ = 1.87 cm/sec) similar bubble clusters were observed at gas flow rates higher than 5 cm/sec, but these bubble clusters coalesced to form a well defined slug. At all other liquid flow rates the upward rolling action of bubble clusters was not observed and the slugs encountered for gas flow rates higher than 5 cm/sec were clearly defined.

The axial distribution of gas holdups, calculated from the longitudinal pressure drop profiles along the column wall, also revealed a different pattern for low liquid flow rates. The gas holdup distributions for a water flow rate of 1.25 cm/sec are shown in Figure 4.9(in which the lines are drawn for making any possible trend in the data perceptible, but have no other significance). It is seen that the gas holdup for the gas flow rate of 3.81 cm/sec remained practically constant, whereas the gas holdup for the gas flow rate of 5.31 cm/sec decreased up the column, indicating that the bubble swarm was accelerating. For higher gas flow rates the reduction in gas holdup with distance was even more pronounced. For the next higher liquid flow rate of 1.87 cm/sec, Figure 4.10 shows the longitudinal gas holdup distribution to have remained practically constant throughout the experimental section except for the highest gas flow rate of 8.44 cm/sec, for which the gas holdup up the column once again showed a marked reduction. For the liquid flow rate of 4.55 cm/sec,

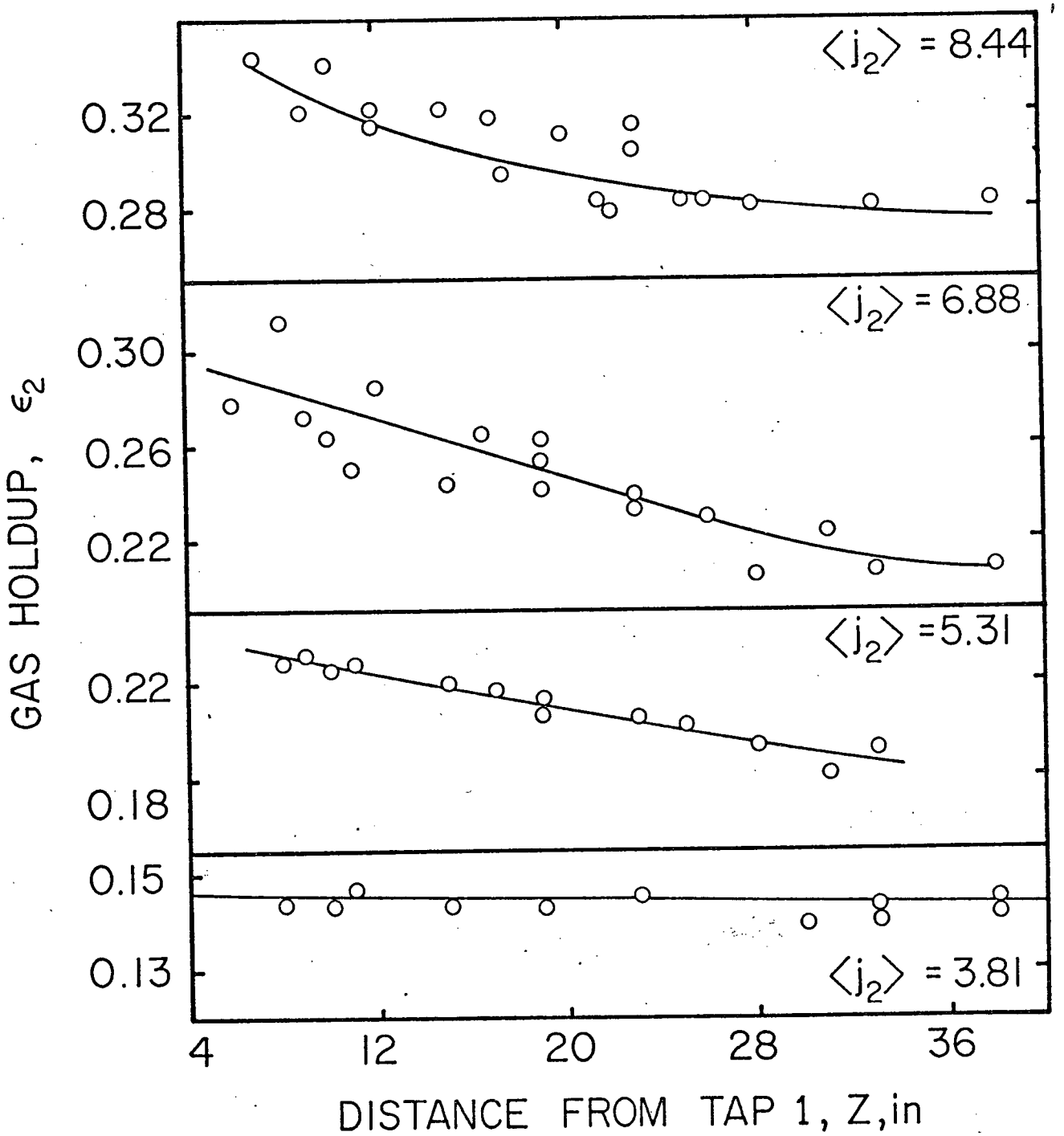

FIGURE 4.9 AXIAL DISTRIBUTION OF GAS HOLDUP IN AIR-WATER FLOW AT $\langle j_1 \rangle$ = 1.25 cm/sec

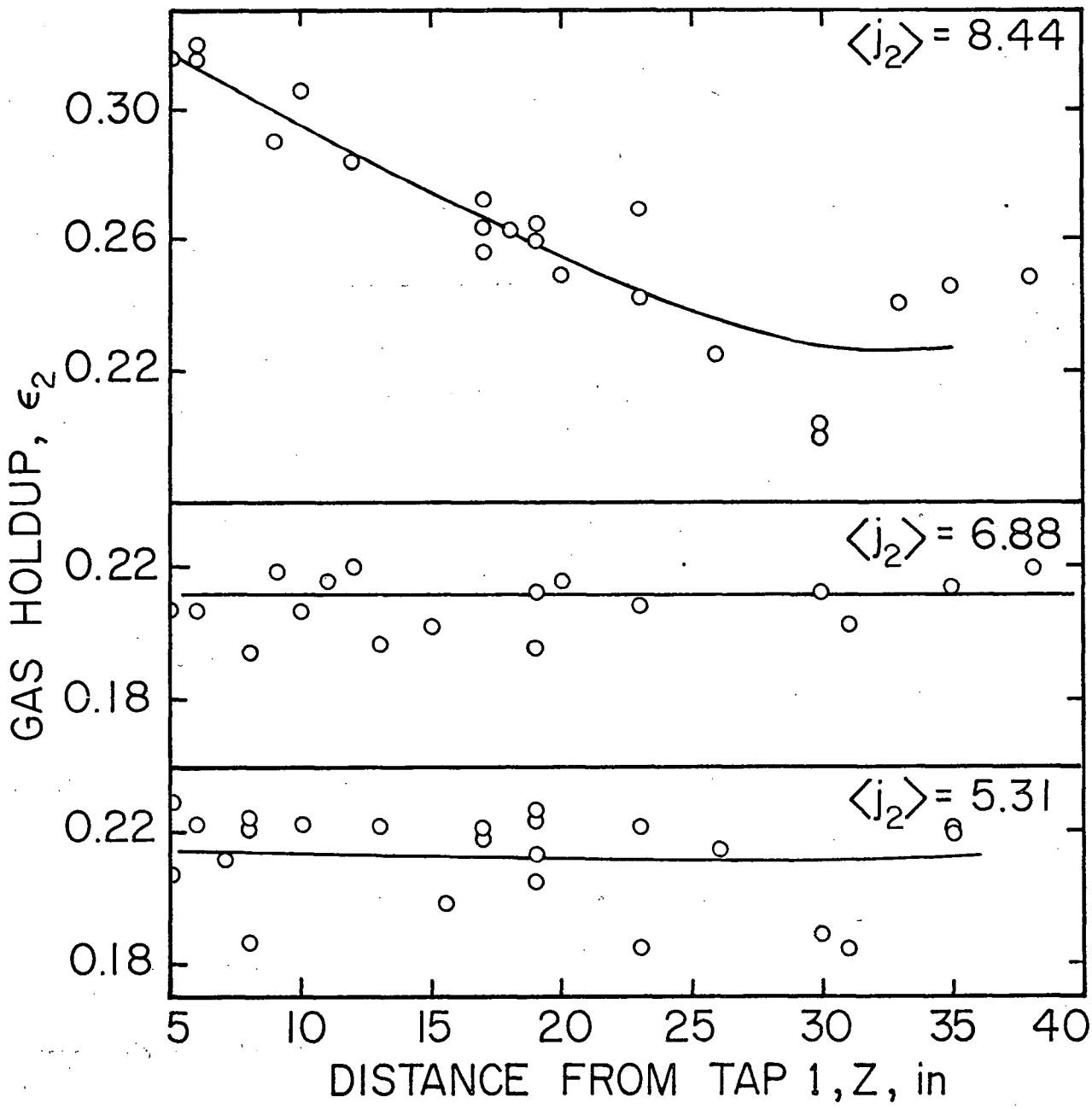

FIGURE 4.10 AXIAL DISTRIBUTION OF GAS HOLDUP IN AIR-WATER FLOW AT $\langle j_1 \rangle$ = 1.87 cm/sec

the longitudinal distribution of gas holdup, shown in Figure 4.11, remained constant for all gas flow rates used. Similar behaviour was found for all the other liquid flow rates studied.

For the air-polyethylene glycol solution flow, the axial distribution of gas holdup is shown in Figure 4.12. At low liquid flow rates it differed substantially from that of air-water flow. In the case of the two lower liquid flow rates, the gas holdup increased markedly up to 20 inches above Tap 1, but above that level, the change in gas holdup was almost insignificant. For two higher liquid flow rates, however, the gas holdup remained practically constant throughout the entire experimental section, as for air-water flow.

The gas holdup was measured by two different techniques in each of the three different sections of the column. As discussed in Appendix 8.2, the results could be misinterpreted if the pressure at the location where the gas holdup was measured were not duly considered. This is illustrated in Table 4.11, where the gas holdup data for a few typical runs are presented both before and after the pressure corrections were applied. As shown earlier, no pressure correction was deemed necessary for gas holdup measurements above the test section and these are therefore presented as measured. The gas holdups measured by the two techniques, in both the test section and the section below it, were

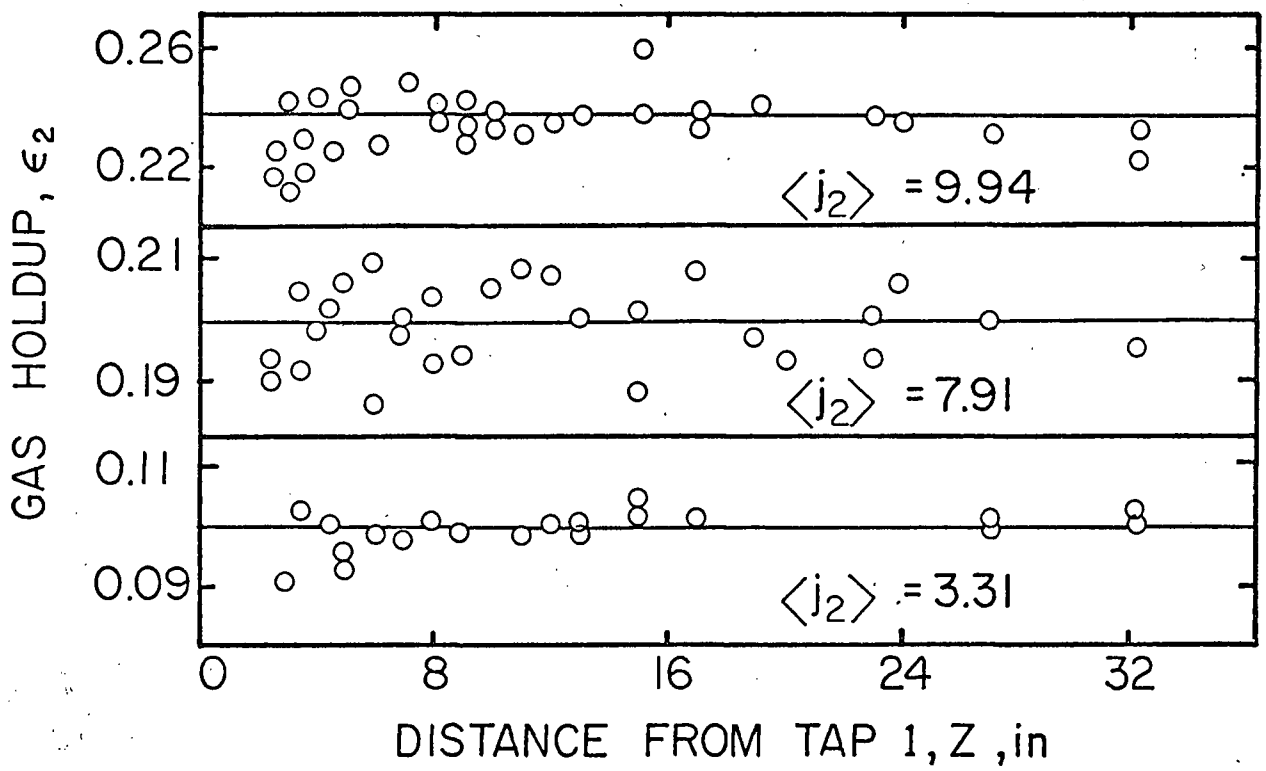

FIGURE 4.11 AXIAL DISTRIBUTION OF GAS HOLDUP IN AIR-WATER FLOW AT $\langle j_1 \rangle$ = 4.55 cm/sec

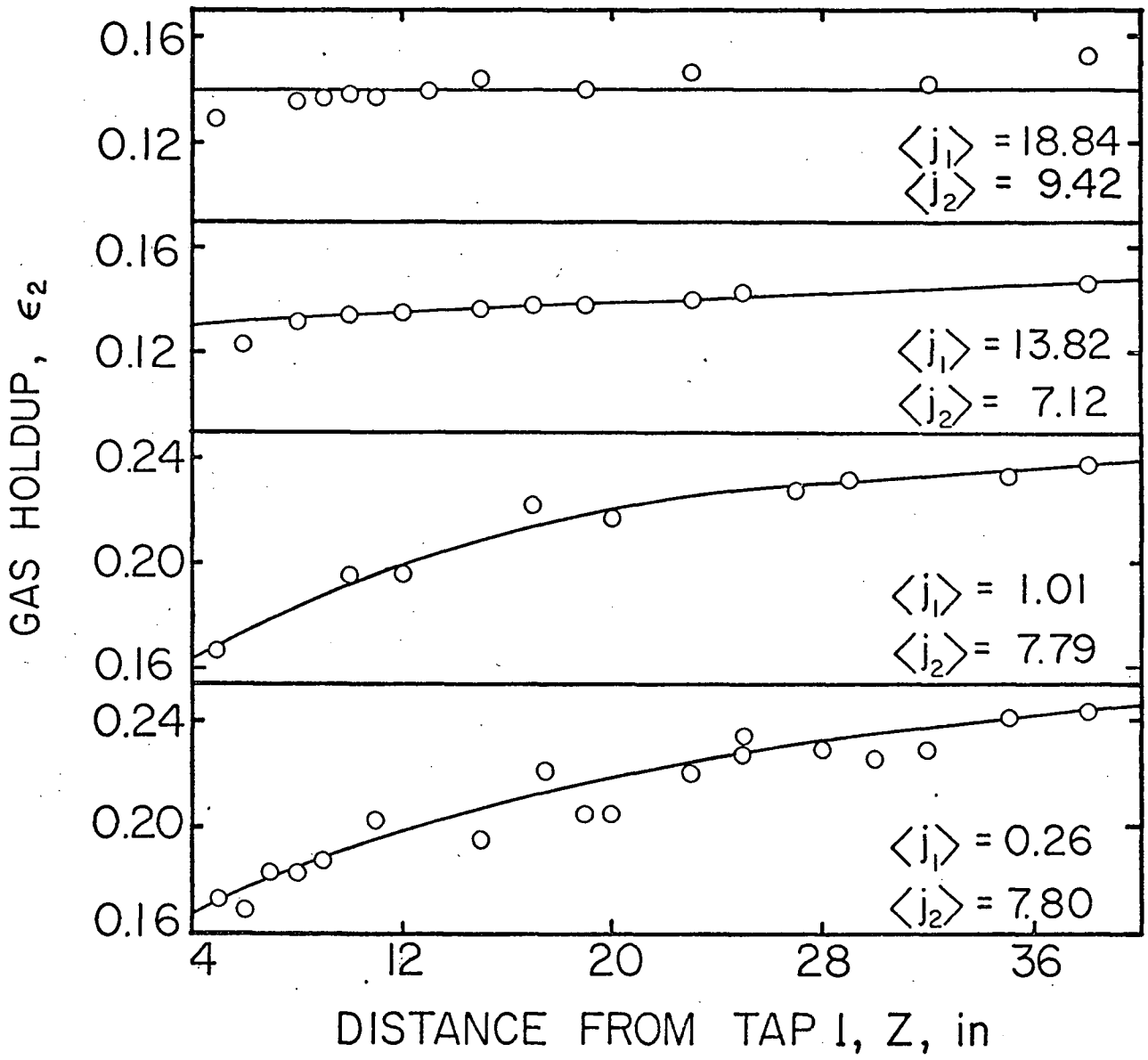

FIGURE 4.12 AXIAL DISTRIBUTION OF GAS HOLDUP IN AIR-PEG SOLUTION FLOW

TABLE 4.11

COMPARISON OF GAS HOLDUPS IN VARIOUS SECTIONS OF THE COLUMN FOR AIR-WATER FLOW

Liquid Flux, $\langle j_1 \rangle$ (cm/sec)	Gas Flux $\langle j_2 \rangle$ (cm/sec)	Measured Gas Holdup in Different Sections of the Column				Corrected Gas Holdup in Different Sections of the Column				Gas Holdup Above The Experimental Section, Measured by	Average Gas Holdup (-)
		Below the Experimental Section by		In the Experimental Section by		Below the Experimental Section by		In the Experimental Section by			
		VSO	PDM	VSO	PDM	VSO	PDM	VSO	PDM	PDM	
1.25	1.97	-	0.049	-	0.068	-	0.061	-	0.076	0.077	0.076
	3.81	0.093	0.091	0.140	0.143	0.123	0.114	0.157	0.160	0.146	0.150
	5.31	0.116	0.123	0.201	0.211	0.150	0.153	0.224	0.234	0.183	0.207
	6.88	0.153	0.159	0.227	0.250	0.198	0.194	0.252	0.276	0.223	0.242
	8.44	0.184	0.197	0.258	0.269	0.242	0.234	0.284	0.296	0.262	0.275
1.87	5.31	0.114	0.127	0.205	0.211	0.148	0.157	0.227	0.234	0.209	0.218
	6.88	0.142	0.163	0.218	0.209	0.184	0.200	0.241	0.231	0.226	0.228
	8.44	0.170	0.192	0.273	0.268	0.217	0.233	0.301	0.295	0.260	0.281
4.55	3.31	0.072	0.076	0.102	0.100	0.096	0.095	0.114	0.111	0.107	0.106
	7.91	0.140	0.158	0.186	0.200	0.183	0.195	0.209	0.221	0.199	0.204
	9.93	0.188	0.198	0.225	0.234	0.243	0.242	0.250	0.257	0.240	0.247

VSO - valve shut-off

PDM - pressure drop measurement

compatible, even though the gas holdups by the valve shut-off technique were generally slightly smaller than those by the pressure drop gradient method, especially below the test section. The uncorrected gas holdups in different sections of the column, even by the same measurement technique, were significantly different. When proper pressure corrections (see Section 3.4) were employed, however, the agreement between gas holdups in different sections of the column was improved, especially at the higher liquid velocities. The average gas holdup for a particular run was obtained by taking an arithmetic mean of the two corrected gas holdups in the experimental section, the two below the experimental section, and the measured gas holdup above the experimental section. It is important to note the near equality of the average gas holdup for a run to the measured gas holdup above the experimental section. This justifies the procedure of not applying any pressure correction to the latter. Similar agreement between the corrected values was achieved for all the other runs.

The measured gas holdups obtained by varying the gas flow rate for various constant liquid flow rates are shown in Figures 4.14 - 4.15, whereas the slopes at the origin for some of these runs are given in Table 4.12. The rise velocity of a single bubble in cocurrent gas-liquid flow was found to be unaffected by liquid flow rate in the sense that the relative velocity of the bubble remained

TABLE 4.12

ESTIMATION OF DISTRIBUTION PARAMETER, C_o, FROM GAS HOLDUP MEASUREMENTS

System	$\langle j_1 \rangle$ (cm/sec)	$\left.\frac{d\langle j_2 \rangle}{d\varepsilon_2}\right\|_{j_2=0}$ (cm/sec)	C_o From Equation 4.16 (-)
Air-Water	0.0	24.7	-
	6.25	32.2	1.20
	7.00	32.8	1.16
	7.65	33.2	1.11
	12.61	42.7	1.42
	17.80	47.8	1.30
Air-PEG Solution	13.82	41.7	1.23
		Average	1.24

the same as in a quiescent stream [65]. For the bubble column, as shown earlier, the bubble rise velocity was found from the slope at the origin to be equal to 24.7 cm/sec. Therefore using this value for $(V_\infty)_B$ and the measured values of the slope at the origin, the values of the distribution parameter, C_0, were calculated from equation 4.16 and are also presented in Table 4.12. Even though this method of estimating C_0 may not be perfectly accurate, it nevertheless provides a good first approximation for C_0, and the final average value of 1.24 compares well with the recommended value of 1.2 [19, 39]. Equation 4.18 can then be justifiably used for describing the data obtained in the 2 inch diameter column, including the data for high viscosity polyethylene glycol solution, since the viscosity of the system was found from literature plots [27] to have little or no effect on the dynamics of the slugs encountered. A comprehensive test of equation 4.18 is shown in Figure 4.13. It can be seen that almost all the data fall within ±10% of the values predicted by equation 4.18, the principal exception being the data for low liquid flow rates ($\langle j_l \rangle$ = 1.25 cm/sec). Thus the model for the slug flow regime, represented by equation 4.18, satisfies most of the data and can be used for estimating the gas holdup for most liquid flow rates (j_l > 2 cm/sec). The gas holdup predicted explicitly by the slug flow model shows excellent agreement with the data, as illustrated in Figures 4.14 - 4.15.

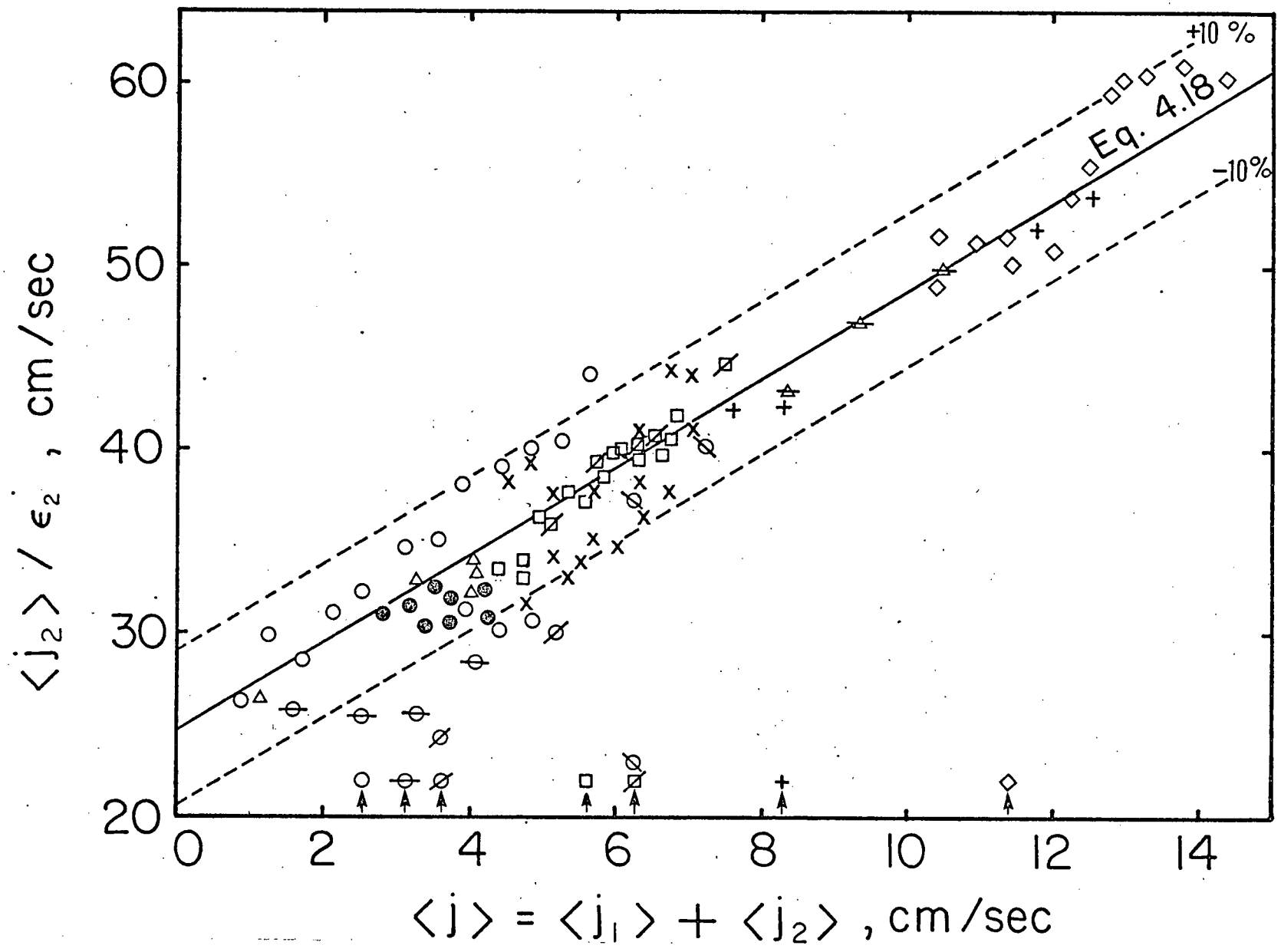

FIGURE 4.13 COMPARISON OF EQUATION 4.18 WITH EXPERIMENTAL DATA IN 2 INCH PERSPEX COLUMN (arrows indicate observed change from bubbly flow to slug flow)

LEGEND FOR FIGURE 4.13

AIR-WATER

○ $\langle j_1 \rangle$ = 0.0 cm/sec

⊖ $\langle j_1 \rangle$ = 1.25 cm/sec

⌀ $\langle j_1 \rangle$ = 1.87 cm/sec

⊘ $\langle j_1 \rangle$ = 4.55 cm/sec

□ $\langle j_1 \rangle$ = 6.25 cm/sec

× $\langle j_1 \rangle$ = 7.00 cm/sec

⌀ $\langle j_1 \rangle$ = 7.65 cm/sec

+ $\langle j_1 \rangle$ = 12.61 cm/sec

◇ $\langle j_1 \rangle$ = 17.75 cm/sec

AIR-PEG SOLUTION

△ $\langle j_1 \rangle$ = 0.26 cm/sec

⍀ $\langle j_1 \rangle$ = 1.01 cm/sec

⏃ $\langle j_1 \rangle$ = 13.82 cm/sec

⍀ $\langle j_1 \rangle$ = 18.84 cm/sec

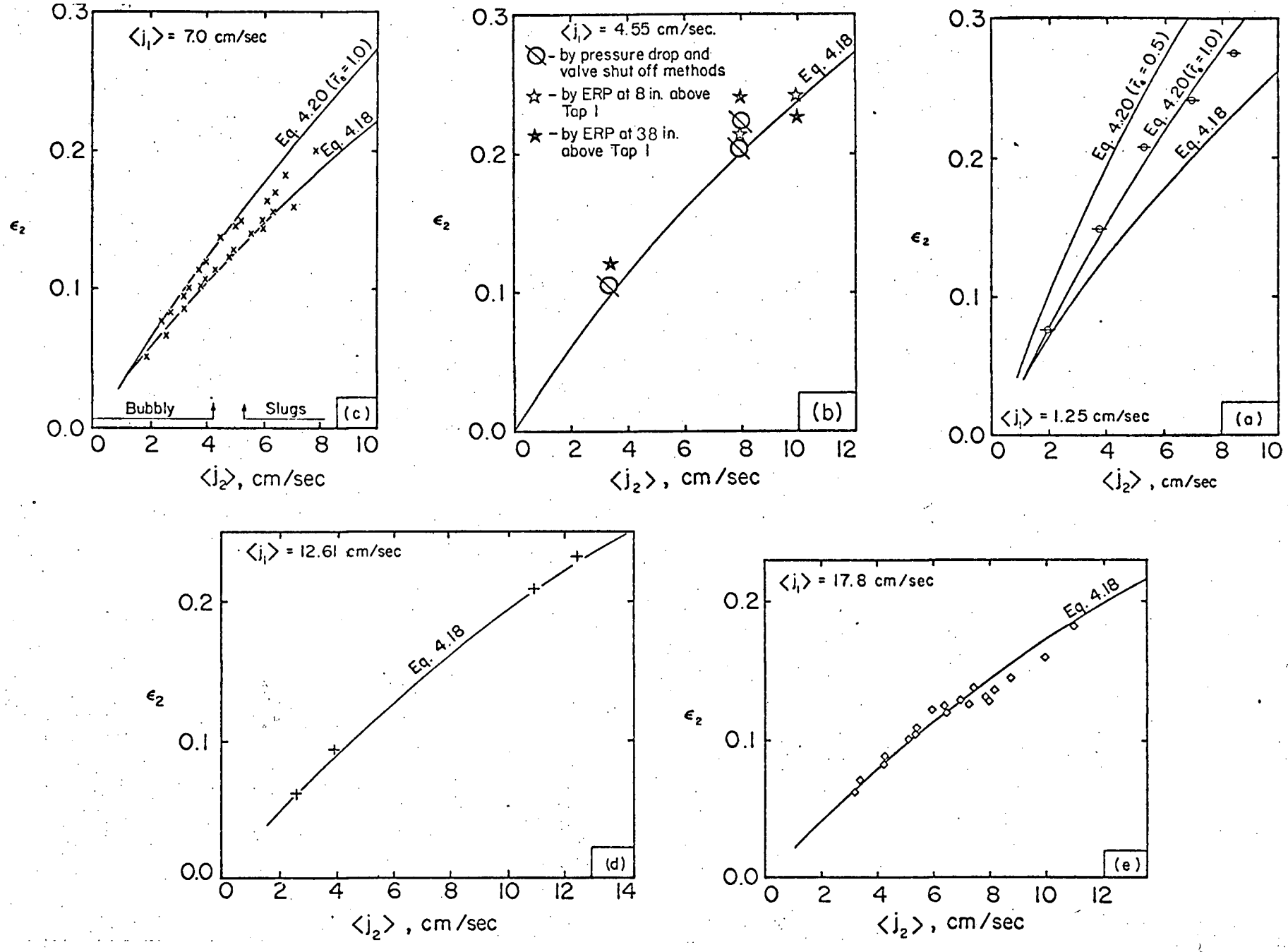

FIGURE 4.14 GAS HOLDUP FOR COCURRENT AIR-WATER FLOW IN 2 INCH PERSPEX COLUMN (ERP measurements at: ☆ - 8 inch above Tap 1, ★ - 38 inch above Tap 1; for other symbols, see legend for Figure 4.13)

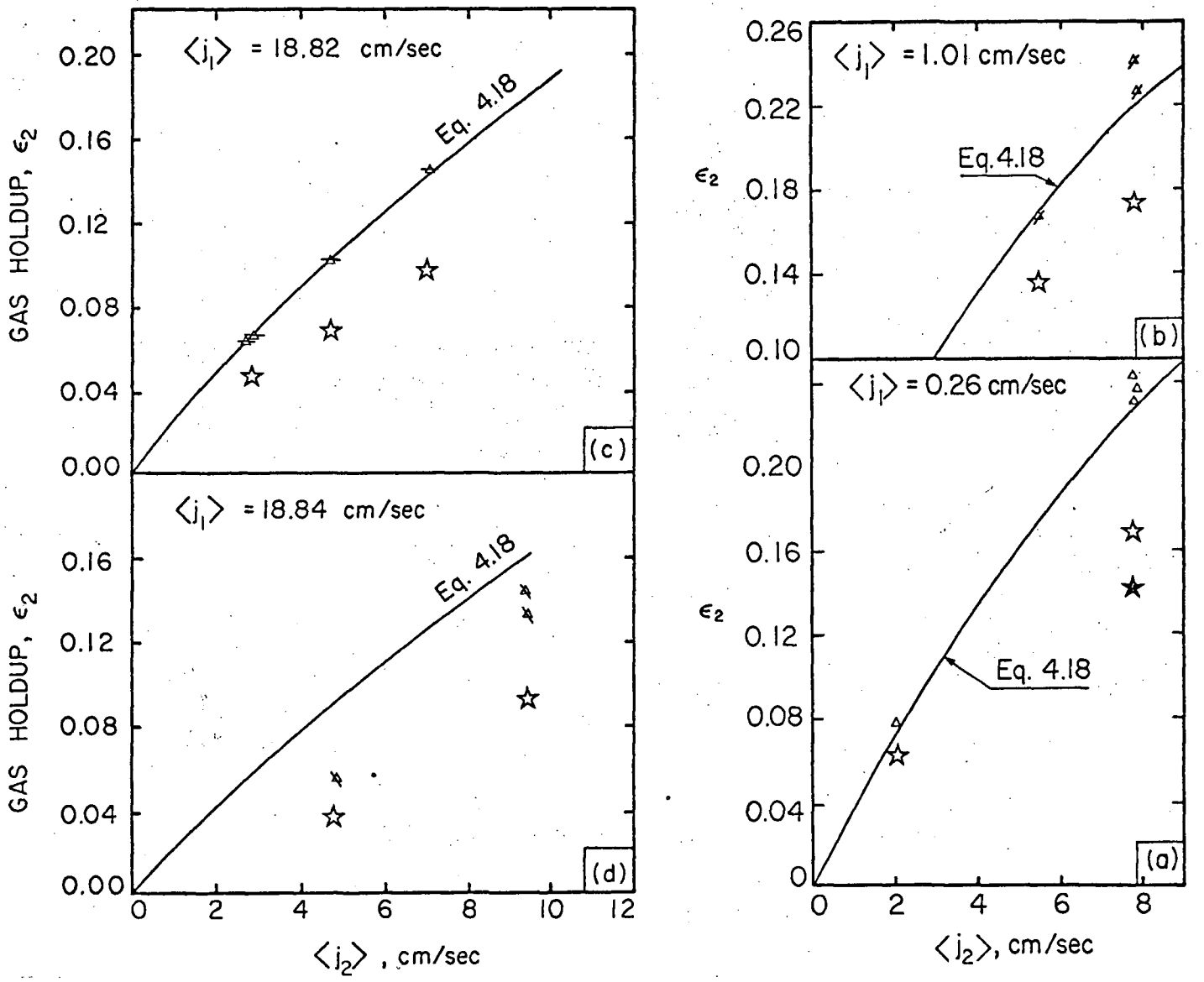

FIGURE 4.15 GAS HOLDUP FOR COCURRENT AIR-PEG SOLUTION FLOW IN 2 INCH PERSPEX COLUMN (ERP measurements at: ☆ - 8 inch above Tap 1, ★ - 38 inch above Tap 1; for other symbols, see legend for Figure 4.13)

For the case of low liquid flow rates, the flow regime encountered for most gas flow rates was predominantly bubbly. The drift velocity for the bubbly flow regime was shown to be given by equation 2.37. Then assuming that $C_0 \simeq 1.0$ [1, 39], equation 4.1 in combination with equation 2.37 becomes

$$\bar{v}_2 = \frac{\langle j_2 \rangle}{\varepsilon_2} = \langle j_1 + j_2 \rangle + (V_\infty)_B \sqrt{\tanh \{0.25(1/\varepsilon_2)^{1/3}\}} \tag{4.20}$$

where $(V_\infty)_B = 24.7$, corresponding to a bubble radius of 0.5 cm from equation 2.10. The values of gas holdup predicted by equation 4.20 for a liquid flow rate of 1.25 cm/sec are compared in Figure 4.14a with experimental data. The measured values are found to lie between the predicted values from equation 4.20 for bubbly flow and equation 4.18 for slug flow. Since, as stated earlier from visual observations, the flow regime was neither truly bubbly nor truly slug flow, it cannot be expected that either equation 4.20 for a single bubble size or equation 4.18 would predict the gas holdup accurately over a range of gas flow rate; and since the bubble size increases with increasing gas flow rate [69], equation 4.20 for a bubble radius of 1.0 cm, also shown in Figure 4.14a, gives a good compromise agreement with the experimental data.

Hence the model for the slug flow regime, represented by equation 4.18, which provides excellent agreement with

most data, will later be used for describing the rise velocity of bubble swarms in three-phase fluidized beds, for water flow rates greater than 2 cm/sec.

Electro-resistivity probe (ERP) measurements

As mentioned earlier, the electro-resistivity probe was used to measure local gas fraction in air-water as well as air-polyethylene glycol solution flow. Even though the data obtained were limited, experimental findings are described below.

(i) Air-water flow

The measured radial profiles of local gas fraction for a water flow rate of 4.55 cm/sec are shown in Figure 4.16. These radial profiles show that the gas holdup was practically uniform in the central core of the column, decreasing gradually, maintaining axial symmetry, to reach zero at the wall. For obtaining the cross-sectional average $\langle\alpha_2\rangle$, these profiles were integrated according to equation 3.5, and the values of gas holdup so obtained are compared in Table 4.13 with the average gas holdup, ε_2, determined directly from valve shut-off and pressure drop measurements. The agreement between the respective values of gas holdup is excellent, in contrast to other reported probes used for measuring local gas fraction which gave average values that were consistently smaller than those

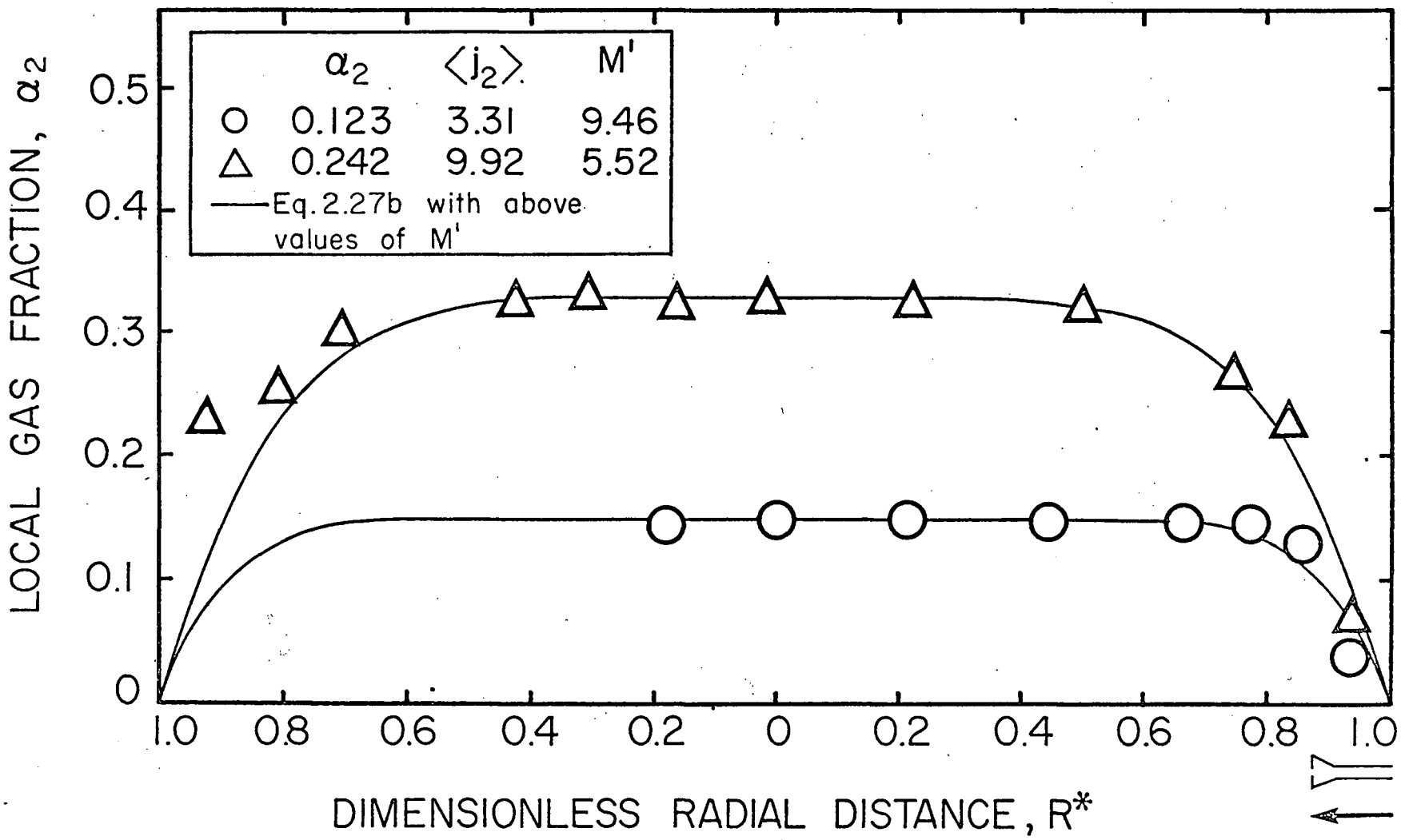

FIGURE 4.16 COMPARISON OF RADIAL GAS HOLDUP PROFILES COMPUTED BY EQUATION 2.27b WITH EXPERIMENTAL DATA (System: Air-water, $\langle j_1 \rangle$ = 4.55 cm/sec)

TABLE 4.13

GAS HOLDUP BY ELECTRO-RESISTIVITY PROBE FOR AIR-WATER FLOW

$\langle j_1 \rangle$ = 4.55 cm/sec

Liquid Flux, $\langle j_2 \rangle$ (cm/sec)	Probe Location Above Tap 1 (inches)	Gas Holdup			Ratio $(\varepsilon_2/\langle\alpha_2\rangle)$	M' From Equation 4.23	C_o From Equation 4.21
		α_{2C}	$\langle\alpha_2\rangle$	ε_2			
3.31	8	0.149	0.123	0.106	0.86	9.46	1.10
7.91	8	0.292	0.211	0.204	0.97	5.23	1.16
7.91	38	0.300	0.213	0.204	0.96	4.90	1.17
9.94	8	0.320	0.226	0.247	1.09	4.82	1.17
9.92	38	0.327	0.242	0.246	1.02	5.52	1.15
					0.98		1.15

measured directly [80, 81, 104]. The axial location of the probe in the column was varied from 8 inches above Tap 1 to 38 inches above Tap 1 in order to establish the effect of hydrostatic head on the radial profiles of gas fraction, as well as on the average values. The radial profiles as well as the averaged values remained unchanged, as shown in Table 4.13, indicating that for the given runs at least, the hydrostatic head had little or no effect on either the radial or the axial distribution of gas holdup.

It was indicated previously that for determining the distribution parameter, C_0, the radial profiles of both local gas fraction and local volumetric flux of the gas-liquid mixture have to be measured simultaneously. However, an estimate for the value of C_0 can be obtained if we assume that the radial profile of mixture flux is similar to that of gas fraction, i.e. the exponents in equations 2.27a and 2.27b are equal. Zuber and Findlay [39] asserted that the assumption of equality of the two exponents is not unreasonable if the volumetric flux of the mixture is considered to be greatly (if not mostly) affected by the volumetric flux of the gas. With this assumption, equation 2.27c reduces to

$$C_0 = \frac{M' + 2}{M' + 1} \qquad (4.21)$$

In order to evaluate M', let us substitute the value of α_2 from equation 2.27b into equation 3.5, giving

$$\langle\alpha_2\rangle = 2 \int_0^1 \alpha_{2C} \{1-(R^*)^{M'}\} R^* \, dR^* \qquad (4.22)$$

which can easily be integrated by parts to yield

$$\frac{\langle\alpha_2\rangle}{\alpha_{2C}} = \frac{M'}{M' + 2} \qquad (4.23)$$

Implicit in equation 2.27b and hence equation 4.23 is the assumption that gas fraction at the wall is zero.

The exponent M' was calculated for each run from equation 4.23 using the values of $\langle\alpha_2\rangle$ and α_{2C} reported in Table 4.13, and then C_0 was evaluated from equation 4.21. It is seen from this table that, as the gas flow rate was increased from 3.3 to 7.9 cm/sec C_0 increased slightly, but a further increase in gas flow rate did not affect the value of C_0. The average value of C_0 for these experiments was 1.15, thus again justifying the assumption of $C_0 = 1.2$, recommended elsewhere [19, 39].

The gas holdup profiles computed by equation 2.27b, using the value of exponent M' calculated from equation 4.23, are compared with the experimental data in Figure 4.16. The agreement between the computed and the experimental values confirms that the radial gas fraction profiles do indeed conform to equation 2.27b.

(ii) Air - PEG solution flow

Some of the measured gas holdup profiles are shown in Figure 4.17. The profiles were found to be axially symmetric for all the gas and liquid flow rates studied, becoming slightly flatter with increasing gas flow rate and more pointed with increasing liquid flow rate. Once again, for obtaining the cross-sectional average of gas holdup, $\langle\alpha_2\rangle$, these profiles were integrated according to equation 3.5, and the values so calculated compared in Table 4.14 with the average gas holdup, ε_2, measured by valve shut-off and pressure drop measurements. The agreement between the two values is poor, becoming worse with increase in flow rate of either phase, the average gas holdup from local measurements being consistently smaller. This discrepancy is believed to be caused by the inability of the electro-resistivity probe to penetrate the bubble front instantly in the PEG solution, the gas bubble becoming markedly deformed in the vicinity of the probe. Also since only slugs were found to exist in this viscous medium, the probe at radial locations receding from the center of the column tended to deflect the bubble and thus failed to penetrate the steep gas-liquid interface at these locations. Thus the probe generally suffered from the same drawbacks as encountered by Nassos and Bankoff [104] with their pointed needle probe. Therefore, while the change in probe design improved the applicability of an electro-resistivity probe for the air-

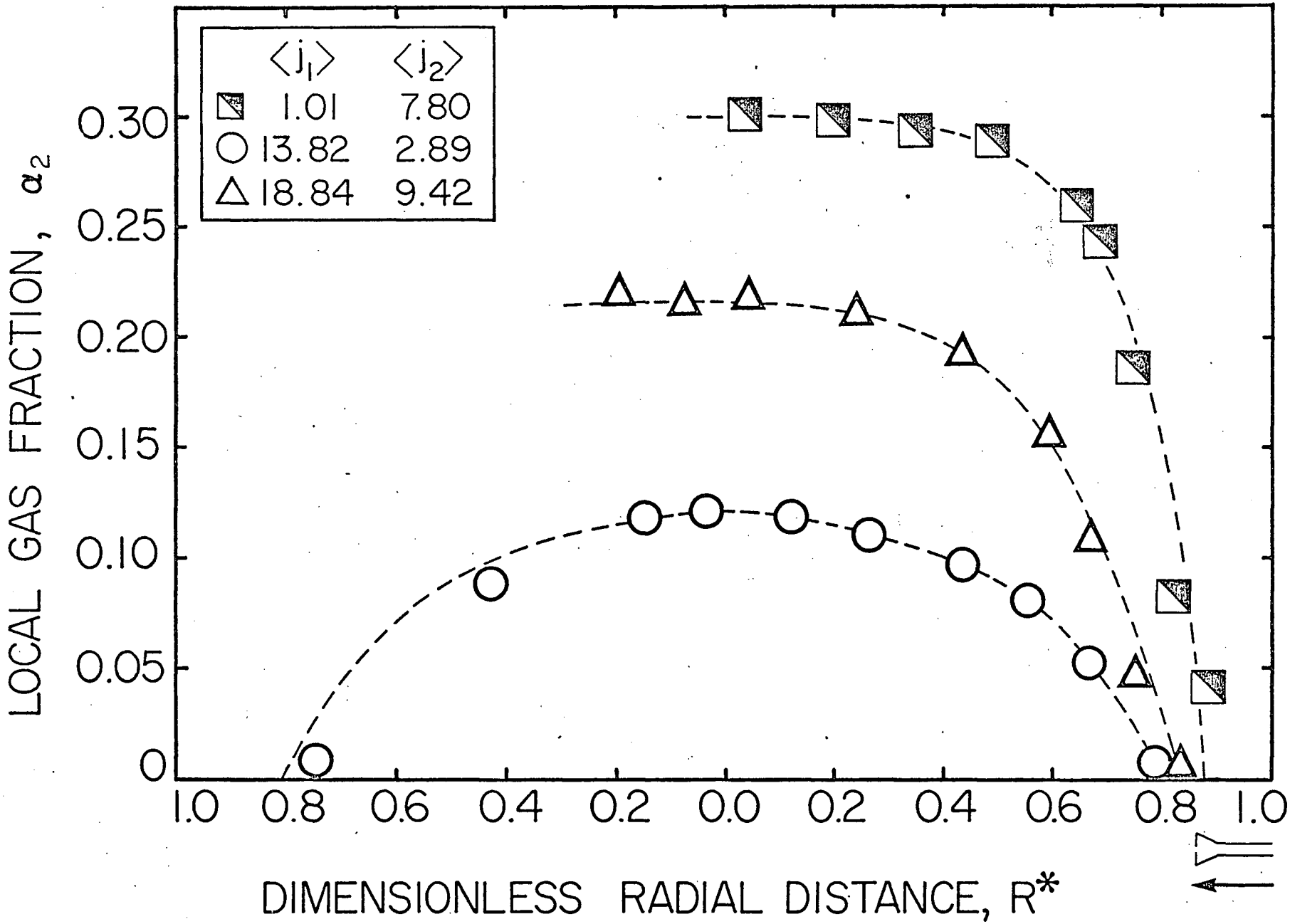

FIGURE 4.17 RADIAL GAS HOLDUP PROFILES IN AIR-PEG SOLUTION FLOW

TABLE 4.14

GAS HOLDUP BY ELECTRO-RESISTIVITY PROBE FOR AIR-PEG SOLUTION FLOW

Liquid Flux, $\langle j_1 \rangle$ (cm/sec)	Gas Flux $\langle j_2 \rangle$ (cm/sec)	Probe Location Above Tap 1 (inches)	Gas Holdup			Ratio $(\varepsilon_2/\langle\alpha_2\rangle$	M' From Eq. 4.23	C_o From Eq. 4.21
			α_{2C}	$\langle\alpha_2\rangle$	ε_2			
0.26	2.03	8	0.112	0.061	0.077	1.26	2.37	1.30
	7.78	8	0.253	0.141	0.238	1.69	2.52	1.28
	7.83	22	0.303	0.168	0.231	1.38	2.49	1.29
1.01	5.47	22	0.246	0.137	0.167	1.22	2.51	1.29
	7.79	22	0.302	0.173	0.235	1.36	2.68	1.27
13.82	2.89	22	0.122	0.046	0.065	1.41	1.22	1.45
	4.77	22	0.163	0.068	0.102	1.50	1.41	1.41
	7.12	22	0.212	0.095	0.143	1.51	1.61	1.38
18.84	4.85	22	0.100	0.036	0.055	1.53	1.14	1.47
	9.42	22	0.210	0.091	0.138	1.52	1.54	1.39

water system, its applicability for the highly viscous air-polyethylene glycol solution system was still not satisfactory.

An estimate of C_0 was obtained as before from the measured profiles, and these calculated values are also presented in Table 4.14. Based as they were on unsatisfactory electro-resistivity probe measurements, little credence was given to these values, which all exceeded 1.2, especially since the value of 1.2 for C_0 was found to satisfactorily describe the bubble rise velocity in Figure 4.13 and the gas holdup data in Figure 4.15 (except the data for $\langle j_l \rangle$ = 18.84 cm/sec). This value will therefore be used for describing the bubble rise velocities in three-phase fluidized bed, even with PEG solution as liquid.

Another important feature to be observed from the measured gas fraction profiles is the existence of a liquid film near the column wall in which the gas fraction is practically zero. The existence of such a film in the rise of a slug has been previously reported [27, 34]. The values of film thickness as obtained from these profiles are reported in Table 4.15. It can be seen that the film thickness changes little with increase in gas flow rate, but increases with increase in liquid flow rate. Due to the presence of this liquid film, equation 2.27b cannot be used for describing the radial profiles since the equation

TABLE 4.15

LIQUID FILM THICKNESS, δ^*, FROM ELECTRO-RESISTIVITY PROBE MEASUREMENTS IN AIR-PEG SOLUTION FLOW

$\langle j_1 \rangle$ (cm/sec)	$\langle j_2 \rangle$ (cm/sec)	δ^* (-)
0.26	7.79	0.09
1.01	5.47	0.11
	7.80	0.12
13.82	2.89	0.19
	4.77	0.19
	7.12	0.19
18.84	4.85	0.22
	9.42	0.17

implicitly assumes that the gas fraction is zero only at the wall (i.e. $\alpha_2 = 0$ only at $R^* = 1$). An alternate scheme, which uses the minimum radial distance at which α_2 becomes zero, instead of the column radius, for making the radial distances dimensionless, is recommended for later analysis of these profiles.

Radial profiles of bubble frequencies were also measured by the electro-resistivity probe and were generally similar to the gas fraction profiles. An estimate of bubble size was obtained by using equation 8.3.6, and the calculated values are presented in Table 4.16. However, it is not possible to confirm these values, as no independent measurements of bubble size were carried out. Nevertheless an order of magnitude analysis can be made by converting the average bubble size, $\bar{r}_e$, to an average cylindrical slug length, λ_s, using

$$\lambda_s = \frac{4}{3} \frac{\bar{r}_e^3}{R^2} \qquad (4.24)$$

and then comparing the slug length so calculated with the values from visual observations. From the values recorded in Table 4.16, the slug lengths calculated from equation 4.24 appear to be at least of the right order of magnitude. It is therefore believed that measurements of bubble frequency profiles can be successfully used for obtaining an estimate of average bubble size in the swarm, and thereby for predicting the bubble rise velocity.

TABLE 4.16

AVERAGE BUBBLE SIZE, $\bar{r}_e$, FROM ELECTRO-RESISTIVITY PROBE MEASUREMENTS IN AIR-PEG SOLUTION FLOW

$\langle j_1 \rangle$ (cm/sec)	$\langle j_2 \rangle$ (cm/sec)	$\bar{r}_e$, From Eq. 8.3.6 (cm)	Slug Length, λ_s	
			From Eq. 4.24 (cm)	From Visual Observations (cm)
1.01	5.47	4.4	15.3	-
	7.79	4.2	17.7	-
13.82	2.89	2.3	2.4	2.5
	4.77	3.2	6.6	10.0
	7.12	4.1	14.6	-
18.84	4.85	3.8	11.1	4.0
	9.42	5.4	33.2	-

4.2.2.2 Gas holdup in three-phase fluidized beds

The measurement of gas holdup in three-phase fluidized beds was conducted mainly in the 2 inch i.d. perspex column. The limited preliminary data obtained in the 20 mm glass column will be discussed first. All the graphs and tables presented in this section are drawn from the data in Appendix 8.7.

(A) 20 mm glass column

The visual observation of the transparent column showed that the slug flow regime existed in this column at almost all the gas and liquid flow rates studied. However, at very small gas and liquid flow rates some large and irregular bubbles were observed in the column, but due to the small size of the column no clear distinction between the bubbly and slug flow regime could be made. The gas holdup data for one liquid flow rate from each of the three systems studied are presented in Figures 4.18-4.20. As can be seen, the agreement between the two techniques of gas holdup measurement is generally quite satisfactory.

It is important to recall that the gas holdup in the 20 mm glass column was measured in a section of the column which included not only the three-phase fluidized bed region, but also the preceding and the following two-phase gas-liquid regions (see Figure 3.1). A comparison of gas holdup so measured with the gas holdup in solids-free gas-

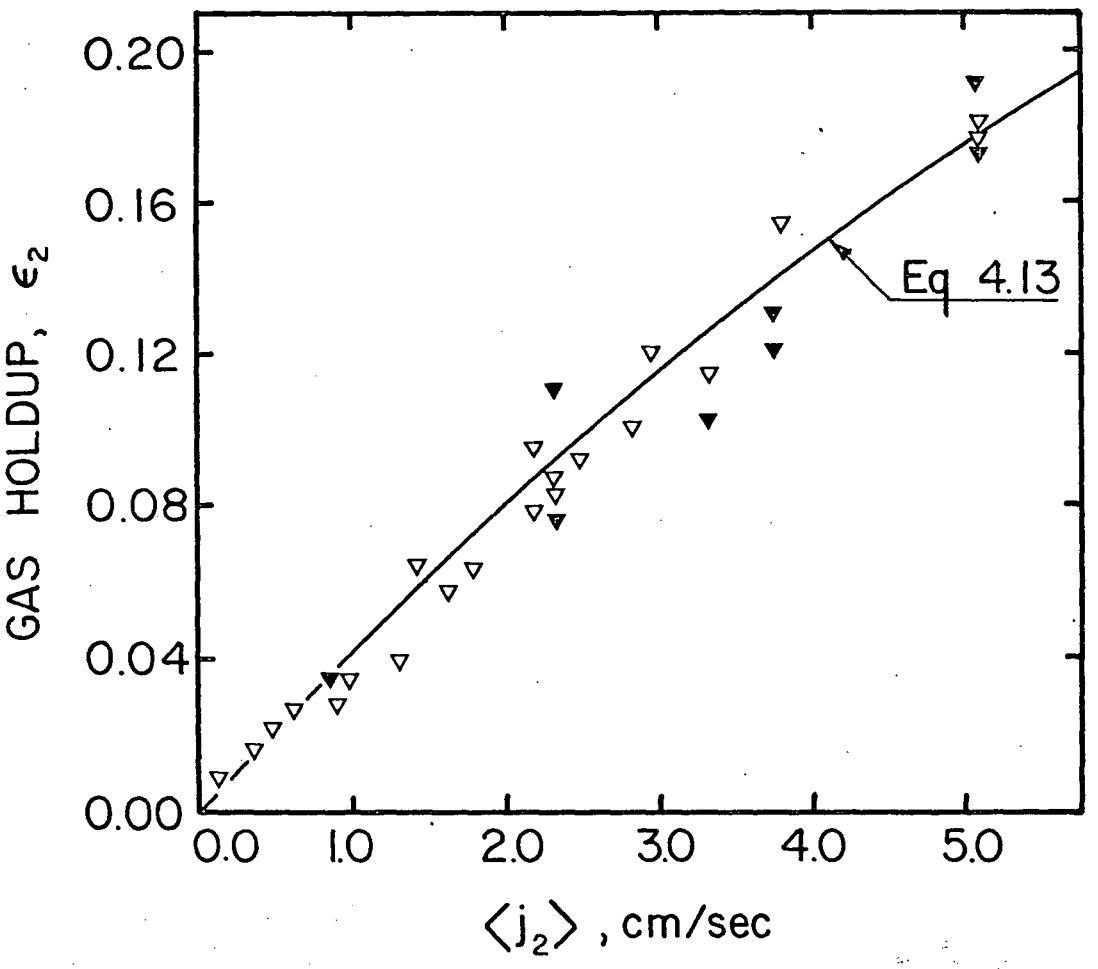

FIGURE 4.18 GAS HOLDUP IN 20 MM GLASS COLUMN FOR THREE-PHASE FLUIDIZATION BY AIR AND WATER OF 1 MM GLASS BEADS (j_1=6.02 cm/sec; W=50 gm; ▽- from pressure drop; ▼- from valve shut-off)

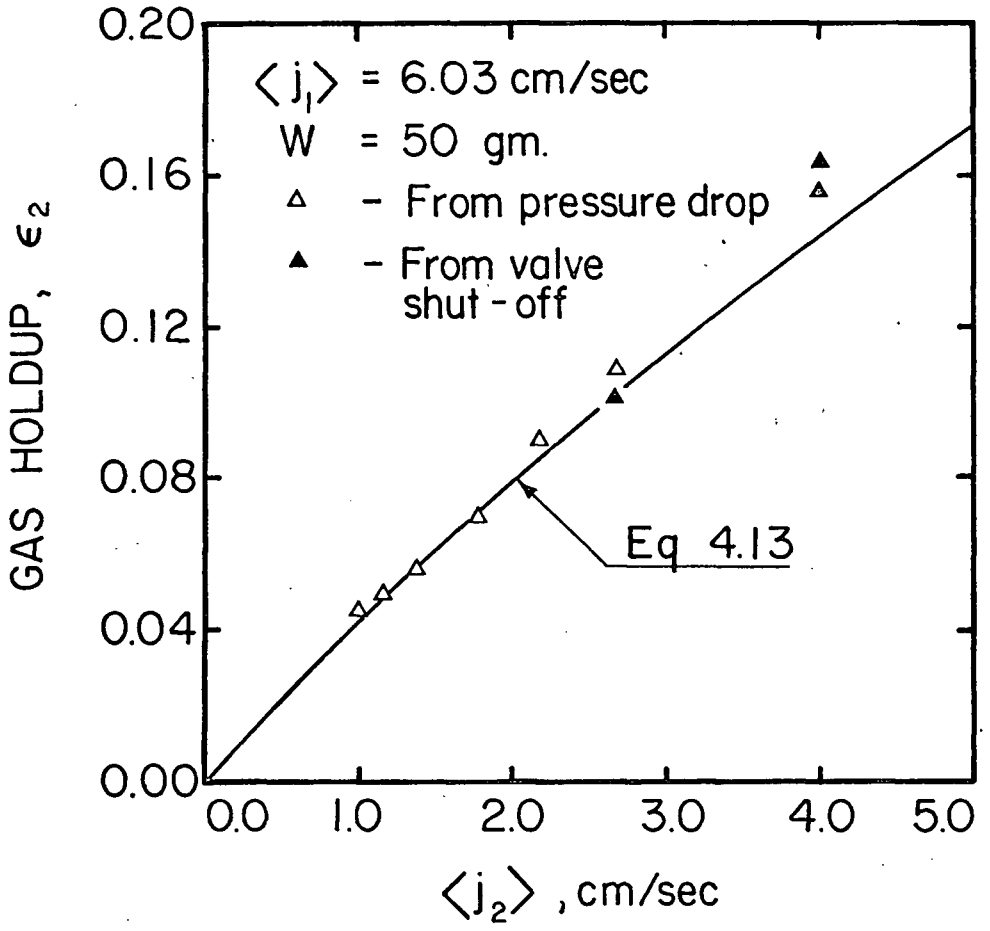

FIGURE 4.19 GAS HOLDUP IN 20 MM GLASS COLUMN FOR THREE-PHASE FLUIDIZATION BY AIR AND AQUEOUS GLYCEROL OF 1 MM GLASS BEADS

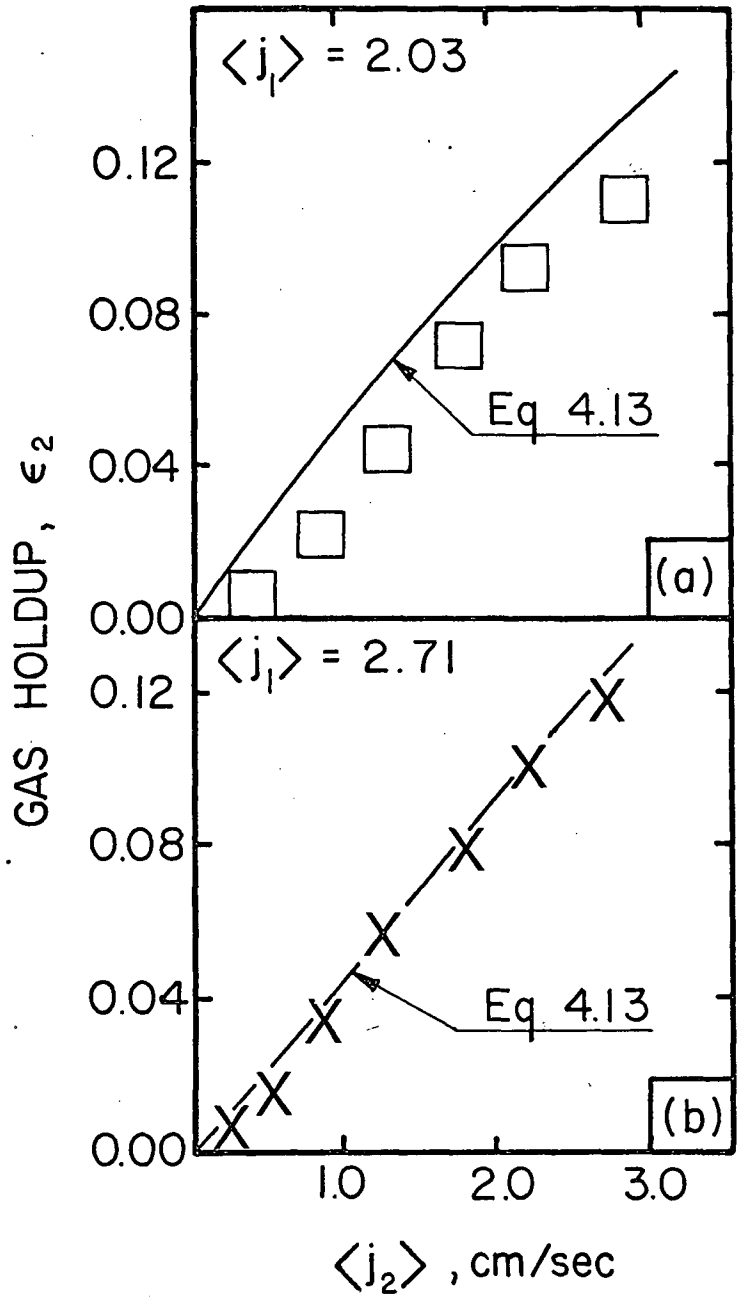

FIGURE 4.20 GAS HOLDUP IN 20 MM GLASS COLUMN FOR THREE-PHASE FLUIDIZATION BY AIR AND WATER OF 1/2 MM SAND PARTICLES

liquid flow could reveal possible effects of the presence of solids on the bubble dynamics. However, since no gas holdup for these combinations of gas and liquid flow rates were obtained in the absence of solids, equation 4.13 was used for predicting the gas holdup in gas-liquid flow.

In Figure 4.18 the gas holdups measured in the presence of a bed of 1 mm glass beads fluidized by a cocurrent stream of air and water are compared with the values predicted from equation 4.13. The two sets of values were found to be in good agreement, indicating that the presence of the 1 mm glass beads did not affect the gas holdup significantly. Similarly, the measured gas holdups in the presence of the same 1 mm glass beads fluidized by a cocurrent stream of air and aqueous glycerol solution (μ_l = 2.1 c.p.) showed good agreement with the predicted values from equation 4.13 (see Figure 4.19), indicating that neither the presence of solid particles nor the small change in liquid viscosity (μ_l doubled) affected the gas holdup. However, the measured gas holdups in the presence of a bed of 1/2 mm sand particles fluidized by a cocurrent stream of air and water at $\langle j_l \rangle$ = 2.03 cm/sec, were found to be consistently smaller than the values predicted by equation 4.13, as shown in Figure 4.20a. Thus the bed of 1/2 mm sand particles, for relatively low bed expansion, tended to reduce the gas holdup by promoting bubble coalescence within the bed. The gas holdups at higher liquid flow rates showed good

agreement with the predicted values from equation 4.13 (see Figure 4.20b), indicating once again that the solid particles had little or no effect on gas holdups.

(B) 2 inch perspex column

Experimental findings for each of the solid species studied are presented separately below.

(i) Air-water-1/4 mm glass beads

The visual observation of the fluidized bed and the region above the bed showed the existence of slugs in the experimental section for gas flow rates greater than 3 cm/sec at all the liquid flow rates studied. It is important to recall that, in contrast, for two of the liquid flow rates, $\langle j_l \rangle$ = 1.25 and 1.87 cm/sec, air-water runs performed in the absence of solids showed only the bubbly flow regime at most gas flow rates. The gas holdups measured in three-phase fluidized beds are shown in Figure 4.21 along with the curve for two-phase gas-liquid flow data reported earlier. It can be seen in Figure 4.21 that, whereas the gas holdups in three-phase fluidized beds for liquid flow rates of 1.25 and 1.87 cm/sec are practically identical, those for a liquid flow rate of 3.18 cm/sec are slightly, but consistently, larger. All these gas holdups are, however, smaller than those for two-phase gas-liquid flow.

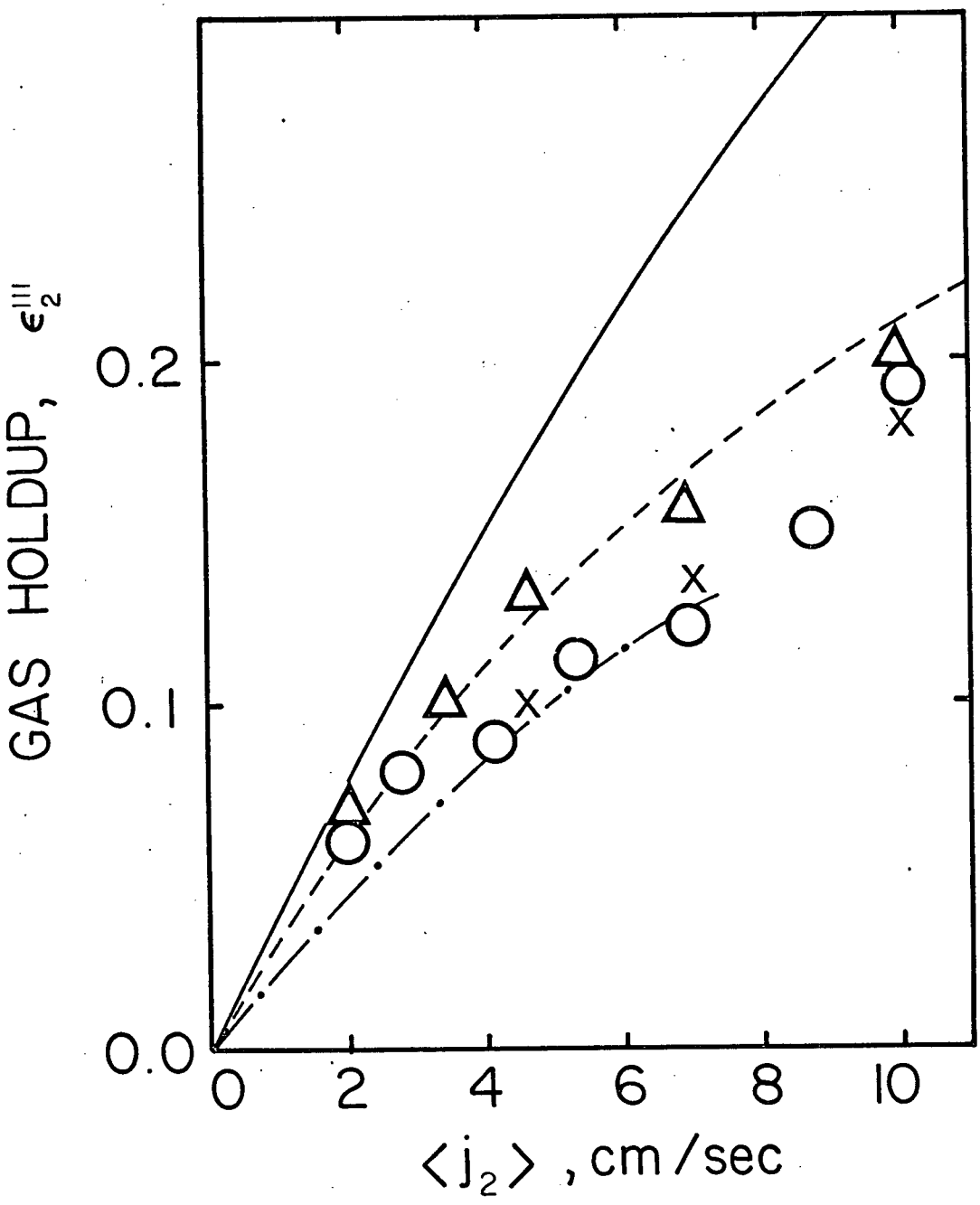

FIGURE 4.21 GAS HOLDUP IN THREE-PHASE BEDS OF 1/4 MM GLASS BEADS FLUIDIZED BY AIR AND WATER (o -j_1=1.25; x -j_1=1.87; Δ -j_1=3.18; ——— two-phase air-water flow, j_1=1.25; generalized wake model with x_k=0.4: —·—·—j_1=1.25, – – – – j_1=3.18)

The gas holdups in three-phase fluidized beds are compared in Table 4.17 with the gas holdups in different gas-liquid regions in the column, as well as with those in gas-liquid flow alone, for the liquid flow rate of 1.25 cm/sec:

1. Since the gas holdups in the two-phase regions above and below the test section were comparable (the former being slightly, but consistently, smaller), an average of all five or six gas holdup measurements in the three gas-liquid regions was taken to represent the gas holdup in the two-phase regions in the presence of a bed of solid particles. These gas holdups were significantly smaller than the gas holdups in the corresponding gas-liquid flow alone. Thus the introduction of a bed of solid particles seemed to affect the structure of gas-liquid flow not only downstream, but surprisingly even upstream, from the bed, apparently causing reduction in gas holdup by promoting bubble coalescence throughout the entire column.
2. The gas holdups in the three-phase fluidized beds as such were considerably smaller than those in gas-liquid flow alone, especially at gas flow rates greater than 4 cm/sec; however, the gas holdups in the three-phase fluidized beds represented on a solids-free basis were slightly larger than those in gas-liquid flow for gas flow rates less than 3 cm/sec, and somewhat smaller

TABLE 4.17

COMPARISON OF GAS HOLDUP IN THREE-PHASE FLUIDIZED BED TO THAT IN TWO-PHASE REGIONS OF THE COLUMN

SYSTEM: Air-Water- 1/4 mm Glass Beads, $\langle j_1 \rangle$ = 1.25 cm/sec, W = 1100 gm, $\varepsilon_3\big|_{j_2 = 0}$ = 0.237

Gas Flux, $\langle j_2 \rangle$ (cm/sec)	Gas Holdup		Average Gas Holdup in Two-Phase Regions	Average Gas Holdup in Gas-Liquid Flow	Gas Holdup in Three-Phase Regions	
	Below the Test Section	Above the Test Section			ε_2''' (measured)	On Solids Free Basis, $\varepsilon_2'''/(1-\varepsilon_3)$
2.03	0.061	0.055	0.054	0.077	0.059	0.092
2.80	0.094	0.075	0.080	0.104	0.080	0.124
4.17	0.128	0.110	0.118	0.155	0.090	0.137
5.30	0.151	0.135	0.140	0.194	0.113	0.173
6.90	0.199	0.175	0.183	0.243	0.122	0.189
8.71	0.234	0.213	0.215	0.278	0.150	0.233
10.00	0.266	0.238	0.244	0.300	0.183	0.278

for gas flow rates greater than 4 cm/sec. A further comparison of gas holdups in the three-phase fluidized beds on a solids-free basis with those in the concurrent two-phase regions showed that, in the slug flow regime ($j_2 >$ 3 cm/sec), the gas-liquid ratio changed only moderately from the two-phase to the three-phase region, the gas fraction being about 13% larger on the average in the three-phase region. Thus, for gas flow rates greater than 3 cm/sec, the presence of solid particles apparently caused the gas-liquid flow structure to be changed in the column as a whole, but not exclusively (to any significant extent) in the three-phase region.

Similar trends were observed for the other liquid flow rates as well.

As was shown earlier in Section 2.3.2, Vail et al. [17] recommended that the ratio of gas holdup in a three-phase fluidized beds to that in the corresponding two-phase gas-liquid flow, $\varepsilon_2'''/\varepsilon_2''$, was only a function of the bed voidage and was well represented by equation 2.120. Efremov and Vakhrushev [16] used the following empirical correlation to represent the ratio $\varepsilon_2'''/\varepsilon_2''$ from their measurements in a 4 inch diameter column:

$$\frac{\varepsilon_2'''}{\varepsilon_2''} = \left[\frac{\rho_1}{\rho_3 \varepsilon_{3H} + \rho_1 (1-\varepsilon_{3H})} \right]^{1.22} \qquad (4.25)$$

where ε_{3H} is the solids holdup in the liquid-solid fluidized bed before the gas is introduced. The ratios of experimentally measured gas holdups in three-phase fluidized beds to those in gas-liquid flow are compared in Table 4.18 with the predictions from equations 2.120 and 4.25. Although the measured ratios were found to vary somewhat with gas flow rates, the average values for gas flow rates between 2 and 10 cm/sec agreed closely with the predicted values from equation 4.25. Predictions from equation 2.120 were significantly smaller, the correlation being based on data in three-phase fluidized beds of 0.73 mm glass beads. Even though the measured absolute values of gas holdup did not agree with the reported data of Efremov and Vakhrushev either in gas-liquid flow or in three-phase fluidized beds, the equality of the gas holdup ratios seems to indicate that the role of solid particles in affecting the bubble dynamics is similar in both small diameter ($D < 4$ inch) and large diameter ($D \geq 4$ inch) columns.

As derived earlier in Section 2.3.1, equation 2.114 provides a general expression for describing the rise velocity of bubble swarms in three-phase fluidized beds, if a proper expression for calculating $\bar{v}'''_{21}$ is used. Equation 2.114, however, cannot be solved independently, but instead equation 2.112 was solved as an integral part of the generalized wake model with the following assumptions:

TABLE 4.18

COMPARISON OF GAS HOLDUP IN THREE-PHASE FLUIDIZED BED TO THAT IN GAS-LIQUID FLOW

SYSTEM: Air-Water- 1/4 mm Glass Beads

$\langle j_2 \rangle$ = 2-10 cm/sec

Liquid Flux, $\langle j_1 \rangle$ (cm/sec)	$\varepsilon_2'''/\varepsilon_2''$ (Experimental)	$\varepsilon_2'''/\varepsilon_2''$ (Eq. 4.25)	$\varepsilon_2'''/\varepsilon_2''$ (Eq. 2.120)	$\varepsilon_2'''/\varepsilon_2''$ (Model with x_k = 0.4)
1.25	0.62 (0.5-0.77)	0.59	0.41	0.55 (0.52-0.60)
1.87	0.64 (0.53-0.86)	0.68	0.48	0.74 (0.72-0.78)

1. Equation 2.46 can be used for describing the voidage in the particulate phase of three-phase fluidized beds, as will be shown later in Section 4.2.3.1.
2. Equation 2.112 can be used for calculating the rise velocity of bubble swarms in conjunction with equation 4.8 for the drift velocity in the slug flow regime, slugs having been observed under most conditions.
3. Equation 4.7 can be used for estimating the wake volume fraction, as discussed in Section 4.1.2.

Now for calculating the gas holdup and the bed voidage from the generalized wake model with these assumptions, the following eight equations have to be solved simultaneously for the eight unknowns involved (ε_1, ε_2, ε_3, ε_k, ε''_{1f}, $\bar{v}_2$, $\bar{v}'''_{21}$, v_{2j}):

$$\varepsilon_2 = \frac{\langle j_2 \rangle}{\bar{v}_2} \tag{2.94}$$

$$\bar{v}_2 = \frac{\langle j_1+j_2 \rangle}{\varepsilon} + \frac{\varepsilon''_{1f}(1-\varepsilon_2-\varepsilon_k)}{\varepsilon} \bar{v}'''_{21} \tag{2.112}$$

$$\bar{v}'''_{21} = \frac{v_{2j}}{\varepsilon'''_1} \tag{2.108a}$$

$$v_{2j} = 0.2 \langle j_1+j_2 \rangle + 0.35 \sqrt{gD} \tag{4.8}$$

$$\varepsilon''_{1f} = \left[\frac{\langle j_1\rangle - \bar{v}_2(1-x_k)\ \varepsilon_k}{V_\infty(1-\varepsilon_2-\varepsilon_k)}\right]^{1/n} \tag{2.106}$$

$$\varepsilon_k = \varepsilon'''_2 \left[\frac{\Omega_k}{\Omega_B}\ \varepsilon^3\right] \tag{4.7}$$

$$\varepsilon = (1-\varepsilon_3) = \varepsilon'''_1 + \varepsilon'''_2 \tag{1.3}$$

$$\varepsilon'''_1 = \varepsilon_k(1-x_k) + \varepsilon''_{1f}(1-\varepsilon_2-\varepsilon_k+x'_k\varepsilon_k) \tag{2.91}$$

A trial and error scheme was developed for solving these equations numerically. The convergence for small gas flow rates (j_2 < 2 cm/sec), even for small liquid flow rates ($\langle j_1\rangle$ = 1.25 cm/sec), was quickly obtained; but for large gas flow rates and small values of x_k ($x_k \simeq 0$), the trial and error scheme adopted failed to converge for 1/4 mm glass beads, as will be illustrated later in Section 4.2.3.2. It was, however, found that neither the wake volume fraction, ε_k, nor the relative particle content of the wake, x_k, affected the value of gas holdup significantly. Thus the values of gas holdup predicted by the generalized wake model are shown in Figure 4.21 for x_k = 0.4 because the trial and error scheme failed to converge for smaller values of

x_k. The agreement between the predicted and the measured values is good enough to confirm the correctness of equation 2.112 for describing the rise velocity of bubble swarms. The predicted values show the gas holdup to increase with increasing gas and liquid flow rates. The ratios of the predicted values of gas holdup in three-phase fluidized beds to the measured values in gas-liquid flow, presented in Table 4.18, show that, although these ratios varied slightly with the gas flow rates, the average values at a given liquid flux were in reasonably good agreement with the predictions from empirical equation 4.25, as well as with the measurements, indicating that equation 2.112 appropriately accounted for the role of particles in affecting the bubble behaviour.

(ii) Air-water- 1/2 mm glass beads

The visual observation of the fluidized bed and the region above the bed, at all liquid flow rates studied, showed that for gas flow rates greater than 4 cm/sec, fully developed slugs were present in the column, while for gas rates less than 3 cm/sec, the flow was primarily bubbly with intermittent occurrence of large irregular bubbles due to coalescence. The bubble motion appeared to be quite chaotic and violent even though the liquid flow, except at the two highest rates, was not turbulent. The increase in liquid flow rate, or bed fluidity, had, in general, a calming effect on the bubble motion.

The measured values of gas holdup in three-phase fluidized beds are shown in Figure 4.22 along with the curve for two-phase gas-liquid flow data reported earlier. The gas holdups at the liquid flow rate of 1.59 cm/sec were found to fluctuate for gas flow rates greater than 7 cm/sec, as particle bridging occurred frequently, causing the bed to be lifted off the bed support screen. No bridging was observed for higher liquid flow rates. The gas holdup was found to increase with increasing gas flow rate, as can be seen from Figure 4.22, but the similar effect of increasing liquid flow rate was not as clearly discernible from the data.

The values of gas holdup measured in the three-phase fluidized bed region are compared in Table 4.19 with those in the corresponding two-phase regions of the column, as well as with those in two-phase gas-liquid flow, at the liquid flow rate of 4.55 cm/sec, for W = 567 gm , W = 1200 gm. As can be seen from this table, the weight of the particles in the column (or the height of the three-phase fluidized bed region) neither affected the gas holdup in the two-phase regions nor that in the three-phase fluidized bed itself, even though the solids holdup was markedly affected, as will be shown later in Section 4.2.3.2. Other inferences from the table are:

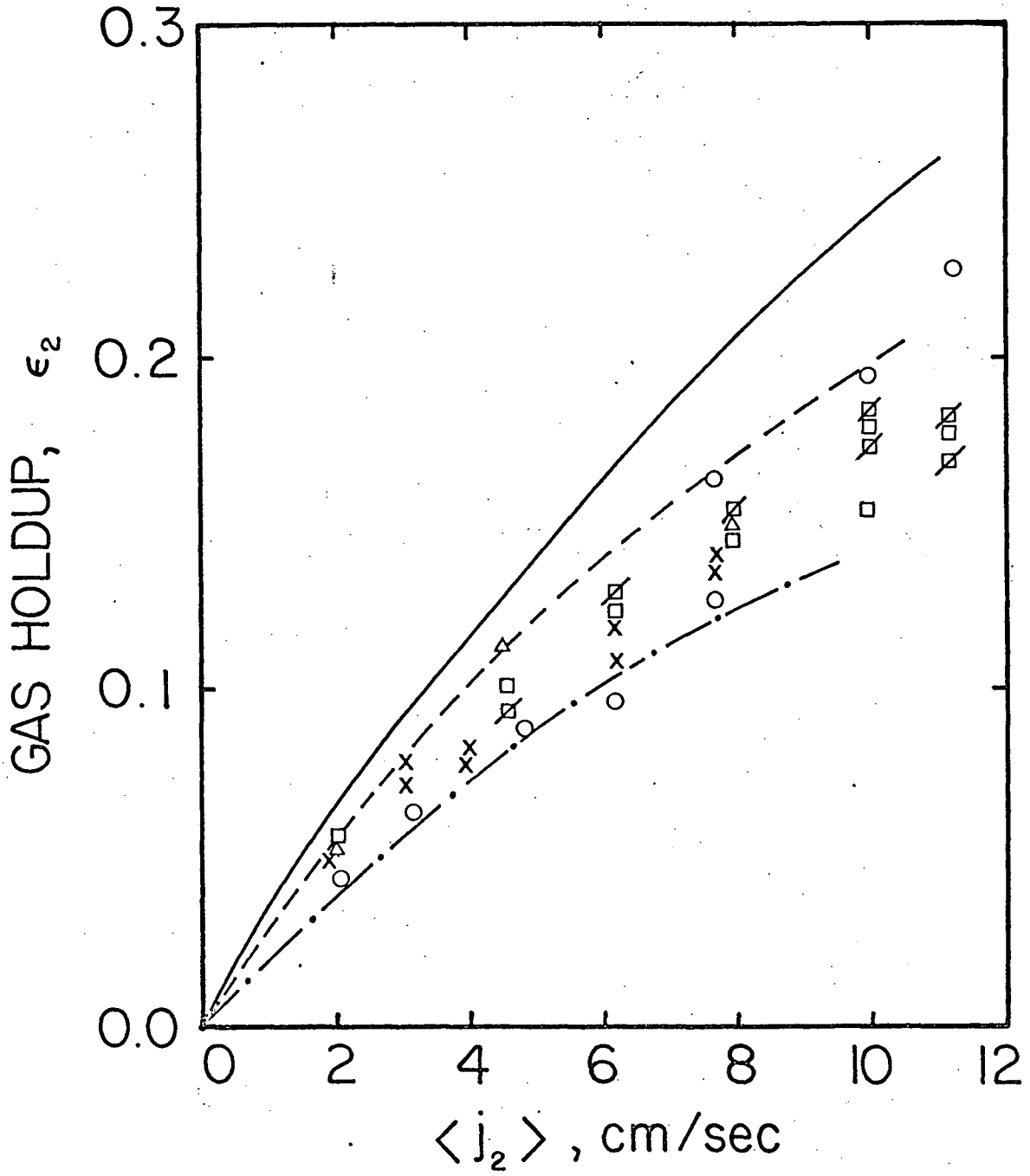

FIGURE 4.22 GAS HOLDUP IN THREE-PHASE BEDS OF 1/2 MM GLASS BEADS FLUIDIZED BY AIR AND WATER (○ -j_1=1.59; x-j_1=3.52; □ -j_1=4.55 (W=1200); ⊘-j_1=4.55 (W=567); △ j_1=5.71; ——— two-phase air-water flow, j_1=4.55; generalized wake model with x_k=0: —·—·— j_1=1.59, — — — — j_1=5.71)

TABLE 4.19

COMPARISON OF GAS HOLDUP IN THREE-PHASE FLUIDIZED BED TO THAT IN TWO-PHASE REGIONS OF THE COLUMN

SYSTEM: Air-Water- 1/2 mm Glass Beads, $\langle j_1 \rangle$ = 4.55 cm/sec

Gas Flux, $\langle j_2 \rangle$ (cm/sec)	Gas Holdup		Average Gas Holdup in Two-Phase Regions	Average Gas Holdup in Gas-Liquid Flow	Gas Holdup in Three-Phase Regions	
	Below the Test Section	Above the Test Section			ε_2'' (measured)	On Solids Free Basis, $\varepsilon_2''/(1-\varepsilon_3)$
			W = 567 gm, $\varepsilon_3\|_{j_2=0}$ = 0.134			
2,00	0.054	0.052	0.054	0.061	0.056	0.073
4.54	0.116	0.112	0.116	0.128	0.093	0.122
6.17	0.152	0.142	0.147	0.163	0.130	0.171
7.92	0.186	0.164	0.177	0.213	0.154	0.204
9.94	0.227	0.213	0.220	0.246	0.172	0.225
11.23	0.265	0.234	0.256	0.258	0.176	0.228
			W = 1200 gm, $\varepsilon_3\|_{j_2=0}$ = 0.148			
2.06	0.057	0.053	0.057	0.065	0.055	0.073
4.51	0.132	0.102	0.116	0.128	0.101	0.139
6.17	0.158	0.138	0.150	0.163	0.125	0.173
7.91	0.192	0.177	0.182	0.204	0.146	0.200
9.94	0.248	0.210	0.225	0.246	0.154	0.211
11.25	0.277	0.247	0.253	0.258	0.177	0.243

1. At a given gas and liquid rate, gas holdups in the two-phase regions above and below the test section are observed to be comparable. Therefore the average of all the gas holdup measurements in the three two-phase regions was taken to represent the gas holdup in these two-phase regions for the given flow rates. These gas holdups are observed to be slightly smaller than those in the corresponding gas-liquid flow without solids in the column. Thus the presence of a bed of 1/2 mm glass beads affected the structure of gas-liquid flow in the adjacent regions only slightly.
2. The gas holdups in the three-phase fluidized beds as such were smaller than those in gas-liquid flow at gas fluxes exceeding 4 cm/sec; however, when represented on a solids-free basis, they approximated both the gas holdups in the adjacent two-phase regions and the gas holdups in gas-liquid flow alone. Thus the gas-liquid ratio remained practically unchanged, from the two-phase region to the three-phase region, from which it can be inferred that the structure of bubble flow through the bed of 1/2 mm glass beads is little different from that of the corresponding two-phase gas-liquid flow.

Similar trends were found for the other liquid flow rates as well.

The ratios of gas holdups measured in three-phase fluidized beds to those measured in two-phase gas-liquid flow are compared with the predictions of equations 4.25 and 2.120 in Table 4.20. Even though the ratios varied somewhat with gas flow rates, the averages of these ratios, for gas flow rates between 2 and 11 cm/sec, are seen to be in excellent agreement with the values predicted from equation 4.25. Predictions from equation 2.120 were significantly lower, as found previously for the 1/4 mm glass beads. The agreement with equation 4.25 once again indicates that the effect of particles on the bubble dynamics is the same in both large ($D \geq 4$ inches) and small ($D = 2$ inch) diameter columns.

In order to check the applicability of the generalized wake model, the eight equations listed above (Equations 2.94, 2.112, 2.108a, 4.8, 2.106, 4.7, 1.3 and 2.91) were solved numerically. The convergence for all the gas and liquid flow rates was in this case quite satisfactory, and the gas holdups calculated from the model with $x_k = 0$ are shown in Figure 4.22 for the highest ($\langle j_l \rangle = 5.71$ cm/sec) and the lowest ($\langle j_l \rangle = 1.59$ cm/sec) liquid flow rates. It was again observed that neither the wake volume fraction, ε_k, nor the relative particle content of the wake, x_k, affected the gas holdup significantly. However, an increase in either the gas or the liquid flow rate caused the gas holdup to increase. The ratios of the predicted values of gas holdup

TABLE 4.20

COMPARISON OF GAS HOLDUP IN THREE-PHASE FLUIDIZED BED TO THAT IN GAS-LIQUID FLOW

SYSTEM: Air-Water- 1/2 mm Glass Beads

$\langle j_2 \rangle$ = 2-11 cm/sec

Liquid Flux, $\langle j_l \rangle$ (cm/sec)	$\varepsilon_2'''/\varepsilon_2''$ (Experimental)	$\varepsilon_2'''/\varepsilon_2''$ (Eq. 4.25)	$\varepsilon_2'''/\varepsilon_2''$ (Eq. 2.120)	$\varepsilon_2''' \varepsilon_2''$ (Model with $x_k = 0$)
4.55	0.74 (0.67-0.84)	0.75	0.55	0.82 (0.80-0.83)
5.71	0.86 (0.76-0.90)	0.85	0.66	0.89 (0.86-0.91)

in three phase fluidized beds to the measured (for $\langle j_l \rangle$ = 4.55 cm/sec) or the predicted(for $\langle j_l \rangle$ = 5.71 cm/sec, at which no gas-liquid flow measurements were made) values in gas-liquid flow, presented in Table 4.20, show that although this ratio varied slightly with gas flow rate, the averaged values were in good agreement with the predictions from equation 4.25, as well as with the measurements, indicating again that equation 2.112 appropriately accounted for the role of particles in affecting the bubble behaviour in three-phase fluidized beds.

The electro-resistivity probe developed for this study and tested successfully in two-phase air-water flow, was used for the purpose of measuring the gas holdup inside the three-phase fluidized bed directly. The operation of the probe was more troublesome than in air-water flow, as it became quite difficult to identify the signal corresponding to the gas phase. The glass beads, being non-conductive, made the datum fluctuate considerably. Thus, in order to assure that only the signal corresponding to the gas phase was integrated, the cut-off level in the comparator had to be raised from 0.05 volt to 0.5 volt above the datum. Measured gas holdup profiles are shown in Figure 4.23 and integrated average gas holdups are presented in Table 4.21. It can be seen that the two gas holdup profiles in Figure 4.23 are both axially symmetric and well represented by

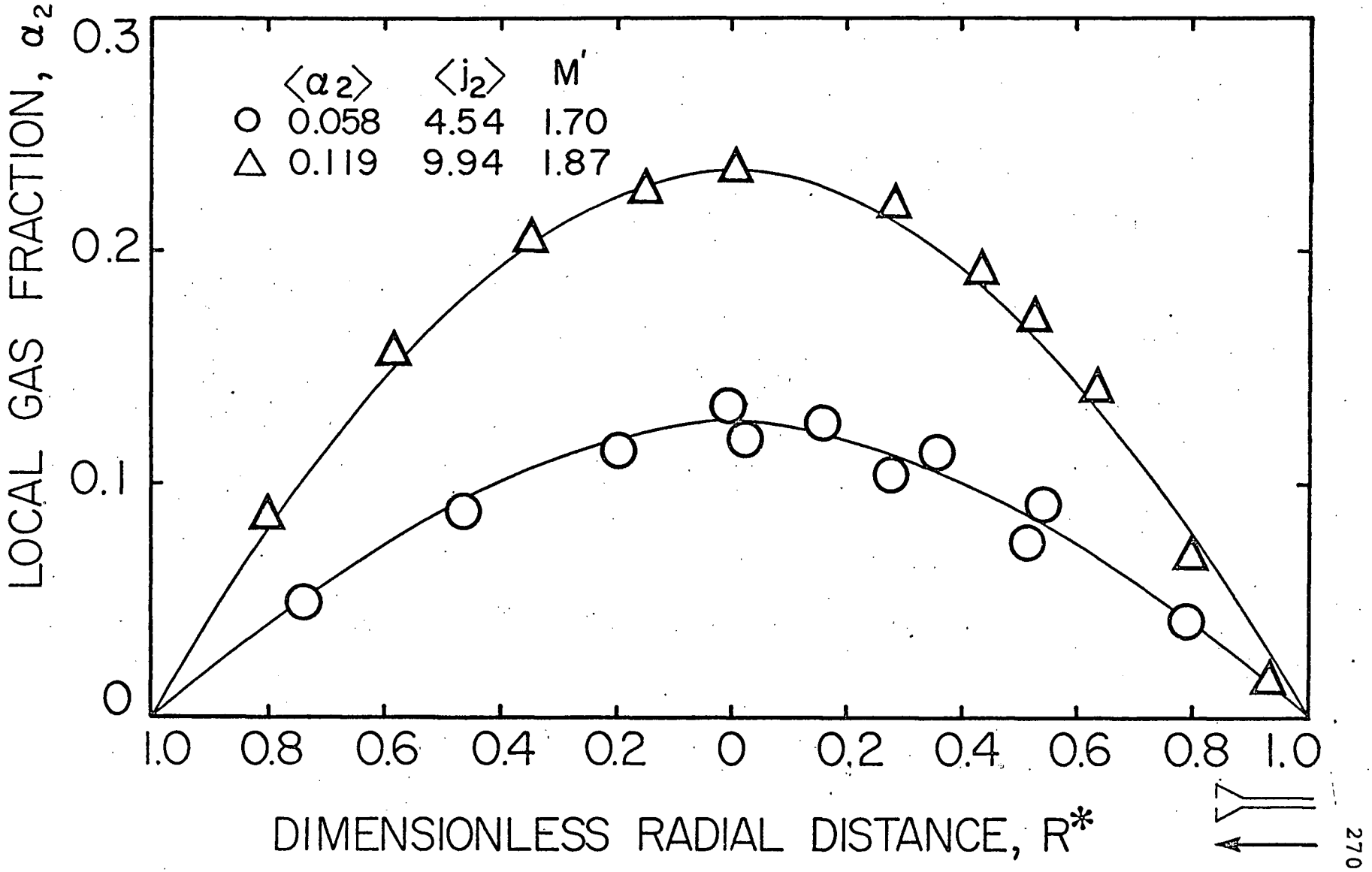

FIGURE 4.23 COMPARISON OF GAS HOLDUP PROFILES COMPUTED BY EQUATION 2.27b WITH EXPERIMENTAL DATA (System: Air-water-1/2 mm glass beads; j_1 = 4.55)

TABLE 4.21

GAS HOLDUP BY ELECTRO-RESISTIVITY PROBE IN THREE-PHASE FLUIDIZED BED

SYSTEM: Air-Water- 1/2 mm Glass Beads,

$\langle j_1 \rangle$ = 4.55 cm/sec

Gas Flux, $\langle j_2 \rangle$ (cm/sec)	α_{2C}	$\langle \alpha_2 \rangle$	ε_2	Ratio ($\varepsilon_2/\langle \alpha_2 \rangle$)	M' From Equation 4.23
4.54	0.127	0.058	0.093	1.60	1.70
7.92	0.228	0.100	0.153	1.52	1.60
9.94	0.235	0.119	0.187	1.57	1.87

equation 2.27b. A comparison of these profiles with those obtained in gas-liquid flow for similar gas and liquid flow rates (cf. Figure 4.16) shows the gas holdup profiles in three-phase fluidized beds to be more pointed, thus indicating that the presence of a bed of 1/2 mm glass beads renders the radial gas holdup distribution more non-uniform.

The average gas holdup was obtained, as before, by integrating these profiles according to equation 3.5. The average gas holdups, so calculated, were found to be consistently smaller than those measured by the pressure drop gradient and valve shut-off techniques. These consistent discrepancies are believed to have been caused by being forced to employ a high cut-off level in the comparator, thereby introducing a small error in the residence time of each bubble as recorded by the integrator; since no independent investigation was undertaken to identify the various sources of errors, these values of gas holdups are not shown in Figure 4.22. It is nevertheless believed that with some further modifications in the design of the probe, along with a better method of processing the probe output, the electroresistivity probe can be successfully used for measuring the local properties of the gas bubble phase in three-phase fluidized beds.

(iii) Air-water- 1 mm glass beads

Visual observation of the fluidized bed and the region above the bed showed the existence of fully developed slugs for gas flow rates greater than 4 cm/sec at all the liquid flow rates studied. The measured values of gas holdup are shown in Figure 4.24 along with the data curve for gas-liquid flow alone. It is clear that the gas holdup in the three-phase fluidized bed increases with increase in gas flow rate, but the effect of liquid flow rate appears to be either small or negligible.

The gas holdups in the three-phase fluidized bed are compared in Table 4.22 with those in various two-phase regions of the column, as well as with those in gas-liquid flow alone, for the liquid flow rate of 12.80 cm/sec:

1. A comparison of the gas holdups in the two-phase regions above and below the test section show them to be almost identical to each other, at a given gas and liquid flow rate. Therefore the average of all the gas holdup measurements in the two-phase regions was taken to represent the gas holdup in these regions for the given flow rates. These gas holdups in turn are equal to those measured in the corresponding gas-liquid flow without solids. Thus the presence of a bed of 1 mm glass beads does not affect the gas holdup, and therefore presumably not the flow structure, in air-water flow.

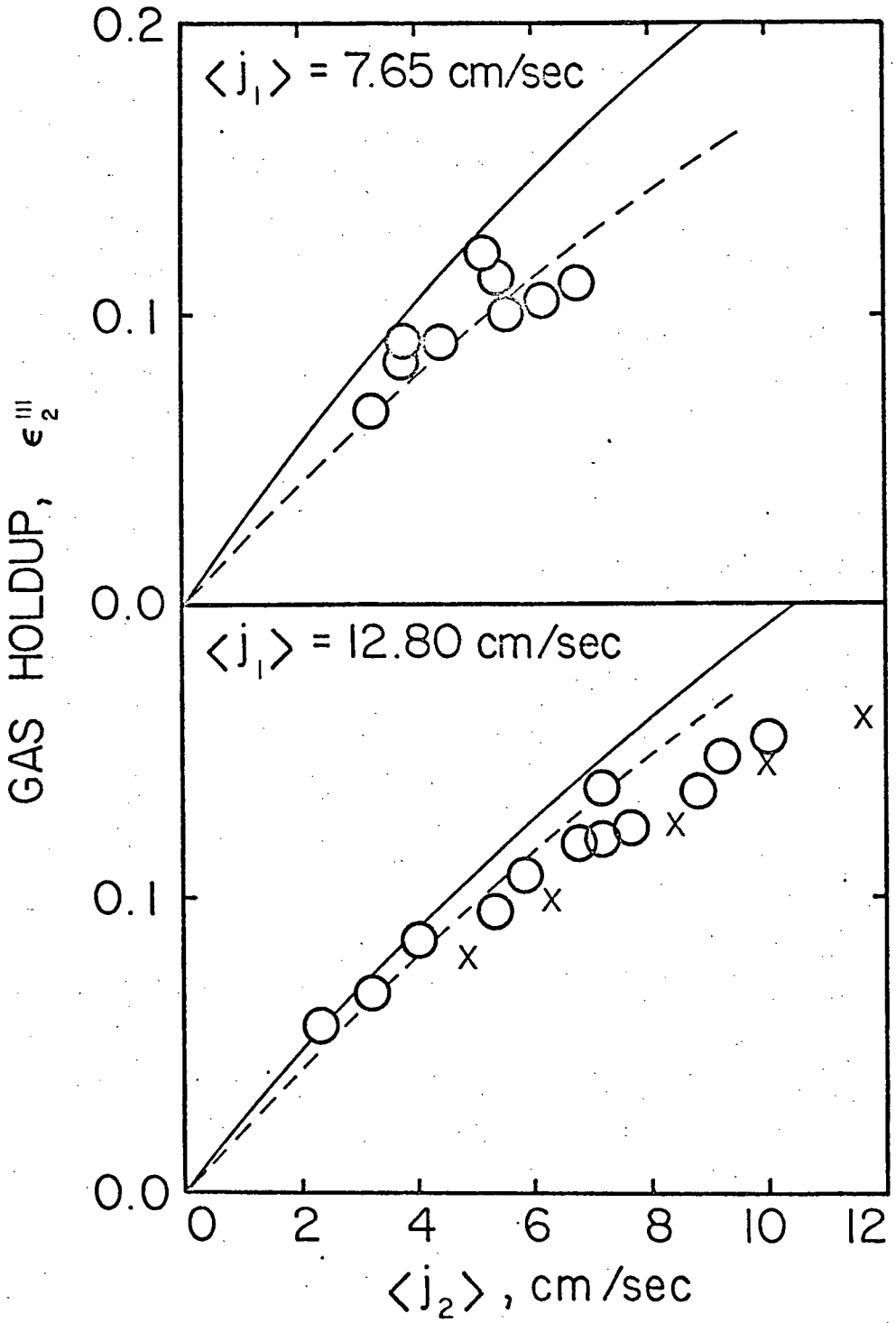

FIGURE 4.24 GAS HOLDUP IN THREE-PHASE BEDS OF 1 MM GLASS BEADS FLUIDIZED BY AIR AND WATER (x - average of 5 repeated runs; – – – – generalized wake model with x_k=0; ——— two-phase air-water flow)

TABLE 4.22

COMPARISON OF GAS HOLDUP IN THREE-PHASE FLUIDIZED BED TO THAT IN TWO-PHASE REGIONS OF THE COLUMN

SYSTEM: Air-Water- 1 mm Glass Beads, $\langle j_1 \rangle$ = 12.80 cm/sec, W = 487.0 gm, $\varepsilon_3\big|_{j_2=0}$ = 0.117

Gas Flux, $\langle j_2 \rangle$ (cm/sec)	Gas Holdup		Average Gas Holdup in Two-Phase Regions	Average Gas Holdup in Gas-Liquid Flow	Gas Holdup in Three-Phase Regions	
	Below the Test Section	Above the Test Section			ε_2''' (measured)	On Solids Free Basis, $\varepsilon_2'''/(1-\varepsilon_3)$
4.85	0.102	0.100	0.100	0.105	0.079	0.093
6.33	0.128	0.123	0.126	0.133	0.100	0.117
8.42	0.168	0.155	0.163	0.169	0.124	0.145
10.06	0.194	0.204	0.192	0.194	0.149	0.173
11.66	0.234	0.230	0.232	0.216	0.162	0.188

2. The gas holdups in the three-phase fluidized bed as such are somewhat smaller than those in gas-liquid flow alone; however, when represented on a solids-free basis, they become almost equal to those in gas-liquid flow. This then indicates that the gas-liquid ratio remains almost unchanged from the two-phase region to the three-phase region. Therefore the bubble flow behaviour within the bed of 1 mm glass beads would appear to be little different than in the corresponding two-phase gas-liquid flow, as also noted earlier for the 1/2 mm particles.

The ratios of gas holdups in three-phase fluidized beds to those in gas-liquid flow, from experimental measurements, are compared in Table 4.23 with the predicted values from equations 4.25 and 2.120. Also included in the table are the gas holdup ratios calculated from the experimental measurements of Michelsen and Østergaard [14] for 1 mm glass beads at a water flow rate of 7.8 cm/sec. It is seen in Table 4.23 that, while the ratios of measured gas holdups for the liquid flow rate of 7.65 cm/sec are in reasonably good agreement with those of Michelsen and Østergaard, both of these ratios are considerably larger than those predicted by either equation 4.25 or equation 2.120. On the other hand, the measured gas holdup ratios for the liquid flow rate of 12.80 cm/sec are in better agreement with the predicted values

TABLE 4.23

COMPARISON OF GAS HOLDUP IN THREE-PHASE FLUIDIZED BED TO THAT IN GAS-LIQUID FLOW

SYSTEM: Air-Water- 1 mm Glass Beads
$\langle j_2 \rangle$ = 2-12 cm/sec

Liquid Flux, $\langle j_1 \rangle$ (cm/sec)	$\varepsilon_2'''/\varepsilon_2''$ (Experimental)	$\varepsilon_2'''/\varepsilon_2''$ (Eq. 4.25)	$\varepsilon_2'''/\varepsilon_2''$ (Eq. 2.120)	$\varepsilon_2'''/\varepsilon_2''$ (Model with $x_k = 0$)	$\varepsilon_2'''/\varepsilon_2''$ [14]
7.65	0.80 (0.72-0.91)	0.59	0.53	0.77 (0.74-0.79)	-
7.80	-	-	-	-	0.73 (0.64-0.80)
12.80	0.82 (0.73-0.94)	0.76	0.72	0.92 (0.90-0.94)	-

from both equation 4.25 and equation 2.120. Therefore only at the larger liquid flux can it be surmised that the effect of 1 mm glass beads on the bubble dynamics is about the same in both large and small diameter columns.

In order to check the applicability of the generalized wake model, the eight equations mentioned earlier were again solved numerically. The convergence for all the gas and liquid flow rates studied was good, and the gas holdups calculated from the model with $x_k = 0$ are shown in Figure 4.24 for liquid flow rates of 7.65 and 12.80 cm/sec. The agreement between the measured and predicted values was quite good, although the predicted gas holdups for the liquid flow rate of 12.80 cm/sec were somewhat high. Once again it was observed that neither the wake volume fraction, ε_k, nor the relative particle content of the wake, x_k, had any significant effect on gas holdups. However, an increase in either the gas or the liquid flow rate caused the gas holdup to increase. The predicted ratios of gas holdup in the three-phase fluidized bed to gas holdup in the corresponding gas-liquid flow, presented in Table 4.23, show that, although the ratio varied somewhat with gas flow rate, the averaged values at a given liquid flux were in reasonably good agreement with the measured values. This then indicates again that equation 2.112 appropriately considers the role of particles in affecting the bubble behaviour.

(iv) Air-water- 2 mm lead shot

The visual observation of the fluidized bed as well as the region above the bed showed that both bubbly and slug flow regimes occurred, depending primarily on the gas flow rate. The transition from bubbly to slug flow was observed to occur between the gas flow rates of 6-8 cm/sec at all the liquid flow rates studied. Below the gas flow rate of 6 cm/sec, in the bubbly flow regime ($d_b \simeq$ 5-10 mm), very little coalescence occurred, especially at the higher liquid flow rates.

The gas holdups measured in the three-phase fluidized beds are shown in Figure 4.25a-d. The gas holdup increased with increase in gas flow rate at all the liquid flow rates studied. No abrupt change in gas holdup due to change in flow regime was clearly noticeable, nor could the effect of an increase in liquid flow rate on the gas holdup be clearly established from the measured data.

The values of gas holdup measured in the three-phase fluidized beds are compared in Table 4.24 with the measured values in various two-phase regions of the column and with those in gas-liquid flow alone, for the liquid flow rate of 26.4 cm/sec:

1. A comparison of gas holdups in the two-phase regions above and below the bed showed that they were not only equal to each other but were also equal to the corresponding gas holdups in gas-liquid flow as calculated from equation 4.18. This then indicates that

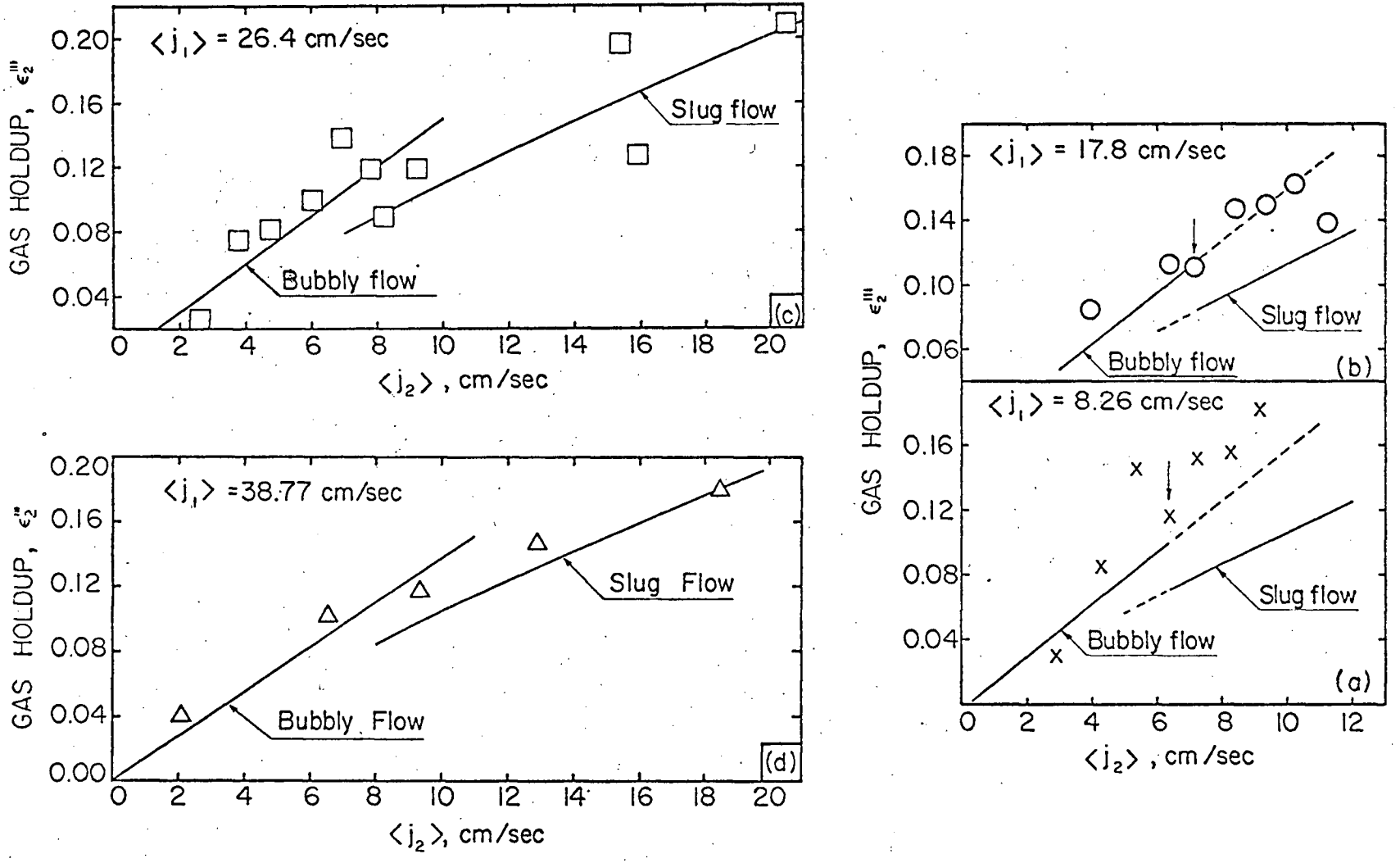

FIGURE 4.25 GAS HOLDUP IN THREE-PHASE BEDS OF 2 MM LEAD SHOT FLUIDIZED BY AIR AND WATER (——— generalized wake model with $x_k = 0$; arrows indicate observed change from bubbly flow to slug flow)

TABLE 4.24

COMPARISON OF GAS HOLDUP IN THREE-PHASE FLUIDIZED BED TO THAT IN TWO-PHASE REGIONS OF THE COLUMN

SYSTEM: Air-Water-Lead Shot, $\langle j_1 \rangle$ = 26.40 cm/sec., W = 3414.0 gm, $\varepsilon_3|_{j_2=0}$ = 0.320

Gas Flux, $\langle j_2 \rangle$ (cm/sec)	Gas Holdup		Average Gas Holdup in Two-Phase Regions	Average Gas Holdup in Gas-Liquid Flow	Gas Holdup in Three-Phase Regions	
	Below the Test Section	Above the Test Section			ε_2''' (measured)	On Solids Free Basis, $\varepsilon_2'''/(1-\varepsilon_3)$
2.56	0.042	0.049	0.043	0.043	0.026	0.037
3.77	0.060	0.060	0.060	0.062	0.074	0.104
4.73	0.077	0.078	0.077	0.076	0.081	0.114
6.00	0.097	0.097	0.100	0.094	0.100	0.138
6.91	0.113	0.114	0.115	0.107	0.139	0.193
7.73	0.125	0.121	0.123	0.118	0.119	0.168
8.15	0.134	0.128	0.132	0.123	0.090	0.127
9.17	0.148	0.142	0.148	0.136	0.118	0.168
15.60	0.205	0.200	0.200	0.208	0.163	0.227
20.50	0.266	0.254	0.262	0.253	0.209	0.286

the gas-liquid ratio in the two-phase regions remained unaffected by the presence of 2 mm lead shot.

2. A comparison of gas holdups in the three-phase fluidized beds to those in the two-phase regions showed that the absolute values of the gas holdups in the three-phase fluidized beds as measured were inconsistently smaller than, equal to, or greater than the corresponding values in gas-liquid flow up to a gas flow rate of 8 cm/sec, above which the three-phase values were consistently smaller. However, almost all the gas holdups in the three-phase fluidized beds, when represented on a solids-free basis, were found to be greater than those in gas-liquid flow alone, indicating that the gas-liquid ratio within the bed was considerably affected by the relatively large and heavy solid particles.

The ratios of gas holdups measured in the three-phase fluidized beds to those measured ($\langle j_l \rangle$ = 17.80 cm/sec) or predicted ($\langle j_l \rangle$ = 26.40 cm/sec) in gas-liquid flow are compared in Table 4.25 with the predicted values from equations 4.25 and 2.120. The former values were many times greater than those predicted by either equation 4.25 or equation 2.120. Since neither of these equations was based on experimental data for large and heavy particles, and since no consideration was given to bubble dynamics in their development, their failure to predict for such systems was

TABLE 4.25

COMPARISON OF GAS HOLDUP IN THREE-PHASE FLUIDIZED BED TO THAT IN GAS-LIQUID FLOW

SYSTEM: Air-Water- Lead Shot
$\langle j_2 \rangle$ = 2.5-21.0 cm/sec

Liquid Flux, $\langle j_1 \rangle$ (cm/sec)	ε_2'' ε_2'' (Experimental)	ε_2'' ε_2'' (Eq. 4.25)	ε_2'' ε_2'' (Eq. 2.120)	ε_2'' ε_2'' (Model)
17.8	0.92 (0.73-1.02)	0.13	0.37	0.73 (0.63-0.86)
26.4	0.93 (0.73-1.20)	0.17	0.50	0.84 (0.75-0.99)

not unexpected. The measurement of gas holdup for a similar system of large heavy particles has not been reported by any of the earlier investigators, and therefore no further comparisons could be made.

In order to check the applicability of the generalized wake model, the following assumptions were made based on visual observations and experimental measurements:

(i) The bed expansion characteristics of lead shot fluidized by water are well represented by the dimensional correlation of Trupp [87], as will be shown in Section 4.2.3.1. Therefore equation 2.106, used for describing the voidage in the particulate phase of the three-phase fluidized bed, is modified for the air-water-lead shot system to

$$\varepsilon''_{1f} = \left[\frac{\langle j_1 \rangle - \bar{v}_2 (1-x_k)\ \varepsilon_k}{0.36\ V_\infty^{1.18} (1-\varepsilon_2-\varepsilon_k)} \right]^{1/2.28} \qquad (4.26)$$

(ii) Since both the bubbly and the slug flow regimes were observed to exist, the drift velocity for the bubbly flow regime is assumed to be given by

$$v_{2j} = (V_\infty)_B \sqrt{\tanh\ [0.25 (1/\varepsilon''_2)^{1/3}]} \qquad (2.37)$$

where $(V_\infty)_B$ is calculated from equation 2.10 for an assumed bubble radius, $\bar{r}_e$ = 4 mm ($d_b \simeq$ 5-10 mm), while equation 4.8 is used for the slug flow regime as before.

The other equations in the model remained the same as before and all eight equations were solved numerically. The convergence for all the gas and liquid flow rates was satisfactory, and the gas holdups calculated from the model with $x_k = 0$ are shown in Figure 4.25a-d. The calculated values showed a break at the transition point between regimes because a constant rather than a steadily increasing bubble radius was assumed in the bubbly flow regime. The measured values, on the other hand, showed a gradual shift from the curve for the bubbly flow regime towards the curve for the slug flow regime, especially at high liquid flow rates (Figure 4.25d). The agreement between the calculated and the predicted values was in general good. The effect of liquid flow rate on the predicted values of gas holdup was small. The ratio of the predicted gas holdup in the three-phase fluidized bed to that in the corresponding gas-liquid flow, presented in Table 4.25, was found to increase with increasing gas flow rate in the bubble flow regime (approaching a value near unity at $\langle j_2 \rangle \simeq 7$ cm/sec), but remained practically constant (but less than unity) in the slug flow regime. The averaged values were also in considerably better agreement with the measured values than those predicted by either equation 4.25 or equation 2.120. This then indicates that equation 2.112 appropriately incorporates the effect of 2 mm lead shot on the air-water bubble behaviour in three-phase fluidized beds.

(v) Air-PEG solution - 1 mm glass beads

The gas holdup data obtained with this system were limited because a stable three-phase fluidization could not be achieved due to consistent elutriation of glass beads even at a gas flow rate as low as 1 cm/sec. All the possible gas holdup measurements were obtained from either the pressure drop measurements (gas holdups were too small to be measurable by the valve shut-off technique) or the electro-resistivity probe measurements, and are shown in Figure 4.26. Also shown is the predicted curve from the generalized wake model, assuming slug flow with $x_k = 0$ (the same eight equations as listed under the section for 1/4 mm glass beads above were solved numerically). It can be seen in Figure 4.26 that, although the scatter in the data is quite large, the values predicted by the generalized wake model are in reasonable agreement with the values obtained from the electro-resistivity probe measurements. The latter cannot, however, be validated in view of the failure of the probe to give reliable results in the air-water- 1/2 mm glass beads system. Some of the characteristic measurements obtained with the electro-resistivity probe are shown in Table 4.26 and Figure 4.27. The results support the optimistic view that, with further refinement, the electro-resistivity probe can be successfully used for measuring the local properties of the gas-bubble phase inside the three-phase

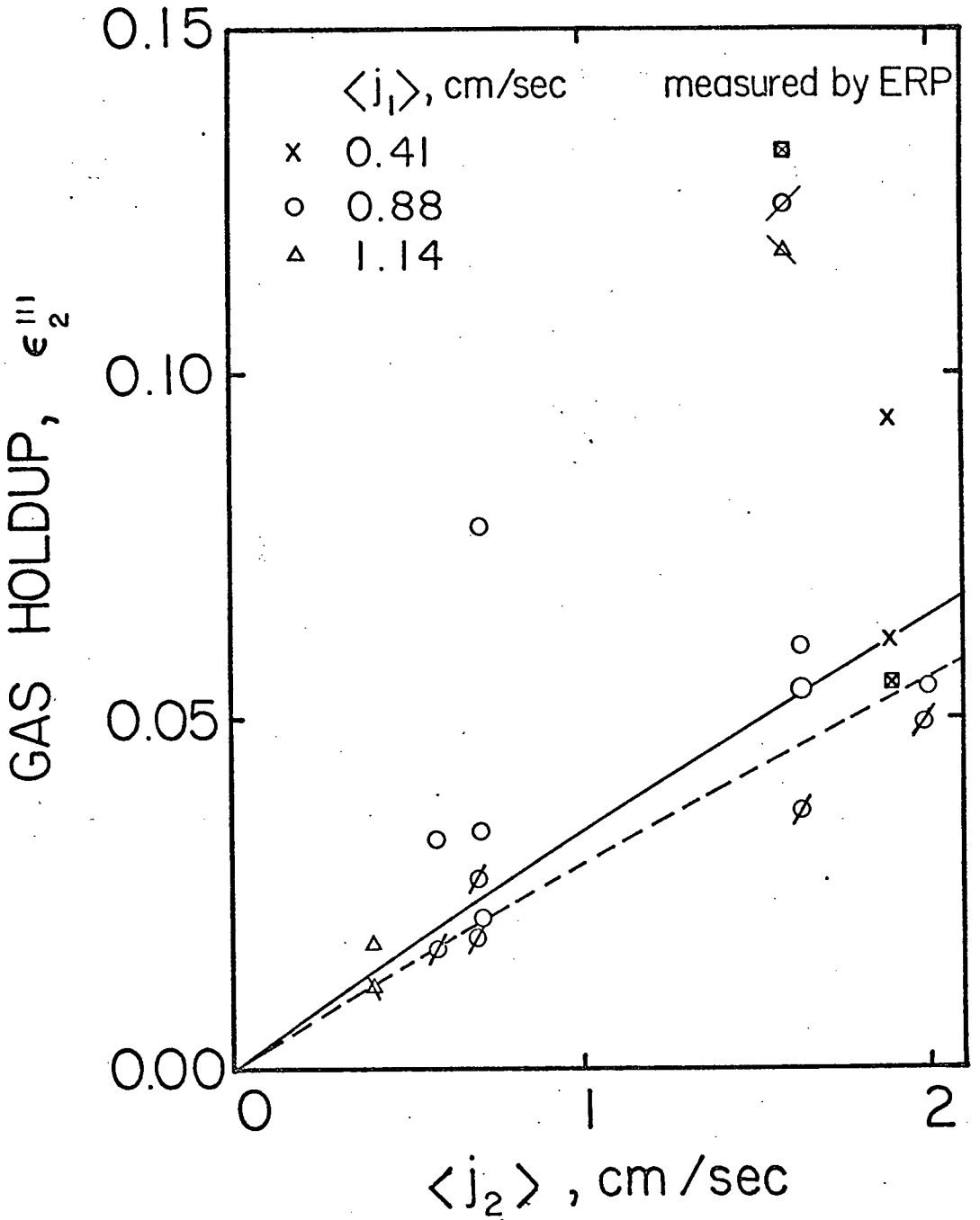

FIGURE 4.26 GAS HOLDUP IN THREE-PHASE BEDS OF 1 MM GLASS BEADS FLUIDIZED BY AIR AND PEG SOLUTION (generalized wake model with x_k=0: – – – – j_1=0.41, ——— j_1=1.14)

TABLE 4.26

CHARACTERISTIC MEASUREMENTS OF GAS-BUBBLE PHASE IN THREE-PHASE FLUIDIZED BED BY ELECTRO-RESISTIVITY PROBE

SYSTEM: Air-PEG Solution - 1 mm Glass Beads,

$\langle j_1 \rangle$ = 0.86 cm/sec

Gas Flux, $\langle j_2 \rangle$ (cm/sec)	$\langle \alpha_2 \rangle$ (-)	$\bar{r}_e$ from Eq. 8.3.6 (cm)	δ^* (-)
0.58	0.017	1.56	0.16
0.71	0.021	1.21	0.17
1.63	0.037	1.73	0.17
1.98	0.050	2.62	0.16

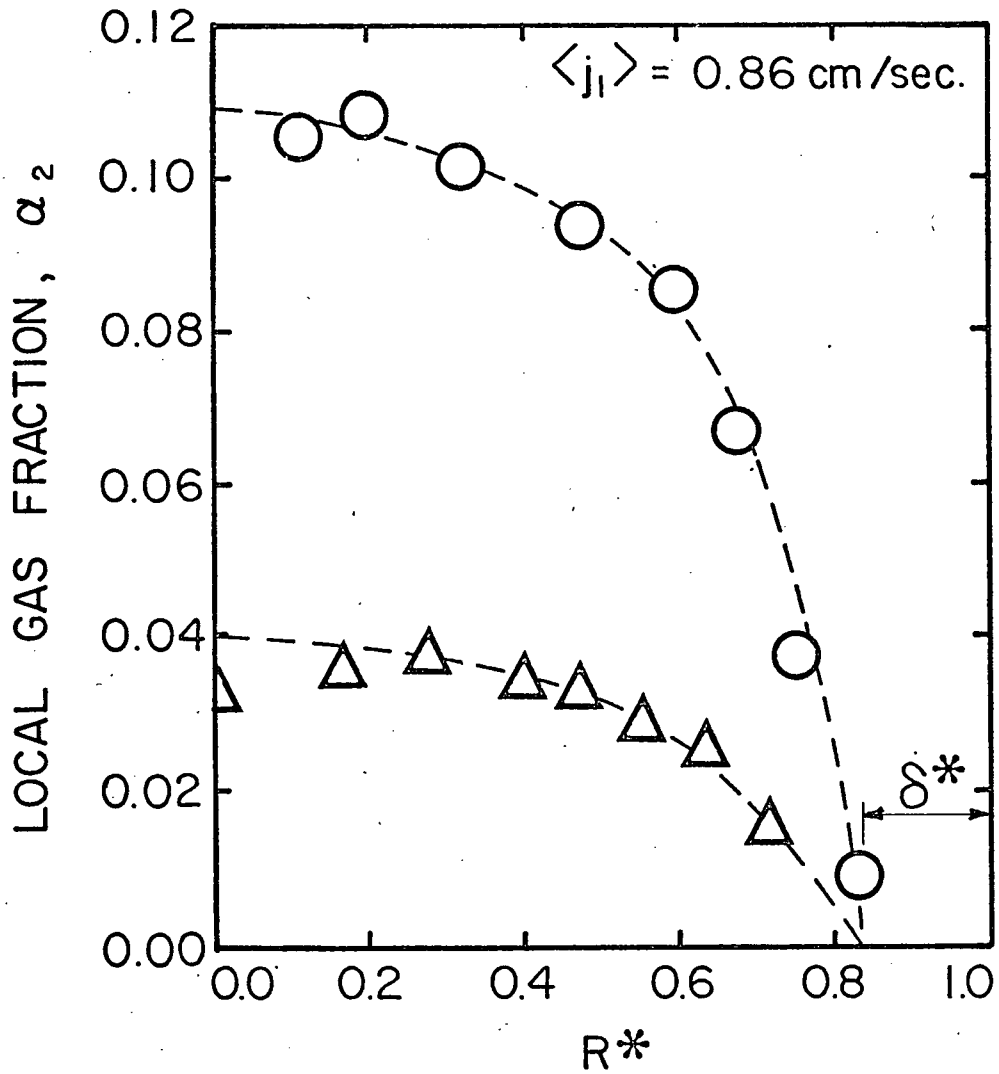

FIGURE 4.27 GAS HOLDUP PROFILES IN THREE-PHASE FLUIDIZED BED (System: air-PEG solution - 1 mm glass beads; o -j_l=0.58; Δ -j_l=1.98)

fluidized bed. For example, the average bubble radii shown in Table 4.26, obtained from equation 8.3.6 using the bubble frequency data, are quite realistic and did compare well with the visual observations.

(vi) Air-PEG solution-steel shot

The visual observation of the fluidized bed and the region above the bed showed that slug flow occurred at all the gas and liquid flow rates studied. The length of the slugs observed in the test section increased with increasing gas flow rate, reaching a length of about 15 cm for a gas flow rate of about 9 cm/sec, when excessive bed fluctuations were noted. No further measurements were therefore attempted. The gas holdups measured in the three-phase fluidized bed are shown in Figure 4.28 along with the data for two-phase air-PEG solution flow, at $\langle j_l \rangle$ = 13.82 cm/sec. It can be seen from this figure that the gas holdup increased quite markedly with increase in gas flow rate but decreased, though only slightly, with an increase in the liquid flow rate.

The gas holdups measured in the three-phase fluidized beds for the liquid flow rate of 13.82 cm/sec are compared in Table 4.27 with the gas holdups measured simultaneously in the two-phase regions of the column, as well as with those measured in gas-liquid flow. It is important to point out that the measurement of gas holdup by the pressure drop gradient method was in this case complicated by the presence of a measurable frictional pressure drop during the flow of

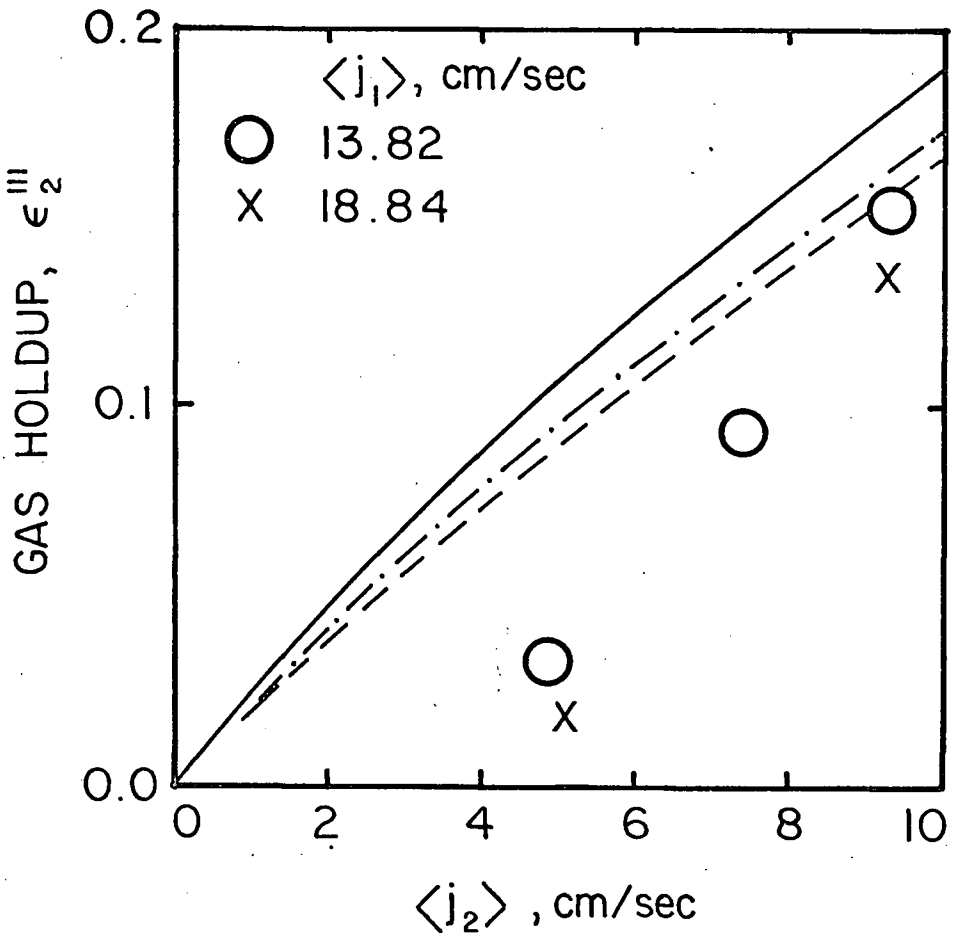

FIGURE 4.28 GAS HOLDUP IN THREE-PHASE BEDS OF 3 MM STEEL SHOT FLUIDIZED BY AIR AND PEG SOLUTION (generalized wake model with x_k=0: —·—·— j_1= 13.82, — — — — j_1=18.84; ———— two-phase air PEG solution flow)

TABLE 4.27

COMPARISON OF GAS HOLDUP IN THREE-PHASE FLUIDIZED BED TO THAT IN TWO-PHASE REGIONS OF THE COLUMN

SYSTEM: Air-PEG Solution - Steel Shot, $\langle j_1 \rangle$ = 13.82 cm/sec; W = 1078 gm,

$\varepsilon_3\big|_{j_2=0} = 0.139$

Gas Flux, $\langle j_2 \rangle$ (cm/sec)	Gas Holdup		Average Gas Holdup in Two-Phase Regions	Average Gas Holdup in Gas-Liquid Flow	Gas Holdup in Three-Phase Region	
	Below the Test Section	Above the Test Section			ε_2'' (measured)	On Solids-Free Basis, $\varepsilon_2''/(1-\varepsilon_3)$
4.89	0.063	0.053	0.062	0.104	0.033	0.039
7.37	0.097	0.106	0.105	0.146	0.094	0.113
9.33	0.134	0.130	0.138	0.178	0.152	0.183

the liquid phase alone at these velocities. Although the gas holdups were calculated from these measurements by suitably subtracting the frictional pressure drop for the liquid phase alone [104], they were found to be consistently larger than the gas holdups by the valve shut-off technique. The averaged gas holdups in the two-phase regions above and below the test section, though equal to each other, were significantly smaller than the corresponding gas holdups in gas-liquid flow without solids, as shown in Table 4.27. This indicates that the introduction of 3 mm steel shot reduced the gas holdup not only above, but even below, the bed. At the same time there was maintained an approximate equality of gas holdups in the two-phase regions with those in the three-phase fluidized beds represented on a solids-free basis.

The electro-resistivity probe was used for a few experiments to determine the average bubble size by means of equation 8.3.6 and measurements of bubble frequency. It was found that the average bubble size in the three-phase fluidized bed was smaller than that in the corresponding gas-liquid flow, as shown in Table 4.28. Apparently the decrease in gas holdup due to solids is accompanied in this instance by a decrease in slug length, an effect which is known to increase the slug rise velocity [27].

In order to check the applicability of the generalized wake model, the gas holdup was calculated by numerically

TABLE 4.28

COMPARISON OF AVERAGE BUBBLE SIZE IN THREE-PHASE FLUIDIZED BED TO THAT IN GAS-LIQUID FLOW

SYSTEM: Air-PEG Solution - Steel Shot, $\langle j_1 \rangle$= 13.82 cm/sec

Gas Flux, $\langle j_2 \rangle$ (cm/sec)	Average Bubble Size, $\bar{r}_e$, cm	
	Three-Phase Fluidized Bed	Gas-Liquid Flow (c.f. Table 4.16)
2.17	1.5	2.3
4.89	2.7	3.2

solving the eight equations listed under the section for 1/4 mm glass beads. The calculated values for x_k=0 are shown in Figure 4.28. The agreement with the measured values is rather poor, but the calculated values nevertheless show the gas holdup to increase with increasing gas flow rate and to decrease with an increase in the liquid flow rate. This agreement with the trends of the measurements would seem to indicate the qualitative correctness of the proposed model.

4.2.3 Voidage results

In this section the measurements of solids holdup ($\varepsilon_3 = 1-\varepsilon$) in liquid-solid and in gas-liquid-solid fluidized beds are reported in both graphical and tabular form. The experimental data from which the graphs and tables were prepared are presented in Appendix 8.7. The physical properties of all the solids and liquids used in this study are recorded in Appendix 8.6.

4.2.3.1 Voidage in liquid-solid fluidized beds

The measurements of solids holdup in the 20 mm glass column as well as in the 2 inch Perspex column were undertaken primarily to establish the relationships for describing the expansion characteristics of liquid-solid fluidized beds, such that the same relationships could then be used for

describing the voidage in the particulate phase of a three-phase fluidized bed.

(A) 20 mm glass column

The measured bed voidages for the three systems studied, obtained from the measurements of solids holdup in liquid-solid fluidized beds, are presented in Table 4.29 along with the predicted values from the Richardson-Zaki correlation, equation 2.46, as well as from the Neuzil-Hrdina correlation, equation 2.51. For beds of 1 mm glass beads fluidized either by water or by aqueous glycerol, the measured values of bed voidage were on the average about 12% greater than the predicted values from equation 2.46, using equation 2.49 for evaluating the exponent n. The agreement was improved to within 5% if the wall correction factor recommended by Richardson and Zaki [2] was employed. However, using the Neuzil-Hrdina correlation, equation 2.51, for predicting the bed voidage in confined media, the agreement between the measured and the predicted values was found to be excellent, as shown in Table 4.29. Therefore equation 2.51 was used subsequently for characterizing the expansion behaviour in the particulate phase of a three-phase fluidized bed of 1 mm glass beads.

The measured values of bed voidage in water fluidized beds of 1/2 mm sand particles were about 15% greater than the predicted values from equation 2.46, using equation 2.49

TABLE 4.29

EXPANSION RESULTS FOR LIQUID-SOLID FLUIDIZATION IN 20 MM COLUMN

Fluidization System	d_p (mm)	Terminal Free Settling Reynolds Number, Re_p (-)	Liquid Flux $\langle j_l \rangle$ (cm/sec)	Measured Voidage, ε (-)	Predicted Voidage	
					$\varepsilon^{(1)}$	$\varepsilon^{(2)}$
Glass Beads Water	1.08	191.4	3.04	0.586	0.512	0.580
			4.01	0.641	0.568	0.642
			4.81	0.700	0.609	0.687
			5.22	0.707	0.628	0.708
			6.02	0.754	0.663	0.747
			6.42	0.769	0.680	0.765
			6.82	0.786	0.696	0.782
			8.02	0.831	0.740	0.830
Glass Beads Aqueous-Glycerol Solution	1.08	74.58	4.06	0.724	0.657	0.718
			4.86	0.777	0.699	0.767
			6.03	0.826	0.753	0.831
Sand-Water	0.458	34.0	1.67	0.751	0.630	0.751*
			2.03	0.787	0.671	0.751*
			2.38	0.823	0.706	0.822*
			2.71	0.844	0.737	0.850*
			3.04	0.873	0.764	0.874*

(1) Calculated from equation 2.46 with $n = 4.45\ Re_p^{-0.1}$

(2) Calculated from equation 2.51

* Calculated from modified Neuzil-Hrdina correlation,

$$\langle j_l \rangle / V_\infty = 0.67\ Re_p^{0.03}\ [1-1.27(d_p/D)^{1.15}]\ \varepsilon_l^{3.95} \qquad (4.27)$$

for evaluating the exponent n. Equation 2.51 could not be used in this case since the free settling Reynolds number of the sand particles was outside the recommended range of its applicability. However the success of equation 2.51 in predicting the voidage in beds of 1 mm glass beads suggested the ideal of modifying the exponent on ε_l in equation 2.51 to fit the experimental data. From a log-log plot of measured bed voidage against liquid flux, Figure 4.29, the slope of the resulting straight line was found to be 3.95 (as compared with the value of 3.21 predicted by equation 2.49). Therefore the Neuzil-Hrdina correlation was modified to

$$\frac{\langle j_l \rangle}{V_\infty} = 0.67\ Re_p^{0.03}\ [1-1.27(d_p/D)^{1.15}]\ \varepsilon_l^{3.95} \qquad (4.27)$$

The voidages predicted by equation 4.27 were found to be in almost perfect agreement with the measured values, as shown in Table 4.29. Therefore equation 4.27, instead of equation 2.51, was used for characterizing the expansion behaviour in the particulate phase of a three-phase fluidized bed of 1/2 mm sand particles.

(B) 2 inch perspex column

The measurements of bed voidages, presented in Table 4.30, were for a wide range of particle sizes (1/4 - 3 mm) and particle densities (2.8 - 11.3 gm/cm^3), and with the two

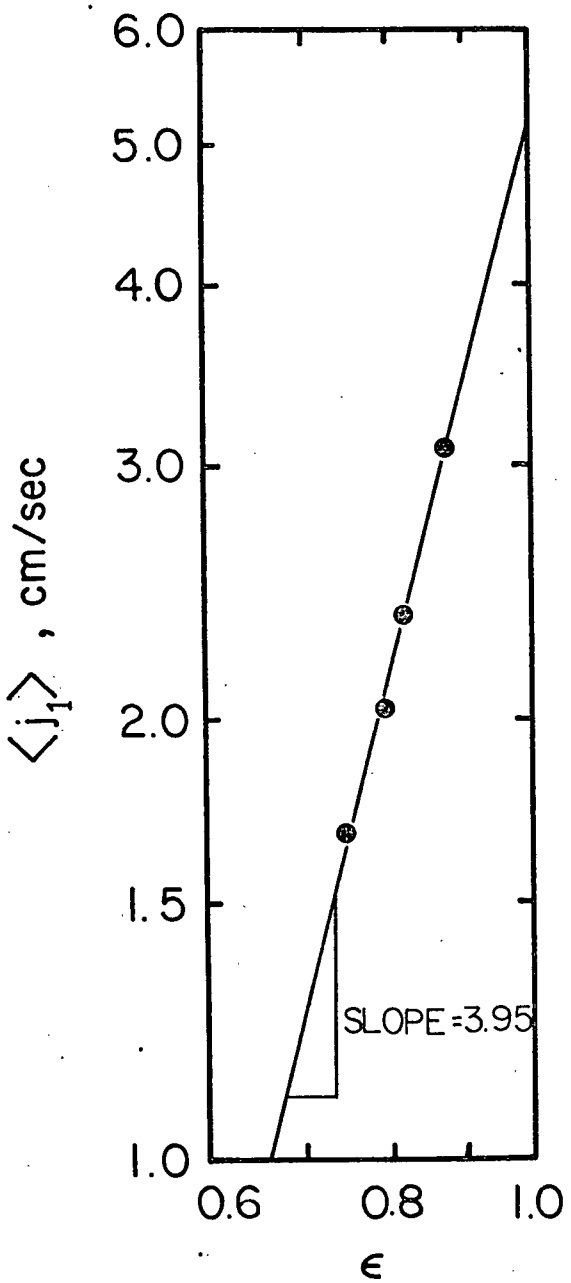

FIGURE 4.29 THE EXPANSION CHARACTERISTICS OF 1/2 MM SAND PARTICLES FLUIDIZED BY WATER

TABLE 4.30

EXPANSION RESULTS FOR LIQUID-SOLID FLUIDIZATION IN 2 INCH COLUMN

Fluidization System	d_p	Terminal Free Settling Reynolds Number, Re_p (-)	Liquid Flux $\langle j_l \rangle$ (cm/sec)	Measured Voidage, ε (-)	Predicted Voidage	
					ε(1)	ε(2)
Glass Beads Water	0.273	10.2	1.25	0.763	0.719	
			1.87	0.834	0.804	
			2.23	0.889	0.844	
			3.18	-	0.931	
Glass Beads Water	0.456	28.0	1.59	0.635	0.628	
			3.52	0.805	0.799	
			4.55	0.866	0.864	
			5.71	0.922	0.925	
Glass Beads Water	1.08	202.2	6.25	0.706	0.680	
		202.2	6.97	0.733	0.706	
		191.4	7.02	0.738	0.724	
		202.2	7.65	0.760	0.730	
		202.2	12.8	0.879	0.875	
Lead Shot-Water	2.18	1762.5	8.26	0.417	0.385*	0.407
			17.80	0.583	0.531*	0.570
			26.40	0.683	0.626*	0.677
			38.77	0.808	0.735*	0.801
Glass Beads PEG Solution	1.08	0.36	0.40	0.732	0.729†	
		0.36	0.86	0.846	0.853†	
		0.40	1.14	0.886	0.893†	
Steel Shot PEG Solution	3.18	15.47	13.82	0.865	0.837	
		15.47	18.84	0.938	0.901	

(1) Calculated from equation 2.46 with $n = (4.45 + 18\ d_p/D)\ Re_p^{-0.1}$

† with $n = (4.35 + 17.5\ d_p/D)\ Re_p^{-0.03}$

* with $n = 2.39$

(2) Calculated from equation 4.28

liquids used, they represented a range of Reynolds number ($0.36 < Re_p < 1770$) from the Stokes' to the Newton's law regimes. Since all the experiments were carried out in the one column, the ratio of particle to column diameter varied from 0.005 to 0.063. These ranges of variables investigated were well within the range of applicability of the Richardson-Zaki correlation (equation 2.46), but were outside the recommended range of applicability of the Neuzil-Hrdina correlation (equation 2.51). Therefore the latter could not be employed when wall effects became important. Instead, the equations recommended by Richardson and Zaki [2] were used and these are:

$$\langle j_l \rangle / V'_\infty = \varepsilon_l^n \qquad (2.46)$$

where

$$n = [4.35 + 17.5\, d_p/D]\, Re_p^{-0.03} \qquad 0.2 < Re_p < 1 \qquad (2.48a)$$

$$n = [4.45 + 18\, d_p/D]\, Re_p^{-0.1} \qquad 1 < Re_p < 200 \qquad (2.49a)$$

$$n = 2.39 \qquad Re_p > 500 \qquad (2.50)$$

and $V'_\infty \simeq V_\infty$, the terminal velocity of particles in an infinite medium estimated from standard relationships [27].

The following discussion of experimental findings results from the measurements conducted for each of the fluidization systems studied.

glass beads - water

The values of bed voidage reported in Table 4.30 were in most cases averages of voidage obtained by two methods, viz. the expanded bed height method and the pressure drop gradient method. The measurements in fluidized beds of 1 mm glass beads did not provide any difficulties and the voidage obtained by either method was satisfactory. The solids holdup remained practically constant from the bottom to the top of the bed, and the expanded bed height obtained from the longitudinal pressure drop profile agreed with the measured bed height by visual observation (Figure 4.30). However, at large bed expansions in fluidized beds of 1/4 mm glass beads, the solids holdup was found to vary along the bed, being higher than average near the bottom and lower near the top. The longitudinal pressure drop profile and the solids holdup distribution (calculated from the differential pressure drop across a differential section of the bed from the unsmoothed data) for such a bed are shown in Figure 4.31. As can be seen, the solids holdup along the bed decreases considerably with distance from the bottom and appears to be responsible for the marked difference in

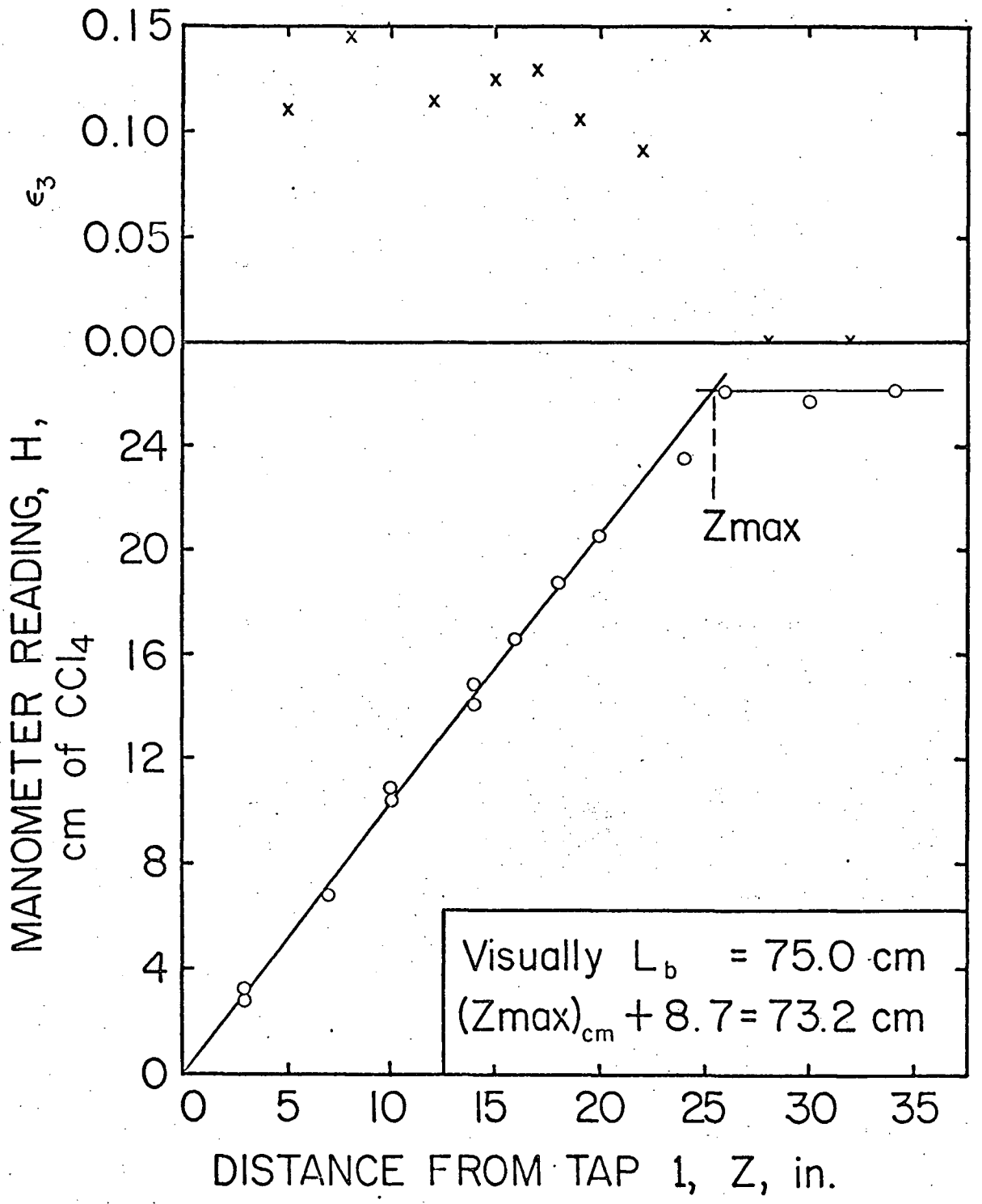

FIGURE 4.30 ESTIMATION OF EXPANDED BED HEIGHT AND SOLIDS HOLDUP DISTRIBUTION FROM LONGITUDINAL PRESSURE DROP PROFILE IN BED OF 1 MM GLASS BEADS FLUIDIZED BY WATER (W=536.4 gm; j_1=12.80 cm/sec; $L_{b,0}$=15.4 cm)

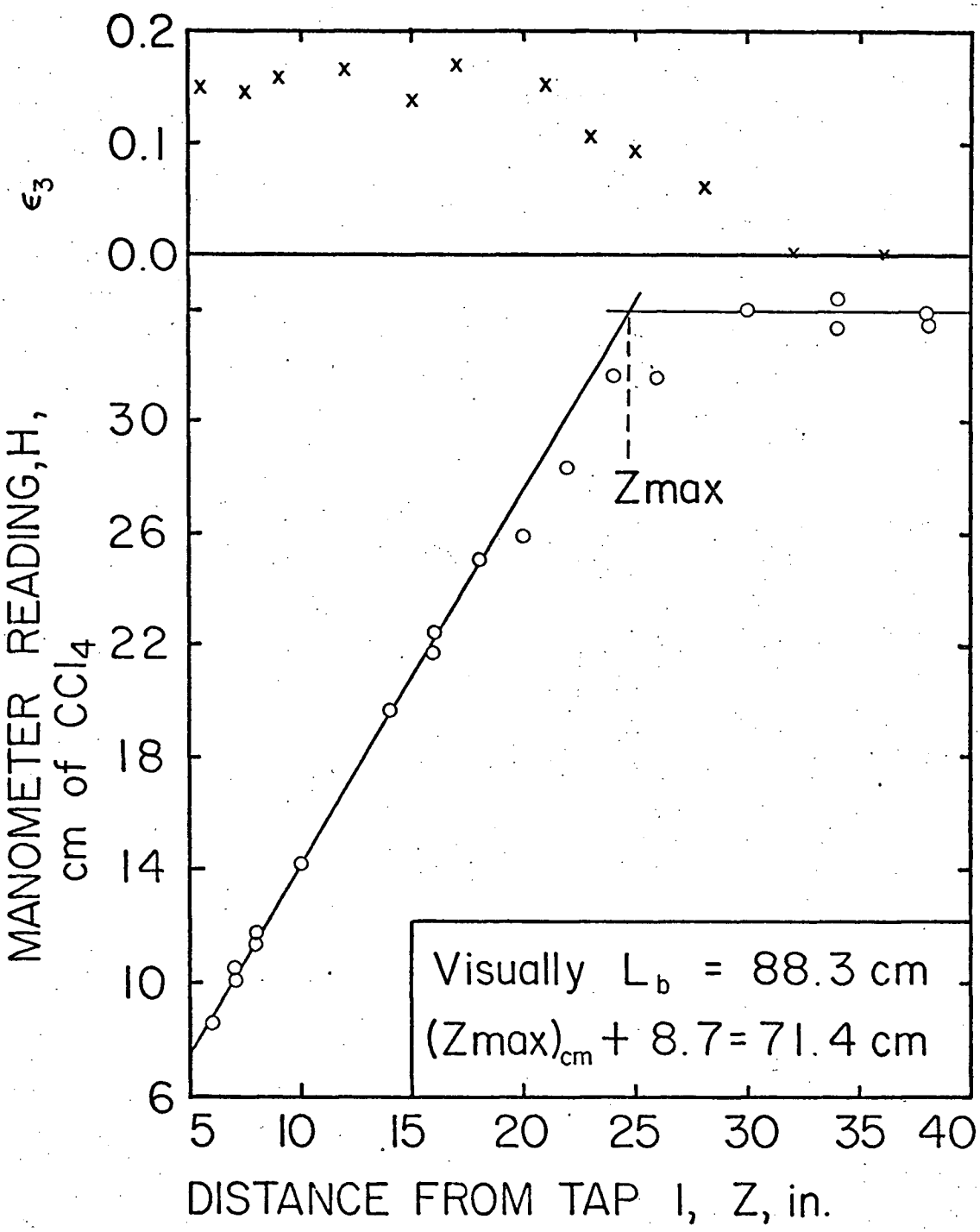

FIGURE 4.31 ESTIMATION OF EXPANDED BED HEIGHT AND SOLIDS HOLDUP DISTRIBUTION FROM LONGITUDINAL PRESSURE DROP PROFILE IN BED OF 1/4 MM GLASS BEADS FLUIDIZED BY WATER (W=739.3 gm; j_l=1.87 cm/sec; $L_{b,0}$=21.5 cm)

bed height obtained by the two methods. The dispersion in solids holdup may have been caused by size segregation in the screen cut selected (0.25 - 0.175 mm). The expanded bed height chosen for determination of average bed voidage in this case, as well as in other similar cases, was the one from the longitudinal pressure drop profile. For fluidized beds of 1/2 mm glass beads the differences were not so great (see Figure 3.10), but nevertheless the same procedure was adopted.

The measured values of bed voidage for the glass beads-water system showed reasonable agreement with the predictions from the Richardson-Zaki correlation, with the exponent n calculated from equation 2.49a, and was therefore used for describing the voidage in the particulate phase of three-phase beds of glass beads fluidized by air and water.

lead shot-water

The two methods used for studying the bed voidage gave excellent agreement with each other, since the observed bed height was found to be in almost perfect agreement with the bed height obtained from the longitudinal pressure prop profile, as illustrated in Figure 4.32. The fluidized bed was observed to expand smoothly, although the existence of agglomerates could not always be ruled out. The measured values of bed voidages were found to be about 10% higher than the predictions from equation 2.46 with n = 2.39. For fluidized beds of such large heavy particles, Trupp [87]

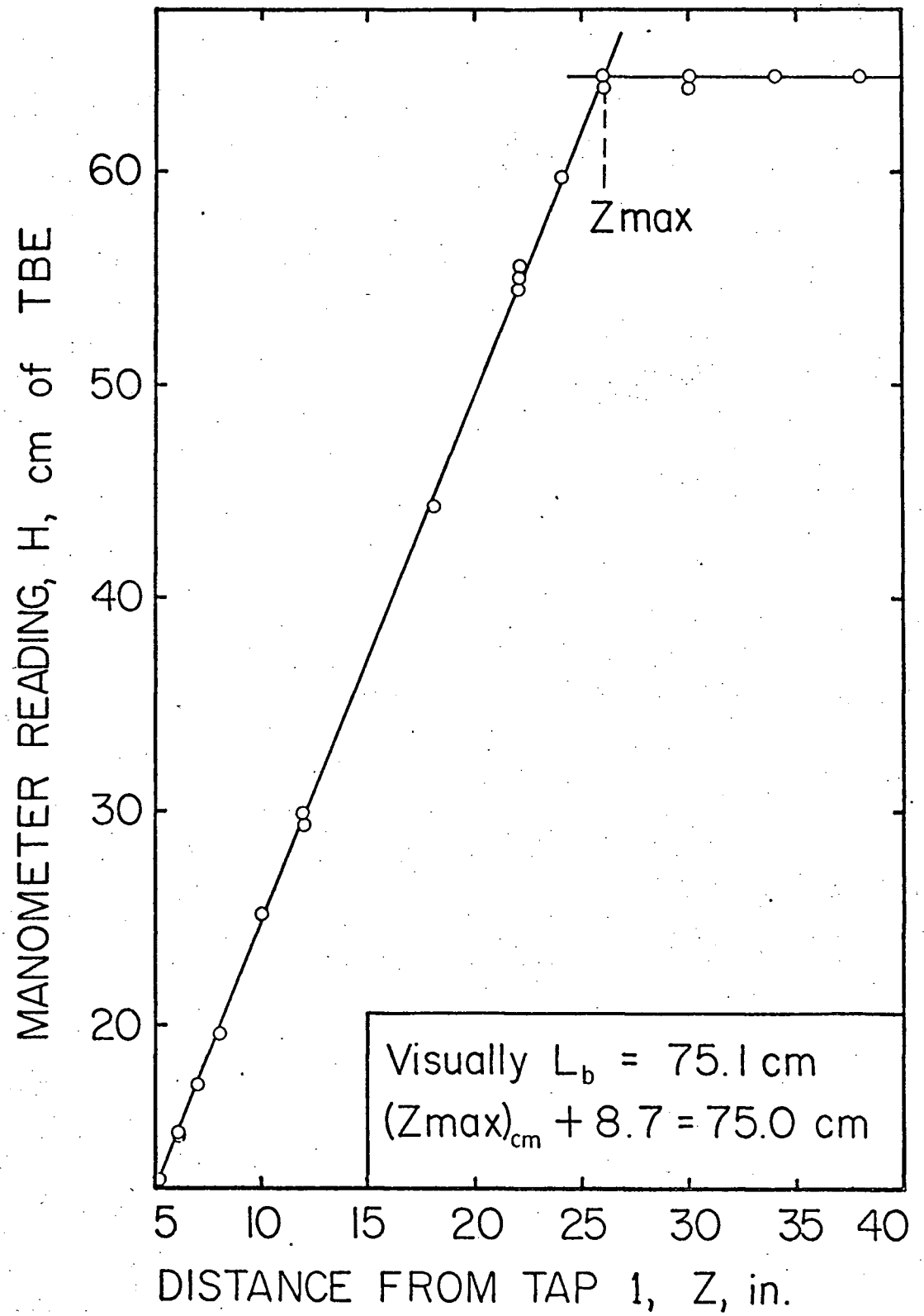

FIGURE 4.32 ESTIMATION OF EXPANDED BED HEIGHT FROM LONGITUDINAL PRESSURE DROP PROFILE IN BED OF 2 MM LEAD SHOT FLUIDIZED BY WATER (TBE=1,1,2,2-tetrabromo-ethane; W=3245.0 gm; j_1=38.77 cm/sec; $L_{b,0}$=25.6 cm)

recommended the correlation

$$\langle j_l \rangle = 0.36\ (V_\infty)^{1.18}\ \varepsilon^{2.28} \qquad (4.28)$$

for $Re_p > 500$ and $d_p/D < 0.06$, based on the assumption that the turbulence generated by the particles affected the bed expansion behaviour. The predictions from equation 4.28 were found to be in excellent accord (Table 4.30) with the measured values, and therefore equation 4.28 was subsequently used for describing the voidage in the particulate phase of three-phase fluidized beds of lead shot.

solid particles - PEG solution

The fluidization of two solid particle species (1 mm glass beads and 3 mm steel shot) with PEG solution provided smooth and uniform bed expansion at all liquid flow rates. As shown in Table 4.30, the measured values of bed voidage were found to be in good agreement with the values predicted from equation 2.46, using calculated values of the exponent n from equations 2.48a and 2.49a as appropriate. Therefore equation 2.46 was used subsequently for describing the voidage in the particulate phase of the corresponding three-phase fluidized beds.

4.2.3.2 Voidage in three-phase fluidized beds

The voidage in three-phase fluidized beds of test particles was measured in both the 20 mm i.d. glass column and the 2 inch i.d. perspex column. For the studies in the 20 mm glass column, the height of the three-phase fluidized bed was obtained by locating the bed boundary visually, while the bed height in the 2 inch perspex column was evaluated from the measured pressure drop profile. The values of bed height calculated by the latter method were found to be realistic and reproducible, even at the high gas flow rates when the bed boundary could no longer be located from visual observation with any degree of confidence. From the measurement of expanded bed height, L_b, the solids holdup was calculated from equation 3.1 and then the bed voidage was obtained from equation 1.3.

(A) 20 mm glass column

The experimental findings for the three systems studied are described below.

(i) Air-water - 1/2 mm sand

The fluidization of sand particles by water alone produced fairly uniform beds. On introduction of air at small flow rates, keeping the liquid flow rate constant, the bed was found to contract quite noticeably, the amount of contraction being dependent on the initial degree of bed

expansion of the liquid-solid fluidized bed. Thus, for highly expanded beds ($\langle j_1 \rangle$ = 3.04 cm/sec), the observed bed contraction amounted to about 34% of the initial bed height, whereas for moderately expanded beds ($\langle j_1 \rangle$ = 1.67 cm/sec) the observed bed contraction was only 14% (Figure 4.33). The minimum value of bed voidage was observed to occur at a volumetric gas flux of about 1 cm/sec for all the liquid flow rates studied. A further increase in the gas flow rate, for a fixed liquid flow rate, produced a slow but gradual bed expansion. Although no particle entrainment was observed, the bed boundary became quite diffuse on increasing the gas flow rate above $\langle j_2 \rangle \simeq 2.5$ cm/sec. No data were therefore taken for much higher gas flow rates.

In order to check the applicability of the generalized wake model, the eight equations listed earlier in Section 4.2.2.2 (Equations 2.94, 2.112, 2.108a, 4.8, 2.106, 4.7, 1.3 and 2.91) were solved numerically with the same assumptions as cited originally, except that the voidage in the particulate phase was assumed to be described by equation 4.27 instead of equation 2.46, as discussed above in Section 4.2.3.1. The curves of bed voidage calculated from the model for various assumed values of x_k are shown in Figure 4.33.From a comparison of the predicted values of bed voidage with the measured values, it is seen that:

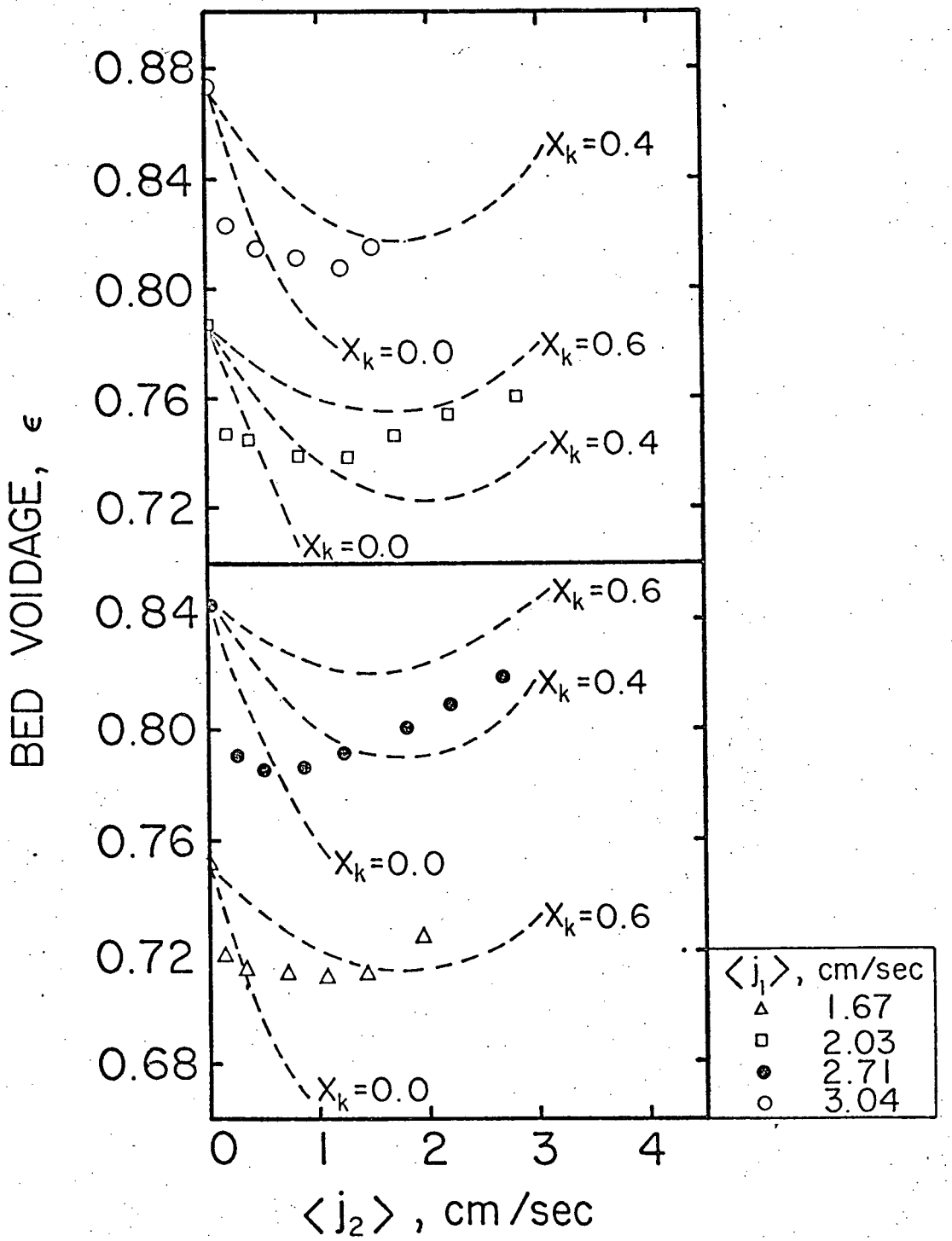

FIGURE 4.33 BED VOIDAGE IN THREE-PHASE BEDS OF 1/2 MM SAND PARTICLES FLUIDIZED BY AIR AND WATER IN 20 MM GLASS COLUMN (— — — generalized wake model)

1. The predictions also show minima in the gas voidage, but these predicted minima occur at a volumetric gas flux of between 1 and 2 cm/sec., which is up to twice the corresponding observed gas fluxes.
2. The measured bed voidages lie between the predicted values for $x_k = 0.0$ and $x_k = 0.6$, the initial bed contraction being closer to the predicted values for $x_k = 0.0$ and the later bed expansion falling between the predicted values for $x_k = 0.4$ and $x_k = 0.6$. The implication of this result, according to the model, is that particle entrainment in the bubble wakes increases as gas flux increases.

(ii) Air-water- 1 mm glass beads

The behaviour of water fluidized beds of 1 mm glass beads, on introduction of air at small flow rates, varied according to the level of initial bed expansion. Thus for a slightly expanded bed ($\langle j_1 \rangle$ = 4.01 cm/sec), no bed contraction was observed; the bed height remained nearly constant for $\langle j_2 \rangle$ up to 1 cm/sec, and thereafter the bed expanded smoothly as the air flow rate was further increased (Figure 4.34). For all other liquid flow rates studied, the bed was found to contract when air was introduced at small flow rates; however, the amount of bed contraction was not as large as for the air-water-sand system. The

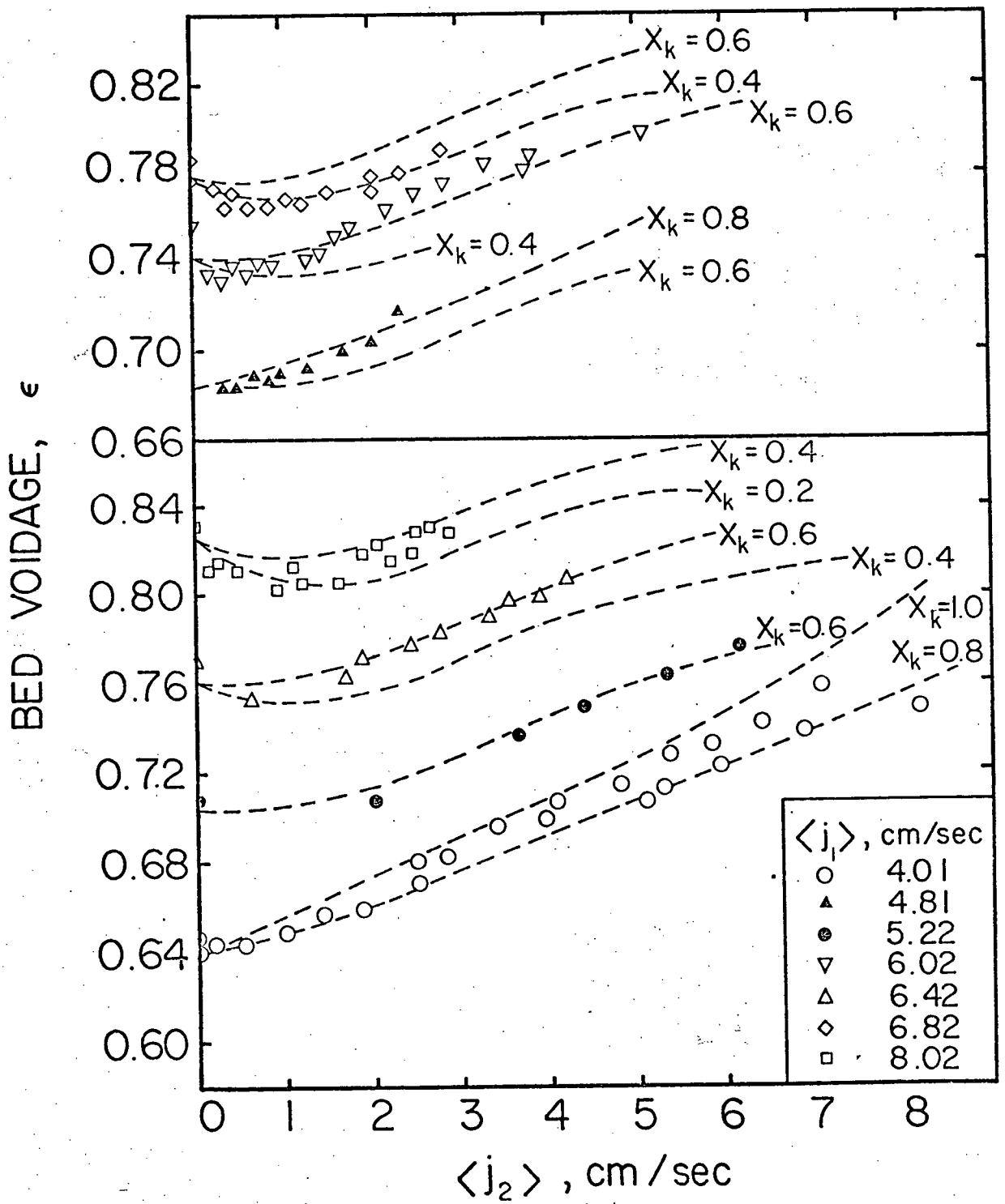

FIGURE 4.34 BED VOIDAGE IN THREE-PHASE BEDS OF 1 MM GLASS BEADS FLUIDIZED BY AIR AND WATER IN 20 MM GLASS COLUMN (- - - - generalized wake model)

maximum bed contraction was only 15% of the initial bed height for the highest liquid flow rate ($\langle j_l \rangle$ = 8.02 cm/sec) investigated. The minima in the measured values of bed voidages occurred at gas flow rates of between 0.5 (for $\langle j_l \rangle$ = 4.81 cm/sec) and 1.5 cm/sec (for $\langle j_l \rangle$ = 8.02 cm/sec). The upper bed boundary eventually became diffuse on increasing the gas flow rate, especially for the initially more expanded beds.

For calculating the bed voidages from the generalized wake model, it was assumed that the voidage in the particulate phase could be described by equation 2.51 instead of equation 2.46, as discussed earlier in section 4.2.3.1. Other assumptions were the same as those cited previously in Section 4.2.2.2. The curves of bed voidage calculated from the model for various assumed values of x_k are shown in Figure 4.34 . As can be seen, the agreement between the predicted and the measured values is excellent if a proper value of x_k can be assumed. It was found that, whereas a large value of x_k ($\simeq$ 1.0) was required to match the data for dense beds ($\langle j_l \rangle$ = 4.01 cm/sec), decreasingly smaller values were needed for progressively less dense beds, the highly expanded bed at $\langle j_l \rangle$ = 8.02 being matched by a value of $x_k \simeq 0.2$. The implication of this result is that particle entrainment in the bubble wakes increases with increasing particle concentration of the liquid phase, an implication which is qualitatively reasonable. However,

no direct measurements on the particle content of wakes were made in this study nor are such measurements available in the literature. Nevertheless the generalized wake model does illustrate the effect of wake particles on the general bed behaviour of three-phase fluidized beds, in contrast to the earlier models of Østergaard [8], who assumed $x_k = 1.0$ with no solids circulation, and Efremov and Vakhrushev [16], who assumed $x_k = 0$.

(iii) Air-aqueous glycerol - 1 mm glass beads

The fluidization of glass beads by aqueous glycerol solution gave a uniformly fluidized bed which expanded smoothly as the volumetric liquid flux was increased. On introduction of air into the liquid-solid fluidized bed at small flow rates, the bed was found to contract at all liquid flow rates. The extent of bed contraction was again found to depend on the initial degree of bed expansion of the liquid-solid fluidized beds; thus for highly expanded beds ($\langle j_l \rangle = 6.03$ cm/sec), the observed bed contraction was about 14% of the initial bed height, whereas for moderately expanded beds ($\langle j_l \rangle = 4.06$ cm/sec), the observed bed contraction was only 7%. Although no entrainment by, or attachment to, the bubbles was observed, the bed boundary became quite diffuse at comparatively smaller air flow rates than for the air-water-glass beads system.

The voidage was calculated from the generalized wake model in the same manner as for the air-water-glass

beads system, and the predicted values for various assumed values of x_k are shown in Figure 4.35. With x_k again as an adjustable parameter, the agreement between the predicted and the measured values is excellent, exhibiting the same trends as were found for the air-water-glass beads system.

A direct comparison of the measured and the predicted values of bed voidages in the air-water-glass beads and the air-aqueous glycerol-glass beads systems, for similar values of $\langle j_l \rangle / V_\infty$ or the initial bed expansion, is shown in Figure 4.36. It can be seen that both the measured and the predicted values for the two systems are in excellent agreement with each other, for intermediate bed expansion. For lower bed expansion, the measured values in the air-water-glass beads system are somewhat smaller than those in the air-aqueous glycerol-glass beads system, as is also the case for the predicted values. For higher bed expansion, the measured values in the air-water-glass beads system are slightly larger than those in the air-aqueous glycerol-glass beads system, as is again the case for the predicted values. Thus it can be said that a relatively small change (e.g. doubling) in the viscosity of the liquid has little or no effect on the voidage of three-phase fluidized beds of 1 mm glass particles, and that the generalized wake model can realistically predict the small effect observed.

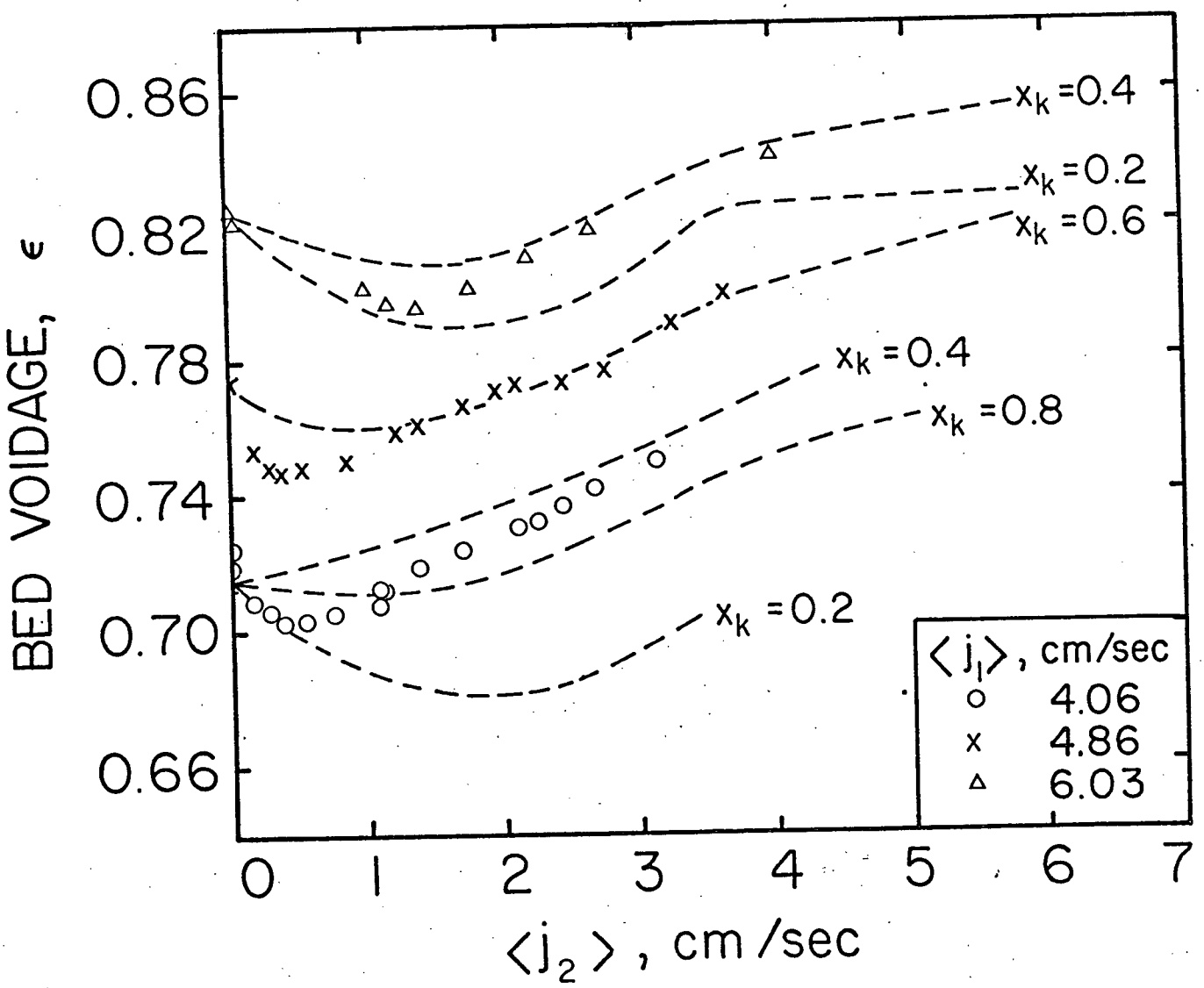

FIGURE 4.35 BED VOIDAGE IN THREE-PHASE BEDS OF 1 MM GLASS BEADS FLUIDIZED BY AIR AND AQUEOUS GLYCEROL IN 20 MM GLASS COLUMN (– – – – – generalized wake model)

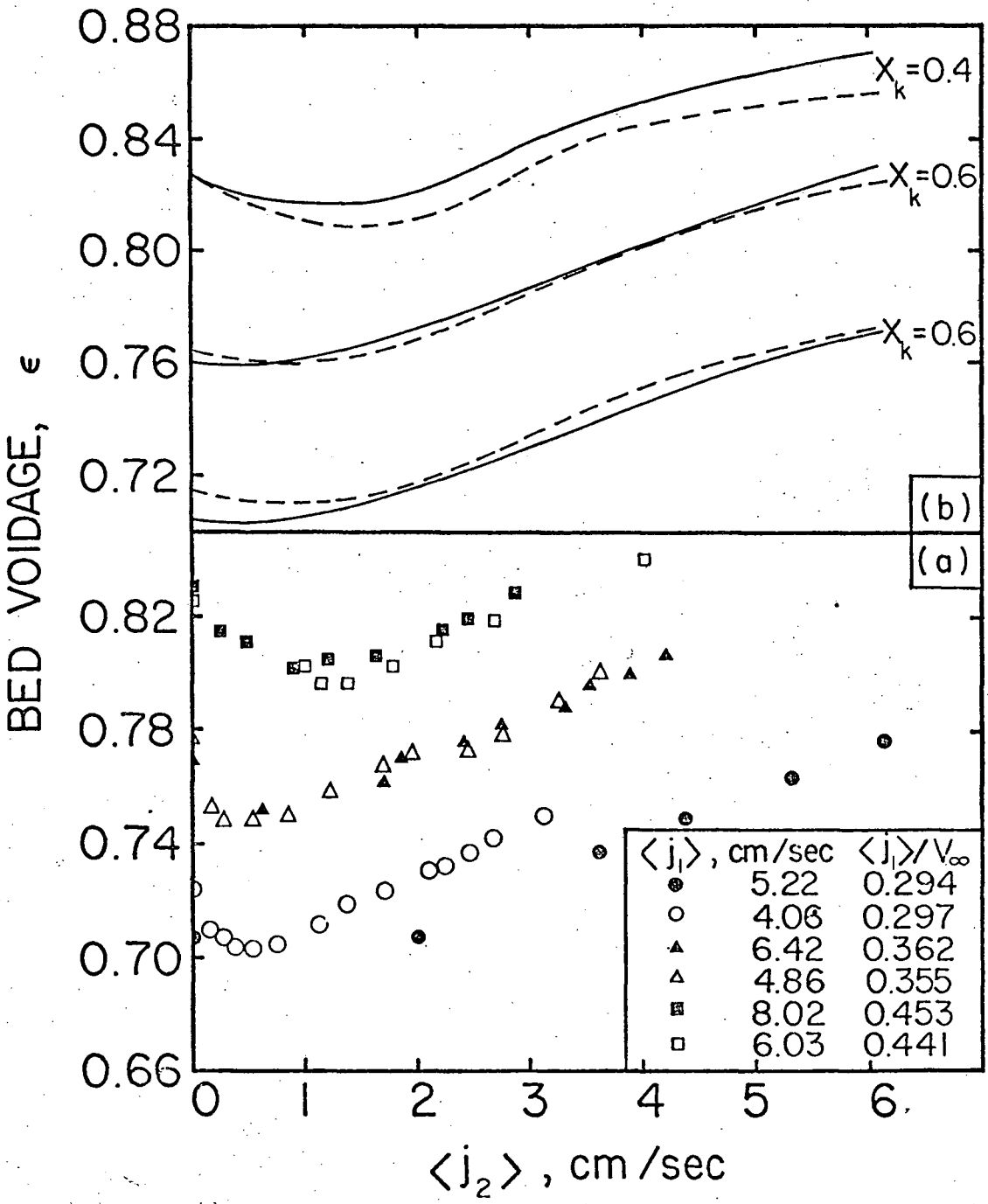

FIGURE 4.36 COMPARISON OF MEASURED (a) AND PREDICTED (b) VALUES OF BED VOIDAGES IN THREE-PHASE BEDS OF 1 MM GLASS BEADS FLUIDIZED BY AIR AND WATER WITH THOSE FLUIDIZED BY AIR AND AQUEOUS GLYCEROL (generalized wake model: ——— air-water - 1 mm glass beads, - - - - - air-aqueous glycerol - 1 mm glass beads; solid symbols are for water and open symbols are for aqueous glycerol)

(B) 2 inch perspex column

The primary objective of this study was to establish the effect of size and density of the particles on the bed voidage in three-phase fluidization. In order to achieve this objective the same wide range of particle sizes (1/4 - 3 mm) and particle densities (2.8 - 11.3 gm/cm^3) were investigated as in liquid-solid fluidization, again covering a free settling particle Reynolds number range of 0.36 to 1770. Attempts to investigate the effect of liquid phase viscosity were not successful, as a stable bed operation with small particles could not be achieved in the present setup using high viscosity liquids. The experimental findings are discussed in the following sections.

(i) Air-water-1/4 mm glass beads

A great deal of attention and care had to be exercised in order to obtain a reproducible set of data with such small particles because the entrainment of particles was found to be an unavoidable phenomenon at large gas flow rates, even for the lowest bed expansion studied. A few runs were carried out in three-phase beds of 1/4 mm glass beads (d_p = 0.323 mm for these runs) to check on whether the entrainment of particles from the system occurred systematically or accidentally. Figure 4.37 shows the variation in observed pressure drop at a particular location in the

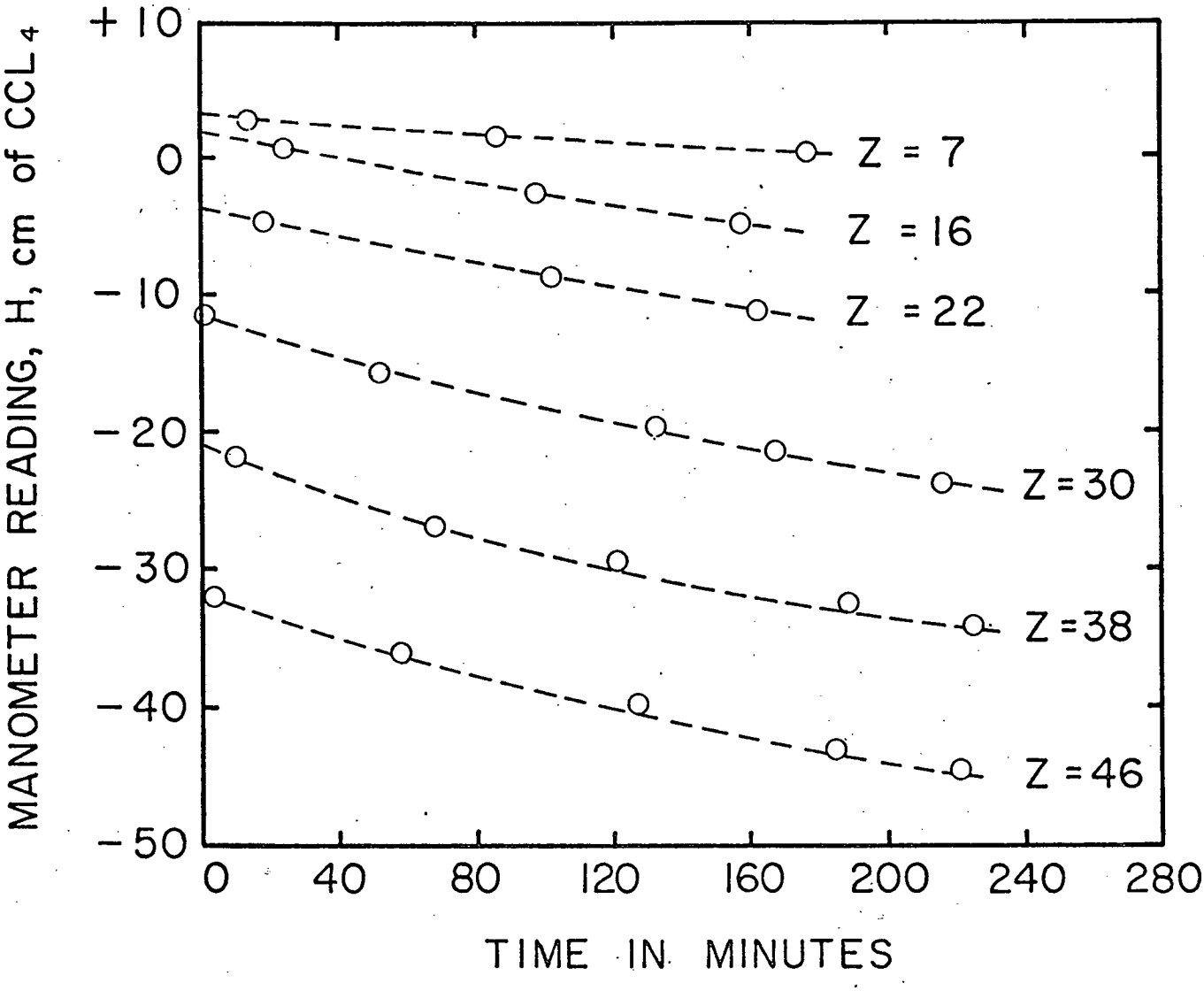

FIGURE 4.37 VARIATION IN OBSERVED PRESSURE DROP FOR ELUTRIATING THREE-PHASE BED OF 1/4 MM GLASS BEADS (d_p=0.323 mm) FLUIDIZED BY AIR ($\langle j_2 \rangle$= 18.0 cm/sec) AND WATER ($\langle j_1 \rangle$ = 3.18 cm/sec) (Z = distance in inches from tap 1)

test section as a function of elapsed time, for one such run ($\langle j_1 \rangle$ = 3.18 cm/sec and $\langle j_2 \rangle$ = 18.0 cm/sec). From these measurements it was confirmed that the particle entrainment did indeed occur systematically (1 gm/min for the quoted experiment). However, these and other similar runs where particle entrainment was disproportionately large were not included in the results, as discussed in Section 3.3, and will be excluded from further discussions.

The introduction of an air stream into a nearly uniform fluidized bed of 1/4 mm glass beads caused a large reduction in bed height, the extent of bed contraction depending on the initial degree of bed expansion, as shown in Figure 4.38. Thus for a highly expanded bed ($\langle j_1 \rangle$ = 3.18 cm/sec), the degree of bed contraction observed was as large as 63% of the initial bed height, whereas for a less expanded bed ($\langle j_1 \rangle$ = 1.25 cm/sec), the bed contraction was only about 33%. On increasing the gas flow rate further, keeping the liquid flow rate constant, no appreciable change in the bed height could be observed. Even a change in the flow regime from bubbly to slug flow (at $\langle j_2 \rangle \simeq 2 - 4$ cm/sec) had relatively little effect, and a further increase in gas flow rate beyond the transition point had no effect, on the bed voidage. Nevertheless the particles were observed to travel a long way up from the main dense bed region before returning back, and some were even swept out of the system at gas flow rates of about 10 cm/sec. Therefore no data were

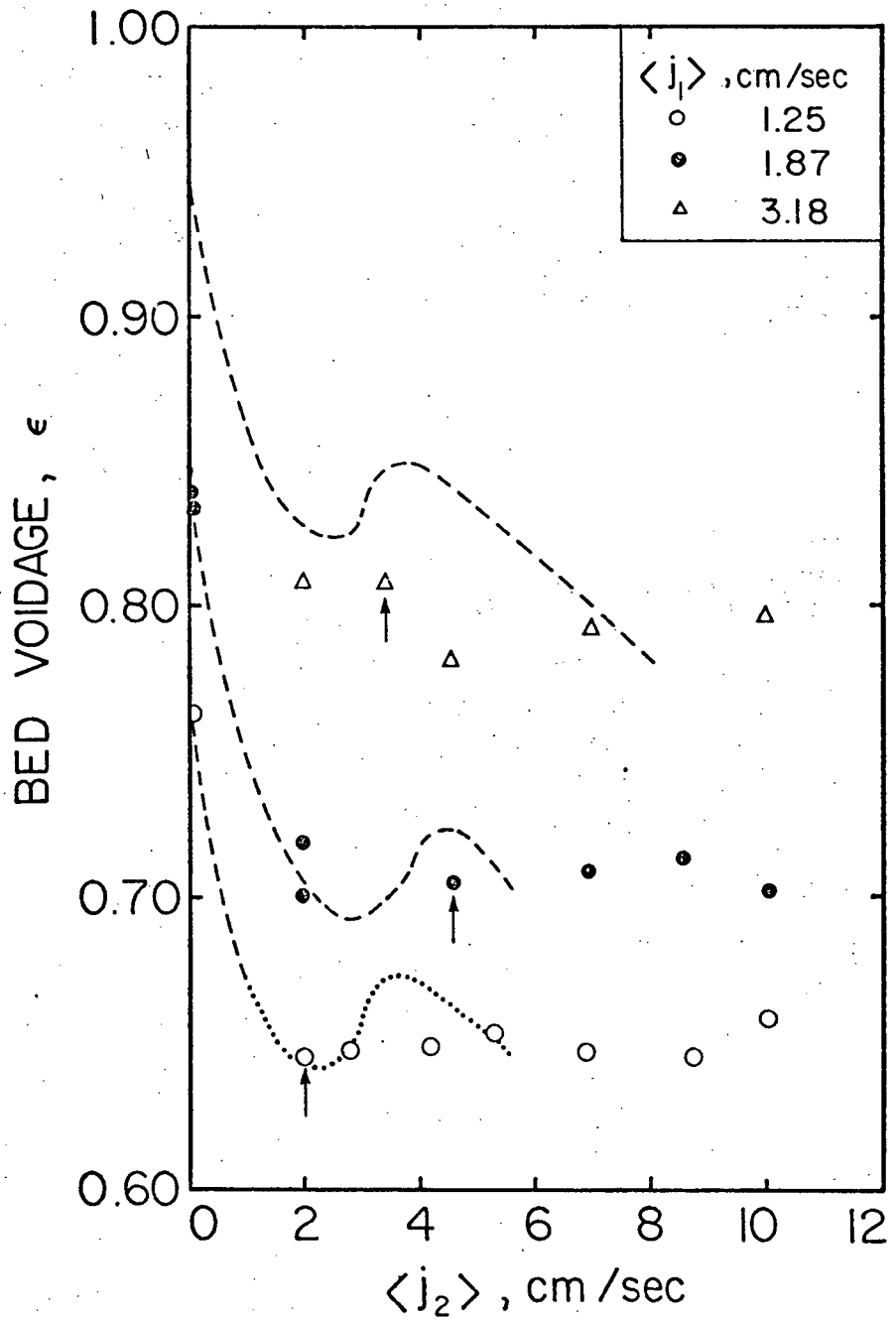

FIGURE 4.38 BED VOIDAGE IN THREE-PHASE BEDS OF 1/4 MM GLASS BEADS FLUIDIZED BY AIR AND WATER (– – – – – generalized wake model with x_k=0.2; arrows indicate observed change from bubbly flow to slug flow)

taken for higher gas flow rates.

In order to check the applicability of the generalized wake model, the bed voidage was calculated by numerically solving the eight equations listed earlier in Section 4.2.2.2, with the same tacit assumptions. However, the numerical scheme adopted failed to converge for low liquid flow rates at gas flow rates greater than 2 cm/sec with small assumed values of $x_k (\simeq 0.0)$. Therefore the predicted curves of bed voidage, shown in Figure 4.38, were obtained from the generalized wake model with $x_k = 0.2$. Even then the convergence at $\langle j_1 \rangle = 1.25$ cm/sec for $j_2 > 1$ cm/sec was not satisfactory. Although the quantitative agreement between the predicted and the measured values, as shown in Figure 4.38, was not entirely unsatisfactory (within 8%), the trends exhibited by the predicted values were not fully compatible with the experimental trends.

The failure of the numerical scheme to converge was believed to have been caused by possible slight inaccuracies in the method of estimating the wake volume fractions. In order to illustrate this point, a few calculations were carried out on a Wang desk calculator by varying the estimated values of ε_k slightly. The calculated results for the liquid flow rate of 1.87 cm/sec are presented in Table 4.31. It can be seen from the table that, at the gas flow rate of 4.0 cm/sec, a slight change in the estimated value of ε_k ($\simeq 3.8\%$) causes the small peak in the predicted

TABLE 4.31

SENSITIVITY OF BED VOIDAGE, ε, PREDICTED FROM GENERALIZED WAKE MODEL WITH $x_k = 0.2$ TO WAKE VOLUME FRACTION, ε_k, IN THREE-PHASE BEDS OF 1/4 MM GLASS BEADS AT $\langle j_1 \rangle = 1.87$ cm/sec

$\langle j_2 \rangle$ (cm/sec)	Predicted by the Model Using Equation 4.7 for ε_k			Calculated by the Model Using Arbitrary Values of ε_k			$\varepsilon_k^{\dagger}$
	ε_2	ε	ε_k	ε_k	ε	ε_2	
3.0	0.072	0.693	0.0396				
4.0	0.095	0.718	0.0373	0.0387	0.701	0.093	0.0356
5.0	0.114	0.715	0.0374	0.0381	0.705	0.112	0.0356
6.0	0.128	0.695	0.0384	0.0377	0.704	0.130	0.0394
7.0				0.0373	0.704	0.146	0.0426

$^{\dagger}\varepsilon_k$ is determined from equation 4.7 using holdups calculated from the arbitrary values of ε_k

bed characteristic curve (ε vs. $\langle j_2 \rangle$) to disappear, and similarly at the gas flow rate of 6 cm/sec, a slight variation in the estimated value of ε_k ($\simeq$ 1.8%) causes the subsequent downward trend in the bed characteristic curve to disappear. It would therefore appear to be necessary that the wake volume fraction be more accurately predictable than by equation 4.7, if the generalized wake model is to correctly predict the voidage behaviour of three-phase fluidized beds of 1/4 mm glass beads.

In order to check the ability of equation 4.7 to estimate the wake volume fraction adequately (since the values of ε_k estimated by the generalized wake model did not agree with the predicted values from equation 2.128, as summarized earlier in Table 4.5), it was decided to calculate the wake volume fraction from the generalized wake model, using the experimental values of gas and solids holdup, as done earlier by Efremov and Vakhrushev [16] and Rigby and Capes [80] for their respective models. The number of unknowns are then reduced to four and the necessary equations are

$$\bar{v}_2 = \langle j_2 \rangle / \varepsilon_2 \tag{2.94}$$

$$\varepsilon_1''' = 1 - \varepsilon_3''' - \varepsilon_2''' \tag{1.3}$$

$$\varepsilon_1''' = \varepsilon_k(1-x_k) + \varepsilon_{1f}'''(1-\varepsilon_k-\varepsilon_2+x_k\varepsilon_k) \tag{2.91}$$

$$\varepsilon''_{lf} = \frac{\langle j_l \rangle - \bar{v}_2(1-x_k)\varepsilon_k}{V_\infty(1-\varepsilon_2-\varepsilon_k)} \qquad (2.106)$$

These four algebraic equations were solved simultaneously for ε_k, using four different value of the parameter x_k. The results obtained are presented in Table 4.32. It can be seen that ε_k increases if the wake is assumed to contain particles, as was also found by Rigby and Capes [80]. Now, since the values of bed voidage predicted by the generalized wake model with $x_k = 0.2$ agreed initially (i.e. at low gas velocities, see Figure 4.38) with the experimental data, values of ε_k for $x_k = 0.2$ are compared in Figure 4.39 with those calculated from equation 4.7, using again the measured values of phase holdups. As can be seen, the agreement is generally acceptable, although the values calculated from equation 4.7 tend to be somewhat larger at high gas flow rates and smaller at low gas flow rates, than those predicted by the model without any reference to experimental data; and as illustrated in Table 4.31, a slight inaccuracy in estimating ε_k can lead to a marked variation in the trends exhibited by the bed characteristic curve.

Thus both the wake volume fraction and the particle content of the wake are critical parameters for determining the behaviour of three-phase fluidized beds of 1/4 mm

TABLE 4.32

ESTIMATED VALUES OF WAKE VOLUME FRACTION, ε_k, FROM EXPERIMENTAL DATA IN THREE-PHASE BEDS OF 1/4 MM GLASS BEADS FLUIDIZED BY AIR AND WATER

$\langle j_1 \rangle$ (cm/sec)	$\langle j_2 \rangle$ (cm/sec)	ε_2	ε_3	ε_k from Generalized Wake Model With				ε_k from Equation 4.7 with p = 3
				x_k=0.0	x_k=0.1	x_k=0.2	x_k=0.4	
1.25	2.03	0.059	0.355	0.025	0.027	0.031	0.041	0.031
	2.79	0.080	0.353	0.025	0.028	0.031	0.042	0.031
	4.17	0.089	0.352	0.019	0.021	0.023	0.031	0.029
	5.30	0.113	0.346	0.019	0.021	0.024	0.032	0.029
	6.91	0.122	0.353	0.016	0.018	0.021	0.028	0.029
	8.71	0.150	0.355	0.017	0.019	0.021	0.028	0.033
	10.01	0.183	0.342	0.018	0.020	0.023	0.030	0.043
1.87	1.98	0.071	0.282	0.044	0.049	0.056	0.075	0.044
	4.60	0.100	0.295	0.029	0.032	0.036	0.048	0.033
	6.95	0.136	0.292	0.027	0.030	0.034	0.045	0.041
	8.54	0.151	0.288	0.024	0.027	0.031	0.041	0.045
	10.05	0.182	0.299	0.027	0.030	0.034	0.045	0.052
3.18	2.00	0.070	0.191	0.071	0.080	0.090	0.123	0.063
	3.40	0.102	0.194	0.064	0.072	0.081	0.110	0.049
	4.58	0.131	0.220	0.069	0.077	0.088	0.118	0.054
	6.95	0.155	0.208	0.053	0.059	0.066	0.089	0.064
	9.97	0.201	0.203	0.049	0.055	0.062	0.084	0.085

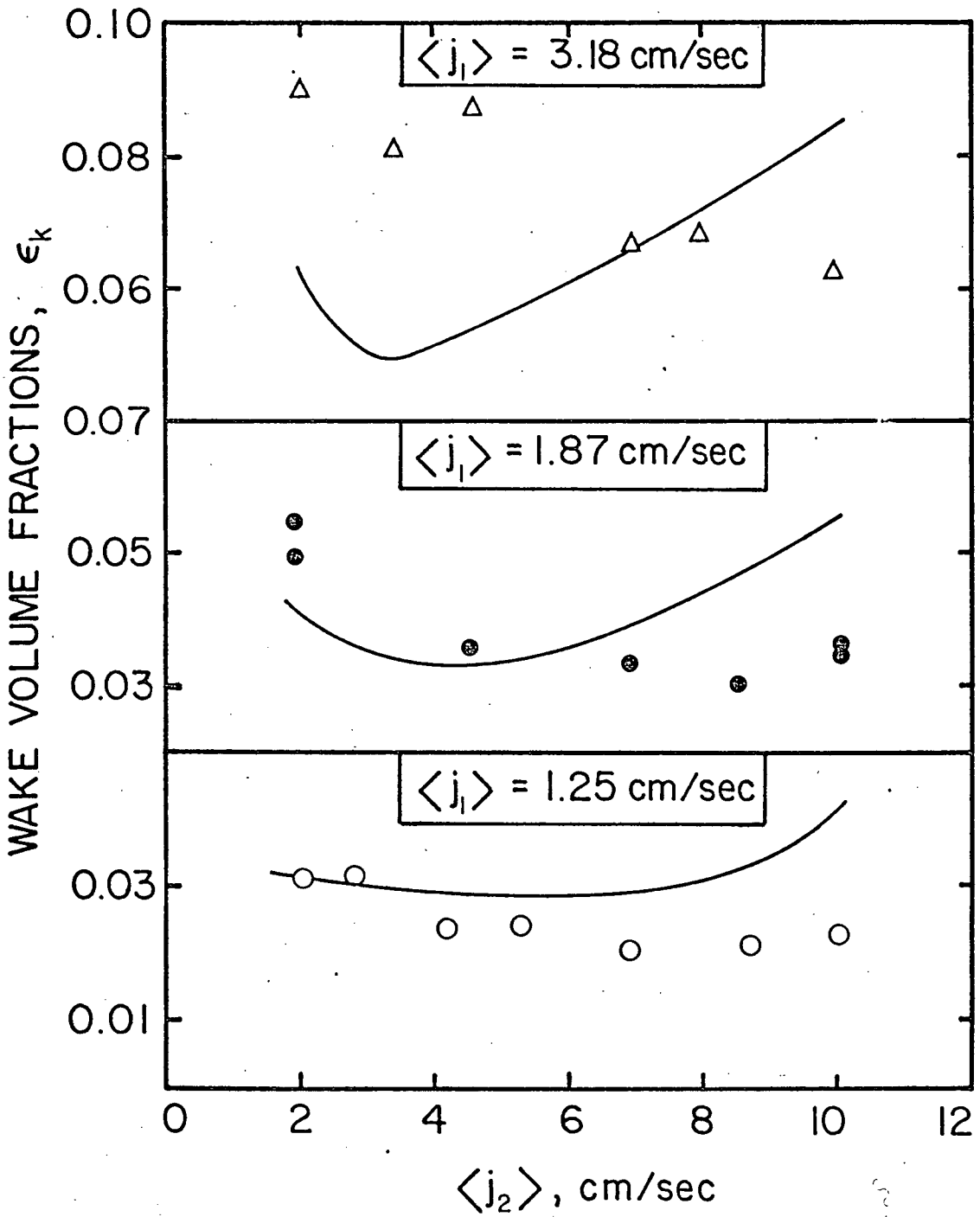

FIGURE 4.39 COMPARISON OF ε_k CALCULATED FROM EQAUTIONS 1.3, 2.91, 2.94 AND 2.106 WITH x_k=0.2, USING THE MEASURED VALUES OF GAS AND SOLIDS HOLDUP IN THREE-PHASE FLUIDIZED BEDS OF 1/4 MM GLASS BEADS, WITH PREDICTED VALUES (——) FROM EQUATION 4.7 WITH p = 3

glass beads. Equation 4.7 does seem to provide an adequate estimate for ε_k and could be used as a first approximation. However, the accuracy, of equation 4.7 can only be fully evaluated when directly measured values of ε_k become available.

(ii) Air-water-1/2 mm glass beads

The behaviour of three-phase fluidized beds of 1/2 mm glass beads was similar in many respects to that of 1/4 mm glass beads. However, in three-phase fluidization of 1/2 mm glass beads, the entrainment of particles did not pose as serious a problem. The fluidization of 1/2 mm glass beads by water alone produced a nearly uniform bed which expanded smoothly when the liquid flux through the column was increased. But the introduction of air into a liquid-solid fluidized bed caused the bed to contract markedly, the amount of contraction observed depending as before upon the initial degree of bed expansion (see Figure 4.40). Thus, at the highest liquid flow rate studied ($\langle j_l \rangle$ = 5.71 cm/sec), the reduction in bed height was as large as 59% of the initial bed height, whereas at the lowest liquid flow rate studied ($\langle j_l \rangle$ = 1.59 cm/sec), the reduction was as small as 15%. Subsequent increase in gas flow rate, for a fixed liquid flow rate, caused no appreciable change in the bed voidage, and even the change in flow regime from bubbly to slug flow, at a gas flow rate of 4 - 5 cm/sec, did not affect the bed voidage noticeably. Increasing the gas flow rate further

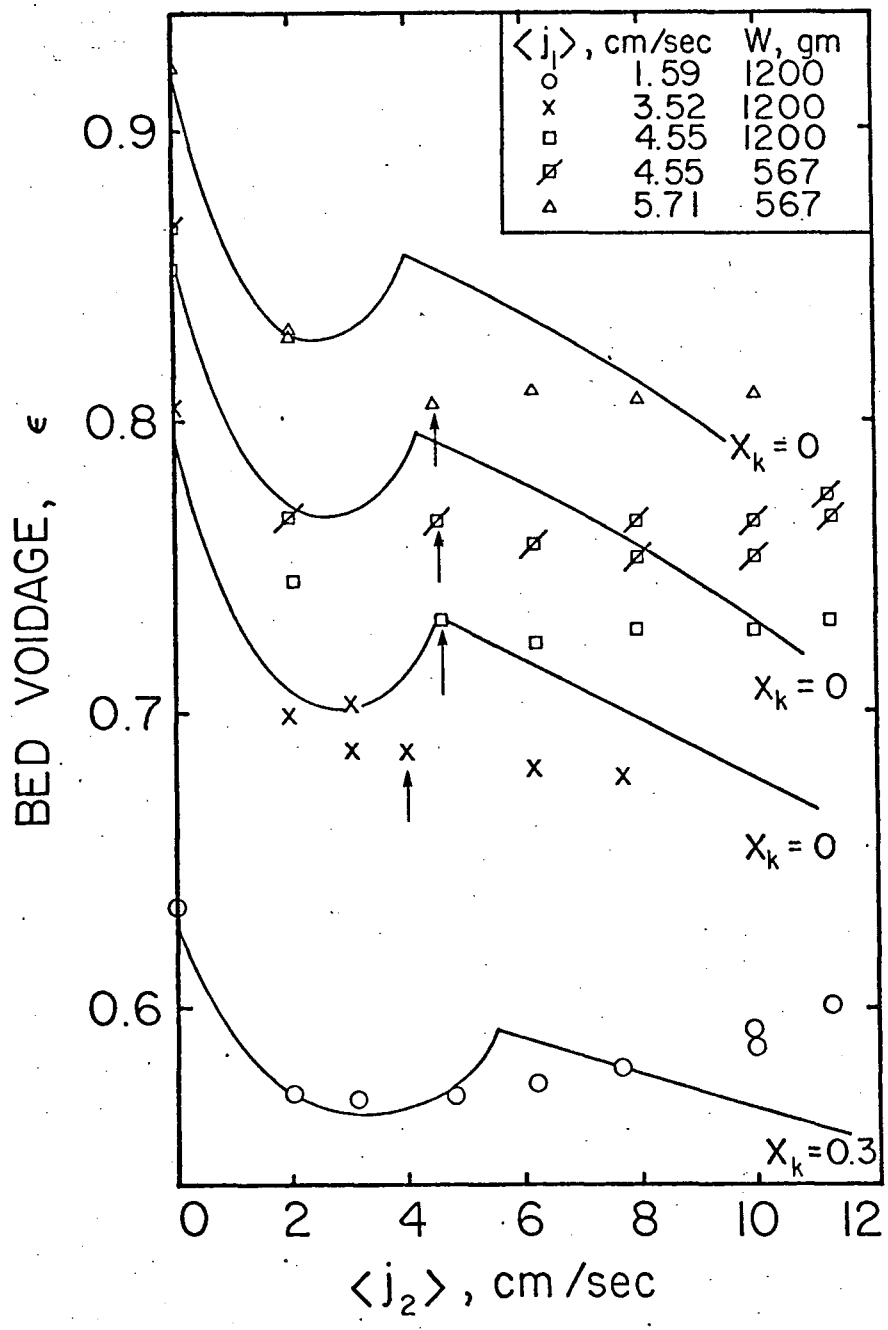

FIGURE 4.40 BED VOIDAGE IN THREE-PHASE BEDS OF 1/2 MM GLASS BEADS FLUIDIZED BY AIR AND WATER (——— generalized wake model; arrows indicate observed change from bubbly flow to slug flow)

beyond the transition point had little or no effect on the bed voidage, except at the lowest liquid flow rate studied ($\langle j_1 \rangle$ = 1.59 cm/sec), when the bed was observed to expand again slowly, as shown in Figure 4.40. At high flow rates of air, the particles were observed a long way up from the dense bed region, but no particles were being elutriated out of the column, even at the highest gas velocity studied.

The numerical scheme used for solving the generalized wake model for 1/2 mm glass beads was the same as that for 1/4 mm glass beads discussed above, the equations to be solved and the assumptions involved being identical. The computation scheme adopted was found to converge successfully, and the resulting bed characteristic curves are shown in Figure 4.40. The bed voidage predicted by the model with $x_k = 0$, for gas flow rates less than 3 cm/sec, agreed very well with the measured values at all the liquid flow rates except the lowest ($\langle j_1 \rangle$ = 1.59 cm/sec), for which the values predicted with $x_k = 0.3$ showed better agreement with the data. The comparison of predicted bed voidages with the measured values at large gas flow rates ($j_2 > 3$ cm/sec) showed reasonable agreement in absolute values (within 8%), but the overall trend of the predictions was not compatible with the experimental trend. A sharp peak in the predicted values of bed voidage occurred at a gas flow rate of between 4 and 6 cm/sec, but this peak could not be attributed to the change in flow regime, since the transition phenomenon

was not (for the present) incorporated into the generalized wake model. Therefore it is believed again that small inaccuracies in the estimates of ε_k from equation 4.7 were responsible for such inexplicable bed characteristic curves.

In order to illustrate the sensitivity of predicted values of bed voidage to ε_k, a few calculations were made on a Wang desk calculator by allowing small variations from the estimated values of ε_k. The results obtained are presented in Table 4.33. It can be seen that a small change in the absolute value of ε_k could change the bed characteristic curve such that the calculated values satisfied the observed bed voidage data plotted in Figure 4.40. Thus the role of wake volume fraction in determining the bed characteristics of 1/2 mm glass beads is important, but not as critical as found for beds of 1/4 mm glass beads.

In order to verify the ability of equation 4.7 to predict the wake volume fraction in beds of 1/2 mm glass beads, measured values of gas and solids holdups were used for evaluating the wake volume fraction from the same four equations as listed above for the 1/4 mm beads. The calculated values for four different values of the parameter x_k are presented in Table 4.34. Again, as with Rigby and Capes [80], ε_k increased with increase in x_k. Since the values of bed voidage predicted by the generalized wake

TABLE 4.33

SENSITIVITY OF BED VOIDAGE, ε, PREDICTED FROM GENERALIZED WAKE MODEL WITH x_k = 0.0 TO WAKE VOLUME FRACTION, ε_k, IN THREE-PHASE BEDS OF 1/2 MM GLASS BEADS

$\langle j_1 \rangle$ (cm/sec)	$\langle j_2 \rangle$ (cm/sec)	Predicted by the Model Using Equation 4.7 for ε_k			Calculated by the Model Using Arbitrary Values of ε_k			$\varepsilon_k^{\dagger}$
		ε_2	ε	ε_k	ε_k	ε	ε_2	
3.52	4.0	0.089	0.716	0.040	0.047	0.690	0.091	0.035
	4.5	0.101	0.733	0.037	0.048	0.686	0.101	0.030
	6.0	0.126	0.718	0.041	0.049	0.684	0.128	0.036
	8.0	0.154	0.699	0.044	0.050	0.680	0.161	0.042
5.71	3.0	0.076	0.830	0.067	0.078	0.818	0.080	0.063
	4.0	0.100	0.858	0.059	0.083	0.808	0.103	0.050
	6.0	0.139	0.836	0.069	0.085	0.808	0.146	0.065
	10.0	0.198	0.786	0.080	0.087	0.808	0.220	0.096

$^{\dagger}\varepsilon_k$ is determined from equation 4.7 using holdups calculated from the arbitrary values of ε_k

TABLE 4.34

ESTIMATED VALUES OF WAKE VOLUME FRACTION, ε_k, FROM EXPERIMENTAL DATA IN THREE-PHASE BEDS OF 1/2 MM GLASS BEADS FLUIDIZED BY AIR AND WATER

$\langle j_1 \rangle$ (cm/sec)	$\langle j_2 \rangle$ (cm/sec)	ε_2	ε_3	ε_k from Generalized Wake Model With				ε_k from equation 4.7 with p = 3
				x_k=0.0	x_k=0.1	x_k=0.2	x_k=0.4	
1.59	2.03	0.042	0.429	0.013	0.015	0.017	0.023	0.019
	3.16	0.063	0.431	0.015	0.016	0.018	0.025	0.022
	4.81	0.088	0.429	0.015	0.017	0.019	0.025	0.020
	6.17	0.096	0.425	0.013	0.014	0.016	0.021	0.019
	7.67	0.164	0.422	0.022	0.025	0.028	0.038	0.026
	9.94	0.195	0.413	0.022	0.024	0.027	0.036	0.033
	11.22	0.227	0.399	0.023	0.026	0.029	0.039	0.041
3.52	2.00	0.050	0.300	0.044	0.049	0.056	0.077	0.038
	3.03	0.079	0.314	0.054	0.060	0.068	0.092	0.038
	4.00	0.082	0.314	0.042	0.047	0.053	0.072	0.037
	6.17	0.118	0.320	0.043	0.048	0.055	0.074	0.033
	7.67	0.136	0.322	0.041	0.046	0.052	0.070	0.036
4.55	2.00	0.056	0.233	0.061	0.068	0.078	0.108	0.052
	4.54	0.093	0.234	0.048	0.054	0.061	0.083	0.046
	6.17	0.130	0.242	0.056	0.063	0.071	0.097	0.049
	7.92	0.154	0.246	0.055	0.062	0.070	0.095	0.055
	9.94	0.172	0.234	0.048	0.054	0.061	0.083	0.064
	11.25	0.169	0.225	0.039	0.044	0.049	0.067	0.065
5.71	2.00	0.053	0.167	0.065	0.073	0.084	0.118	0.065
	4.46	0.113	0.193	0.084	0.094	0.107	0.149	0.054
	6.15	0.123	0.189	0.064	0.072	0.081	0.112	0.058
	7.96	0.149	0.192	0.064	0.071	0.081	0.111	0.066
	9.97	0.180	0.191	0.065	0.072	0.082	0.112	0.079

model with $x_k = 0$ agreed initially with the measured values (Figure 4.40), estimated values of ε_k for $x_k = 0$ are compared in Figure 4.41 with the predicted values from equation 4.7. It can be seen that, even though the overall agreement is quite reasonable, the predictions from equation 4.7 tend to overestimate the wake volume fraction at large gas flow rates ($j_2 > 8$ cm/sec).

Thus the wake volume fraction and particle content of the wake are important parameters for describing the behaviour of three-phase fluidized beds of 1/2 mm glass beads. Yet in most instances the generalized wake model with $x_k \simeq 0$ can adequately predict the bed voidage. Further experimental evidence is, however, necessary for assessing equation 4.7 as a means for predicting the wake volume fraction in such three-phase systems.

The effect of column diameter on bed voidages is illustrated in Figure 4.42, where the bed voidage data for beds of 1/2 mm sand in the 20 mm i.d. glass column are compared with that of 1/2 mm glass beads in the 2 inch i.d. perspex column, even though the method of estimating the expanded bed height in the two instances were different. Also shown in Figure 4.42 is the curve representing the limited bed voidage data of Østergaard and Theisen [18] for beds of 0.58 mm glass beads in 4 in i.d. columns. Equality or near equality of initial bed voidage was chosen as the basis for comparisons. Although it is difficult to glean

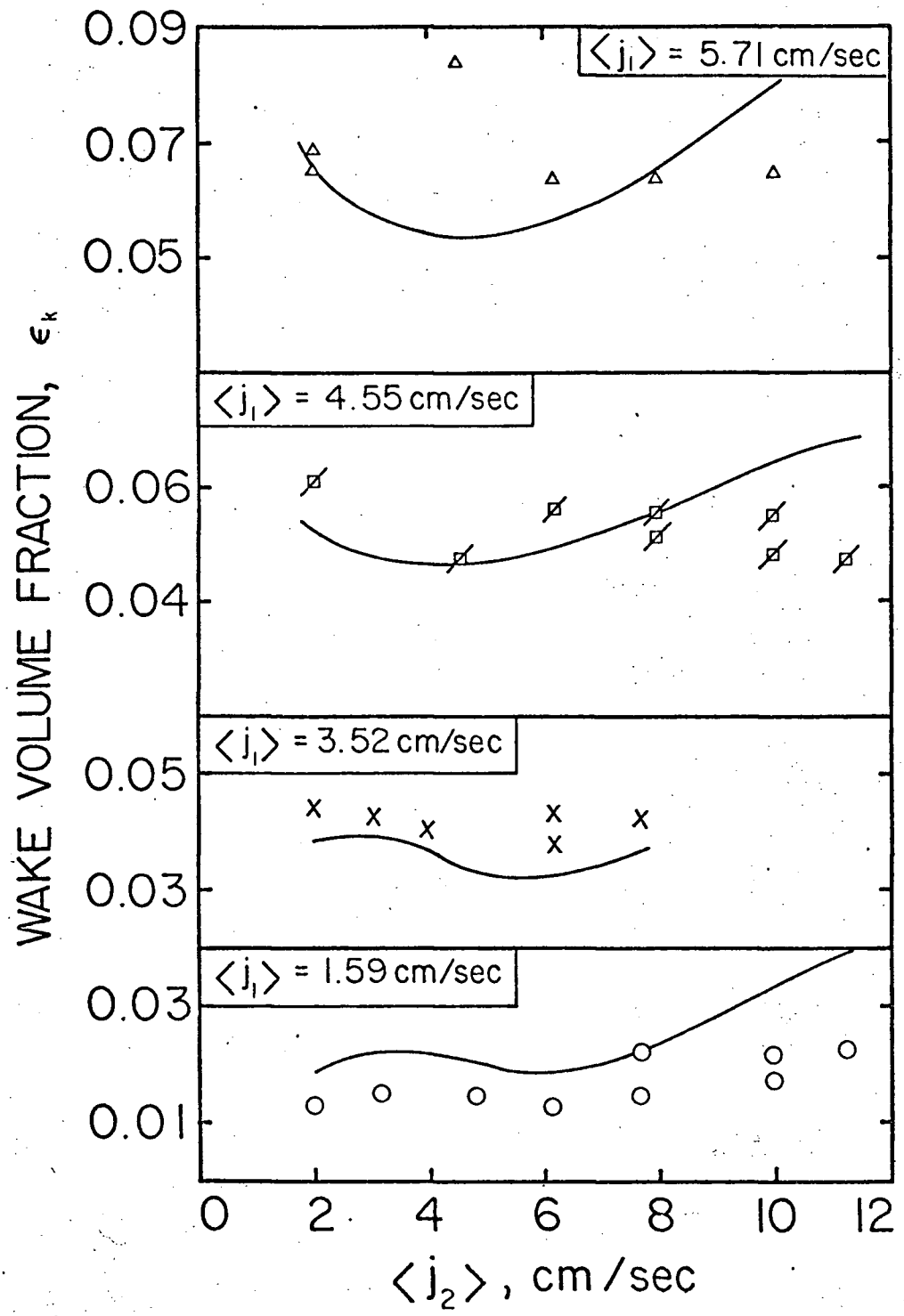

FIGURE 4.41 COMPARISON OF ϵ_k CALCULATED FROM EQUATIONS 1.3, 2.91, 2.94 AND 2.106 WITH x_k=0, USING THE MEASURED VALUES OF GAS AND SOLIDS HOLDUP IN THREE-PHASE FLUIDIZED BEDS OF 1/2 MM GLASS BEADS, WITH PREDICTED VALUES (——) FROM EQUATION 4.7 WITH p=3

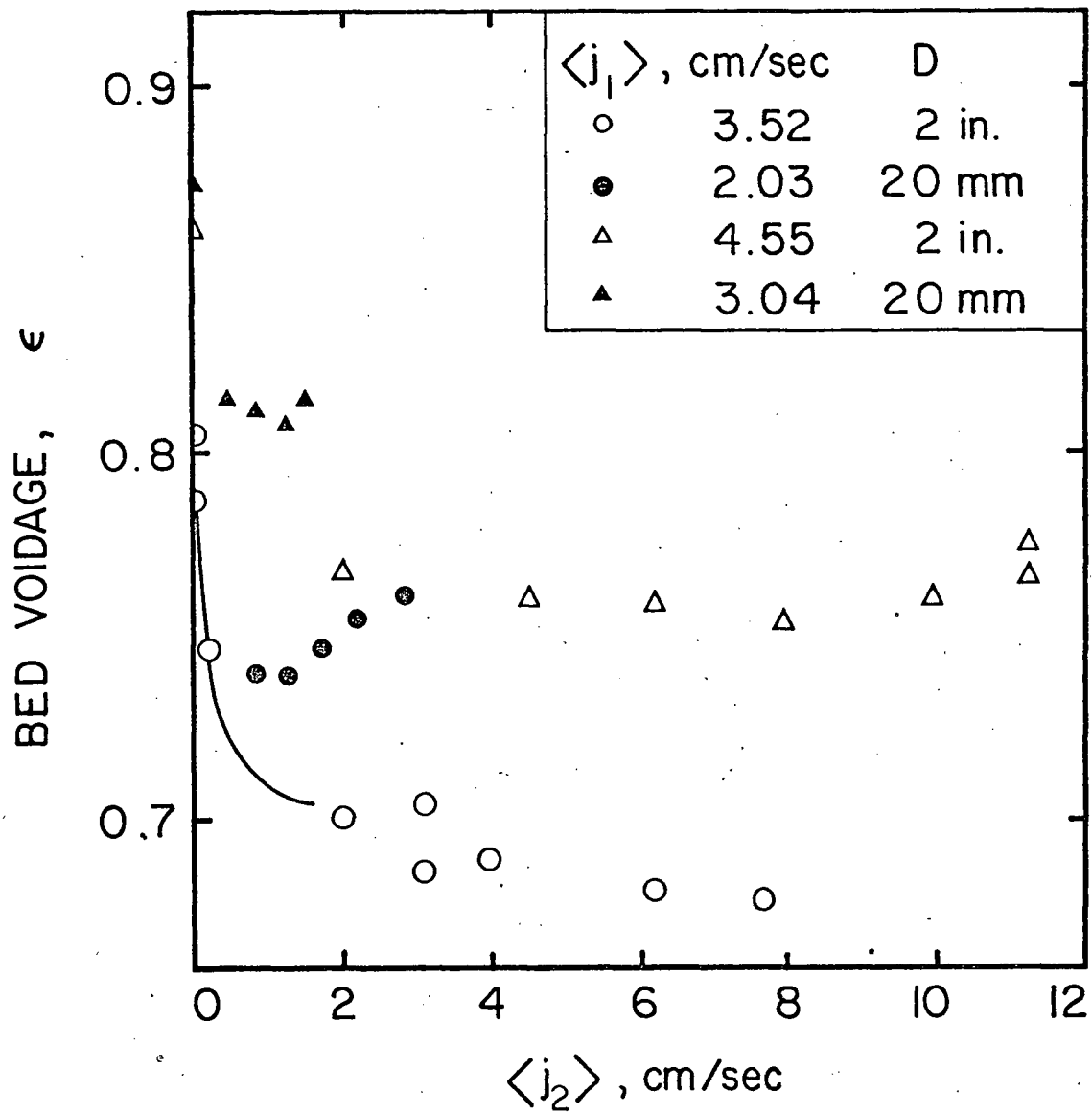

FIGURE 4.42 COMPARISON OF BED VOIDAGE DATA FOR 1/2 MM SAND PARTICLES IN 20 MM GLASS COLUMN WITH THOSE FOR 1/2 MM GLASS BEADS IN 2 INCH PERSPEX COLUMN (——— data of Østergaard and Theisen [18] for 0.58 mm glass beads at j_1=3.6 cm/sec in 4 inch column)

any comparative pattern from the sparse data of Østergaard and Theisen [18], the data obtained here from the 20 mm and 2 inch columns clearly indicate that the degree of bed contraction in the smaller column is significantly smaller than in the larger one. This difference in bed behaviour of similar particles could be attributable to either one or both of the following factors:

(i) The difference in the absolute depths of the respective three-phase fluidized bed regions (the 2 inch diameter beds were always deeper than the 20 mm diameter beds), as postulated by Rigby and Capes [80].

(ii) The difference in the wake characteristics of slugs in 20 mm and 2 inch diameter columns.

(iii) Air-water-1 mm glass beads

On introducing air into a liquid-solid fluidized bed of 1 mm glass beads, a measurable bed contraction was observed to occur. The amount of bed contraction in a highly expanded bed ($\langle j_l \rangle$ = 12.80 cm/sec) was about 20% of the initial expanded bed height, whereas in a moderately expanded bed ($\langle j_l \rangle$ = 7.02 cm/sec), it amounted to about 15%. A further increase in gas flow rate, at constant liquid flow rates of 7.02 and 7.65 cm/sec, caused the bed to expand slowly and reach a plateau at a gas flow rate of about 6 cm/sec, as shown in Figure 4.43a and b. At the higher liquid flow rate of 12.8 cm/sec, the bed continued to contract up to a gas flow rate of about 4 cm/sec, but increasing the gas flow rate further, from 4 to 12 cm/sec, did not affect the bed voidage appreciably, as shown in Figure 4.43c. The particles were observed to travel a long way up in the test section before returning back into the main dense bed region, but no particles were observed to leave the column, even at the highest gas flow rates studied.

For predicting the bed voidage from the generalized wake model, the same numerical scheme as before was used for solving the set of eight equations listed earlier. A good convergence was quickly obtained, and the curves of bed voidage calculated from the model are presented for specific values of x_k in Figure 4.43. The predicted values of bed voidage for x_k = 0.0 are in good agreement with the measured

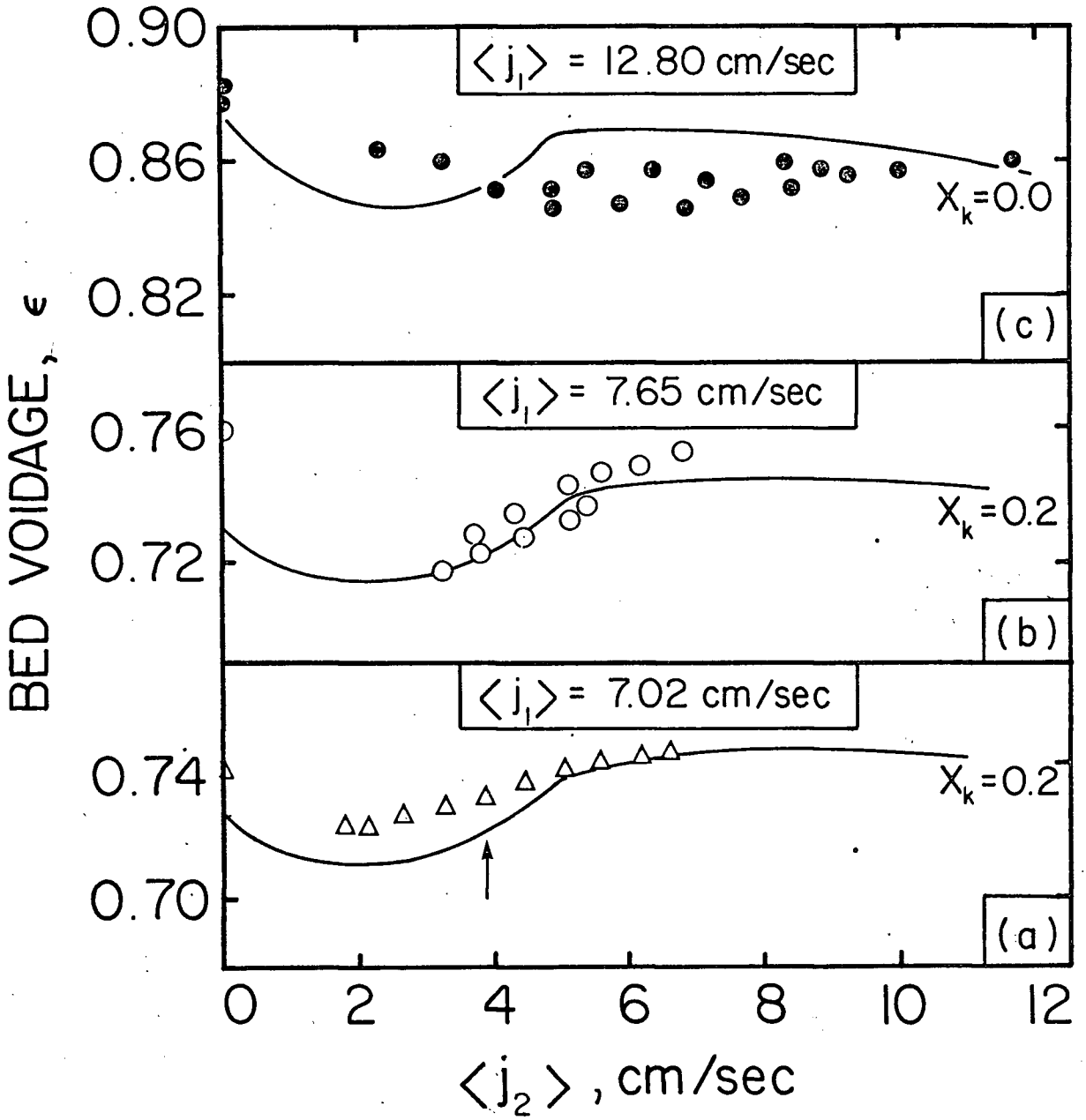

FIGURE 4.43 BED VOIDAGE IN THREE-PHASE BEDS OF 1 MM GLASS BEADS FLUIDIZED BY AIR AND WATER (——— generalized wake model; arrow indicates observed change from bubbly flow to slug flow)

values at the liquid flow rate of 12.80 cm/sec, but the predicted values for x_k = 0.2 showed better agreement with the measured values at the other two liquid flow rates. Thus the generalized wake model can satisfactorily predict the voidage in three-phase fluidized beds of 1 mm glass beads if the bubble wakes are assigned an appropriate particle content, which exceeds zero for the denser (lower liquid velocity) beds.

In order to test the ability of equation 4.7 to predict the wake volume fraction in three-phase fluidized beds of 1 mm glass beads, measured values of gas and solids holdups were used for calculating ε_k from equation 4.7, as well as from the same four equations which were applied to the smaller beads, for four different values of the parameter x_k. The calculated values are presented in Table 4.35 and show that ε_k increases with increasing x_k. Now a comparison of ε_k thus calculated, using the values of x_k at each liquid flux for which the generalized wake model was found to give good agreement with the measured values of bed voidage, with the predicted values from equation 4.7 is shown in Figure 4.44. Even though a considerable scatter exists in the calculated values of ε_k, the overall agreement with the predicted values from equation 4.7 is reasonable, indicating that the simple equation 4.7 can be used in preference to the more complex equation 2.128 (the predictions from these two equations showed moderate agreement in Table 4.5) for

TABLE 4.35

ESTIMATED VALUES OF WAKE VOLUME FRACTION, ε_k, FROM EXPERIMENTAL DATA IN THREE-PHASE BEDS OF 1 MM GLASS BEADS FLUIDIZED BY AIR AND WATER

$\langle j_1 \rangle$ (cm/sec)	$\langle j_2 \rangle$ (cm/sec)	ε_2	ε_3	ε_k from Generalized Wake Model				ε_k from equation 4.7 ith p = 3
				x_k=0.0	x_k=0.1	x_k=0.2	x_k=0.4	
7.02	1.78	0.052	0.279	0.034	0.039	0.046	0.072	0.042
	2.12	0.050	0.279	0.023	0.027	0.031	0.046	0.042
	2.63	0.076	0.276	0.047	0.054	0.064	0.098	0.045
	3.28	0.073	0.273	0.027	0.031	0.036	0.052	0.046
	3.87	0.090	0.270	0.036	0.041	0.047	0.069	0.041
	4.44	0.138	0.266	0.087	0.100	0.117	0.178	0.047
	5.01	0.076	0.262	0.011	0.013	0.015	0.021	0.047
	5.57	0.068	0.260	0.006	0.007	0.008	0.011	0.048
	6.17	0.132	0.258	0.040	0.045	0.052	0.076	0.047
	6.60	0.132	0.257	0.036	0.040	0.047	0.067	0.047
7.65	3.23	0.067	0.283	0.038	0.044	0.050	0.073	0.044
	3.80	0.091	0.278	0.054	0.062	0.072	0.107	0.040
	4.45	0.088	0.273	0.037	0.042	0.048	0.070	0.042
	5.14	0.121	0.268	0.060	0.069	0.080	0.118	0.042
	5.60	0.101	0.253	0.024	0.027	0.031	0.045	0.039
	6.80	0.123	0.247	0.028	0.032	0.036	0.053	0.047
12.80	2.31	0.055	0.136	0.055	0.065	0.078	0.134	0.074
	3.23	0.068	0.141	0.055	0.064	0.076	0.129	0.076
	4.07	0.085	0.149	0.075	0.086	0.102	0.163	0.069
	5.36	0.095	0.143	0.057	0.066	0.077	0.119	0.063
	6.33	0.100	0.144	0.051	0.058	0.068	0.102	0.059
	7.14	0.119	0.146	0.066	0.075	0.088	0.132	0.066
	8.42	0.139	0.148	0.074	0.085	0.099	0.147	0.073
	9.24	0.148	0.145	0.072	0.082	0.096	0.142	0.077
	10.06	0.154	0.143	0.069	0.078	0.091	0.134	0.080
	11.66	0.162	0.141	0.061	0.069	0.080	0.117	0.085

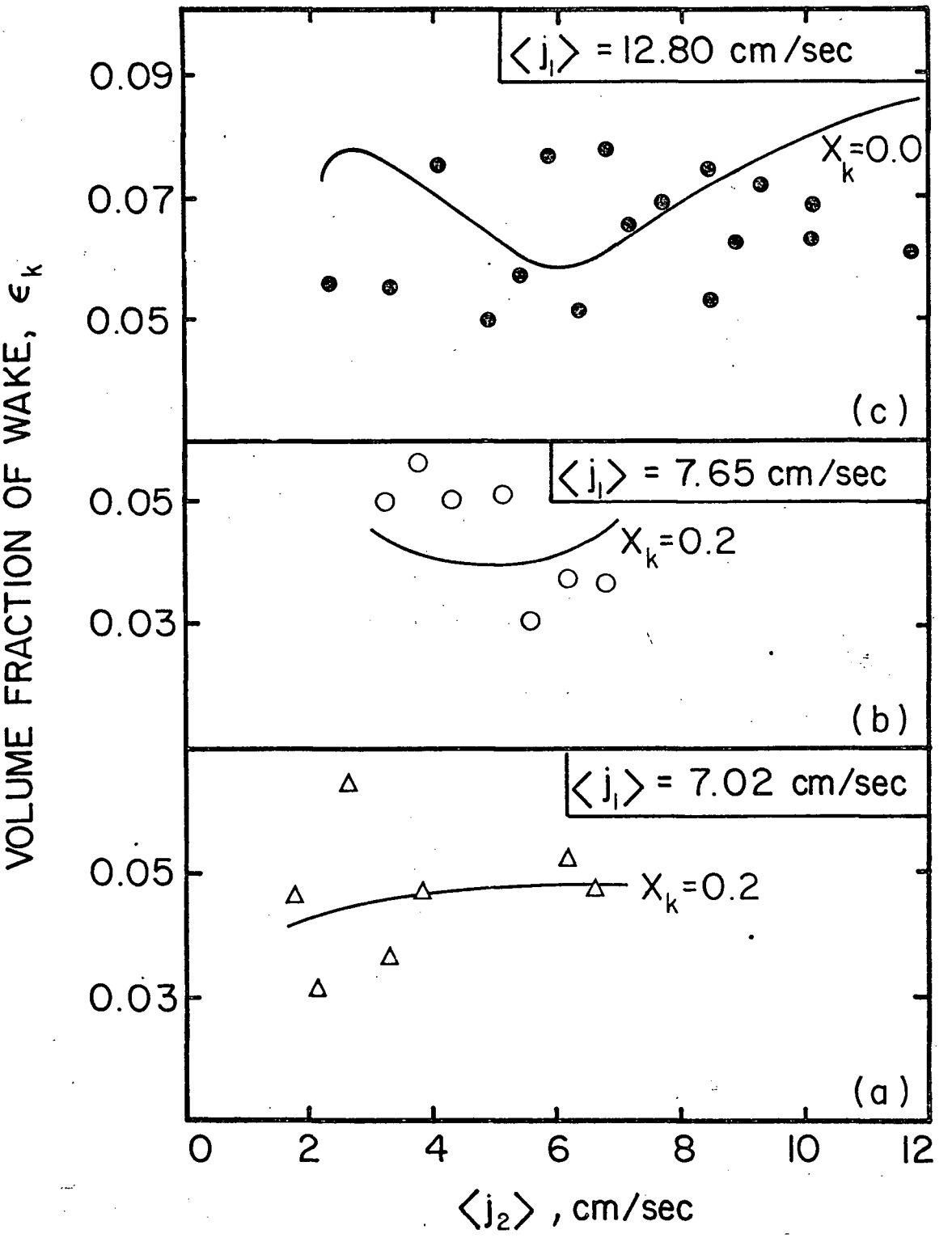

FIGURE 4.44 COMPARISON OF ϵ_k CALCULATED FROM EQUATIONS 1.3, 2.91, 2.94 AND 2.106, USING THE MEASURED VALUES OF GAS AND SOLIDS HOLDUP IN THREE-PHASE FLUIDIZED BEDS OF 1 MM GLASS BEADS, WITH PREDICTED VALUES (——) FROM EQUATION 4.7 WITH p=3

estimating the wake volume fraction in three-phase fluidized beds of 1 mm glass beads.

The effect of column diameter on bed voidages is illustrated in Figure 4.45, where the voidage data are presented for beds of 1 mm glass beads in 20 mm and 2 inch diameter columns. Also shown in Figure 4.45 is the curve representing the voidage data of Michelsen and Østergaard (14) for beds of 1 mm glass beads in 6 inch diameter column. The basis of selecting the data for this comparison was the near equality of bed voidage in the initial liquid-solid fluidized beds. It is quite clearly indicated that the degree of bed contraction increases with increase in column diameter. This change in bed behaviour with column diameter was also observed previously with the 1/2 mm particles, and could again be explained by either or both of the factors cited for the smaller particles.

(iv) Air-water-lead shot

The behaviour of three-phase beds of 2 mm lead shot fluidized by a cocurrent stream of air and water was quite different than described hertofore for beds of glass beads. The introduction of air into the water fluidized bed of 2 mm lead shot did not bring about any contraction in bed height at any of the liquid flow rates studied. On the contrary, a slight initial bed expansion was always noted. Increasing the air flow rate, at a fixed liquid flow rate,

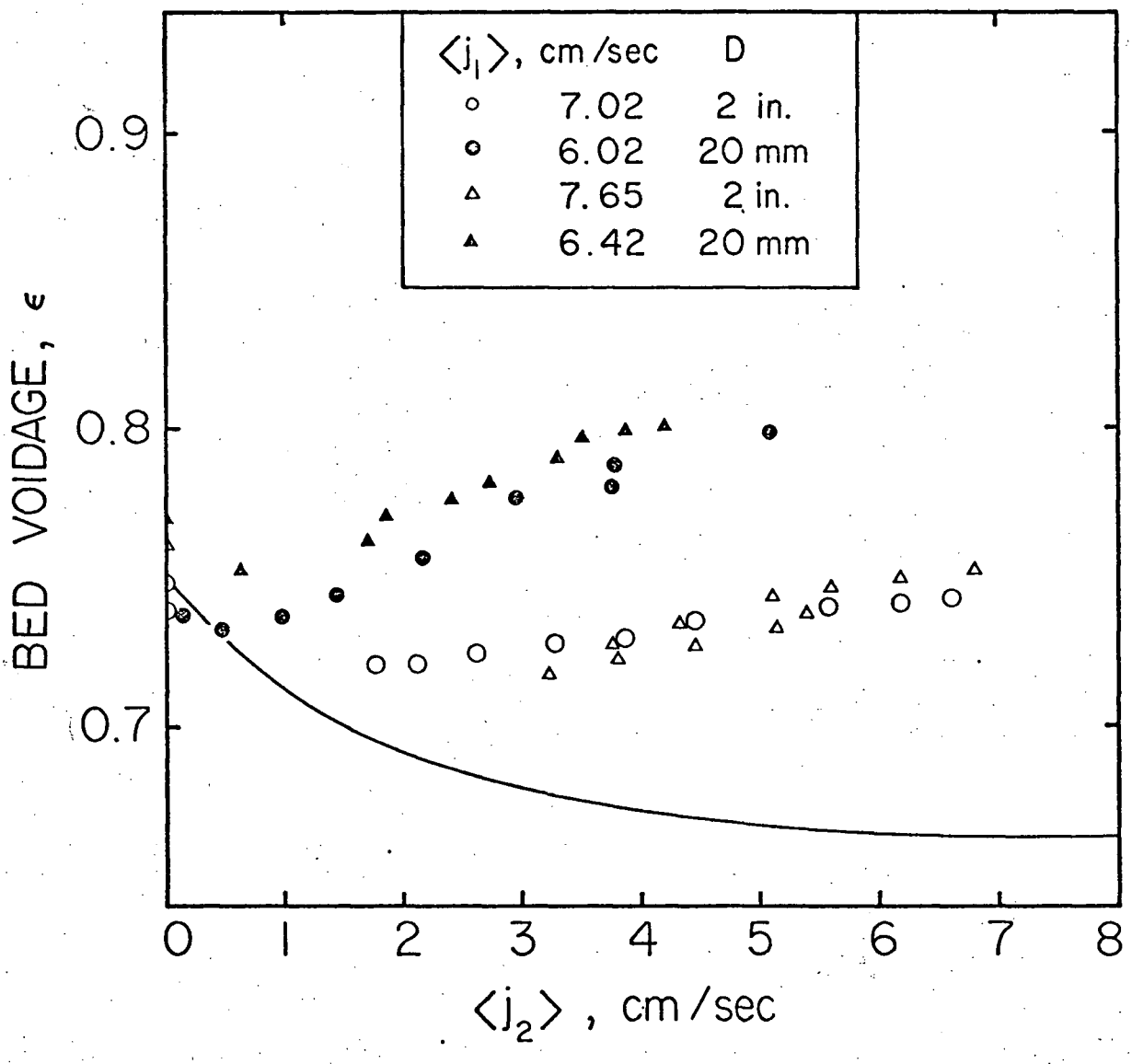

FIGURE 4.45 COMPARISON OF BED VOIDAGE DATA FOR 1 MM GLASS BEADS IN 20 MM GLASS COLUMN WITH THOSE IN 2 INCH PERSPEX COLUMN (——— data of Michelsen and Østergaard [14] for 1 mm glass beads at j_1=6.6 cm/sec in 6 inch column)

resulted in further expansion of the bed up to a gas flow rate of about 6 cm/sec. But increasing the air flow rate beyond this velocity caused the bed characteristic curve to change abruptly as the bed began to contract. The bed continued to contract on increasing the air flow rate until a plateau was reached ($10.0 < j_2 < 12.0$), after which the bed was observed to expand again, but only slightly, as shown in Figure 4.46.

The first break in the bed characteristic curve coincided with transition from bubbly to slug flow, which was visually observed to occur at an air flow rate of between 6 and 8 cm/sec at all the liquid flow rates studied. Thus the flow regime was primarily bubbly up to the air flow rate of 6 cm/sec, while for air flow rates greater than 8 cm/sec, large slugs were observed to travel through the column with smaller bubbles rising in their respective wakes. For slightly higher gas flow rates, at the two lower liquid flow rates ($\langle j_1 \rangle$ = 8.26 and 17.8 cm/sec), the beds were occasionally lifted off the bed support screen, due presumably to particle bridging. No readings were taken under such conditions. For the higher liquid flow rates, no such bridging effect was observed even at the highest air flow rate studied. Under all conditions, even though the beds were in a vigorous state of fluidization, no particles were observed to leave the column.

In order to check the ability of the generalized wake model to predict the bed voidage in these three-phase

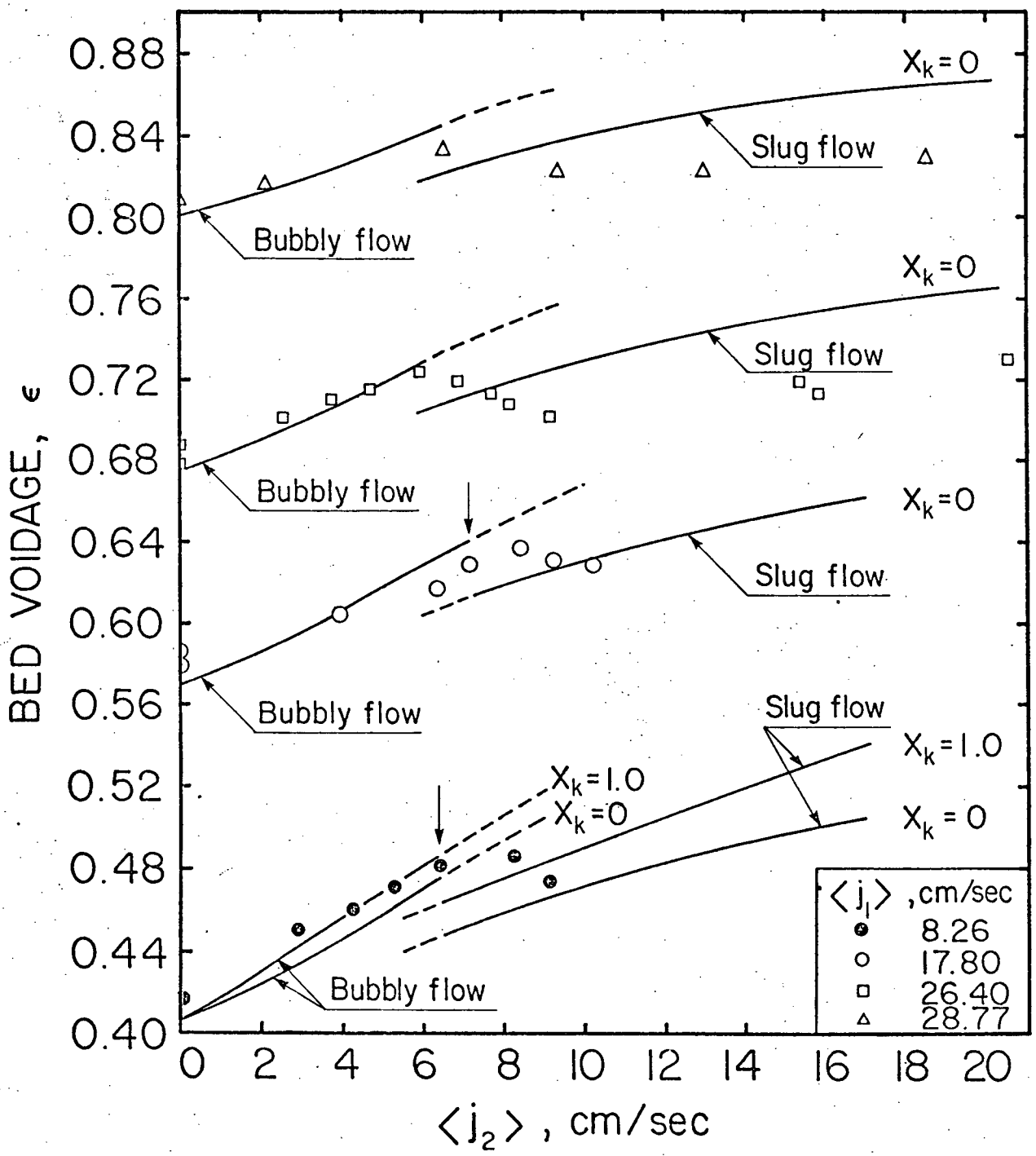

FIGURE 4.46 BED VOIDAGE IN THREE-PHASE BEDS OF 2 MM LEAD SHOT FLUIDIZED BY AIR AND WATER (——— generalized wake model; arrows indicate observed change from bubbly flow to slug flow)

fluidized beds, the first two assumptions made in formulating the necessary mathematical equations were modified in view of the differences in observed bed behaviour. The modified assumptions are:

(i) Equation 4.28 can be used for predicting the voidage in the particulate phase of the three-phase fluidized beds, as discussed above in section 4.2.3.1.

(ii) Equation 2.112 can be used for calculating the rise velocity of bubble swarms, where the drift velocity for bubbles at $j_2 < 6$ cm/sec can be calculated from equation 2.37 with $\bar{r}_e = 0.4$ cm (an approximation from visual observations), and for slugs at $j_2 > 8$ cm/sec, from equation 4.8, as discussed in Section 4.2.2.2.

Thus, following the first assumption, equation 2.106, in the set of eight equations necessary for solving the generalized wake model, was modified to

$$\varepsilon''_{1f} = \left[\frac{\langle j_1 \rangle - \bar{v}_2 (1-x_k) \varepsilon_k}{0.36\ V_\infty^{1.18} (1-\varepsilon_2-\varepsilon_k)} \right]^{1/2.28} \qquad (4.29)$$

and following the second assumption, equation 2.37 was modified to

$$v_{2j} = (V_\infty)_B \sqrt{\tanh \{0.25 (1/\varepsilon''_2)^{1/3}\}} \quad \text{for } j_2 < 6 \qquad (4.30)$$

but for the slug flow regime, as before

$$v_{2j} = 0.2(<j_1+j_2>)+ 0.35\sqrt{gD} \quad \text{for } j_2> 8 \qquad (4.8)$$

The other six equations from the earlier set of eight remained intact. The new set of eight simultaneous equations were then solved numerically for different values of the parameter x_k, varying from 0.0 to 1.0.

The calculated values of bed voidage for $x_k = 0.0$ are compared with the measured values in Figure 4.46, and showed a fairly good overall agreement over the wide range of gas flow rates studied. The agreement was particularly good for $j_2 < 6$ cm/sec, whereas for $j_2 > 8$ cm/sec the predicted values were somewhat larger than the measured values, the maximum deviation being about 5%. Thus the agreement of the bed voidage data with the predictions from the generalized wake model using the bubbly flow model for $j_2 < 6$ cm/sec, and their gradual shift at higher gas velocities towards the predicted values using the slug flow model, justifies the use of the respective expressions for drift velocities and adds to the credibility of the generalized wake model.

The variation in the bed voidage due to a change in the value of x_k from 0.0 to 1.0 is shown in Figure 4.46 for one of the liquid flow ratio ($<j_1> = 8.26$ cm/sec). The variation in bed voidage due to a change in the assumed

particle content of the wakes is very small, indicating that for beds of such large and heavy particles, the role of the wake particles is either small or insignificant. Further, if ε_k in equation 4.29 is neglected, it being tacitly assumed that the effect of the wake on bed voidage is insignificant, then this equation simplified to

$$\varepsilon''_{lf} = \left[\frac{\langle j_l \rangle}{0.36\ V_\infty^{1.18} (1-\varepsilon'''_2)} \right]^{1/2.28} \tag{4.31}$$

which, in combination with equations 1.3 and 2.60, yields

$$\varepsilon = \varepsilon''' + (1-\varepsilon'''_2) \left[\frac{\langle j_l \rangle}{0.36\ V_\infty^{1.18} (1-\varepsilon'''_2)} \right]^{1/2.28} \tag{4.32}$$

Equation 4.32 is equivalent to equation 2.62 derived earlier for the gas-free model, which can thus be considered a special case (wake-free case) of the generalized wake model.

The values of bed voidage calculated from equation 4.32, using the measured values of gas holdup in the three-phase fluidized beds, are presented in Table 4.36 along with the measured values of bed voidage. As can be seen, the agreement between the respective values at all the gas and liquid flow rates studied is surprisingly good, considering that the mechanism postulated [10] for deriving the gas-free model is presumed to be oversimplified. It can there-

TABLE 4.36

COMPARISON OF MEASURED BED VOIDAGES IN THREE-PHASE BED OF 2 MM LEAD SHOT FLUIDIZED BY AIR AND WATER WITH THE VALUES PREDICTED BY THE GAS-FREE MODEL

$\langle j_1 \rangle$ (cm/sec)	$\langle j_2 \rangle$ (cm/sec)	Measured Bed Voidage, ε	Predicted Bed Voidage, ε, From Equation 4.32
8.26	0.0	0.417	0.407
	2.91	0.451	0.430
	5.36	0.471	0.518
	7.22	0.489	0.523
	9.14	0.474	0.546
17.80	0.0	0.583	0.570
	3.97	0.605	0.626
	7.18	0.629	0.645
	9.33	0.631	0.670
	10.21	0.629	0.678
	11.22	0.609	0.662
26.40	0.0	0.683	0.677
	2.56	0.701	0.693
	4.73	0.716	0.727
	6.91	0.719	0.761
	8.15	0.708	0.732
	15.85	0.714	0.754
	20.50	0.729	0.802
38.77	0.0	0.809	0.801
	2.14	0.816	0.824
	6.56	0.833	0.856
	9.33	0.822	0.865
	12.93	0.822	0.880
	18.50	0.829	0.897

fore be said that, in determining the bed characteristics of large heavy particles, the role played by the bubble wakes can be neglected and the bed voidage well approximated from equation 2.62 or its equivalents.

(v) Air-PEG solution-glass beads

A great deal of attention and care had to be exercised for obtaining any three-phase fluidization data in beds of glass beads fluidized by a cocurrent stream of air and PEG solution. Not only was the phenomenon of particle entrainment encountered at practically all the gas and liquid flow rates obtainable in the present set-up, but a slight change in the temperature of the viscous liquid could also change the results radically. With 1/4 and 1/2 mm glass beads a stable bed operation could not be achieved at any flow rates, and therefore no data were recorded. In beds of 1 mm glass beads particle entrainment also occurred, but it was relatively small, thus making it possible to obtain limited data by taking every precaution to determine the weight of particles actually in the bed, as discussed in Section 3.3. Since the weight of particles inside the column could not always be accurately known and the temperature not always properly controlled for the relatively low liquid velocities required for these particles, the accuracy of these data is doubtful. They are nevertheless considered here briefly, as they represent the only data taken in the viscous domain ($Re_p \simeq 0.36$).

The introduction of air into the liquid-solid fluidized bed of 1 mm glass beads invariably resulted in slight expansion of the bed (Figure 4.47). However, even at the smallest air flow rate studied ($<j_2>$ = 0.4 cm/sec), particles were observed a long way up from the main dense bed region, their return being extremely slow. On increasing the air flow rate, the three-phase fluidized bed became quite chaotic but still showed a slight net expansion.

The calculation of bed voidage from the generalized wake model was not attempted. However, estimation of bubble radii from bubble frequency profiles measured by the electroresistivity probe (see Appendix 8.3) revealed that the Reynolds number, Re_b, of the bubbles in such a viscous system is about 200. Levich [38] has reported that for an almost spherical bubble in a liquid without impurities, the separation zone extends only to 2° from the line of symmetry at a bubble Reynolds number as high as 625. Therefore a bubble in the PEG solution can be assumed to carry an insignificant wake. It has been shown before that, when the wake volume fraction is insignificant, the generalized wake model simplifies to the gas-free model. Thus for the present system the bed voidage should be predictable by equation 2.62.

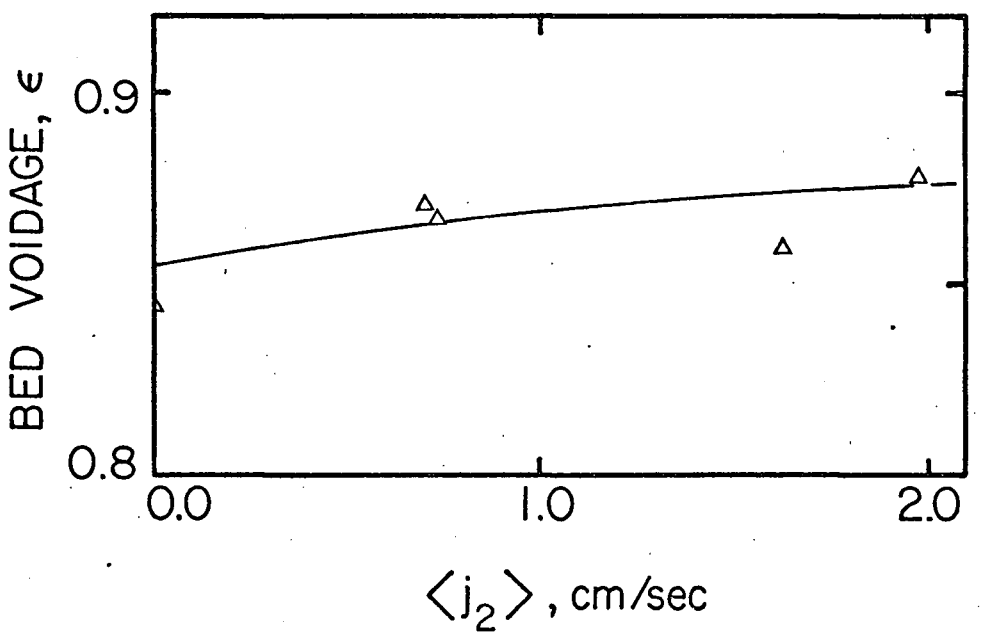

FIGURE 4.47 BED VOIDAGE IN THREE-PHASE BEDS OF 1 MM GLASS BEDS FLUIDIZED BY AIR AND PEG SOLUTION (△ -j_1=0.86≃0.88 cm/sec; ——— gas-free model)

The values of bed voidage calculated from equation 2.62, using the measured values of ε_2''', are compared in Table 4.37 with the measured values of ε'''. The agreement between the two sets of values appears to be reasonable, as also shown in Figure 4.47. Thus we can expect the gas-free model to describe the bed voidage of three-phase fluidized beds in the viscous domain (as well as of large heavy particles at considerably higher Reynolds numbers). It is interesting to note that the cell model derived in Appendix 8.1 for the Stokes regime also indicates that a three-phase fluidized bed operated in a viscous liquid medium will only expand on increasing the gas flow rate. A quantitative comparison with the cell model has not been made since the Happel two-phase cell model [49], of which the three-phase model is an extension, does not satisfactorily represent a liquid-solid fluidized bed in the voidage range (ε = 0.73 - 0.89) of the gas-free measurements.

(vi) Air-PEG solution-steel shot

The three-phase fluidization of 3 mm steel shot by a cocurrent stream of air and PEG solution occurred without appreciable particle elutriation. The introduction of an air stream into the liquid-solid fluidized bed did not affect the bed height significantly. However, increasing the air flow rate for a fixed liquid flow rate produced a measurable contraction in bed height, depending on the

TABLE 4.37

COMPARISON OF MEASURED BED VOIDAGES IN THREE-PHASE BED OF 1 MM GLASS BEADS FLUIDIZED BY AIR AND PEG SOLUTION WITH THE VALUES PREDICTED BY THE GAS-FREE MODEL

$\langle j_1 \rangle$ (cm/sec)	$\langle j_2 \rangle$ (cm/sec)	Experimental Values		Predicted Bed Voidage, ε, From Equation 2.6.2*
		Gas Holdup, ε_2'''	Bed Voidage, ε	
0.40	-	-	0.732	0.729
0.43	1.88	0.062	0.858	0.755
0.86	-	-	0.846	0.855
0.86	0.58	0.033	0.815	0.870
0.86	1.98	0.055	0.877	0.872
0.88	0.70	0.033	0.871	0.866
0.88	0.71	0.034	0.867	0.866
0.88	1.63	0.060	0.860	0.875
1.14	-	-	0.887	0.893
1.14	0.40	0.017	0.847	0.898

* $$\varepsilon = \varepsilon_2''' + (1-\varepsilon_2''') \left[\frac{\langle j_1 \rangle}{V_\infty \ (1-\varepsilon_2''')} \right]^{1/n} \qquad (2.62)$$

initial degree of bed expansion. Thus, for a highly expanded bed ($\langle j_1 \rangle$ = 18.84 cm/sec), the reduction in bed height was as much as 50% of the initial height, whereas for a less expanded bed ($\langle j_1 \rangle$ = 13.82 cm/sec), the reduction in bed height was only about 20%. The less expanded bed at high air flow rates ($\langle j_2 \rangle \simeq$ 10 cm/sec) was occasionally lifted off the bed support screen, indicating the probable occurrence of particle bridging across the column. Under such conditions it became difficult to maintain a constant liquid flow rate, and therefore no further data were obtained for any higher gas or any lower liquid flow rates. No bridging was encountered in beds at the higher liquid flow rate. The individual particle movement as well as the overall bed behaviour was apparently quite chaotic, analogous to the bed behaviour of 1 mm glass beads in a non-viscous system.

The calculation of bed voidages from the generalized wake model was carried out with the same assumptions as used for the 1 mm glass beads in the non-viscous system. The appropriate equations were then solved numerically, and the calculated bed voidages are shown in Figure 4.48 along with the measured values . The predicted curves of bed voidage for x_k = 0.0 appear to agree substantially with the measured values, at least in absolute values if not in trend, indicating the suitability of the generalized wake model for predicting the bed voidage in such highly viscous systems as well as in the non-viscous systems discussed previously.

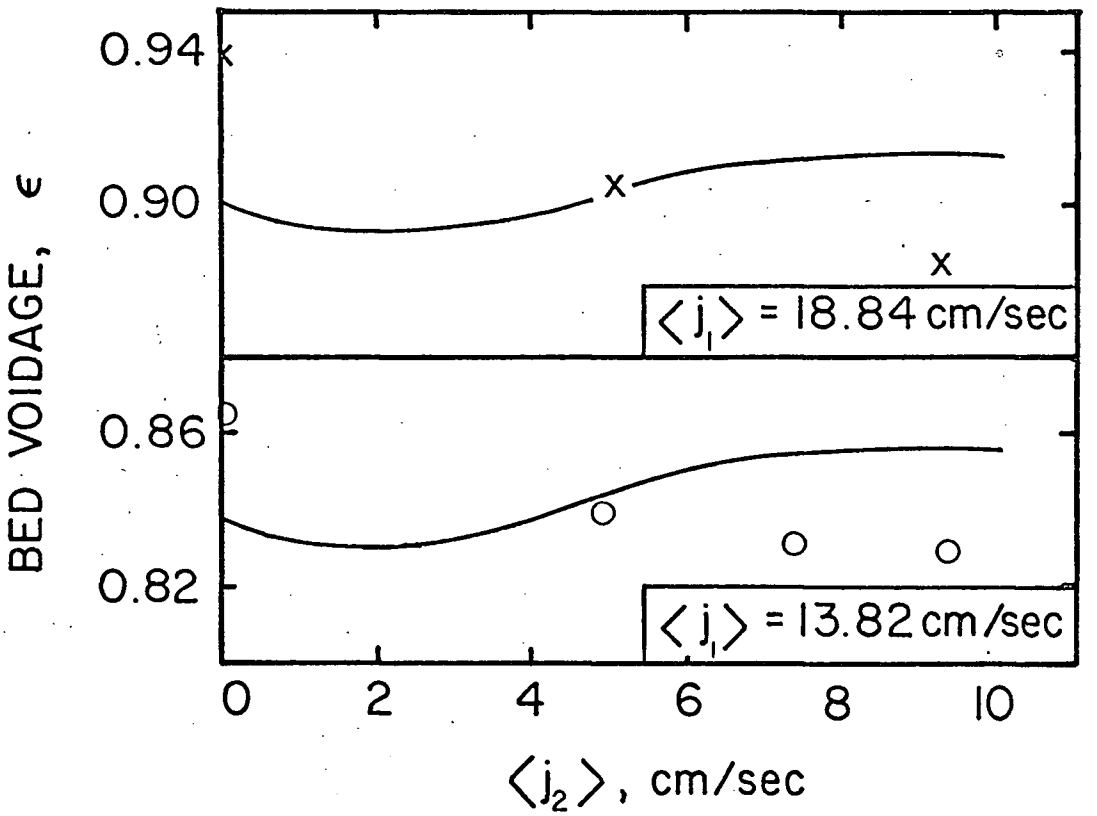

FIGURE 4.48 BED VOIDAGE IN THREE-PHASE BEDS OF 3 MM STEEL SHOT FLUIDIZED BY AIR AND PEG SOLUTION (——— generalized wake model with x_k=0)

CHAPTER 5

CONCLUSIONS

The major findings of the experimental studies on gas holdup in (A) gas-liquid flow and (B) three-phase fluidized beds, and solids holdup in (C) liquid-solid fluidized beds and (D) three-phase fluidized beds, are summarized as follows:

(A) Gas holdup in gas-liquid flow

(i) The two techniques used for gas holdup measurements in different sections of the column, viz. the pressure drop gradient method and the valve shut-off technique, gave matching results if, and only if, the pressures at which these measurements were made, were duly considered. The necessary pressure correction to the gas holdup, particularly by the valve shut-off technique, could be as large as 30%, depending on the location in the column.

(ii) The proposed model for drift velocities of bubble swarms (equation 2.37 for bubbly flow and equation 2.39 for slug flow), in conjunction with equation 4.1, described almost all the gas holdup data satisfactorily.

(iii) The electro-resistivity probe developed for this study was used successfully for measuring the local characteristics in air-water flow, and showed that

(a) the radial gas holdup profiles were axially symmetric and could be well represented by equation 2.27b, and

(b) the average gas holdup obtained by integrating these profiles was essentially equal to that measured by the pressure drop gradient and valve shut-off techniques.

Since the probe could not penetrate the air bubbles instantly, the measurements in the air-PEG system were not as successful.

(B) Gas holdup in three-phase fluidized beds

(i) Although the two techniques for measuring the gas holdups, viz. the pressure drop gradient method and the valve shut-off technique, were satisfactory for present purposes, more accurate techniques based on local measurements are required for future investigations of gas flow structure in three-phase fluidized beds.

(ii) Since the gas fraction in three-phase fluidized beds on a solids-free basis, was found to be only slightly larger than that in the co-existing gas-liquid regions, but smaller than that in the corresponding gas-liquid flow without solids, it is believed that the presence

of light small particles caused the gas flow structure in the entire column, (and not exclusively in the three-phase bed region), to be altered. For the light particles, increasing the particle size had a progressively smaller effect; but the use of heavy large particles caused the gas fraction in the three-phase fluidized bed, on a solids-free basis, to be increased significantly, thus indicating bubble breakup to be predominant, which was visually observable as well.

(iii) Even though the attempts to measure the local structure of gas flow through the three-phase region, using the electro-resistivity probe, were not entirely successful, it could be observed that

(a) the radial gas holdup profiles were axially symmetric, and

(b) the average bubble size, estimated from measured bubble frequency, was representative.

(C) Solids holdup in liquid-solid fluidized beds

(i) When the wall effects were significant, the Neuzil-Hrdina correlation (equation 2.51), within the recommended range of its applicability, was found to represent the bed voidage better than the Richardson-Zaki correlation (equation 2.46).

(ii) When particle Reynolds number was greater than 1,000, the dimensional correlation recommended by Trupp [87] was found to represent the bed voidage better than the Richardson-Zaki correlation.

(iii) The Richardson-Zaki correlation provided satisfactory agreement with the experimental data in most other circumstances.

(D) Solids holdup in three-phase fluidized beds

(i) The method developed for estimating the expanded bed height from longitudinal pressure drop profiles was found to give bed heights that were not only representative, but also reproducible and meaningful.

(ii) The fluidized beds of small light particles were found to contract on introduction of the gas phase, the degree of contraction depending mainly on the initial level of bed expansion. Thus, for initially highly expanded beds, the degree of bed contraction was as large as 60%. With further increase in gas flow rates, the bed height remained practically unchanged, but the height of the dilute phase above the main three-phase region increased progressively, ultimately reaching the top of the column, when a systematic elutriation of solid particles was recorded.

(iii) With light particles of increasing particle sizes, the degree of bed contraction became progressively smaller. For heavy large particles, introduction of gas phase caused the liquid-fluidized bed to expand. The transition from the bubbly to the slug flow regime at higher gas flow rates gave rise to a measurable reduction in the bed height, but subsequent increases in gas flow rate caused the bed to expand again, until a plateau was eventually reached.

(iv) The three-phase fluidization of particles in the Stokes' law regime failed to produce a steady bed, since a systematic elutriation was observed for as small a gas flow rate as 1 cm/sec. However, the experimental results did indicate that these fluidized beds too expanded on introduction of the gas phase.

Modelling three-phase fluidized beds

A general model for a three-phase fluidized bed was derived, based on the concept of relative velocity between the dispersed phase and the continuous phase proposed by Lapidus and Elgin [67] for any dispersed phase operation. The three main features of the generalized wake model are:

1. Equation 2.105 represents the relative velocity between the liquid and the solid particles in the particulate phase, taking the presence of gas and wake phases into consideration.

2. Equation 2.111 represents the relative velocity between the gas phase and the liquid phase, taking the presence of solids in the particulate phase into consideration.
3. Equation 4.7 estimates the wake size while the parameter x_k considers the particle content of the wakes and its effect on particle circulation in the bed.

The other equations in the generalized wake model were developed to represent the inter-relationship between the gas phase, the particulate phase and the wake phase.

The generalized wake model not only gave satisfactory agreement with most of the available data on solids holdup, and with the present data on gas holdup, in three-phase fluidized beds, but it also identified the relevant parameters for further study. Thus, while the influence of bubble wake size has been clearly established by earlier workers [7, 8, 14, 16, 18, 80], the role of wake particles has not been clear, in spite of the analysis by Rigby and Capes [80]. The generalized wake model clearly shows the importance of wake size and of wake particle content for three-phase beds of small particles. The comparison with experimental measurements presently available suggests that the particle content of the wakes was either small or zero, except for initially dense beds or for high gas flow rates. However, direct measurements of sizes and particle contents of bubble wakes in three-phase fluidized beds (which can also be

obtained indirectly from measurements of particle circulation rates) are needed to substantiate the predictions from the model, and are recommended for future investigations.

On the other hand, for beds of large and/or heavy particles, in which initial contraction is no longer observed, the properties of the bubble wakes apparently become unimportant, since the simple gas-free model, to which the generalized wake model reduces in the absence of wakes, predicts the bed behaviour quite successfully. Therefore a detailed study of wake characteristics (wake size, particle content of wakes, and circulation rate of particles) in such beds is not required. What is needed, however, is a precise criterion for predicting whether a designated bed of solid particles fluidized by a given liquid at a specific velocity will initially expand or initially contract on introducing a given gas. From the information available in the literature, as well as from that obtained in this investigation, it is believed that such a criterion can be developed; it is therefore recommended for further study.

NOMENCLATURE

Some symbols defined in the Appendix and used only once are not included here

a	radius of particle
A	column cross-sectional area
b_1, b_2, b_3, b_4	constants in equation 8.1.3
C	phase velocity of surface wave on liquids of shallow depth
C_1	constant
C_∞	phase velocity of surface wave on liquids of infinite depth
C_o	gas distribution parameter
d_b	bubble diameter, $d_b = 2\ r_e$
d_o	orifice diameter
d_p	particle diameter
D	column diameter
f	function of; friction factor
F	drag force exerted by the fluid on the particle
g	acceleration due to gravity
h	depth of undisturbed liquid
H	manometer reading
j_i	local volumetric flux (or local superficial velocity) of phase i
j	local volumetric flux (or local velocity) of gas-liquid mixture
k_1	constant for rise velocity of slugs, equation 2.11

L_b	expanded bed height or height of three-phase region
$L_{b,0}$	static bed height
L_i	length of various sections (A, E or C) of the column, as defined in Figure 3.5
m	exponent in equation 2.31
M	exponent in equation 2.27a
M'	exponent in equation 2.27b
n	exponent in Richardson-Zaki correlation, equation 2.46
N	total number of bubbles passing through a point in time T
n'	bubble frequency
N_{Eo}	Eötvös number based on tube radius, $N_{Eo} = g\rho_l R^2/\sigma$
P_i	pressure at various locations in the column, see Figure 8.2.4
P_{ATM}	reference pressure at top of column (barometric pressure)
Δp	pressure drop as measured by a differential manometer
Q_i	volumetric flow rate of phase i
r	radial distance from pipe center
r_e	radius of sphere having the same volume as the bubble
R	column radius
R*	dimensionless radial distance from pipe center, $R^* = r/R$
R_s	radius of curvature of spherical capped bubbles in region of front stagnation point
Re_b	Reynolds number of isolated rising bubble, $Re_b = \frac{d_b V_\infty \rho_l}{\mu_l}$

Re_p terminal free settling Reynolds number of particles,

$$Re_p = \frac{d_p V_\infty \rho_l}{\mu_l}$$

S slope of H vs. Z from longitudinal pressure drop profile

t_i residence time of the i^{th} bubble on the probe

T sample interval

v_i local linear velocity of phase i

$\bar{v}_i$ weighted mean velocity of phase i,

$$\bar{v}_i = \frac{\langle \alpha_i v_i \rangle}{\langle \alpha_i \rangle} = \frac{\langle j_i \rangle}{\langle \alpha_i \rangle}$$

v_{il} local relative velocity of phase i with respect to continuous liquid phase, $v_{il} = -v_{li}$

v_{ij} local drift velocity of phase i with respect to local gas-liquid mixture velocity j

V rise velocity of single bubble, or fall velocity of a single particle, in a cylindrical column

V_∞ terminal rise velocity of a bubble or free settling velocity of a solid particle in an infinite medium

V'_∞ liquid fluidization velocity of particle swarm extrapolated to $\varepsilon = 1$

V_0 energy destroying velocity of a bubble swarm

W weight of solid particles in the test section

We Weber number, $We = 2\rho_l V_\infty^2 r_e/\sigma$

x_k ratio of solids fraction in the wake to that in the particulate phase, see equation 2.89

Z vertical distance from tap 1 (in inches) or vertical coordinate along the column axis

$\langle\ \rangle$ denotes the property is averaged over the flow cross-sectional area. However, when the averaging process is evident, e.g. for j_l (see equations VII and VIII under Notation), these brackets will be omitted for convenience

Greek Letters

α_i	local volume fraction (or holdup) of phase i in the column
γ	ratio of radii, equation 2.17
λ	wave length
δ^*	dimensionless liquid film thickness in gas-liquid flow, δ^* = liquid film thickness/R
ε_i	average volume fraction (or holdup) of phase i in the column, $\varepsilon_i = \langle\alpha_i\rangle$
ε	average bed voidage defined as the volume of gas and liquid phases per unit volume of three-phase mixture
θ	spherical coordinate (r, θ)
μ_i	dynamic viscosity of phase i
ρ_i	density of phase i
ρ_M	density of manometric fluid
τ	shear stress
ψ	stream function
Ω_i	volume of phase i
σ	surface tension of liquid

Subscripts

i	dummy index or refers to phase i, i = 1 liquid phase, i = 2 gas phase and i = 3 solid phase
C, W	local values at column axis and at column wall respectively
k	wake phase
f	particulate phase
r	radial
θ	angular
z	axial
mf	minimum fluidization
B	bubble
s	solid particle

Superscripts

", "'	represents two-phase and three-phase regions, respectively
-	average value

If the term is specifically identified otherwise, the superscripts are dropped for brevity

LITERATURE CITED

1. Bhaga, D., M. Eng. Thesis, McGill University, Montreal (1969).

2. Richardson, J.F., and W.N. Zaki, Trans. Inst. Chem. Engrs., 32, 35 (1954).

3. Jackson, R., Trans. Inst. Chem. Engrs., 42, CE107 (1964).

4. Bhatia, V.K., M. Tech. Thesis, Indian Institute of Technology, Kharagpur, India (1965).

5. Robinson, S.P., U.S. Pat. 2, 614, 035 (Oct. 14, 1952); Chem. Eng., 60, 338 (1953).

6. Turner, R., Joint Symp. on Fluidization London, Soc. Chem. Ind., Inst. of Chem. Engrs., 47 (1963).

7. Stewart, P.S.B., and J.F. Davidson, Chem. Eng. Sci., 19, 319 (1964).

8. Østergaard, K., Chem. Eng. Sci., 20, 165 (1965).

9. Adlington, D., and E. Thompson, Proc. Third European Symp. Chem. Reaction Eng., 203 (1965).

10. Volk, R., Master's Thesis, Brooklyn Polytech. (1962).

11. Dakshinamurty, P., V. Subrahmanyam, and J.N. Rao, Ind. Eng. Chem. Process Des. Develop., 10, 322 (1971).

12. Evans, K., B.A.Sc. Thesis, University of British Columbia, Vancouver (1970).

13. Guha, D.K., N.K. Roy, and M.N. Rao, Chem. Eng. Sci., 19, 215 (1964).

14. Michelsen, M.L., and K. Østergaard, Chem. Eng. J., 1, 37 (1970).

15. Massimilla, L., A. Solimando, and E. Squillace, Brit. Chem. Eng., 6, 232 (1961).

16. Efremov, G.I., and I.A. Vakhrushev, Int. Chem. Eng., 10, 37 (1970).

17. Vail, Yu. K., N. Kh. Manakov, and V.V. Manshilin, Int. Chem. Eng. 10, 244 (1970).

18. Østergaard, K., and P.I. Theisen, Chem. Eng. Sci., 21, 413, 470 (1966).

19. Nicklin, D.J., Chem. Eng. Sci., 17, 692 (1962).

20. Davidson, J.F., and D. Harrison, "Fluidized Particles," Cambridge University Press, New York (1963).

21. Levenspiel, O., and D. Kunii, "Fluidization Engineering," John Wiley and Sons, Inc., New York (1969).

22. Rowe, P.N., and B.A. Partridge, Chem. Eng. Sci., 19, 974 (1964).

23. Scott, D.S., "Properties of cocurrent gas-liquid flow," Advances in Chemical Eng., 4,200-278, Academic Press, New York (1964).

24. Hodossy, L., Int. Chem. Eng., 8, 427 (1968).

25. Kasturi, G., J. Stepanek, and F.A. Holland, Brit. Chem. Eng., 16, 335, 511 (1971).

26. Gouse, Jr., S.W., "An index to two-phase gas-liquid flow literature," Massachusetts Inst. Tech Report No. 9 (1966).

27. Wallis, G.B., "One-dimensional two-phase flow," McGraw Hill, New York (1969).

28. Haberman, W.L., and R.K. Morton, The David Taylor Model Basin Report No. 802 (1953).

29. Haberman, W.L., and R.K. Morton, Trans. Am. Soc. Civil Engrs., 121, 227 (1956).

30. Peebles, F.N., and H.J. Garber, Chem. Eng. Progr., 49, 88 (1953).

31. Aybers, N.M., and A. Tapucu, Wärme - und Stoffubertragung, 2, 118 (1969).

32. Hadamard, J., Comp. Rend., 154, 1735 (1911).

33. Rybczynski, W., B. Int. Acad. Sci. Cracovie (A), p. 40 (1911).

34. Davies, R.M., and G.I. Taylor, Proc. Roy. Soc. (London), 200A, 375 (1950).

35. Edge, R.M. and C.D. Grant, Chem. Eng. Sci., 26, 1001 (1971).

36. Letan, R. and E. Kehat, AIChE J., 14, 398 (1968).

37. Magarvey, R.H., and R.L. Bishop, Can. J. Phys., 39, 1418 (1961).

38. Levich, G.V., "Physico-chemical Hydrodynamics," p. 435 ff., Prentice-Hall, Englewood Cliffs, N.J. (1962).

39. Zuber, N., and J.A. Findlay, Trans. ASME, J. Heat Transfer, 87C, 453 (1965).

40. Moore, D.W., J. Fluid Mech., 23, 749 (1965).

41. Mendelson, H.D., AIChE J. 13, 250 (1967).

42. Lamb, H., "Hydrodynamics," Sixth Ed., pp. 366, 458, 602, Dover Publications, New York (1945).

43. Dumitrescu, D.T., Z. angew. Math U. Mech., 23, 139 (1943).

44. White, E.T., and R.H. Beardmore, Chem. Eng. Sci., 17, 351 (1962).

45. Uno, S., and R.C. Kintner, AIChE J., 2, 3 (1956).

46. Harmathy, T.Z., AIChE J., 6, 281 (1960).

47. Neuzil, L., and M. Hrdina, Coll. Czechoslov. Chem. Commun., 30, 752 (1965).

48. Mendelson, H.D., and C.C. Maneri, AIChE J., 14, 295 (1968).

49. Happel, J., and H. Brenner, "Low Reynolds Number Hydrodynamics," pp. 115, 387, Prentice-Hall, Englewood, Cliffs, N.J. (1965).

50. Happel, J., and P.A. Ast, Chem. Eng. Sci., 11, 286 (1960).

51. Freedman, W., and J.F. Davidson, Trans. Inst. Chem. Engrs., 47, 251 (1969).

52. Hughmark, G.A., Ind. Eng. Chem. Process Des. Develop., 6, 218 (1967).

53. Shulman, H.L., and M.C. Molstad, Ind. Eng. Chem., 42, 1058 (1950).

54. Østergaard, K., "Studies of Gas-Liquid Fluidization," Thesis for Doctor Technices, Technical University of Denmark (1968).

55. Volpicelli, G., and L. Massimilla, Pulp and Paper Mag. Can., 64, T512 (1965).

56. Andersson, K.E.B., Chem. Eng. Sci., 15, 276 (1961).

57. Ergun, S., Chem. Eng. Progr., 48, 89 (1952).

58. Anderson, J.L., and J.A. Quinn, Chem. Eng. Sci., 25, 338 (1970).

59. Towell, G.D., C.P. Strand, and G.H. Ackerman, "Mixing Theory Related to Practice," AIChE-I. Chem. E. Symp. Ser., 10, 97 (1965).

60. Ellis, J.E., and E.L. Jones, Two-Phase Flow Symposium, Exeter, England (June 1965).

61. de Nevers, N., and Jen-Liang Wu, AIChE J., 17, 182 (1971).

62. Yoshitome, H., and T. Shirai, J. Chem. Eng. Japan, 3, 29 (1970).

63. Hinze, J.O., "Turbulence," McGraw-Hill, New York (1959).

64. Calderbank, P.H., Trans. Inst. Chem. Engrs., 36, 443 (1958).

65. Baker, J.L.L., and B.T. Chao, AIChE J., 11, 268 (1965).

66. Efremov, G.I., and I.A. Vakhrushev, Int. Chem. Eng., 9, 614 (1969).

67. Lapidus, L., and J.C. Elgin, AIChE J., 3, 63 (1957).

68. Reith, T., S. Renken, and B.A. Israel, Chem. Eng. Sci., 23, 619 (1968).

69. Patrick, M., Argonne Natl. Lab. Report 6581 (1962).

70. Lockhart, R.W., and R.C. Martinelli, Chem. Eng. Progr., 45, 39 (1949).

71. Powley, M.W., "Two-Phase Flow," DuPont of Canada Ltd., Maitland (1965).

72. Dukler, A.E., Moyce Wicks, III, and R.G. Cleveland, AIChE J., 10, 38 (1964).

73. Hughmark, G.A., Chem. Eng. Progr., 58, 62 (1962).

74. Zuber, N., and J. Hench, General Electric Co. Report No. 62GL100, Schencetady, N.Y. (1962).

75. Marrucci, G., Ind. Eng. Chem. Fundamentals, 4, 224 (1964).

76. Bhatia, V.K., AIChE J., 15, 465 (1969).

77. Rietema, K., and S.P.P. Ottengraf, Trans. Inst. Chem. Engrs., 48, 54 (1970).

78. Crabtree, J.R., and J. Bridgwater,Chem. Eng. Sci., 24, 1755 (1969).

79. Rigby, G.R., G.P. van Blockland, W.H. Park, and C.E. Capes, National Research Council of Canada, Ottawa (Sept. 1969).

80. Rigby, G.R., and C.E. Capes, National Research Council of Canada, NRCC11544, Ottawa (October 1970).

81. Delhaye, J.M., Comp. Rend. Acad. Sc., Paris, 267A, 290 (1968).

82. Masliyah, J.H., and N. Epstein, J. Fluid Mech., 44, 493 (1970).

83. Bhatia, V.K., K. Evans, and N. Epstein, Ind. Eng. Chem. Process Des. Develop., 11, 151 (1972).

84. Yeheskel, J., and E. Kehat, Chem. Eng. Sci., 26, 1223 (1971).

85. Yeheskel, J., and E. Kehat, Chem. Eng. Sci., 27, 2037 (1972).

86. Gal-Or, B., and S. Waslo, Chem. Eng. Sci., 23, 1431 (1968).

87. Trupp, A.C., "Fluidization," Proc. of Symp., Tripartite Chem. Eng. Conf., Montreal, Canada (September 1968).

88. Rowe, P.N., "Fluidization," Chem. Eng. Progr. Symp. Ser., 58, 42 (1962).

89. Smith, T.N., Trans. Inst. Chem. Engrs., 45, 311 (1967).

90. LeClair, B.P., and A.E. Hamielec, Ind. Eng. Chem. Fundamentals, 7, 542 (1968).

91. Smith, T.N., Trans. Inst. Chem. Engrs., 43, 69 (1965).

92. Bird, R.B., W.E. Stewart, and E.N. Lightfoot, "Transport Phenomena," p. 91 ff., John Wiley and Sons Inc., New York (1960).

93. Steinour, H.H., Ind. Eng. Chem., 52, 277 (1949).

94. Clamen, A., and W.H. Gauvin, AIChE J., 15, 184 (1969).

95. Torobin, L.B., and W.H. Gauvin, AIChE J., 7, 615 (1961).

96. McLaren, F.G., A.F.C. Sherath, and A.S. Morton, Nature, 223, 828 (1969).

97. Hanratty, T.J., G. Latinen, and R.H. Wilhelm, ALChE J., 2, 372 (1956).

98. Zenz, F.A., and D.F. Othmer, "Fluidization and Fluid Particle Systems," Reinhold Publishing Corp., New York (1960).

99. Hendrix, C.D., S.B. Dave, and H.F. Johnson, 52nd National AIChE Meeting, Memphis, Tenn. (February 1964).

100. Viswanathan, S., A.S. Kakar, and P.S. Murti, Chem. Eng. Sci., 20, 903 (1964).

101. LeClair, B., M.A. Sc. Thesis, University of British Columbia, Vancouver (1963).

102. Yoshida, F. and K. Akita, 50th AIChE Meeting, Buffalo (May 1963).

103. Neal, L.G., and S.G. Bankoff, AIChE J., 9, 490 (1963).

104. Nassos, G.P., and S.G. Bankoff, Chem. Eng. Sci., 22, 661 (1967).

105. "Applications Manual," Philbrick Researches Inc., Massachusetts (1966).

106. Perry, R.H., C.H. Chilton, and S.D. Kirkpatrick, ed., "Chemical Engineers Handbook," 4th edit., pp. 3-86, McGraw-Hill, New York (1963).

107. Mathur, K.B., Ph.D. Thesis, University of Birmingham, England (1958).

108. Govier, G.W., B.A. Radford, and J.S.C. Dunn, Can. J. Chem. Eng., 38, 62 (1960).

109. Bennett, C.A., and N.L. Franklin, "Statistical Analysis in Chemistry and Chemical Industry," John Wiley & Sons, Inc., New York (1954).

110. Hsu, Y.Y., F.F. Simon, and R.W. Graham, Multi-Phase Flow Symposium, ASME, New York (1963).

111. Delhaye, J.M., Centre d'Etudes Nucléaires de Grenoble, Rapport CEA-R-3465(E) (1968).

112. Mehta, N.C., J.M. Smith, and E.W. Comings, Ind. Eng. Chem., 49, 989 (1957).

113. Smissaert, G.E., Argonne Natl. Lab. Report 6755 (1963).

114. Nicklin, D.J., J.O. Wilkes, and J.F. Davidson, Trans. Inst. Chem. Engrs., 40, 61 (1962).

115. "Two-Phase Flow Instrumentation," 11th National ASME/AIChE Heat Transfer Conf., Minneapolis, Minn. (1969).

APPENDIX 8.1

A CELL MODEL FOR THREE-PHASE FLUIDIZATION

The mechanism for bed contraction in three-phase fluidized beds as postulated by Stewart and Davidson [7] and Østergaard [8] suggests that the solid particles are supported entirely by the liquid phase, whereas the gas phase passes through the bed as discrete bubbles each followed by their liquid wake. Thus it is possible that the characteristic behaviour of a three-phase fluidized bed can be synthesized from the behaviour of two simpler two-phase systems, namely--cocurrent gas-liquid flow and liquid-solid fluidization.

The ability of the cell model technique to describe the motion of a gas bubble in a bubble swarm has been demonstrated recently by Gal-Or and Waslo [86], whereas for sedimentation and fluidization of a single species of solid particles Happel and Brenner [49] have demonstrated the applicability of several different cell models. Smith [89] advanced the Happel [49] cell model to represent the sedimentation of particles of various species by considering that each single species can be represented by an individual spherical cell which, when combined with the spherical cells representing each of the other species in the assemblage by

imposing suitable conditions at the envelope boundaries, is assumed to represent the assemblage. Therefore, in the cell model suggested for three-phase fluidization, it is envisaged that individual spherical cells can be used to represent cocurrent gas-liquid flow and liquid-solid fluidization respectively, along with suitable conditions to match these individual cells such that the combined cells constitute a representative model for the three-phase fluidized bed. The advantage of such a physical model is that it simplifies to its component two-phase systems in limiting cases. A schematic drawing of the cell model for three-phase fluidization is shown in Figure 8.1.1. By analogy to Smith's analysis it can be seen that it is not necessary to impose any restriction on the sizes of solid particles and/or gas bubbles. However, in order to keep the model tractable, it will be assumed that all the particles are of a single species (fixed size and density), and that all the gas bubbles are equi-sized.

The solution of the Navier-Stokes equations, linearized for creeping flow of liquid between a solid sphere and a concentric spherical boundary, has been given by Lamb [42]. Happel and Brenner [49] have shown that the specific solution is dependent on the boundary conditions assumed for the spherical cell. Though the boundary conditions employed for the two spherical cells are formulated here slightly differently than was done by Happel [49] for

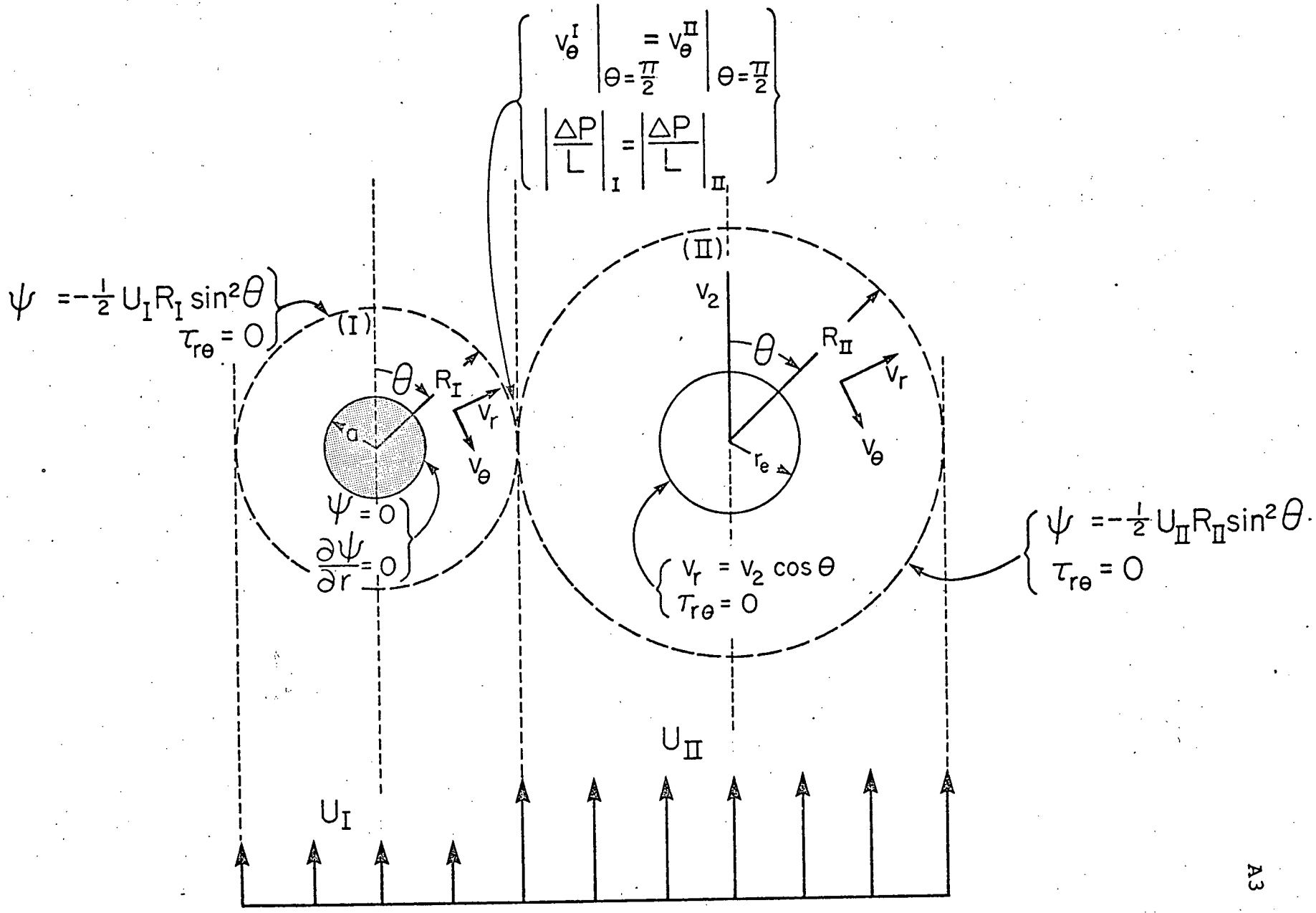

FIGURE 8.1.1 SCHEMATIC OF CELL MODEL FOR THREE-PHASE FLUIDIZATION

solid particles and by Gal-Or and Waslo [86] for gas bubbles, the solution to the present cell model can nevertheless be derived from their solutions. However, for clarity, the solution of the linearized Navier-Stokes equation for each of the two limiting cases will first be considered briefly.

1. The case of a stationary solid particle with vertically upwards liquid flow

The Navier-Stokes equation for viscous, incompressible and axisymmetric creeping flow ($Re_p << 1$) in terms of the stream-function, ψ, is given by Lamb [42] as

$$E^4\psi = 0 \qquad (8.1.1)$$

where

$$E^2 = \left[\frac{\partial^2}{\partial r^2} + \frac{\sin\theta}{r^2} \left\{ \frac{\partial}{\partial\theta} \left(\frac{1}{\sin\theta}\right) \frac{\partial}{\partial\theta} \right\} \right] \qquad (8.1.2)$$

The Stokes solution to equation 8.1.1 is given by Lamb [42]:

$$\psi = \left(\frac{b_1}{r} + b_2 r + b_3 r^2 + b_4 r^4\right)\sin^2\theta \qquad (8.1.3)$$

The velocity components are now related to the stream function, ψ, as follows:

$$v_r = - \frac{1}{r^2 \sin \theta} \frac{\partial \psi}{\partial \theta} \qquad (8.1.4)$$

and

$$v_\theta = \frac{1}{r \sin \theta} \frac{\partial \psi}{\partial r} \qquad (8.1.5)$$

while the tangential shear stress is given by

$$\tau_{r\theta} = \mu \left[\frac{1}{r} \frac{\partial v_\theta}{\partial \theta} + \frac{\partial v_\theta}{\partial r} - \frac{v_\theta}{r} \right] \qquad (8.1.6)$$

All vectorial quantities are taken as positive in the vertically upward direction.

In order to evaluate the four constants b_1, b_2, b_3 and b_4 in equation 8.1.3, a physically realistic and consistent set of boundary conditions is needed. One such set of boundary conditions is:

At the surface of the stationary particle ($r = a$),

$$v_r = 0 \qquad (8.1.7)$$

$$v_\theta = 0 \qquad (8.1.8)$$

and at the surface of the spherical envelope, ($r = R_I$),

$$\tau_{r\theta} = 0 \qquad (8.1.9)$$

$$\psi = - \frac{1}{2} U_I R_I^2 \sin^2 \theta \qquad (8.1.10)$$

Substituting the value of ψ from equation 8.1.3 into equations 8.1.4 - 8.1.6 gives

$$v_r = -2\left(\frac{b_1}{r_3} + \frac{b_2}{r} + b_3 + b_4 r^2\right) \cos\theta \qquad (8.1.11)$$

$$v_\theta = \left(-\frac{b_1}{r^3} + \frac{b_2}{r} + 2b_3 + 4b_4 r^2\right) \sin\theta \qquad (8.1.12)$$

and

$$\tau_{r\theta} = 6\mu\left(\frac{b_1}{r^4} + b_4 r\right) \sin\theta \qquad (8.1.13)$$

Now applying the boundary conditions 8.17 and 8.18 at r=a to equations 8.1.11 and 8.1.12, respectively, yields

$$b_1 + b_2 a^2 + b_3 a^3 + b_4 a^5 = 0 \qquad (8.1.14)$$

and

$$-b_1 + b_2 a^2 + 2b3a^3 + 4b4a^5 = 0 \qquad (8.1.15)$$

Similarly applying the boundary conditions 8.1.9 and 8.1.10 at $r = R_I$ to equations 8.1.13 and 8.1.3, respectively, gives

$$\frac{b_1}{R_I^4} + b_4 R_I = 0 \qquad (8.1.16)$$

and

$$\frac{b_1}{R_I} + b_2 R_1 + b_3 R_I^2 + b_4 R_I^4 = -\frac{1}{2} U_I R_I^2 \qquad (8.1.17)$$

The four constants b_1, b_2, b_3 and b_4 can now be evaluated explicitly by solving the four algebraic equations 8.1.14 - 8.1.17 simultaneously. After much manipulation, the values of the four constants are found to be

$$b_1 = -U_I R_I^6 a^3/2\ S(a,R_I) \tag{8.1.18}$$

$$b_2 = +U_I a R_I (2a^5 + 3R_I^5)/2\ S(a,R_I) \tag{8.1.19}$$

$$b_3 = -U_I R_I (3a^5 + 2R_I^5)/2\ S(a,R_I) \tag{8.1.20}$$

$$b_4 = +U_I R_I a^3/2\ S(a,R_I) \tag{8.1.21}$$

where $S(a,R_I) = 2\ R_I^6 + 3a^5 R_I - 3aR_I^5 - 2a^6$ (8.1.22)

The tangential velocity at the surface of the envelope, $v_\theta|_{r=R_I}$, can now be obtained from equation 8.1.12. After substitution and simplification it is given by

$$v_\theta|_{r=R_I} = -\frac{U_I \sin\theta\,(4R_I^6 + 6a^5 R_I - 3aR_I^5 - 5a^3 R_I^3 - 2a^6)}{2\ S(a,\ R_I)} \tag{8.1.23}$$

The total volumetric flow rate of liquid through the envelope, Q_l, is obtained by integrating the tangential velocity at the equator, $v_\theta|_{\theta=\pi/2}$, over the annular area, i.e.

$$Q_1 = \int_0^{2\pi} \int_a^{R_1} v_\theta|_{\theta=\pi/2} \; r dr \, d\theta$$

After substitution and simplification,

$$Q_1 = \pi R_I^2 U_I \tag{8.1.24}$$

The drag force, F_Z, exerted by the fluid on the particle is given by [49]

$$F_Z = \mu\pi \int_0^{\pi} r^3 \sin^3\theta \, \frac{\partial}{\partial r} \left[\frac{E^2 \psi}{r^2 \sin^2\theta}\right] r \, \partial\theta \tag{8.1.25}$$

where the operator E^2 is defined by equation 8.1.2. After carrying out the required operation on ψ, given by equation 8.1.3, the result is

$$E^2\psi = \left[-\frac{2b_2}{r} + 10b_4 r^2\right] \sin^2\theta \tag{8.1.26}$$

Substituting the value of $E^2\psi$ from equation 8.1.26 into equation 8.1.25 and simplifying we get

$$F_Z = 8 \, b_2 \, \mu\pi \tag{8.1.27}$$

Since the spherical particle is held suspended in a fluidized state by the vertically streaming flow of liquid, the drag force experienced by the particle must be balanced exactly

by the gravitational force, corrected for buoyancy, on the particle. Therefore

$$F_Z = 8b_2\mu\pi = + \frac{4}{3}\pi a^3(\rho_3-\rho_1)\ g \qquad (8.1.28)$$

Substituting the value of b_2 from equation 8.1.19 and simplifying we get

$$\frac{R_I U_I (2a^5 + 3R_I^5)}{S(a,R_I)} = \frac{1}{3}\frac{a^2(\rho_3-\rho_1)g}{\mu} = -\frac{3}{2}(V_\infty)_S \qquad (8.1.29)$$

where $-(V_\infty)_S$ is the Stokes free settling velocity of a solid particle in the negative Z-direction, given by

$$(V_\infty)_S = -\frac{2}{9}\frac{a^2(\rho_3-\rho_1)g}{\mu} \qquad (8.1.30)$$

For the model under consideration, Happel and Brenner [49] suggested that the viscous drag force divided by the cell volume will equal $-\Delta p/L$, the frictional pressure drop per unit length of the bed. Thus

$$-\Delta p/L = F_Z/(\tfrac{4}{3}\pi R_1^3) = (\frac{a}{R_1})^3(\rho_3-\rho_1)g \qquad (8.1.31)$$

which is equivalent to

$$-\frac{\Delta p}{L} = (1-\varepsilon)(\rho_3-\rho_1)g \qquad (8.1.32)$$

a well known condition for particulate fluidization.

2. The case of a rising bubble in a cocurrent liquid flow

The cell model for the case of a rising bubble in a cocurrent liquid flow is similar (though not identical) to the case of a stationary solid particle with vertically upward liquid flow if the internal circulation within the gas bubble is neglected. Therefore we need only solve the Navier-Stokes equations for the liquid side (equation 8.1.1, the general solution of which is given by equation 8.1.3) for a physically realistic and consistent set of boundary conditions. One such set of boundary conditions is:
At the surface of the bubble ($r = r_e$),

$$v_r = v_2 \cos\theta \qquad (8.1.33)$$

$$\tau_{r\theta} = 0^{(\dagger)} \qquad (8.1.34)$$

---

†It is important to recall from the discussion by Levich [38] that this is only an approximation. The correct form of this boundary condition would be the continuity of tangential shear stress across the interface. However, if we consider that $\mu_2 << \mu_1$, the solutions obtained by employing the correct and the approximate boundary condition are identical. Nevertheless, for internal circulation within the bubble to exist the tangential shear stress, though small, must be non-zero.

and at the surface of the spherical envelope ($r=R_{II}$),

$$\tau_{r\theta} = 0 \tag{8.1.35}$$

$$\psi = -\frac{1}{2} U_{II} R_{II}^2 \sin^2 \theta \tag{8.1.36}$$

Using equations 8.1.11 and 8.1.13, and applying the boundary conditions at the surface of the bubble, we get

$$b_1 + b_2 r_e^2 + b_3 r_e^3 + b_4 r_e^5 = -\frac{v_2 r_e^3}{2} \tag{8.1.37}$$

$$\frac{b_1}{r_e^4} + b_4 r_e = 0 \tag{8.1.38}$$

Similarly, from the boundary conditions at the surface of the envelope applied to equations 8.1.13 and 8.1.3, we get

$$\frac{b_1}{R_{II}^4} + b_4 R_{II} = 0 \tag{8.1.39}$$

$$b_1 + b_2 R_{II}^2 + b_3 R_{II}^3 + b_4 R_{II}^5 = -\frac{U_{II} R_{II}^3}{2} \tag{8.1.40}$$

The four constants b_1, b_2, b_3 and b_4 can now be evaluated explicitly by solving the four algebraic equations 8.1.37 - 8.1.40 simultaneously. The values of the four constants are found, after many manipulations, to be

$$b_1 = b_4 = 0 \tag{8.1.41}$$

$$b_2 = - \frac{R_{II}\, r_e (v_2 - U_{II})}{2(R_{II} - r_e)} \tag{8.1.42}$$

$$b_3 = - \frac{U_{II} R_{II} - v_2 r_e}{2(R_{II} - r_e)} \tag{8.1.43}$$

The tangential velocity at the surface of the envelope, $v_\theta|_{r=R_{II}}$ can now be obtained from equation 8.1.12. After substituting the values of the constants and simplifying, this velocity is given by

$$v_\theta|_{r=R_{II}} = - \left[\frac{U_{II}(2R_{II} - r_e) - r_e\, v_2}{2(R_{II} - r_e)}\right] \sin\theta \tag{8.1.44}$$

The total volumetric flow of liquid through the envelope Q_1, is then obtained by integrating the tangential velocity at the equator, $v_\theta|_{\theta=\pi/2}$, over the annular area:

$$Q_1 = \int_0^{2\pi} \int_{r_e}^{R_{II}} v_\theta|_{\theta=\pi/2}\, r\, dr\, d\theta = \pi(U_{II} R_{II}^2 - v_2 r_e^2) \tag{8.1.45}$$

The drag force, F_z, exerted by the fluid on the bubble is given by equation 8.1.27, which, after substitution of the value of the constant b_2 from equation 8.1.42, yields

$$F_Z = 8b_2\mu\pi = -\frac{4\mu\pi R_{II} r_e (v_2 - U_{II})}{(R_{II} - r_e)} \qquad (8.1.46)$$

If it is now assumed that a bubble in a swarm of bubbles rises steadily without acceleration, then the drag force experienced by the bubble must be balanced exactly by the buoyant force on the bubble due to gravity. Thus

$$-\frac{4\mu\pi R_{II} r_e (v_2 - U_{II})}{(R_{II} - r_e)} = \frac{4}{3}\pi r_e^3 (\rho_2 - \rho_1) g \qquad (8.1.47)$$

Since $\rho_2 << \rho_1$, equation 8.1.47 after simplification can be written as

$$(v_2 - U_{II}) = \frac{1}{3}\frac{\rho_1 r_e^2 g}{\mu}(1 - r_e/R_{II}) = (V_\infty)_B (1 - r_e/R_{II}) \qquad (8.1.48)$$

where $(V_\infty)_B$ is the rise velocity of a bubble in an infinite medium, given by

$$(V_\infty)_B = \frac{1}{3}\frac{\rho_1 r_e^2 g}{\mu} \qquad (8.1.49)$$

The frictional pressure drop per unit length of the bed, $-\Delta p/L$, as suggested by Happel and Brenner [49], in combination with equation 8.1.47, is then given by

$$-\Delta p/L = F_Z/(\frac{4}{3}\pi R_{II}^3) = -\rho_l(\frac{r_e}{R_{II}})^3 g \qquad (8.1.50)$$

The cell models derived for cases (1) and (2) above represent the two two-phase systems, namely liquid-solid fluidization and cocurrent gas-liquid flow, respectively, from which the behaviour of a three-phase fluidized bed could be synthesized, if these cell models could be coupled both dynamically and statistically. Smith [89, 91], in an attempt to predict the simultaneous sedimentation of two different solid particle species by cell models, postulated that the equality of all tangential velocities at the equator of a spherical cell makes it possible to couple two horizontally contiguous cells by stipulating equality of tangential velocities at their point of contact (see Figure 8.1.1). The other coupling condition used here is the equality of drag forces per unit cell volume (or the pressure drop per unit length of the bed, $-\Delta p/L$), which ensures that at any height within the bed no radial pressure gradients exist. The latter condition is similar to that used by Smith in his earlier work [91]. Therefore, it is postulated here that the necessary and sufficient boundary conditions to dynamically link the two cell models are

$$v_\theta^{(I)}\big|_{r=R_{II}} = v_\theta^{(II)}\big|_{r=R_{II}} \quad \text{at } \theta=\pi/2,\ 3\pi/2 \qquad (8.1.51)$$

and

$$\left|\frac{\Delta p}{L}\right|_I = \left|\frac{\Delta p}{L}\right|_{II} \tag{8.1.52}$$

It should be emphasized that these are a set of physically consistent boundary conditions which may not necessarily be unique.

Substitution from equations 8.1.23 and 8.1.44 into equation 8.1.5. yields

$$\frac{U_I[4+6(a/R_I)^5-3(a/R_I)-5(a/R_I)^3-2(a/R_I)^6]}{[2+3(a/R_I)^5-3(a/R_1)-2(a/R_I)^6]}$$

$$= \frac{U_{II}(2-r_e/R_{II})-(r_e/R_{II})v_2}{(1-r_e/R_{II})} \tag{8.1.53}$$

where U_I is obtained from the solution for the liquid-solid cell (equation 8.1.29) and is given by

$$U_I/(V_\infty)_S = -\frac{3+4.5(a/R_I)^5-4.5(a/R_I)-3(a/R_I)^6}{3+2(a/R_I)^5} \tag{8.1.54}$$

while (v_2-U_{II}) is similarly obtained from equation 8.1.48:

$$\frac{(v_2-U_{II})}{(V_\infty)_B} = (1-r_e/R_{II}) \tag{8.1.55}$$

Substitution from equations 8.1.31 and 8.1.50 into equation 8.1.52 yields

$$\left(\frac{a}{R_I}\right)^3 \left(\frac{\rho_3-\rho_1}{\rho_1}\right) = \left(r_e/R_{II}\right)^3 \qquad (8.1.56)$$

If these cells thus coupled together are a true statistical representation of a three-phase fluidized bed, the total volumetric flux of gas and liquid through the cells should be equal to the overall volumetric flux of gas and liquid through the three-phase bed. Thus from equations 8.1.24 and 8.1.45, the total volumetric flow of liquid through the two cells is

$$Q_1 = Q_1^{(I)} + Q_1^{(II)} = \pi(U_I R_I^2 + U_{II} R_{II}^2 - v_2 r_e^2) \qquad (8.1.57)$$

Then the volumetric flux of liquid through the two cells will be

$$\frac{Q_1}{\pi(R_I^2 + R_{II}^2)} = \frac{U_I R_I^2 + U_{II} R_{II}^2 - v_2 r_e^2}{R_I^2 + R_{II}^2} = \langle j_1 \rangle \qquad (8.1.58)$$

Similarly, for the volumetric flux of gas through the two cells, we obtain

$$\frac{v_2 r_e^2}{R_I^2 + R_{II}^2} = \langle j_2 \rangle \qquad (8.1.59)$$

Simple geometric considerations provide the volumetric fraction of gas and solid in the combined cells. These are given by

$$\varepsilon_2 = \frac{r_e^3}{R_I^3 + R_{II}^3} \qquad (8.1.60)$$

and

$$\varepsilon_3 = \frac{a^3}{R_I^3 + R_{II}^3} \qquad (8.1.61)$$

respectively.

The eight equations (8.1.53 - 8.1.56 and 8.1.58 - 8.1.61) derived here provide a self-consistent set of equations to predict the volumetric fractions of gas and solid in the three-phase fluidized bed along with r_e and v_2, if the solid particle size and the volumetric flux of gas and liquid through the bed are known.

Results

It can be easily observed that an analytical solution to the above set of non-linear equations can not be obtained so readily. Therefore a numerical method was used to solve these equations based on the simple algorithm outlined below:

Step 1 - for assumed values of ε_2, ε_3 and a, equations 8.1.56, 8.1.60 and 8.1.61 are solved simultaneously for r_e, R_I and R_{II} by a scheme involving successive iterations with rapid convergence (about three iterations required).

Step 2 - having obtained the values of r_e, R_I and R_{II}, the remaining equations are solved in a straightforward manner to obtain U_I, U_{II}, v_2, $\langle j_1 \rangle$ and $\langle j_2 \rangle$.

By keeping the particle radius, a, and ε_3 constant, the values of $\langle j_1 \rangle$ and $\langle j_2 \rangle$ were obtained for various values of ε_2, by following the two steps outlined above. Figure 8.1.2 shows the results obtained by solving the above set of equations for arbitrarily chosen physical properties of the liquid and the solid particles (ρ_1=1.0 gm/cc, ρ_3=2.5 gm/cc and μ=1.0 poise). Then for a constant volumetric liquid flux, $\langle j_1 \rangle$, values of ε_3 can be obtained as a function of volumetric gas flux, $\langle j_2 \rangle$, from Figure 8.1.2. The total bed voidage, ε, is determined from

$$\varepsilon = \varepsilon_1 + \varepsilon_2 = 1 - \varepsilon_3 \qquad (8.1.62)$$

and is shown plotted in Figure 8.1.3 as a function of $\langle j_2 \rangle$ for fixed values of $\langle j_1 \rangle$. It can be seen from Figure 8.1.3

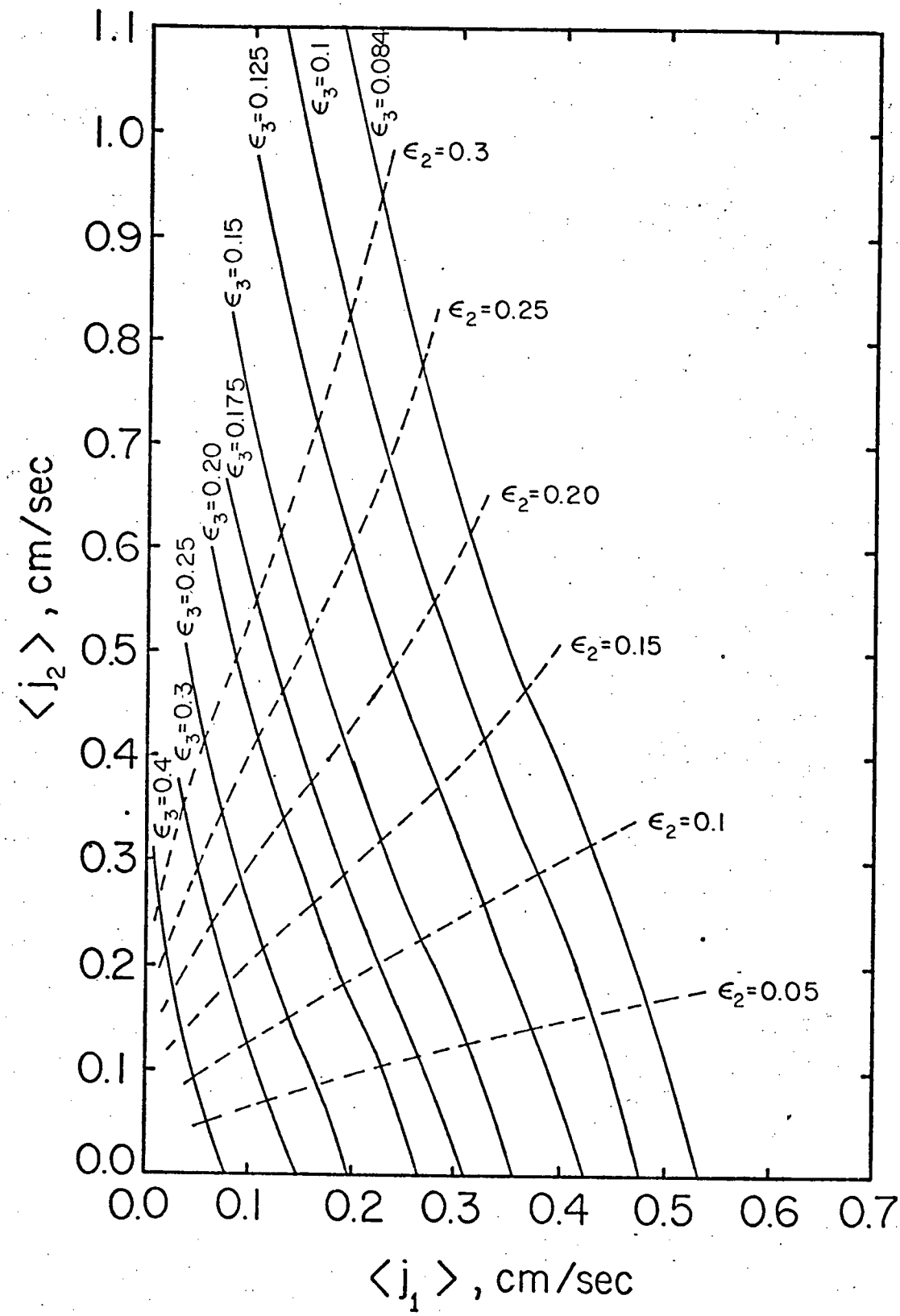

FIGURE 8.1.2 SOLUTION OF CELL MODEL FOR THREE-PHASE FLUIDIZATION UNDER ARBITRARILY CHOSEN CONDITIONS (d_p=1.35 mm, ρ_3=2.5 gm/cm^3; ρ_1=1.0 gm/cm^3, μ_1=1.0 poise)

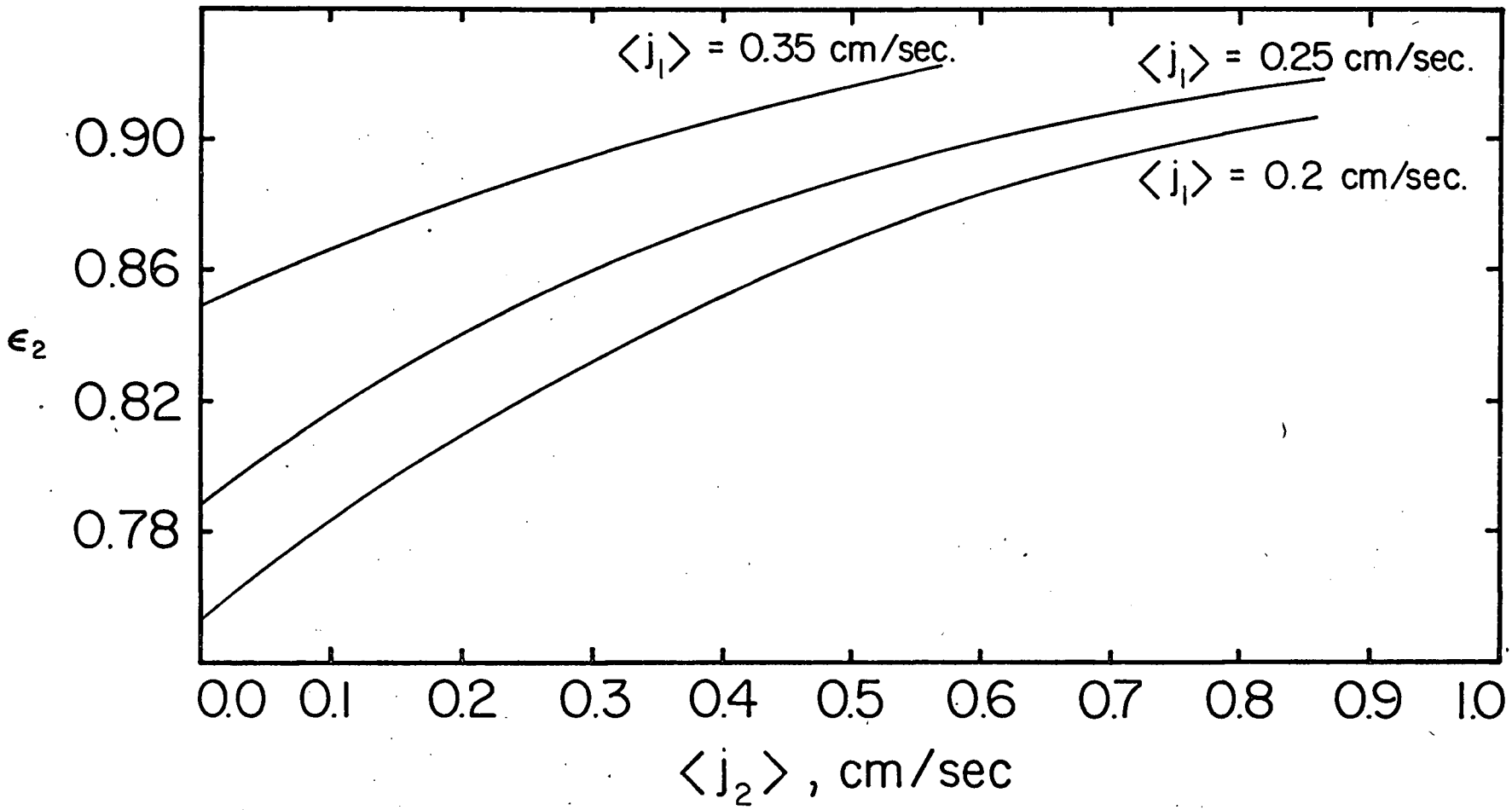

FIGURE 8.1.3 EXPANSION BEHAVIOUR OF A THREE-PHASE FLUIDIZED BED AS PREDICTED BY THE CELL MODEL (d_p=1.35 mm, ρ_3=2.5 gm/cm^3; ρ_1=1.0 gm/cm^3, μ_1=1.0 poise)

that, at a fixed volumetric flux of liquid, the fluidized bed expands further on introduction of the gas stream, which is contrary to the observed bed contraction phenomenon in many three-phase fluidized beds. However, it is interesting to note that the cell model presented here describes the distribution between the liquid-gas bubble cell in a manner whereby the average volumetric flux of liquid through the liquid-solid cell, U_I, is found to be smaller than the overall volumetric liquid flux, $\langle j_1 \rangle$, indicating that the rest of the liquid is associated with the rising gas bubbles.

Another interesting aspect of a three-phase fluidized bed is the rise velocity of a bubble through the bed, which can be obtained from equations 8.1.55 to 8.1.57 and is given by

$$v_2''' = \langle j_1 \rangle + \langle j_2 \rangle + (V_\infty)_B \left[1-(r_e/R_{II})\right] + \left[\langle j_1 \rangle + \langle j_2 \rangle - U_I\right] \left[\frac{(\rho_3-\rho_1)}{\rho_1} \frac{\varepsilon_3}{\varepsilon_2}\right]^{2/3} \qquad (8.1.63)$$

The rise velocity of a bubble swarm in cocurrent gas-liquid flow was obtained by Gal-Or and Waslo [86] using the cell model technique, and their result can also be obtained by substituting $\varepsilon_3=0$ into equation 8.1.63:

$$v_2'' = \langle j_1 \rangle + \langle j_2 \rangle + (V_\infty)_B \left[1-(r_e/R_{II})\right] \qquad (8.1.64)$$

A comparison of equations 8.1.63 and 8.1.64 shows that for the same volumetric liquid flux, volumetric gas flux and bubble size, the rise velocity of a bubble swarm in a three-phase fluidized bed is higher than in cocurrent gas-liquid flow, and that the difference between the rise velocities is a function of the overall bed voidage. Experimental results in conformity with this trend were found by Vail et al. [17].

Since most of the bed expansion data obtained for three-phase fluidized beds are for large Reynolds numbers where the omission of the inertial terms from the Navier-Stokes equations cannot be justified, no comparison of experimental data with the predictions from this cell model is attempted. However, it has been demonstrated here that a cell model representation of a three-phase fluidized bed is mathematically feasible and physically credible. In order to be able to compare the predictions of this model with the existing experimental data, the full Navier-Stokes equations should be solved for the coupled cell model by already existing numerical techniques [82, 90] and is recommended for later investigations. Attempts by the present author to obtain bed expansion data for very small glass beads (0.5 mm diam.) in a highly viscous liquid ($\mu \simeq 0.65$ poise) were unsuccessful, as no stable bed could be obtained at such low gas flow rates as $j_2 \leq 2.0$ cm/sec. However, limited data on three-phase fluidization of 1 mm glass beads by air and the same viscous liquid showed no bed contraction, in keeping with the predictions of the cell model.

APPENDIX 8.2

MEASUREMENT TECHNIQUES FOR GAS HOLDUP (AND BED HEIGHT) IN THREE-PHASE FLUIDIZED BEDS AND RELATED SYSTEMS

The measurement of gas holdup in two-phase gas-liquid flow has been the subject of considerable attention over the years, and numerous sophisticated methods have been proposed, developed and used [109]. All these methods can be classified into two broad groups:

(i) methods to measure the overall average gas fraction, and

(ii) methods to measure the point or local gas fraction.

The latter group uses various electrical, isokinetic sampling, hot film and other probes for studying the local structure of two-phase flow. A considerable amount of work has been done by Bankoff [103, 104], Hsu [110] and Delhaye [111] for the advancement of these probes and for a better understanding of the measurement techniques themselves.

In the former group fall the two most common methods for measurement of gas holdup. They are

1. Modified pressure drop gradient method.
2. Direct volumetric measurements using quick closing valves.

Undoubtedly any local information is lost by using these techniques because of the averaging process involved in the techniques themselves. Nevertheless they are most commonly employed for their simplicity and ease of measurements. Although the pressure drop method has received some attention [103], the details of these techniques are seldom discussed. An attempt is therefore made here to provide some background of these techniques so as to identify the shortcomings and precautions to be exercised in using them.

1. Modified pressure drop gradient method

The pressure drop in two-phase gas-liquid flow in a vertical pipe has been considered by Nicklin [19] and can basically be expressed as

$$-\Delta p = (-\Delta p)_f + (-\Delta p)_a + (-\Delta p)_Z \qquad (8.2.1)$$

where $(-\Delta p)_f$ = pressure drop due to friction between the liquid and the column wall

$(-\Delta p)_a$ = pressure drop due to acceleration of bubble swarm

$(-\Delta p)_Z$ = pressure drop due to hydrostatic head of liquid.

Now if we consider that the velocities of the phases employed are small, then the frictional component may be negligibly small. However, if the velocities of phases

employed are not small, Nassos and Bankoff [104] recommend that an approximate correction for the frictional pressure drop can be made by noting the pressure drop when the liquid phase is flowing alone; alternatively it can be estimated from the well established relation for single phase flow:

$$(-\Delta p)_f = 4fLv_l^2\rho_l/2D \qquad (8.2.2)$$

In practice, the frictional pressure drop is usually small and can be neglected. Furthermore, if the gas volume fraction does not change appreciably between the two measuring stations, the pressure drop component due to acceleration, $(-\Delta p)_a$, is zero. Under these circumstances equation 8.2.1 simplifies to

$$(-\Delta p) = (-\Delta p)_z \qquad (8.2.3)$$

which simply states that the pressure drop between two measuring points is due only to the hydrostatic head of liquid. Therefore the use of this method to measure gas holdup in two-phase gas-liquid flow simply amounts to the measurement of static pressure drop gradients along the column wall.

The following precautions for measurement of static pressure drop must be carefully observed in the design and location of pressure taps:

1. Static pressure taps mounted flush to the inside of the column wall provide the most reliable results [106], whereas pressure taps protruding into the column perpendicular to the flow axis (such pressure probes were used by Efremov and Vakhrushev [16]) give pressure drop readings which are normally too low.

2. In deciding on the distance between the pressure taps, it must be remembered that for measurements over very short lengths, a small absolute error in reading the manometer level could introduce a large percentage error, whereas for measurements over very long lengths, equation 8.2.3 may not hold, since the pressure drop due to acceleration is then less likely to be negligible.

3. Usual care must be taken to ensure that no air bubbles are trapped inside the manometer lines.

This method could be easily modified to obtain also the gas holdup in a three-phase fluidized bed. The pressure drop in a two-phase fluidized bed was considered by Mehta et al. [112]. Combining their approach with that of Nicklin [19] for gas-liquid flow, the total pressure drop in a three-phase fluidized bed may be considered as the sum of several contributions:

$$(-\Delta p) = (-\Delta p)_{fl} + (-\Delta p)_{fs} + (-\Delta p)_{ag} + (-\Delta p)_{al} + (-\Delta p)_{Zl} + (-\Delta p)_{Zs} \qquad (8.2.4)$$

where

$(-\Delta p)_{fl}$ = frictional pressure drop between the liquid and the column wall

$(-\Delta p)_{fs}$ = frictional pressure loss due to particle-particle and particle-wall collisions

$(-\Delta p)_{ag}$ = pressure loss due to acceleration of gas bubble swarm

$(-\Delta p)_{al}$ = pressure loss due to acceleration of liquid

$(-\Delta p)_{Zl}$ = pressure drop due to hydrostatic head of liquid

$(-\Delta p)_{Zs}$ = pressure drop due to hydrostatic head of solids

By arguments similar to those presented above it can be assumed that all the frictional and accelerational components of pressure drop are either negligible or zero. Then equation 8.2.4 simplifies to

$$-\Delta p = (-\Delta p)_{Zl} + (-\Delta p)_{Zs} \qquad (8.2.5)$$

which simply states that the pressure drop between two measuring points is due only to the hydrostatic head of liquid and solid particles. Therefore, to measure the gas holdup by this method, static pressure drop gradient along the column wall must be measured. In addition to the precautions listed above, care has to be taken to ensure that

no solid particles are trapped inside the manometer lines.

Next we consider the manometric equations required to obtain the gas volume fraction from the observed manometer readings in the three-phase region. The corresponding relations for the two-phase region can be obtained from these by suitable manipulations. Let us consider the test section of the experimental column as shown in Figure 8.2.1, where Section I represents the three-phase fluidized region and Section II the two-phase gas-liquid regions above and below the bed. Considering the manometer reading between the points (i) and (ii), it can be shown by a static pressure balance that

$$(-\Delta p) = (P_i - P_{ii}) = Z\rho_l + H(\rho_M - \rho_l) \qquad (8.2.6)$$

If it is assumed that both the gas and the solid particles are uniformly distributed in Section I, then the average density in Section I is given by

$$\begin{aligned}(\rho_{av})_I &= \rho_1\varepsilon_1''' + \rho_2\varepsilon_2''' + \rho_3\varepsilon_3 \\ &= \rho_1(1-\varepsilon_2'''-\varepsilon_3) + \rho_2\varepsilon_2''' + \rho_3\varepsilon_3 \\ &= \rho_1 + \varepsilon_3(\rho_3-\rho_1) - \varepsilon_2'''(\rho_1-\rho_2) \qquad (8.2.7)\end{aligned}$$

Similarly, if it is assumed that the gas distribution in Section II is uniform, the average density in Section II is then given by

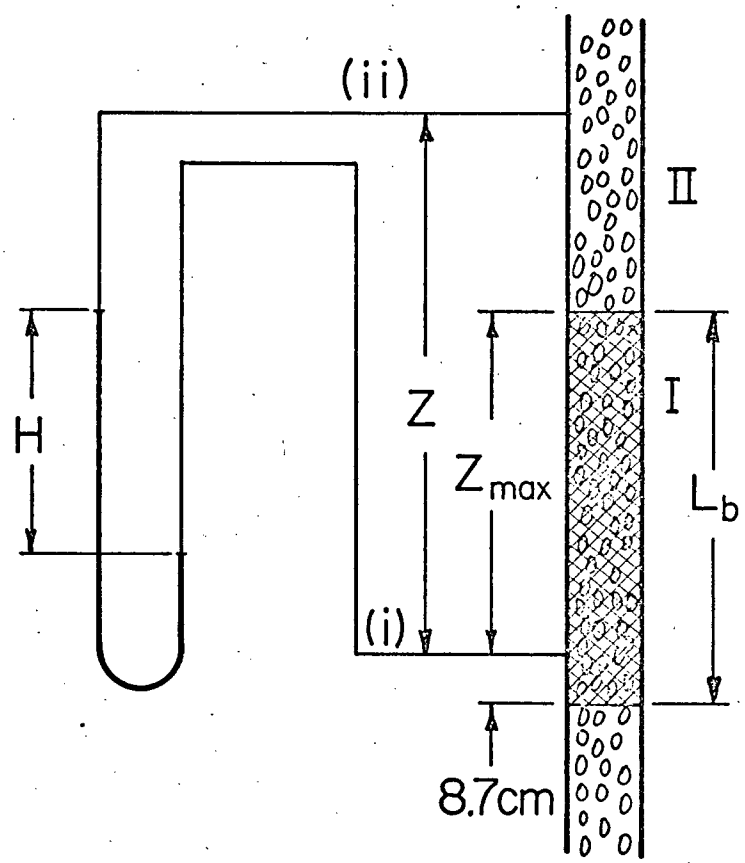

FIGURE 8.2.1 SCHEMATIC OF STATIC PRESSURE DROP GRADIENT ALONG THE TEST SECTION

$$(\rho_{av})_{II} = \rho_1 - \varepsilon_2''(\rho_1 - \rho_2) \qquad (8.2.8)$$

As stated above, the pressure drop in the absence of any significant dynamic pressure losses is equal to the hydrostatic head of liquid and solid. Then

$$-\Delta p = Z_{max}\,(\rho_{av})_I + (Z - Z_{max})(\rho_{av})_{II} \qquad (8.2.9)$$

Substituting equations 8.2.6, 8.2.7 and 8.2.8 into equation 8.2.9 and rearranging we get

$$H(\rho_M - \rho_1) = Z_{max}\{\varepsilon_3(\rho_3 - \rho_1) + (\varepsilon_2'' - \varepsilon_2''')(\rho_1 - \rho_2)\} - Z\,\varepsilon_2''(\rho_1 - \rho_2) \qquad (8.2.10)$$

which for $Z = Z_{max}$ simplifies to

$$H_{max}\,(\rho_M - \rho_1) = Z_{max}\{\varepsilon_3(\rho_3 - \rho_1) - \varepsilon_2'''(\rho_1 - \rho_2)\} \qquad (8.2.11)$$

For $Z < Z_{max}$ it can be shown similarly that

$$H(\rho_M - \rho_1) = Z\{\varepsilon_3(\rho_3 - \rho_1) - \varepsilon_2'''(\rho_1 - \rho_2)\} \qquad (8.2.12)$$

Both equations 8.2.10 and 8.2.12 are linear relationships between H and Z, as shown in Figure 8.2.2, and their point of intersection is given by equation 8.2.11. Therefore, following equation 8.2.12, a plot of H versus Z for $Z < Z_{max}$ will be a straight line whose slope is given by

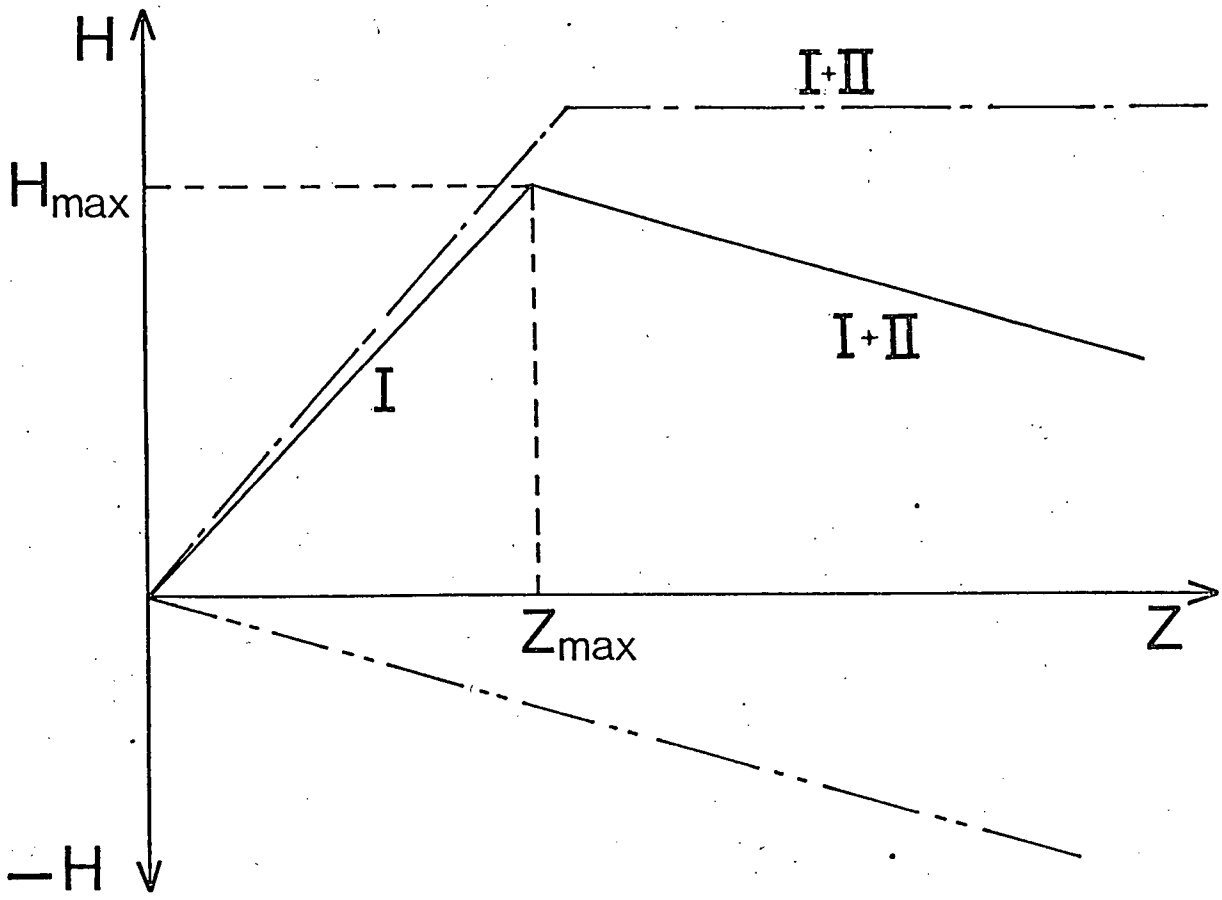

FIGURE 8.2.2 PLOT OF MANOMETRIC EQUATIONS: ——— THREE-PHASE FLUIDIZED BED; —·—·— LIQUID-SOLID FLUIDIZED BED; —··—··— TWO-PHASE GAS-LIQUID FLOW

$$S_I = \frac{\varepsilon_3(\rho_3-\rho_1)-\varepsilon_2'''(\rho_1-\rho_2)}{\rho_M - \rho_1} \qquad (8.2.13)$$

Similarly a plot of H versus Z for $Z > Z_{max}$ following equation 8.2.10 will be another straight line whose slope is given by

$$S_{II} = -\varepsilon_2'' (\rho_1-\rho_2)/(\rho_M-\rho_1) \qquad (8.2.14)$$

As is evident from equation 8.2.13, the slope of the straight line in Section I is a positive quantity as long as the following inequality is satisfied:

$$\varepsilon_3(\rho_3-\rho_1) > \varepsilon_2''' (\rho_1-\rho_2) \qquad (8.2.15)$$

whereas the slope of the straight line in Section II is always a negative quantity. This abrupt change of slope from Section I to Section II at $Z = Z_{max}$ provides a reliable and consistent definition for the expanded bed height, L_b, which for the present setup is given by

$$L_b = Z_{max} + 8.7 \qquad (8.2.16)$$

The manometric equation for two-phase gas-liquid flow can be obtained by substituting $\varepsilon_3=0$ into equation 8.2.10 and noting that the gas holdup is ε_2'' throughout the entire section. Then

$$H\ (\rho_M-\rho_1) \quad = \quad -Z\ \varepsilon_2''\ (\rho_1-\rho_2) \tag{8.2.17}$$

Similarly, the manometric equation for a liquid-solid fluidized bed can be obtained by substituting $\varepsilon_2'' = \varepsilon_2''' = 0$ into equation 8.2.10 and equation 8.2.12. Then

$$H(\rho_M-\rho_1) = Z\ \varepsilon_3\ (\rho_3-\rho_1) \text{ for } Z < Z_{max} \tag{8.2.18}$$

and

$$H(\rho_M-\rho_1) = Z_{max}\ \varepsilon_3\ (\rho_3-\rho_1) \text{ for } Z \geq Z_{max} \tag{8.2.19}$$

Equations 8.2.17 - 8.2.19 are shown graphically in Figure 8.2.2.

2. Direct volumetric measurements using quick closing valves

This method of measuring the gas holdup has been used most frequently, yet the details for applying this technique have been least discussed. The method by itself is quite simple, but the interpretation of data, due to compressibility of the gas phase, becomes complicated. The method consists of isolating a large volume of the flow channel by two valves that can be shut instantaneously. The distance between the valves should be large so that all longitudinal variations in the section are properly averaged. When the valves are shut, the volume of either the liquid

or the gas collected is measured, and knowing the volume of the system, the volume fraction of either fluid phase can be determined.

Since the success of this method requires that the distance between the valves be large, in vertical pipe flow there would be a considerable variation in static pressure from the bottom to the top of the isolated section. Due to this variation, the pressure at which the gas is collected below the top valve is some average of the static pressures existing between the two valves during flow. Since the volumetric gas flow rate also varies with pressure, for consistency it should be corrected to the same pressure at which the gas holdup is measured. Thus, Govier et al. [108], who used this technique in their entire study of two-phase gas-liquid flow, corrected the gas flow rate to the pressure at the midpoint of the test section under running conditions. This correction is sufficient to make the results consistent. Most other investigators do not specifically mention if any such correction factor was employed by them [17, 100]. It is therefore shown below how this correction factor was arrived at for the present study. The correction is derived for a three-phase system, from which the corresponding simpler case of a two-phase gas-liquid system can be easily obtained.

Figure 8.2.3(a) shows the experimental column, which is open to atmosphere at the top, running under steady state

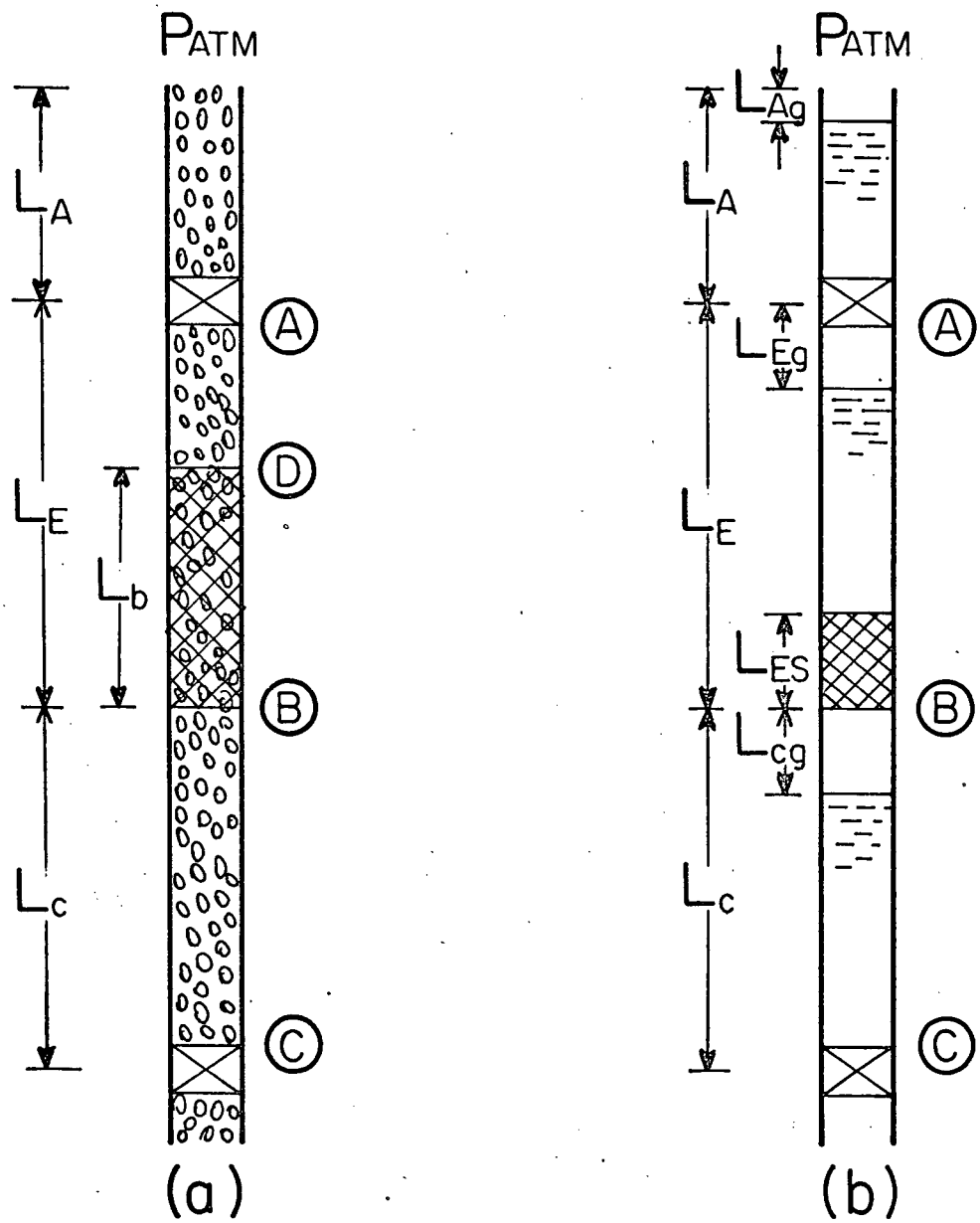

FIGURE 8.2.3 DIAGRAMATIC REPRESENTATION OF THE EXPERIMENTAL COLUMN (a) UNDER RUNNING CONDITION, AND (b) WITH VALVES CLOSED

conditions just before the valves are shut off. Under these conditions, the bubbles are present in the column under a varying pressure head from C, where the hydrostatic head is quite large, to almost atmospheric pressure near the top. The pressure inside a bubble is slightly higher than the pressure around it, the excess pressure being due to surface tension of the liquid. However, for bubbles larger than 1 mm diameter, the excess pressure is insignificant [38]. Then from equation 8.2.3 it follows that the pressure at point A is given by

$$(P)_A = (L_A - L_{Ag})\ \rho_l g + P_{ATM} \tag{8.2.20}$$

and the pressure at point C is given by

$$(P)_C = (L_C - L_{Cg})\ \rho_l g + (P)_B \tag{8.2.21}$$

Similarly, from equation 8.2.5 the pressure at point B is given by

$$(P)_B = [L_E - L_{Eg} - (W/\rho_3 A)]\ \rho_l g + \frac{Wg}{A} + (P)_A \tag{8.2.22}$$

If it is assumed that the longitudinal gas distribution throughout the experimental column, as well as the longitudinal distribution in the fluidized bed region, are uniform, than the longitudinal pressure distribution existing in the

column during steady-state operation can be graphically illustrated as shown in Figure 8.2.4.

When the two valves are shut simultaneously, then just at that instant there are bubbles present between them whose inside pressures vary from $(P)_C$ to $(P)_A$. Now the bubbles below the test section rise and collect below the bed support screen. Since the volume of this section is fixed, the volume of gas collected below point B is the sum of the volumes of all the individual bubbles formerly present between B and C, whereas the pressure at which the gas is collected is a weighted mean of the contributions from each individual bubble. Since it has been assumed that the gas distribution in this section is uniform, the longitudinal pressure distribution between C and B is linear and the average pressure at which the gas is collected below point B can be simply given by

$$(\bar{P})_B = [(P)_B + (P)_C] / 2 \qquad (8.2.23)$$

which is the pressure at the midpoint of this section when the column is running at steady state.

Similarly with the assumption of uniform gas and solid distribution in the test section, it can easily be shown by averaging the area under BDA in Figure 8.2.4 that the pressure at which the gas is collected below point A is given by

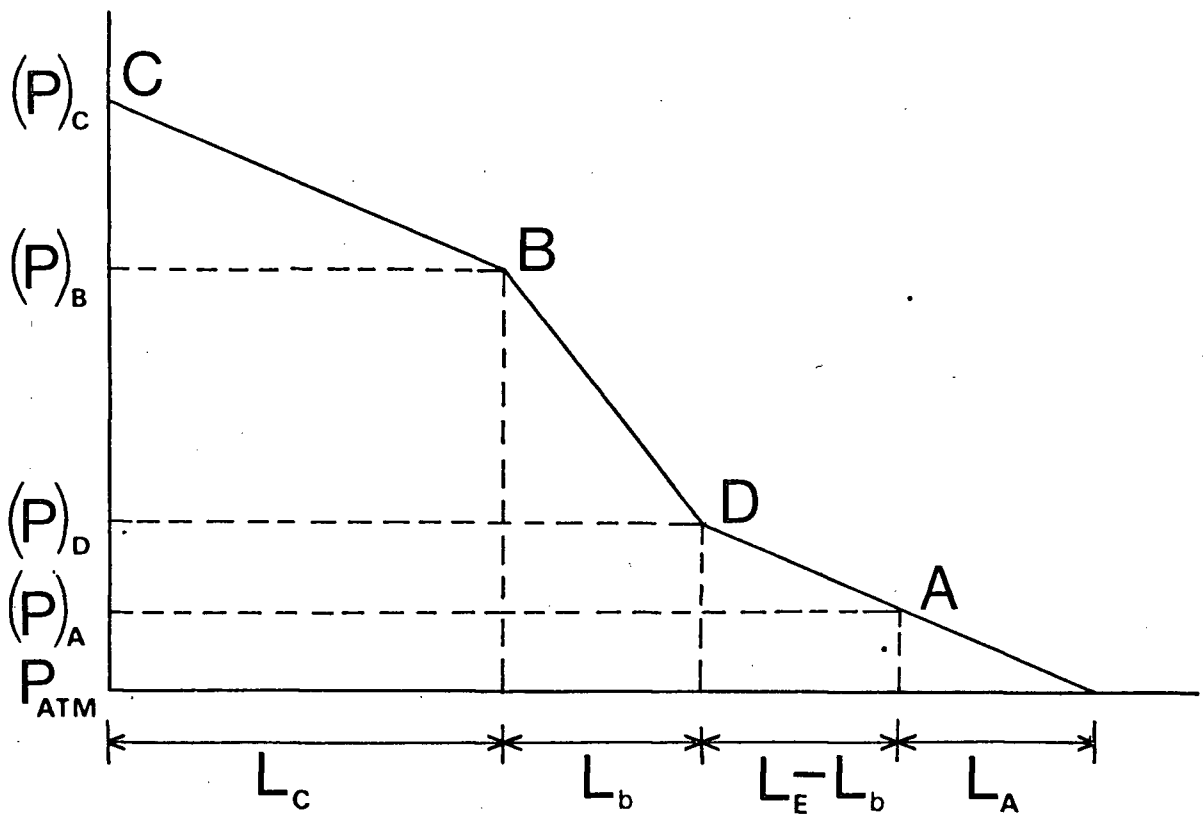

FIGURE 8.2.4 LONGITUDINAL DISTRIBUTION OF ABSOLUTE PRESSURE IN THE EXPERIMENTAL COLUMN WITH VALVES OPEN

$$(\bar{P})_A''' = [(P)_B - (P)_A]\frac{L_b}{2L_E} + [(P)_A + (P)_D] / 2 \qquad (8.2.24)$$

When no solid particles are present in the test section, $L_b = 0$ and the pressure at which the gas is collected at point A is simply given by

$$(\bar{P})_A'' = [(P)_A + (P)_B] / 2 \qquad (8.2.25)$$

which is then the midpoint pressure in the test section when the column is running at steady state.

Since the gas flow rate should be corrected to the pressure at which the gas is collected, the procedure adopted by Govier et al. [108] is shown by this simple analysis to be consistent for a uniform gas distribution in the test section.

It has been shown above that gas is collected in different sections of the experimental column at different pressures, viz. gas above the test section is collected at atmospheric pressure, gas in the test section is collected at pressure $(\bar{P})_A$, and gas below the test section is collected at pressure $(\bar{P})_B$. Since one of the aims of this study was to compare the measured gas holdups in different sections of the experimental column, it was necessary that all the gas holdups as well as the gas flow rates be referred to the same pressure. Also, since the above analysis is

approximate at best, the actual pressure at which the gas was collected in the test section was measured by an open mercury manometer located 40.9 cm below valve A. The pressure at which the gas was collected below the test section could then be easily obtained by adding the observed additional hydrostatic head to the test section pressure. All the measured gas holdups were then corrected from the pressure at which they were measured to a standard atmospheric pressure of 760 mm Hg. No correction was deemed necessary for the gas holdup measured above the test section. The actual numerical procedure adopted for applying these corrections is now outlined.

Let

h_1 = reading of the open mercury manometer when only liquid is flowing

h_2 = reading of the open mercury manometer when gas and liquid are flowing

h_3''' = reading of the open mercury manometer when the valves are shut after a three-phase fluidization run.

Then from direct measurements as shown in Figure 8.2.3(b)

Gas holdup above the test section, $\varepsilon_{2A} = L_{Ag}/L_A$ (8.2.26)

Gas holdup in the test section, $\varepsilon_{2E} = L_{Eg}/L_E$ (8.2.27)

Gas holdup below the test section, $\varepsilon_{2C} = L_{Cg}/L_C$ (8.2.28)

The following routine was used to obtain the necessary correction factors:

$$DE = h_1 - (98.5\ \rho_1)/(\rho_M - \rho_1)$$

$$PR = (h_2 - DE)(\rho_M - \rho_1)/13.6$$

$$PS = (h_3'' - DE)(\rho_M - \rho_1)/13.6$$

$$PSC = PS - [(40.9 - L_{Eg})\ \rho_1/13.6]$$

$$HE = [L_E - L_{Eg} - (W/\rho_3 A)]\ \rho_1/13.6$$

$$HS = W/(A\ 13.6)$$

$$HC = (L_C - L_{Cg})\ \rho_1/13.6$$

$$PCC = PSC + HE + HS + (HC/2)$$

Then

$$CORR1 = (PSC + 76)/76 \qquad (8.2.29)$$

and

$$CORR2 = (PCC + 76)/76 \qquad (8.2.30)$$

Now the corrected gas holdups are obtained from

$$\varepsilon_{2EC} = \varepsilon_{2E}\ CORR1 \qquad (8.2.31)$$

$$\varepsilon_{2CC} = \varepsilon_{2C}\ CORR2 \qquad (8.2.32)$$

In this case, since the gas collected in the test section is the sum of gas in the three-phase fluidized bed and in the two-phase gas-liquid region above the bed, a simple material balance is used to obtain the gas holdup in the three-phase fluidized bed, the result of which is

$$\varepsilon_2''' = \varepsilon_2'' + [\varepsilon_{2EC} - \varepsilon_2''] \, L_E/L_b \qquad (8.2.33)$$

where ε_2'' is the gas holdup in the two-phase gas-liquid region and is measured independently by a separate U-tube manometer provided near the top of this section.

The procedure adopted for correcting the gas holdup measurements in two-phase gas-liquid flow is principally the same as outlined above. The quantity PSC in the above routine gives the measured value of the pressure at which gas is collected in the test section. This was compared in all runs with the pressure $(\bar{P})_A$ given by equation 8.2.24 from the above analysis. It was found that the measured pressure PSC was usually slightly greater than the pressure $(\bar{P})_A$, the difference,however, always being very small.

Thus the simple analysis given above provides some insight into this technique and a method for estimating the pressure under which gas is collected in different sections of the column. In order to obtain results that can be compared, it is necessary that all the measured gas holdups be corrected to the same pressure consistently. Failure to take these correction factors into account would provide erroneous results [17], which may also lead to wrong conclusions, as for example those reported by Volk [10].

APPENDIX 8.3

ESTIMATION OF BUBBLE SIZE FROM LOCAL BUBBLE FREQUENCY MEASUREMENTS

Let n_r' be the frequency at any particular radial position in the column and let Ω_B be the volume of each individual bubble in the bubble swarm. If it is further assumed that all bubbles in the swarm are equi-sized spheres of radius $\bar{r}_e$, then the volumetric flow rate of gas bubbles whose centers fall within the probe detection area (see Figure 8.3.1) is given by

$$Q_{2r} = n_r' \Omega_B \tag{8.3.1}$$

the probe detection area being

$$A_r = \pi \bar{r}_e^2 \tag{8.3.2}$$

where $\bar{r}_e$ is the maximum distance from the probe tip to the centers of detectable bubbles. This distance is the same as the radius of a bubble due to the assumption of equi-sized spherical bubbles in the swarm.

The overall volumetric gas flow rate can now be obtained by integrating equation 8.3.1 over the cross-section of the column. Thus

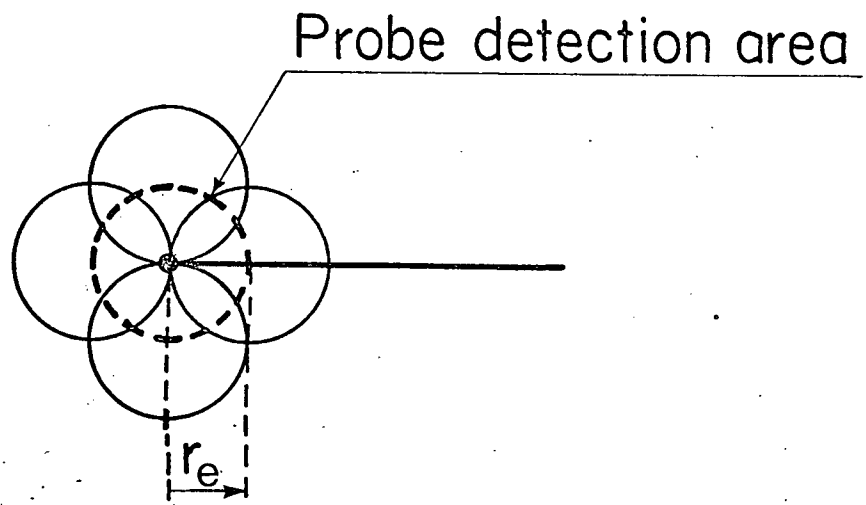

FIGURE 8.3.1 A PLAN VIEW OF BUBBLE TRAVERSE OVER THE PROBE

$$Q_2 = \int\int \frac{Q_{2r}}{A_r}\, dA = \int\int \frac{n_r' \Omega_B}{\pi \bar{r}_e^2}\, dA \qquad (8.3.3)$$

or

$$Q_2 = \frac{4}{3} \bar{r}_e \int_0^R \int_0^{2\pi} n_r' \, r \, dr \, d\theta \qquad (8.3.4)$$

If it is assumed that the radial profile of local bubble frequency is axially symmetric, equation 8.3.4 can be further simplified to

$$Q_2 = \frac{8\pi}{3} \bar{r}_e \int_0^R n_r' \, r \, dr = \frac{8}{3} \bar{r}_e \pi R^2 \int_0^1 n_r' \, R^* dR^* \qquad (8.3.5)$$

where R^* is the dimensionless distance from the center of the pipe.

Now if the radial profile of local bubble frequency can be measured, an estimate for the average bubble size in the swarm can be obtained by rearranging equation 8.3.5:

$$\bar{r}_e = \frac{3 \langle j_2 \rangle}{8 \int_0^1 n_r' \, R^* \, d \, R^*} \qquad (8.3.6)$$

APPENDIX 8.4

CALIBRATION OF LIQUID FLOW METERS

The liquid flow meters in the 2 inch circulation loop were calibrated by recording the time taken to collect 50 - 100 lbs of liquid. Special care was taken to keep the liquid temperature nearly constant when calibrating the flow meters for polyethylene glycol (PEG) solutions. The calibration curves of various flow meters for water and PEG solutions are shown in Figures 8.4.1 and 8.4.2, respectively.

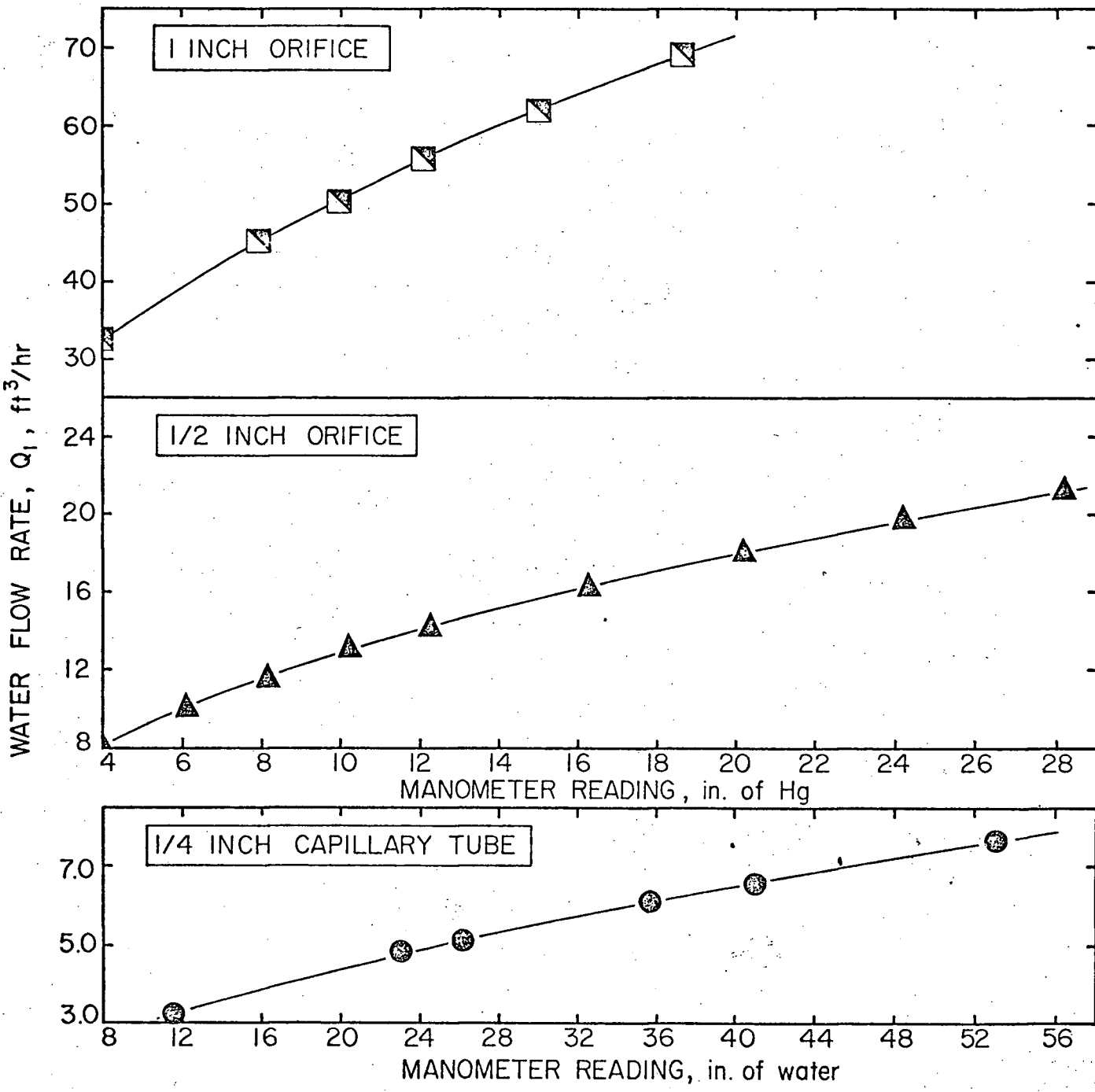

FIGURE 8.4.1 CALIBRATION CURVES FOR WATER FLOW METERS IN 2 INCH CIRCULATION LOOP

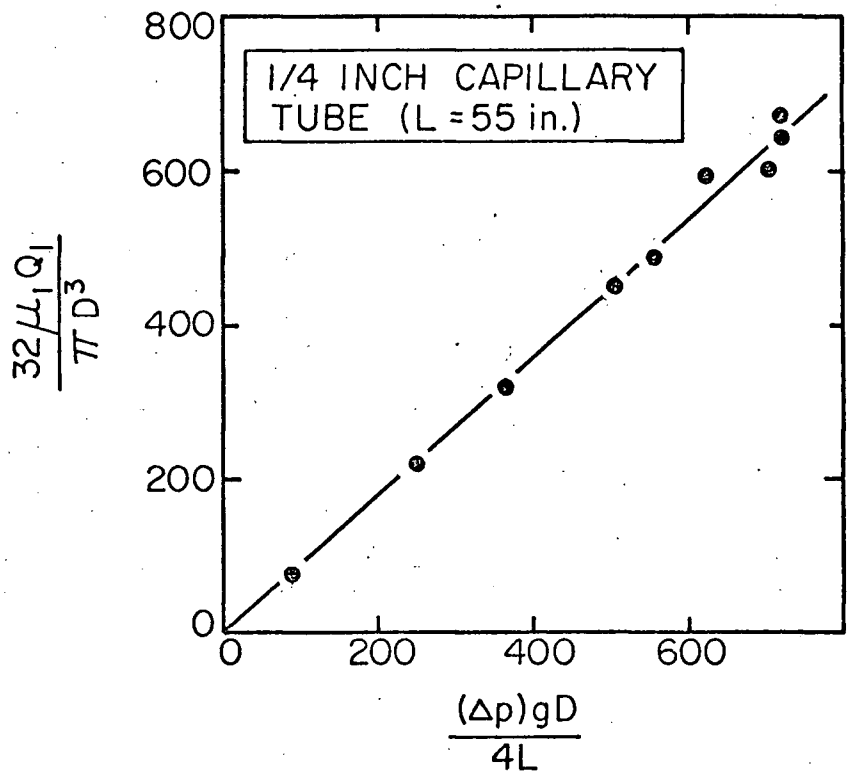

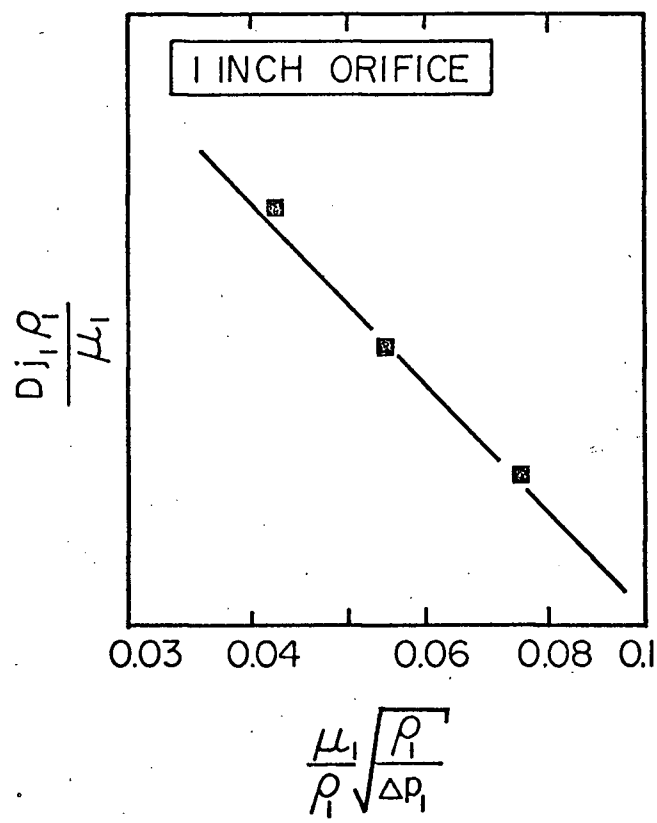

FIGURE 8.4.2 CALIBRATION CURVES FOR PEG SOLUTION FLOW METERS IN 2 INCH CIRCULATION LOOP

APPENDIX 8.5

CALIBRATION OF ROTAMETERS

In the 20 mm glass column setup rotameters were used for measuring both the air and the water flow rates. Calibration curves for these rotameters are presented in Figures 8.5.1 and 8.5.2, respectively.

For measuring the air flow rate in the 2 inch circulation loop, one rotameter was used most frequently. For calibrating this rotameter, the air line was pressurized by controlling the opening of the vent valve. Air was then metered with a wet-test gas meter for a period of 2 - 4 minutes. The calibration curves thus obtained are shown in Figure 8.5.3 for several supply pressures in the air line.

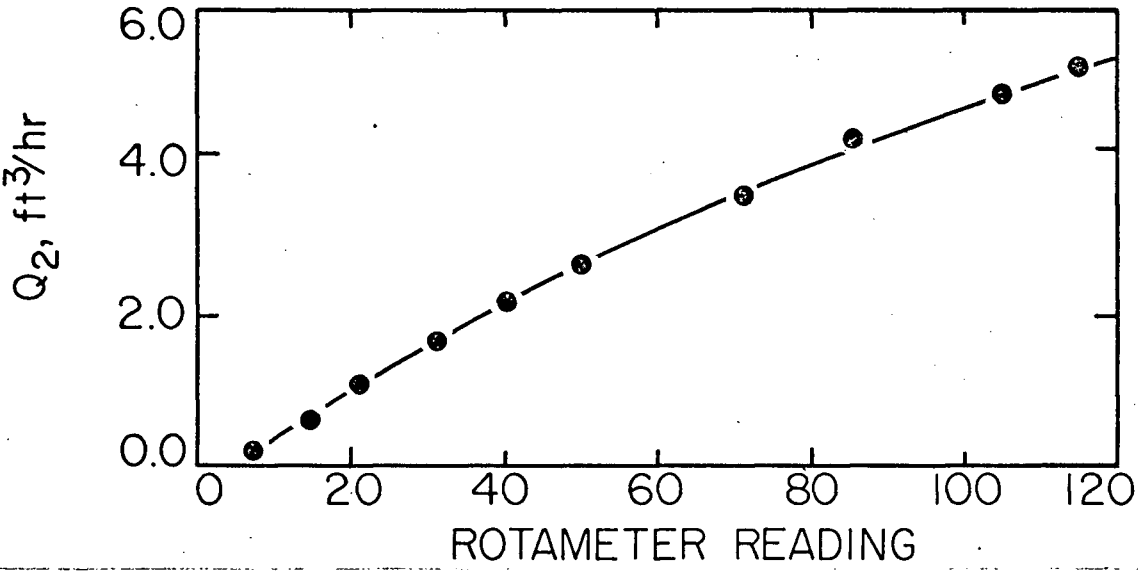

FIGURE 8.5.1 CALIBRATION CURVE FOR AIR ROTAMETER IN 20 MM GLASS COLUMN SETUP

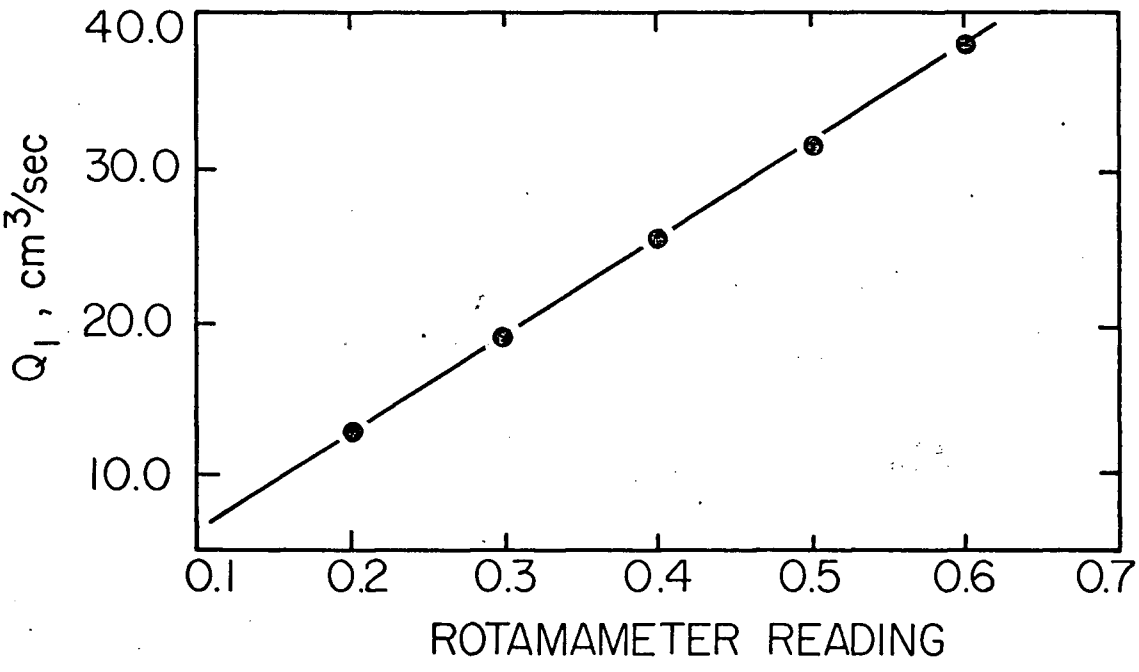

FIGURE 8.5.2 CALIBRATION CURVE FOR WATER ROTAMETER IN 20 MM GLASS COLUMN SETUP

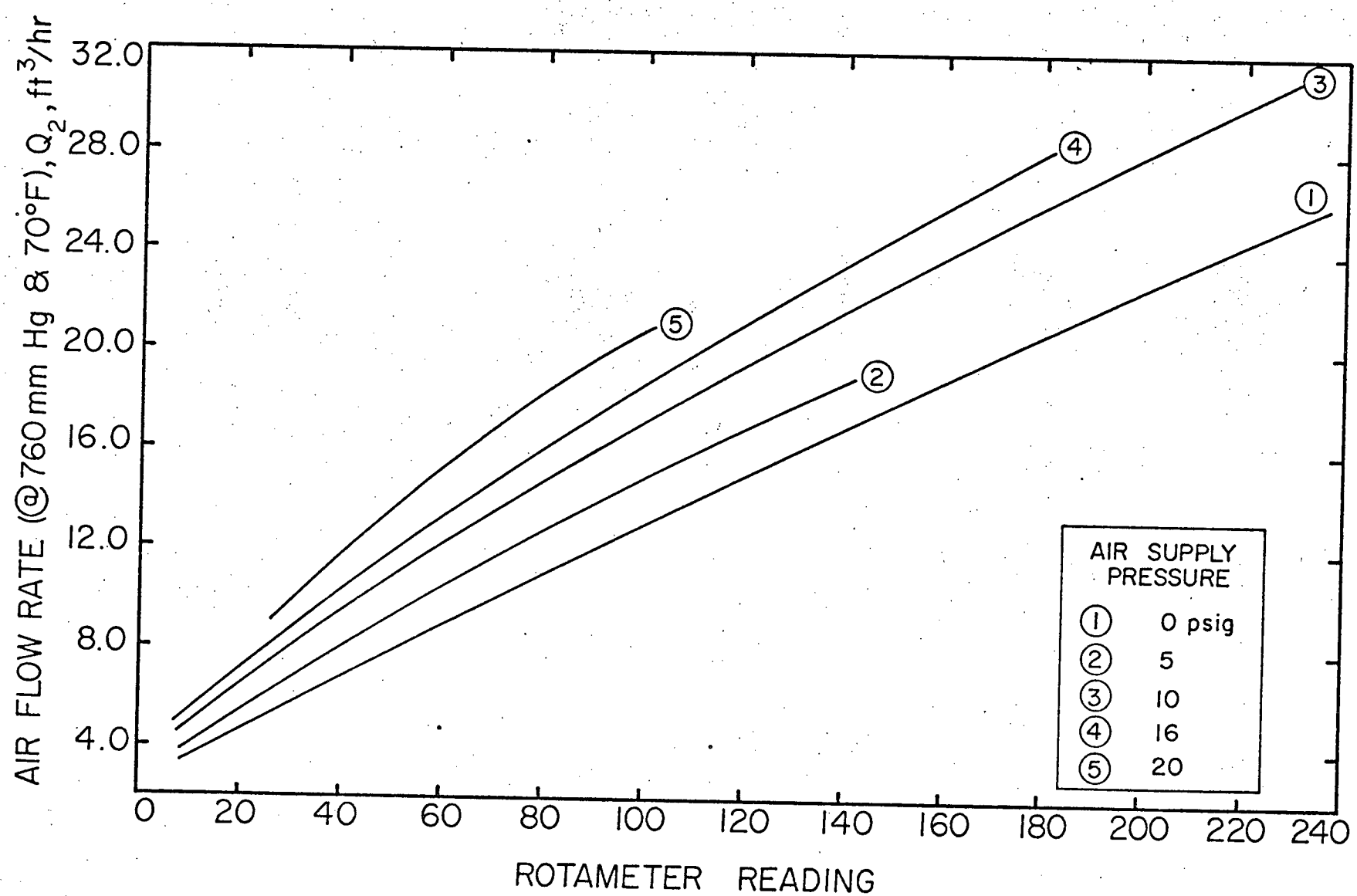

FIGURE 8.5.3 CALIBRATION CURVES FOR AIR ROTAMETER IN 2 INCH CIRCULATION LOOP

APPENDIX 8.6

PHYSICAL PROPERTIES OF THE MATERIALS USED

(A) Solid densities and particle sizes

TABLE 8.6.1

Particles		Density (gm/cm^3)	Particle diam. (mm)
0.25 mm	Glass	2.938	0.273
0.50 mm	Glass	2.935	0.456
0.50 mm	Sand	2.578	0.458
1.0 mm	Glass (A)	2.824	1.08
1.0 mm	Glass (B)	2.949	1.08
No. 9	Lead	11.03	2.18
1/8 in	Steel	7.756	3.18

(B) Densities and viscosities of liquids

TABLE 8.6.2

SYSTEM: GLYCEROL-WATER SOLUTION

% by Weight Glycerol	Specific Gravity (25°/25°C) [106]	Viscosity (cp) [107]		
		20°C	25°C	30°C
0.0	0.997	1.005	0.894	0.801
20	1.048	1.769	1.542	1.360
21	1.051	1.829	1.592	1.403
22	1.054	1.892	1.644	1.447
24	1.059	2.025	1.754	1.541
25	1.061	2.095	1.810	1.590
26	1.064	2.167	1.870	1.641
30	1.074	2.501	2.157	1.876

TABLE 8.6.3

CALIBRATION OF CANON VISCOMETER (300-H-304)

Standard	Temp. (°F)	Kinematic Viscosity (cs)	Density (gm/cm^3)	Dynamic Viscosity (cp)	Time Constant
S-20-57-4j	77	35.37	0.8506	30.09	0.22301
					0.22273
"	68	45.21	0.8538	38.60	0.22271
					0.22238
560	77	121.2	0.8733	105.8	0.22210
					0.22206
"	100	59.09	0.8654	51.14	0.22281
					0.22281
"	68	167.1	0.8763	146.4	0.22150
					0.22146
				Average	0.22215

TABLE 8.6.4

SYSTEM: POLYETHYLENE GLYCOL-WATER SOLUTION (I)

Sample	Density (at room temperature) (gm/cm^3)	Temperature (°F)	Viscosity (cp)
1	1.055	77.0	66.94
1	1.055	80.0	63.41
1		74.0	70.84
1		69.9	76.81
2	1.057	68.7	79.88
2	1.058	72.2	74.60
2		75.6	69.92
2		80.0	64.50
2		77.0	69.10
3	1.058	72.0	72.38
3	1.056	68.5	77.62
3		76.0	67.14
3		79.6	62.86
	Average 1.057		

TABLE 8.6.5

SYSTEM: POLYETHYLENE GLYCOL-WATER SOLUTION (II)

Sample	Density (at room temperature) (gm/cm^3)	Temperature (°F)	Viscosity (cp)
1	1.050	67.0	64.45
1	1.050	70.0	60.71
1		73.1	57.13
1	1.052	76.1	54.09
1	1.052	79.2	51.10
2	1.052	72.0	55.55
2	1.053	79.1	52.45
3	1.047	68.0	63.30
3	1.050	68.0	63.30
3		71.5	59.08
3		76.0	54.29
3		80.0	50.53
3		66.1	65.56
	Average 1.050		

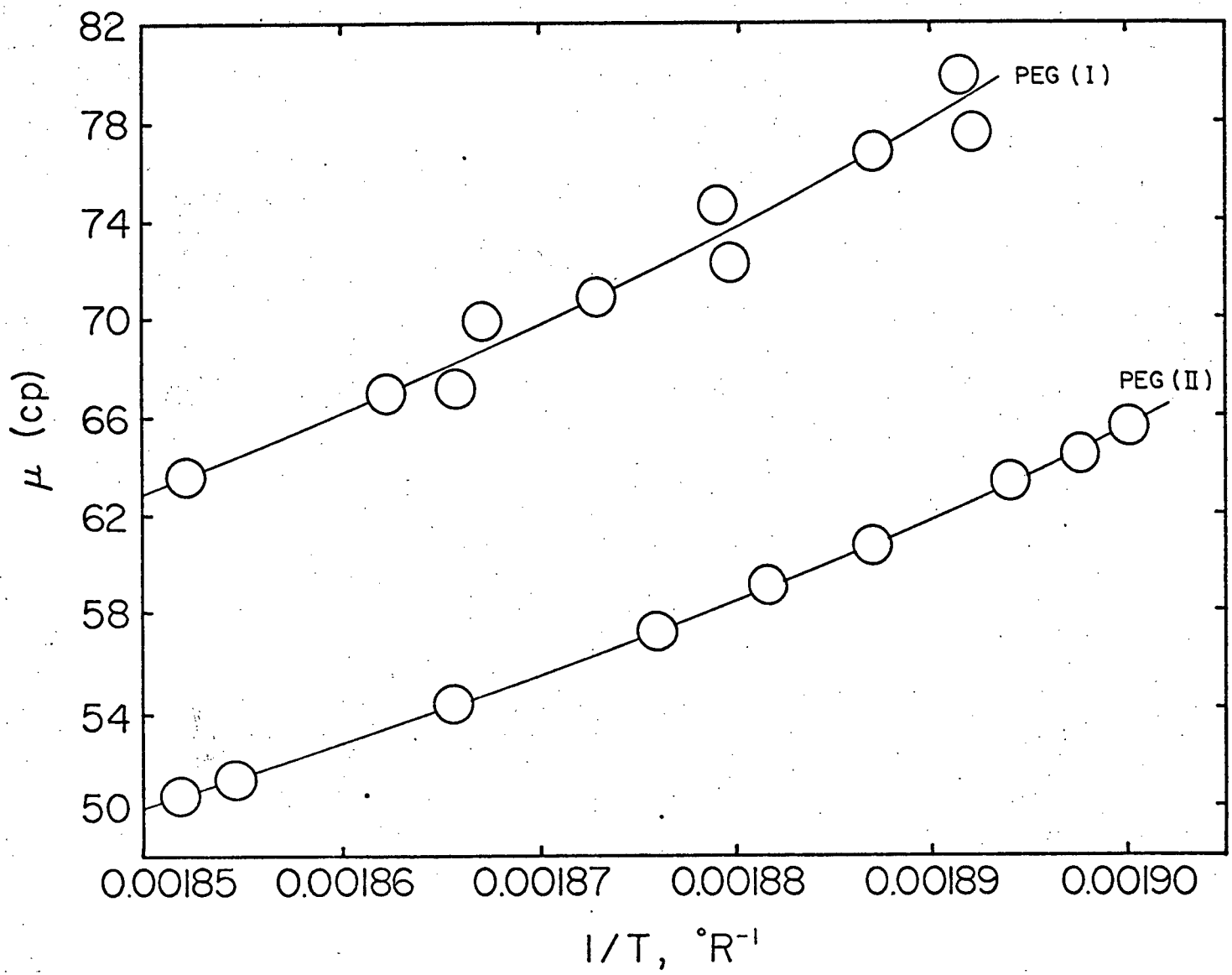

FIGURE 8.6.1 DYNAMIC VISCOSITY OF POLYETHYLENE GLYCOL SOLUTIONS

APPENDIX 8.7

PROCESSED DATA AND RESULTS

The following symbols in addition to those defined in the nomenclature are used in Appendix 8.7

A or B	after the weight of solid particles in the test section, W, indicates whether glass beads (A) or glass beads (B) were used (see Table 8.6.1)
I or II	after the PEG solution flow rate identifies whether solution I or solution II was used
EBH	expanded bed height
PDM	pressure drop measurement
VSO	valve shut-off technique
ε_{2A}	gas holdup above the test section
ε_{2E}	gas holdup in the test section
ε_{2C}	gas holdup below the test section
ε_{2P}	gas holdup by pressure drop measurement
ε_{2V}	gas holdup by valve shut-off technique
T	temperature in °F
Bubbly (LI)	mainly bubbly flow with occasional large irregular bubbles
$L\uparrow$	the height (in cm) up to which the particles were visually observed to exist
d_b	approximate bubble diameter in cm
λ_s	approximate slug length in cm

TABLE 8.7.1

GAS HOLDUP DATA FOR AIR-WATER FLOW IN 20 MM GLASS COLUMN

$\langle j_1 \rangle$ (cm/sec)	$\langle j_2 \rangle$ (cm/sec)	ε_2	$\bar{v}_2$ (cm/sec)	$\langle j \rangle$ (cm/sec)
0.0	5.33	0.329	16.20	5.33
4.01	5.33	0.234	22.81	9.35
	10.18	0.329	30.93	14.19
	17.34	0.430	40.38	21.95
6.02	5.33	0.200	26.72	11.35
	10.18	0.307	33.18	16.20
	17.34	0.408	42.52	23.36
8.02	5.33	0.182	29.37	13.36
	10.18	0.283	35.96	18.21
	17.34	0.375	46.29	25.36
10.03	5.33	0.163	32.64	15.36
	10.18	0.247	41.20	20.21
	17.34	0.367	47.30	27.37
12.04	5.33	0.163	32.80	17.37
	10.18	0.238	42.89	22.22
	17.34	0.342	50.71	29.38
14.20	10.18	0.247	41.24	24.34
	17.34	0.344	50.47	31.54
16.12	10.18	0.216	47.07	26.33
	17.34	0.353	49.11	33.44

TABLE 8.7.2

GAS HOLDUP DATA IN 2 INCH PERSPEX COLUMN FOR

(A) AIR - WATER FLOW

$\langle j_1 \rangle$ (cm/sec)	$\langle j_2 \rangle$ (cm/sec)	ϵ_2	$\bar{v}_2$ (cm/sec)	$\langle j \rangle$ (cm/sec)
0.0	1.79	0.068	26.38	1.79
	2.52	0.085	29.88	2.52
	3.45	0.121	28.53	3.45
	4.27	0.137	31.18	4.27
	5.05	0.156	32.26	5.05
	6.21	0.179	34.68	6.21
	7.10	0.202	35.13	7.10
	7.76	0.204	38.09	7.76
	8.85	0.227	39.04	8.85
	9.66	0.242	40.00	9.66
	10.48	0.260	40.42	10.48
	11.25	0.255	44.15	11.25
1.25	1.97	0.076	25.90	3.22
	3.81	0.150	25.46	5.06
	5.31	0.207	25.61	6.56
	6.88	0.242	28.40	8.13
	8.44	0.275	30.67	9.69
1.87	5.31	0.218	24.38	7.18
	6.88	0.228	30.23	8.75
	8.44	0.281	30.09	10.31
4.55	3.31	0.106	31.3	7.85
	7.91	0.204	38.73	12.45
	7.94	0.213	37.35	12.48
	9.92	0.247	40.20	14.46
	9.94	0.246	40.34	14.48
6.25	1.79	0.056	32.08	8.03
	2.52	0.075	33.49	8.77
	3.16	0.093	33.98	9.41
	3.73	0.103	36.28	9.97
	4.39	0.116	37.67	10.63
	4.85	0.131	37.15	11.10
	5.39	0.140	38.52	11.64
	5.86	0.147	40.00	12.11
	6.37	0.161	39.44	12.61
	6.99	0.176	39.72	13.23
	7.37	0.176	41.94	13.62
7.00	1.98	0.052	38.44	8.99
	2.60	0.066	39.30	9.63
	3.21	0.085	37.58	10.23

(B) air - PEG solution flow

$\langle j_1 \rangle$ (cm/sec)	$\langle j_2 \rangle$ (cm/sec)	ϵ_2	$\bar{v}_2$ (cm/sec)	$\langle j \rangle$ (cm/sec)
0.26	2.03	0.077	26.41	2.29
	7.76	0.242	32.13	8.02
	7.80	0.230	33.97	8.06
	7.86	0.236	33.26	8.11
1.01	5.47	0.167	32.83	6.48
	7.79	0.235	33.20	8.8
13.82	2.81	0.065	43.24	16.64
	4.77	0.102	46.97	18.60
	7.12	0.143	49.8	20.95
18.84	4.85	0.055	87.94	23.69
	9.42	0.138	68.33	28.26

TABLE 8.7.2 continued

	3.80	0.103	37.07	10.78
	4.32	0.115	37.73	11.34
	4.83	0.123	39.28	11.86
	4.94	0.130	38.04	11.97
	5.59	0.136	40.98	12.62
	5.99	0.145	41.31	13.03
	6.45	0.146	44.29	13.48
	7.02	0.159	44.06	14.05
7.00	2.45	0.078	31.56	9.42
	2.60	0.086	30.21	9.58
	2.64	0.084	31.58	9.60
	2.72	0.083	32.68	9.68
	2.79	0.082	34.17	9.75
	3.22	0.094	34.15	10.20
	3.44	0.100	34.24	10.40
	3.57	0.119	29.91	10.55
	3.73	0.113	33.05	10.68
	4.00	0.107	37.37	10.96
	4.02	0.120	33.55	11.00
	4.17	0.131	31.82	11.15
	4.33	0.123	35.16	11.31
	4.48	0.137	32.80	11.44
	4.83	0.122	39.55	11.79
	5.05	0.146	34.62	12.02
	5.20	0.15	34.79	12.17
	5.59	0.140	39.94	12.55
	5.71	0.151	37.79	12.68
	5.78	0.159	36.31	12.74
	5.86	0.164	35.68	12.84
	5.98	0.149	40.10	12.94
	6.17	0.164	37.65	13.15
	6.26	0.169	37.16	13.22
	6.37	0.158	40.43	13.32
	6.42	0.171	37.68	13.40
	6.75	0.182	37.10	13.73
	7.12	0.173	41.07	14.08
	7.61	0.200	38.07	14.58
7.65	1.79	0.054	33.03	9.43
	2.52	0.070	36.00	10.17
	3.16	0.085	37.13	10.81
	3.84	0.098	39.34	11.49
	4.27	0.107	39.80	11.91
	4.95	0.123	40.27	12.59
	5.39	0.132	40.79	13.04
	5.82	0.143	40.59	13.47
	6.40	0.167	38.35	14.05
	7.34	0.164	44.66	14.98
12.61	2.62	0.062	42.26	15.23
	3.99	0.094	42.45	16.60
	10.93	0.210	52.05	23.54
	12.49	0.232	53.84	25.10
17.75	3.08	0.063	48.84	20.79
	3.17	0.062	51.61	20.85
	3.18	0.062	51.29	20.98
	3.34	0.071	46.81	21.02
	4.18	0.082	51.28	21.86
	4.22	0.083	50.84	22.02
	4.26	0.086	49.85	22.01
	5.04	0.098	51.68	22.72
	5.07	0.101	50.20	22.87
	5.38	0.107	50.31	23.05
	5.98	0.123	48.62	23.66
	6.37	0.125	50.99	24.04
	6.47	0.120	54.02	24.21
	6.91	0.128	53.86	24.59
	7.23	0.131	55.49	24.97
	7.45	0.138	53.93	25.13
	7.80	0.131	59.54	25.60
	8.02	0.135	59.33	25.74
	8.13	0.135	60.22	25.93
	8.77	0.145	60.48	26.57
	9.75	0.160	60.94	27.55
	10.93	0.181	60.39	28.73
3.61	1.94	0.063	31.03	5.55
2.64	3.66	0.116	31.44	6.30
4.83	1.94	0.064	30.30	6.77
3.37	3.66	0.112	32.52	7.02
4.89	2.52	0.079	31.94	7.41
4.83	2.59	0.085	30.45	7.42
4.00	3.66	0.115	31.70	7.66
4.83	3.49	0.108	32.25	8.33
5.09	3.44	0.108	31.77	8.53
4.89	3.66	0.119	30.64	8.55

TABLE 8.7.3

SOLIDS HOLDUP DATA FOR LIQUID-SOLID FLUIDIZATION IN 20 MM GLASS COLUMN

Fluidization System	d_p (mm)	W (gms)	$L_{b,0}$	L_b	$\langle j_l \rangle$ (cm/sec)	T (°F)	ε_3 from E.B.H.
Sand-Water	0.458	45.0	12.1	22.3	1.67	68~70	0.249
				26.1	2.03		0.213
				31.3	2.38		0.178
				35.7	2.71		0.156
				43.8	3.04		0.127
Glass beads-Water	1.08	50.0(A)	10.7	13.6	3.04	72.0	0.414
				15.7	4.01	-	0.359
				18.8	4.81	65.0	0.300
				19.2	5.22	82.0	0.245
				22.9	6.02	73.0	0.245
				24.4	6.82	73.0	0.214
				33.0	8.02	73.0	0.830
Glass beads-Water-glycerol solution	1.08	50.0	10.5	20.4	4.06	67.0	0.276
				20.2	4.06	70.0	0.280
				25.0	4.86	65.5	0.225
				32.3	6.03	69.5	0.175

TABLE 8.7.4

SOLIDS HOLDUP DATA FOR LIQUID-SOLID FLUIDIZATION IN 2 INCH PERSPEX COLUMN

Fluidization System	d_p (mm)	W (mm)	$L_{b,0}$ (cm)	L_b (cm)	$\langle j_1 \rangle$ (cm/sec)	T (°F)	Solids Holdup, ϵ_3	
							From E.B.H.	From P.D.M.
Glass beads-Water	0.273	1100.0	31.7	77.6	1.25	62.0	0.238	0.236
		739.3	21.5	71.4	1.87	62.0	0.166	0.163
		721.1	21.2	109.4	2.23	62.0	0.111	-
Glass beads-Water	0.456	1200.0	34.2	54.8	1.59	60.0	0.370	0.365
		1200.0	34.5	102.7	3.52	60.0	0.197	0.193
		1200.0	34.2	136.5	4.55	60.0	-	0.148
		566.5	16.7	72.2	4.55	60.0	0.132	0.134
		566.5	16.6	121.4	5.71	60.0	-	0.078
Glass beads-Water	1.08	488.1	14.3	27.4	6.25	70.0	0.294	0.294
		488.1	14.3	30.2	6.97	70.0	0.267	0.267
		576.6(A)	19.3	40.1	7.02	65.0	0.251	0.262
		488.1	14.3	34.1	7.65	68.0	0.236	0.240
		536.4	15.4	73.2	12.80	65.0	0.121	0.120
		487.0	13.9	68.8	12.80	63.0	0.117	0.116
Lead Shot-Water	2.18	4936.4	37.1	38.0	8.26	64.0	0.582	0.585
		5094.3	40.1	54.4	17.80	60.0	0.414	0.420
		3267.3	25.6	46.0	26.40	57.0	0.318	0.310
		3414.3	27.1	48.3	26.40	56.0	0.316	0.324
		3245.0	25.6	75.0	38.77	58.0	0.194	0.192
Glass beads-PEG Solution	1.08	413.0	11.8	25.9	0.40(I)	71.0	0.268	-
		378.0/280.0	10.8/8.0	40.5/28.8	0.86(I)	71.0	0.158	0.152
		385.0	11.0	57.0	1.14(I)	74.0	0.114	-
Steel Shot-PEG Solution	3.18	1078.3	12.3	50.9	13.82(II)	68.0	0.135	0.143
		1078.3	12.3	111.3	18.84(II)	68.0	0.062	0.070

TABLE 8.7.5

GAS AND SOLIDS HOLDUP DATA IN 20 MM GLASS COLUMN
FOR THREE-PHASE BEDS OF
(A) air-water-1/2 mm sand
W=45; $L_{b,0}$=12.1

$\langle j_1 \rangle$ ($\frac{cm}{sec}$)	$\langle j_2 \rangle$ ($\frac{cm}{sec}$)	L_b (cm)	Δp (in. of CCl_4)	$\epsilon_{2P}/\epsilon_{2V}$	ϵ_3	T (°F)
1.67	0.0	22.3	6.47	-	0.249	
	0.13	19.7	6.43	0.002	0.282	
	0.33	19.4	6.40	0.003	0.286	
	0.70	19.3	6.20	0.009	0.288	
	1.05	19.2	5.66	0.025	0.289	
	1.43	19.3	4.86	0.050	0.288	
	1.93	20.2	4.16	0.072	0.275	
	0.0	22.3	6.48	-	0.249	
2.03	0.0	26.1	6.55	-	0.213	
	0.0	26.1	6.50	-	0.213	
	0.18	21.9	6.43	0.004	0.254	
	0.38	21.8	6.39	0.005	0.255	
	0.83	21.3	5.84	0.022	0.261	
	1.28	21.2	5.10	0.045	0.262	
	1.70	21.9	4.23	0.072	0.254	
	2.18	22.6	3.60	0.091	0.246	
	2.80	23.2	3.03	0.109	0.239	
2.38	0.0	31.3	6.55	-	0.178	
	0.25	25.2	6.00	0.017	0.220	
	0.45	24.6	6.00	0.017	0.226	
	1.00	23.9	5.43	0.035	0.232	
	1.50	24.7	4.69	0.058	0.225	
	2.13	25.5	3.94	0.081	0.218	
2.71	0.0	35.7	6.65	-	0.156	
	0.25	26.7	6.44	0.007	0.208	
	0.50	25.9	6.19	0.014	0.215	
	0.83	26.0	5.55	0.034	0.213	
	1.23	26.6	4.84	0.056	0.209	
	1.78	27.8	4.12	0.078	0.200	
	2.18	29.1	3.42	0.100	0.191	
	2.68	30.8	2.84	0.118	0.180	
3.04	0.0	43.8	6.73	-	0.127	
	0.18	31.4	6.58	0.005	0.177	
	0.45	30.1	6.43	0.009	0.185	
	0.83	29.4	5.82	0.028	0.189	
	1.23	28.9	5.30	0.044	0.192	
	1.50	30.0	4.39	0.072	0.185	
	0.0	43.7	9.71	-	0.127	

TABLE 8.7.5 continued

(C) air-aqueous glycerol-1 mm glass beads
W=50 (A); $L_{b,0}$=10.7

$\langle j_1 \rangle$ ($\frac{cm}{sec}$)	$\langle j_2 \rangle$ ($\frac{cm}{sec}$)	L_b (cm)	Δp (cm. of CCl_4)	$\epsilon_{2P}/\epsilon_{2V}$	ϵ_3	T (°F)	
4.06	0.0	20.4	21.8	-	0.276	67.0	
	0.0	20.2	-	-	0.279	70.0	
	0.15	19.4	-	-	0.291	70.0	
	0.27	19.2			0.294		
	0.38	19.0			0.297		
	0.53	19.0			0.297	70.5	
	0.75	19.1			0.295		
	1.08	19.3		/0.045	0.292	71.5	
	1.13	19.6	19.5	0.028	0.288		
	1.38	20.0	18.3	0.043	0.282		
	1.70	20.4	18.3	0.043	0.276	68.0	
	2.10	20.9	18.2	0.044	0.270		
	2.25	21.0	13.4	0.102	0.268		
	2.68	21.0	11.5	0.125	0.259		
	3.13	22.5	10.0	0.144/0.136	0.251	72.0	
4.86	0.0	25.3	22.0	-	0.223	65.0	
	0.18	22.8			0.247	70.0	
	0.38	22.3			0.253		
	0.53	22.4			0.252		
	0.85	22.6		/0.035	0.249	70.0	SLUGS
	1.23	23.3	18.9	0.038	0.242	65.0	
	1.38	23.5	17.9	0.050	0.240	66.0	
	1.70	24.1	16.4	0.068	0.234		
	1.95	24.6	15.6	0.078	0.229		
	2.10	24.9	14.9	0.087/0.101	0.226	66.0	
	2.45	24.8	14.5	0.091	0.227	67.0	
	2.75	25.3	13.2	0.107	0.223		
	3.26	26.9			0.210	69.0	
	3.63	28.1	10.4	0.142/0.138	0.201		
6.03	0.0	32.3	24.3	-	0.175	59.5	
	1.00	28.5	20.7	0.045	0.198	72.5	
	1.15	27.8	20.3	0.050	0.203		
	1.38	27.7	19.9	0.054	0.204		
	1.78	28.5	18.6	0.070	0.198		
	2.18	29.8	16.9	0.091	0.189		
	2.68	31.0	15.4	0.109/0.101	0.182	74.0	
	4.01	35.3	10.9	0.163/0.156	0.160		

TABLE 8.7.5 continued

(B) air-water-1 mm glass beads

W=50(A); $L_{b,0}$=10.7

$\langle j_1 \rangle$ ($\frac{cm}{sec}$)	$\langle j_2 \rangle$ ($\frac{cm}{sec}$)	L_b (cm)	Δp (in. of CCl_4)	$\epsilon_{2P}/\epsilon_{2V}$	ϵ_3	T (°F)
3.04	0.0	13.6	7.54	-	0.414	72.0
4.01	0.0	15.7	8.28	-	0.359	
	0.0	15.9	8.00	-	0.354	79.0
	0.0	16.2	8.09	-	0.347	72.0
	0.18	15.8	8.27	0.005	0.356	72.0
	0.53	15.8	7.85	0.018	0.356	72.0
	0.90	16.2	8.03	0.037/0.055	0.371	
	1.00	16.0	7.28	0.036	0.352	72.0
	1.43	16.4	6.51	0.059	0.343	42.0
	1.88	16.5	5.31	0.083	0.341	79.0
	2.50	17.6	4.99	0.106	0.320	72.0
	2.50	17.1	4.72	0.110/0.111	0.330	-
	2.83	17.7	4.02	0.123	0.318	79.0
	3.40	18.5	3.58	0.150	0.304	72.0
	3.95	18.7	2.86	0.159	0.301	79.0
	4.08	19.2	2.30	0.190	0.293	72.0
	4.80	19.7	2.31	0.189	0.286	72.0
	5.08	19.2	1.69	0.195	0.293	79.0
	5.28	19.6	3.33	0.182/0.185	0.288	
	5.35	20.7	1.48	0.215	0.272	72.0
	5.83	21.0	0.95	0.221	0.268	73.0
	5.93	20.3	0.75	0.224	0.277	80.0
	6.40	21.8	0.20	0.244	0.258	73.0
	6.88	21.5	-0.13	0.251	0.262	81.0
	7.08	23.3	-0.60	0.269	0.242	73.0
	8.20	22.4	-1.28	0.287	0.251	81.0
4.81	0.0	18.8	7.64	-	0.300	65.0
	0.0	18.8	7.67	-	0.300	68.0
	0.35	17.8	7.60	0.001	0.317	
	0.48	17.8	7.56	0.003	0.317	66.0
	0.70	18.1	7.51	0.004	0.311	
	0.85	18.0	7.42	0.007	0.313	67.0
	1.00	18.2	6.97	0.021/0.043	0.310	68.0
	1.30	18.3	6.62	0.33	0.308	69.0
	1.70	18.8	5.95	0.053	0.300	
	2.03	19.1	5.53	0.066	0.295	70.0
	2.33	19.9	5.02	0.082/0.097	0.283	70.5
5.22	0.0	19.2	8.00	-	0.293	82.0
	2.00	19.2	5.37	0.081	0.293	
	3.63	21.4	3.86	0.128	0.263	
	4.38	22.4	3.31	0.145	0.251	
	5.30	23.7	2.11	0.182	0.237	
	6.13	25.1	1.39	0.204	0.224	82.0
6.02	0.0	22.9	8.49	-	0.246	73.0
	0.0	22.8	8.55	-	0.247	
	0.13	21.4	8.20	0.009	0.263	73.0
	0.48	21.0	7.80	0.021	0.268	
	0.95	21.3	7.38	0.034	0.264	
	1.43	22.0	6.41	0.064	0.256	
	2.18	23.1	5.41	0.095	0.244	73.0
	2.33	23.4	5.86	0.083/0.111	0.241	
	2.33	24.1	5.76	0.086/0.076	0.234	
	2.95	25.2	4.57	0.121	0.223	
	3.76	25.5	4.36	0.130/0.131	0.221	73.0
	3.76	25.8	4.24	0.133/0.121	0.218	
	3.80	26.5	3.51	0.154	0.212	
	5.08	27.9	2.96	0.173/0.191	0.202	
	5.08	27.4	2.73	0.180/0.173	0.206	73.0
6.02	0.0	23.1	8.26	-	0.244	69.5
	0.19	21.2	8.14	0.004	0.266	69.5
	0.35	21.0	8.02	0.007	0.268	
	0.48	21.5	7.72	0.017	0.262	70.5
	0.63	21.3	7.39	0.027	0.265	
	0.75	21.6	7.40	0.027	0.261	
	0.85	21.1	7.58	0.021/0.035	0.267	71.0
	0.90	21.5	7.36	0.028	0.262	71.5
	1.30	21.9	6.98	0.039	0.257	
	1.63	22.7	6.40	0.058	0.248	72.0
	1.78	23.1	6.20	0.064	0.244	
	2.20	23.8	5.73	0.078	0.237	
	2.50	24.5	5.28	0.092	0.230	
	2.83	25.1	4.97	0.102	0.225	
	3.33	26.2	4.51	0.116/0.103	0.215	73.0
	0.0	23.0	7.76	-	0.245	71.0
6.42	0.0	24.4	8.18	-	0.231	78.0
	0.0	24.4	9.49	-	0.231	
	0.63	22.7	9.40	0.003	0.248	
	1.70	23.6	8.44	0.033	0.239	
	1.88	24.5	6.09	0.065	0.230	
	2.43	25.1	6.40	0.096	0.224	
	2.75	25.8	5.37	0.087	0.218	
	3.30	26.6	5.41	0.126	0.212	
	3.53	27.6	4.24	0.122	0.204	
	4.20	29.2	3.69	0.179	0.193	78.0
6.82	0.0	25.3	7.92	-	0.223	76.0
	0.0	26.3	7.96	-	0.214	74.5
	0.18	23.9	7.81	0.005	0.236	
	0.35	23.7	7.79	0.005	0.238	
	0.48	24.7	7.81	0.005	0.228	
	0.53	24.1	7.99	/0.024	0.234	
	0.63	23.7	7.77	0.006	0.238	
	0.85	24.0	7.74	0.007	0.235	
	1.08	24.4	7.52	0.014/0.039	0.231	
	1.25	24.1	7.02	0 .029	0.234	
	1.63	24.6	6.47	0.046	0.229	
	2.03	25.5	6.07	0.058/0.083	0.221	
	2.33	25.6	5.92	0.063	0.220	
	2.83	26.9	5.53	0.075	0.210	
	2.88	27.3	5.36	0.080/0.101	0.206	79.0

TABLE 8.7.6

GAS AND SOLIDS HOLDUP DATA IN 2 INCH PERSPEX COLUMN FOR THREE-PHASE BED OF

(A) air-water-1/4 mm glass beads

$\langle j_1 \rangle$ (cm/sec)	$\langle j_2 \rangle$ (cm/sec)	L_b (cm)	ϵ_3	ϵ_{2C}		ϵ_{2E}	ϵ_{2A}		ϵ_2''	ϵ_2'''	$\frac{\epsilon_2'''}{(1-\epsilon_3)}$	Observations
				PDM	VSO		PDM	VSO				
1.25	0.0	77.6	0.237									W=1100
	2.03	52.9	0.355	0.066	0.057	0.052	0.054	0.056	0.054	0.059	0.092	SLUGS
	2.80	53.2	0.353	0.098	0.089	0.070	0.075	0.076	0.080	0.080	0.124	
	4.17	53.2	0.352	0.128	0.128	0.096	0.109	0.112	0.118	0.089	0.137	
	5.30	53.3	0.346	0.154	0.149	0.118	0.135	0.134	0.140	0.113	0.173	
	6.91	52.1	0.353	0.194	0.204	0.143	0.170	0.179	0.183	0.122	0.189	
	8.71	51.6	0.355	0.240	0.008	0.174	0.206	0.220	0.215	0.150	0.233	
	10.01	53.2	0.342	0.279	0.253	0.207	0.233	0.244	0.244	0.183	0.278	
1.87	0.0	105.5	0.166									W=1067
	1.98	60.8	0.299	0.063	0.055	0.049	0.054	0.046	0.054	0.061	0.088	
	10.05	59.3	0.298	0.272	0.253	0.211	0.228	0.207	0.234	0.193	0.275	
1.87	0.0	76.3	0.163									W=739
	1.98	43.8	0.282	0.065	0.057	0.057	0.059	0.052	0.058	0.071	0.099	BUBBLY(LI)
	4.60	41.5	0.295	0.140	0.130	0.108	0.121	0.119	0.125	0.100	0.141	
	6.95	42.0	0.292	0.193	0.186	0.158	0.170	0.134	0.173	0.136	0.192	SLUGS
	8.54	42.6	0.288	0.234	0.222	0.165	0.203	0.218	0.214	0.151	0.211	
	10.05	42.1	0.299	0.287	0.286	0.200	0.237	0.258	0.270	0.182	0.260	
3.18	2.00	57.6	0.191	0.062	0.049	0.065	0.068	0.058	0.059	0.070	0.086	W=655 , BUBBLY
	3.40	56.4	0.194	0.108	0.096	0.103	0.106	0.075	0.106	0.102	0.126	BUBBLY(LI)
	4.58	50.0	0.220	0.130	0.120	0.125	0.123	0.128	0.122	0.131	0.168	SLUGS
	6.95	50.9	0.208	0.187	0.156	0.167	0.169	0.151	0.172	0.155	0.196	
	9.97	48.7	0.203	0.255	0.249	0.191	0.228	0.214	0.234	0.201	0.253	W=590

TABLE 8.7.6 continued

(B) air-water-1/2 mm glass beads

$\langle j_1 \rangle$ (cm/sec)	$\langle j_2 \rangle$ (cm/sec)	L_b (cm)	ϵ_3	ϵ_{2C}		ϵ_{2E}	ϵ_{2A}		ϵ_2''	ϵ_2'''	$\frac{\epsilon_2'''}{(1-\epsilon_3)}$	Observations
				PDM	VSO		PDM	VSO				
1.59	0.0	54.7	0.365									W=1200
	2.03	47.1	0.429	0.064	0.052	0.048	0.054	0.061	0.058	0.042	0.074	BUBBLY(LI)
	3.16	46.8	0.431	0.109	0.098	0.073	0.084	0.077	0.090	0.063	0.111	BUBBLY(LI)
	4.81	47.1	0.429	0.143	0.132	0.105	0.124	0.128	0.132	0.088	0.154	SLUGS , λ_s=10
	6.17	47.4	0.425	0.178	0.171	0.124	0.156	0.177	0.167	0.096	0.167	SLUGS , λ_s=10-12
	7.67	48.0	0.421	0.212	0.197	0.165	0.187	0.197	0.195	0.146	0.252	SLUGS , λ_s=12-15
	9.94	49.1	0.411	0.269	0.263	0.205	0.233		0.249	0.194	0.312	SLUGS , λ_s=18-20
	11.22	50.6	0.396	0.302	0.285	0.246	0.261	0.232	0.271	0.227	0.377	SLUGS , λ_s=18-20
3.52	0.0	102.7	0.195									W=1200
	2.00	67.2	0.300	0.059	0.048	0.051	0.052	0.055	0.054	0.054	0.072	BUBBLY(LI)
	3.03	66.2	0.305	0.098	0.086	0.071	0.080	0.067	0.087	0.075	0.108	BUBBLY(LI)
	4.00	64.5	0.313	0.122	0.109	0.089	0.103	0.113	0.110	0.081	0.118	SLUGS , λ_s=10
	6.17	63.1	0.320	0.167	0.158	0.128	0.145	0.139	0.151	0.113	0.167	SLUGS , L_f=80
	7.67	62.7	0.322	0.200	0.190	0.147	0.176	0.187	0.183	0.138	0.203	SLUGS
4.55	0.0	136.5	0.148									W=1200
	2.06	79.2	0.255	0.058	0.056	0.052	0.057	0.050	0.057	0.055	0.073	BUBBLY
	4.51	74.7	0.270	0.127	0.137	0.104	0.111	0.094	0.116	0.101	0.139	SLUGS , λ_s=6
	6.17	73.2	0.276	0.161	0.154	0.131	0.143	0.132	0.150	0.125	0.173	SLUGS , λ_s=6
	7.91	74.2	0.272	0.200	0.184	0.149	0.177		0.182	0.146	0.200	SLUGS , λ_s=10
	9.94	74.2	0.272	0.244	0.252	0.175	0.210		0.225	0.154	0.211	SLUGS , λ_s=12
	11.25	72.8	0.271	0.278	0.278	0.188	0.233	0.271	0.254	0.178	0.245	SLUGS , λ_s=12
	11.25	72.8	0.268	0.278	0.276	0.209	0.240	0.243	0.252	0.177	0.241	SLUGS , λ_s=15
4.55	0.0	72.2	0.134									W=567
	2.00	41.0	0.233	0.054	0.053	0.055	0.054	0.051	0.054	0.056	0.073	BUBBLY(LI) , L_f=52
	4.54	40.7	0.234	0.122	0.111	0.101	0.107	0.118	0.116	0.093	0.122	SLUGS , λ_s=5 , L_f=64
	6.17	39.4	0.242	0.158	0.147	0.135	0.134	0.150	0.147	0.130	0.171	SLUGS L_f=80
	7.92	38.7	0.243	0.196	0.176	0.182	0.171	0.157	0.177	0.154	0.204	SLUGS , λ_s=12 , L_f=80
	9.94	40.7	0.234	0.241	0.212	0.208	0.209	0.217	0.215	0.179	0.234	SLUGS , λ_s=12
	11.25	42.4	0.225	0.272	0.272	0.208	0.234	0.288	0.259	0.169	0.218	SLUGS , λ_s=12 , L_f=90
	11.22	40.8	0.233	0.271	0.248	0.201	0.233		0.253	0.182	0.237	
	7.92	39.7	0.240	0.199	0.185	0.173	0.178	0.219	0.188	0.152	0.200	
	9.98	38.9	0.245	0.245	0.254	0.182	0.216	0.214	0.227	0.184	0.243	
	9.94	38.7	0.246	0.247	0.239	0.179	0.216		0.226	0.187	0.248	
5.71	0.0	121.4	0.078									W=567
	2.0	56.5	0.168	0.051	0.052	0.055	0.057	0.051	0.053	0.055	0.067	BUBBLY
	4.46	49.3	0.193	0.116	0.115	0.130	0.115	0.119	0.116	0.113	0.140	SLUGS , λ_s=4 , L_f=90
	6.15	50.4	0.189	0.151	0.136	0.134	0.140	0.145	0.145	0.123	0.151	SLUGS , λ_s=8
	7.96	49.7	0.192	0.193	0.191	0.156	0.177	0.200	0.187	0.149	0.184	SLUGS , λ_s=12
	9.97	50.0	0.191	0.236	0.219	0.205	0.217	0.297	0.224	0.180	0.223	SLUGS , λ_s=18 , L_f=110

TABLE 8.7.6 continued

(C) air-water-1 mm glass beads

$\langle j_1 \rangle$ (cm/sec)	$\langle j_2 \rangle$ (cm/sec)	L_b (cm)	ϵ_3	ϵ_{2C}		ϵ_{2E}	ϵ_{2A}		ϵ_2''	ϵ_2'''	$\frac{\epsilon_2'''}{(1-\epsilon_3)}$	Observations
				PDM	VSO		PDM	VSO				
7.02	0.0	40.1	0.262									W=577 (A)
	1.78	36.1	0.279			0.050		0.042	0.046	0.052	0.072	
	2.12	36.2	0.279		0.059	0.059		0.052	0.057	0.050	0.070	
	2.63	36.6	0.276		0.067	0.075		0.066	0.069	0.076	0.106	
	3.28	36.9	0.273		0.091	0.090		0.089	0.091	0.073	0.100	SLUGS
	3.87	37.3	0.270		0.109	0.099		0.063	0.108	0.090	0.124	SLUGS
	4.44	38.0	0.266		0.120	0.124		0.125	0.138	0.138	0.189	
	5.01	38.4	0.262		0.130	0.106		0.102	0.122	0.076	0.103	
	5.57	38.7	0.260		0.136	0.106		0.063	0.068	0.068	0.092	
	6.17	39.0	0.258		0.133	0.128		0.176	0.145	0.132	0.178	
	6.60	39.2	0.257		0.170	0.138		0.148	0.152	0.132	0.178	
7.65	0.0	34.1	0.240									W=488 (B)
	3.23	28.5	0.283		0.083	0.068		0.053	0.067	0.067	0.094	
	3.76	29.5	0.273		0.099	0.086		0.086	0.094	0.085	0.116	
	4.32	30.3	0.266		0.105	0.096		0.101	0.104	0.094	0.128	
	5.11	31.3	0.257		0.130	0.103		0.109	0.125	0.111	0.149	
	5.40	30.6	0.263		0.123	0.116		0.120	0.118	0.113	0.153	
	6.80	32.6	0.247		0.163	0.119		0.165	0.159	0.123	0.164	
12.80	0.0	73.2	0.121									W=536 (B)
	2.31	63.6	0.139			0.050	0.053	0.058	0.055	0.055	0.063	
	3.23	62.7	0.141		0.069	0.066	0.089	0.079	0.089	0.068	0.079	
	4.07	59.5	0.149		0.086	0.083	0.085	0.091	0.085	0.085	0.100	
	4.85	57.5	0.154		0.100	0.104	0.101	0.080	0.101	0.103	0.122	
	5.36	61.0	0.143		0.106	0.085	0.105	0.076	0.105	0.095	0.111	
	5.84	57.6	0.154		0.120	0.110	0.108	0.126	0.108	0.107	0.126	
	6.33	60.8	0.144		0.132	0.110	0.117	0.113	0.117	0.100	0.117	
	6.80	57.0	0.155		0.139	0.116	0.139	0.181	0.139	0.118	0.140	
	7.70	58.4	0.152		0.162	0.136	0.149	0.137	0.149	0.124	0.146	
	8.42	59.7	0.148		0.178	0.154	0.162	0.130	0.162	0.139	0.163	
	8.83	61.8	0.143		0.174	0.131	0.183	0.134	0.183	0.136	0.159	
	9.24	59.5	0.145		0.188	0.160	0.181	0.155	0.181	0.148	0.174	
	10.06	61.8	0.143		0.184	0.188	0.199	0.182	0.199	0.154	0.180	
12.80	0.0	68.8	0.116									W=487 (B)
	4.85	53.8	0.150	0.102		0.088	0.103	0.097	0.100	0.079	0.093	
	6.33	55.7	0.143	0.133	0.124	0.115	0.119	0.127	0.126	0.100	0.117	
	8.42	56.6	0.141	0.175	0.161	0.149	0.153	0.158	0.162	0.124	0.145	
	10.06	55.3	0.143	0.208	0.180	0.179	0.204	0.131	0.192	0.149	0.173	
	11.66	55.4	0.141	0.238	0.230	0.186	0.219	0.241	0.232	0.162	0.188	

TABLE 8.7.6 continued

(D) air-water-2 mm lead shot

$\langle j_1 \rangle$ (cm/sec)	$\langle j_2 \rangle$ (cm/sec)	L_b (cm)	ϵ_3	ϵ_{2C} PDM	ϵ_{2C} VSO	ϵ_{2E}	ϵ_{2A} PDM	ϵ_{2A} VSO	ϵ_2''	ϵ_2'''	$\frac{\epsilon_2'''}{(1-\epsilon_3)}$	Observations
8.26	0.0	38.0	0.583									
	2.91	40.2	0.549	0.073	0.083	0.078	0.093	0.088	0.087	0.030	0.067	BUBBLY
	4.27	41.0	0.539	0.116	0.124	0.115	0.128	0.113	0.126	0.085	0.185	
	5.36	41.7	0.529	0.142	0.163	0.151	0.146	0.131	0.149	0.145	0.309	
	6.40	42.5	0.520	0.164	0.181	0.147	0.153	0.102	0.167	0.118	0.245	SLUGS
	7.22	43.2	0.511	0.172	0.191	0.163	0.163	0.135	0.177	0.152	0.310	
	8.26	43.0	0.514	0.188	0.207	0.174	0.179	0.125	0.189	0.155	0.318	
	9.14	42.0	0.526	0.204	0.227	0.198	0.194	0.196	0.206	0.182	0.385	
17.80	0.0	54.4	0.414									
	3.97	57.7	0.395	0.081	0.081	0.082	0.084	0.086	0.083	0.084	0.139	BUBBLY
	6.37	59.2	0.383	0.124	0.133	0.115	0.121	0.124	0.126	0.113	0.183	W=5062
	7.18	61.1	0.371	0.137	0.145	0.127	0.142	0.139	0.143	0.115	0.177	SLUGS
	8.42	62.3	0.363	0.156	0.163	0.154	0.152	0.148	0.155	0.147	0.231	W=5056
	9.33	61.3	0.369	0.171	0.195	0.158	0.167	0.173	0.170	0.150	0.237	
	10.21	60.5	0.371	0.183	0.205	0.162	0.181	0.181	0.182	0.163	0.258	W=5018
	11.22	57.5	0.391	0.159	0.193	0.146	0.158	0.177	0.167	0.138	0.227	
26.40	0.0	48.3	0.322									W=3414
26.40	0.0	46.0	0.313									W=3267
	2.56	51.1	0.299	0.038	0.047		0.043	0.055	0.043	0.026	0.037	W=3414
	3.77	52.8	0.289	0.059	0.061	0.066	0.060	0.059	0.060	0.074	0.104	W=3408
	4.73	53.7	0.284	0.077	0.077	0.085	0.079	0.076	0.077	0.081	0.114	
	5.96	55.2	0.276	0.097	0.097	0.103	0.101	0.094	0.099	0.100	0.138	W=3402
	6.91	54.2	0.281	0.111	0.114	0.123	0.114	0.127	0.115	0.139	0.193	
	7.73	52.9	0.288	0.120	0.129	0.118	0.121	0.098	0.123	0.119	0.168	
	8.15	52.1	0.292	0.131	0.138	0.118	0.128	0.147	0.132	0.090	0.127	
	9.17	51.0	0.298	0.146	0.150	0.138	0.142	0.142	0.148	0.118	0.168	
	15.85	53.2	0.286	0.202	0.215	0.176	0.193	0.204	0.200	0.127	0.178	
	15.38	51.9	0.282	0.203	0.199	0.177	0.205	0.191	0.201	0.198	0.275	W=3267
	20.50	53.9	0.271	0.262	0.269	0.213	0.254	0.233	0.261	0.208	0.286	W=3267
38.77	0.0	75.0	0.191									W=3245
	2.14	79.6	0.184	0.024	0.036	0.030	0.019	0.030	0.024	0.041	0.050	W=3267
	6.56	86.9	0.167	0.081	0.086	0.094	0.082	0.085	0.085	0.102	0.122	W=3245
	9.33	81.1	0.178	0.118	0.124	0.104	0.118	0.124	0.121	0.118	0.143	W=3223
	12.95	81.1	0.178	0.146	0.149	0.139	0.145	0.146	0.146	0.145	0.179	
	18.50	84.4	0.171	0.206	0.229	0.168	0.204	0.223	0.209	0.180	0.217	

TABLE 8.7.6 continued

(E) air-PEG solution (I) - 1 mm glass beads

$\langle j_1 \rangle$ (cm/sec)	$\langle j_2 \rangle$ (cm/sec)	L_b (cm)	ϵ_3	ϵ_{2C}		ϵ_{2E}	ϵ_{2A}		ϵ_2''	ϵ_2'''	$\frac{\epsilon_2'''}{(1-\epsilon_3)}$	Observations
				PDM	VSO		PDM	VSO				
0.40	0.0	25.9	0.268									T=71 , W=413
0.43	1.88	48.9	0.142	0.102	0.066	0.040	0.076	0.057	0.078	0.062	0.072	T=74
0.86	0.0	40.5	0.154									T=71 , W=387
	0.58	25.5	0.185	0.019	0.033		0.023	0.018	0.022	0.033	0.040	T=68 , W=280
	1.98	39.8	0.123	0.089	0.058	0.070	0.085	0.086	0.085	0.055	0.063	T=70 , W=291
0.88	0.71	45.5	0.133	0.049	0.032	0.034	0.047	0.034	0.043	0.034	0.039	T=72 , W=360
	0.70	44.5	0.130	0.047			0.044	0.042	0.044	0.033	0.038	T=72 , W=343
	1.63	36.9	0.140	0.073	0.041	0.060	0.069	0.053	0.066	0.055	0.064	T=72 , W=308
1.14	0.0	57.0	0.114									T=74 , W=385
	0.40	42.4	0.153	0.017			0.015	0.017	0.015	0.017	0.020	

TABLE 8.7.6 continued

(F) air-PEG solution (II) - steel shot

$\langle j_1 \rangle$ (cm/sec)	$\langle j_2 \rangle$ (cm/sec)	L_b (cm)	ϵ_3	ϵ_{2C}		ϵ_{2E}	ϵ_{2A}		ϵ_2''	ϵ_2'''	$\frac{\epsilon_2'''}{(1-\epsilon_3)}$	Observations
				PDM	VSO		PDM	VSO				
13.82	0.0	50.9	0.135									T=68 , W=1078
	4.89	42.3	0.162	0.063		0.048	0.061	0.044	0.062	0.033	0.039	
	7.37	40.5	0.169	0.118	0.076	0.101	0.106		0.105	0.093	0.113	
	9.33	40.2	0.171	0.158	0.109	0.100	0.141	0.119	0.138	0.152	0.183	
18.84	0.0	111.3	0.062									T=68 , W=1078
	5.03	72.2	0.095	0.050	0.043	0.032	0.049	0.034	0.046	0.020	0.022	
	9.28	58.6	0.117	0.179	0.135	0.141	0.160	0.132	0.159	0.134	0.152	

APPENDIX 8.8

PUBLICATIONS

Reprinted from AIChE JOURNAL, May 1969

Gas Holdup of a Bubble Swarm in Two Phase Vertical Flow

V. K. BHATIA

University of British Columbia, Vancouver, British Columbia

The rise of a gas bubble in a confined liquid medium is somewhat analogous to the corresponding sedimentation of a solid particle; but this analogy has been misinterpreted in the past by various authors who were therefore obliged either to set narrow operating limits on the validity of their equations (*3*) or to correct them by means of empirical factors (*4*). Marrucci (*7*) derived an expression for the rise velocity of a swarm of bubbles and concluded that the rise velocity showed a weaker dependence on the fraction of solid in suspension than the settling velocity of a multiparticle suspension of rigid spheres following Happel's free surface model (*8*) (Figure 1.). He noted qualitatively that the sparse data of Nicklin (*10*) and his own data indicated a relatively small decrease in rise velocity with increasing ϵ, but quantitatively his model failed to agree with the experimental data of various other investigators. Although no explicit mention is made of the radius of bubbles which make up the swarm, Marrucci's model does implicitly indicate the effect of bubble radius on the rise velocity of the swarm.

Mendelson (*6*) recently derived an equation for predicting the rise velocity of single bubbles in infinite media

from the interfacial disturbance analogy between the motion of waves on an ideal liquid and the rise of bubbles in a low viscosity liquid.

$$V_\infty = \sqrt{\frac{\sigma}{\rho r_e} + g r_e} \qquad (1)$$

This equation was found to represent the experimental data well for the rise velocity of single bubbles larger than 1.5 mm. in diameter.

Later, Maneri and Mendelson (5) extended this analogy for predicting the rise velocity of large single bubbles in bounded media. They showed that for large N_{Eo}, that is for large tube diameters such that $1/N_{Eo} << 1$, the rise velocity of a single bubble could be represented by

$$V/V_\infty = \sqrt{\tanh\left[0.25(r/r_e)\right]} \qquad (2)$$

Equation (2) was found to correlate experimental data well for $1/\lambda = (r/r_e)$ between 1 and 10, the lower value of which corresponds to a slug.

In this paper an attempt is made to extend Mendelson's wave analogy further, to describe the rise velocity of a swarm of bubbles, by employing the cell model technique proposed by Happel and Ast (9) for sedimentation and subsequently used by Marrucci (7). Following their approach we have the necessary relationship between λ and gas volume fraction, ϵ, given by

$$\epsilon = \lambda^3 \qquad (3)$$

Now combining Equations (2) and (3) we get

$$V_o = V_\infty \sqrt{\tanh\left[0.25(1/\epsilon)^{1/3}\right]} \qquad (4)$$

Thus Equation (4) would predict the energy destroying velocity [as defined by Nicklin (10)] of a bubble swarm in tubes of large diameters. It should, however, be pointed out here that Equation (4) will not give the true rise velocity, V_o, for slugs and is applicable only for a swarm consisting of large spherical bubbles. But Equation (2), with $r = r_e$, does represent the rise velocity of slugs in a quiescent liquid medium, for which it then simplifies (5) in combination with Equation (1) for large N_{Eo} to

$$V_s = 0.35\sqrt{gD} \qquad (5)$$

which is the familiar Dumitrescu equation (11). Equation (5) should, however, be modified as suggested by Nicklin (10), to be used for predicting the energy destroying velocity, V_o, for slugs:

$$V_o = 0.2\,(u_g + u_L) + V_s \qquad (6)$$

The gas velocity, u_g, for which a certain gas volume fraction, ϵ, would exist at the given liquid flow rate, u_L, is given by

$$u_g = \frac{\epsilon(V_o + u_L)}{(1-\epsilon)} \qquad (7)$$

a relationship derivable directly from Nicklin's equations. The rise velocity of the bubble swarm will then be given by

$$V_B = V_o + u_g + u_L \qquad (8)$$

DISCUSSION

Equation (4) represents the simplest expression that can be derived for the rise velocity of bubble swarms. Equation (4) predicts the ratio V_o/V_∞ to be a function of gas holdup, ϵ, only, but V_o itself depends on bubble diameter as well as on gas holdup. Figure 1 shows a plot of Equation (4) along with plots of Marrucci's equation for bubble swarms and Happel's equation for sedimentation of solid spheres. The discrepancy between the curves for bubble swarms and solid particles arises from the fact that the tangential liquid velocity is zero at the surface of a solid particle but not zero at the surface of a bubble. As a result, the energy dissipation is smaller and therefore the relative velocity higher for the bubble swarm. The reason

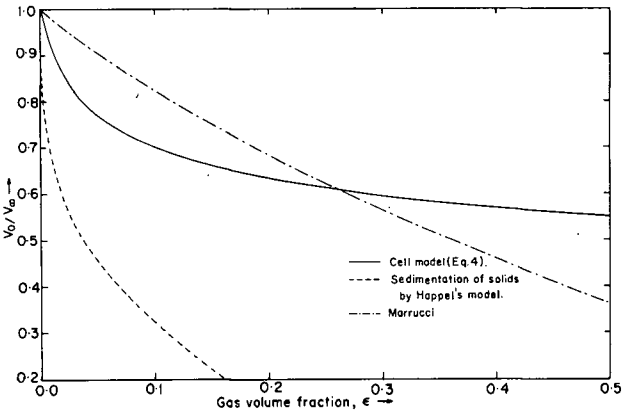

Fig. 1. Effect of gas volume fraction on the rise velocity of bubble swarms.

for the discrepancy between the two models for rise velocity of a bubble swarm is that Marrucci based his derivation on potential flow theory, whereas the model described herein is based on Mendelson's wave analogy (5). Nicklin reported data for V_o as a function of u_g, but did not report the bubble diameter as a function of gas velocity. No reliable correlation exists for predicting the diameter of bubbles that form the swarm. But the operating conditions of Nicklin probably gave rise to bubble diameters between 2 and 6 mm. (14).

To check the validity of the above equations, we need systematic data for gas holdup, average bubble diameter, and a description of flow regimes as a function of gas and liquid velocities. Figure 2 shows data of Bridge, et. al. (12), Nicklin (10), and Deraux (13) for the air-water system with zero net water flow, compared with the present model [Equation (1), (4), and (7)] for a bubble diameter of 3 mm. Although average diameters of bubbles are not reported (except for data of Bridge) we see that the theoretical relationship for 3 mm. diameter bubbles does follow the data well, whereas the empirical correlation of Davidson, et. al. (15) follows the data only at the lower gas velocities corresponding to the bubble flow regime.

The experimental data of Ellis and Jones (19) and Towell and Strand (20) are of special interest since they employed large column diameters and therefore introduced the additional phenomenon of recirculation, which is absent in smaller pipes (less than 4 in. in diameter). Towell and Strand (19) used a 16 in. diameter column and reported that bubble diameter was essentially constant (0.21 in.) for all gas rates except the highest (1.0 ft./sec.), where occasional large irregular masses of gas were observed. Ellis and Jones (20) used circular pipes of 1, 2, 4, and 12 in. diameters and reported that, although no time slugs (gas bubble bridging the pipe diameter) were observed in pipes greater than 4 in. in diameter, large bubbles and irregular masses of gas appeared to be moving up these columns. In pipes up to 2 in. in diameter, slugs were reported to appear at gas velocities exceeding 0.1 ft./sec. Ellis and Jones gave an empirical correlation for the transition from bubble to slug flow as

$$u_g = 0.2\,u_L + 0.1$$

Therefore it seems reasonable to conclude that bubbles of up to about 2 in. in diameter could be present in vertical two-phase flow depending on gas flow rate and pipe diameter.

Since the model described herein is dependent on the bubble diameter, it is necessary to know the time average diameter of the bubble in the swarm in order to correctly predict the gas holdup. Also it is important to note that since the model does not account for bulk recirculation, which is present in large diameter columns (19, 20), it

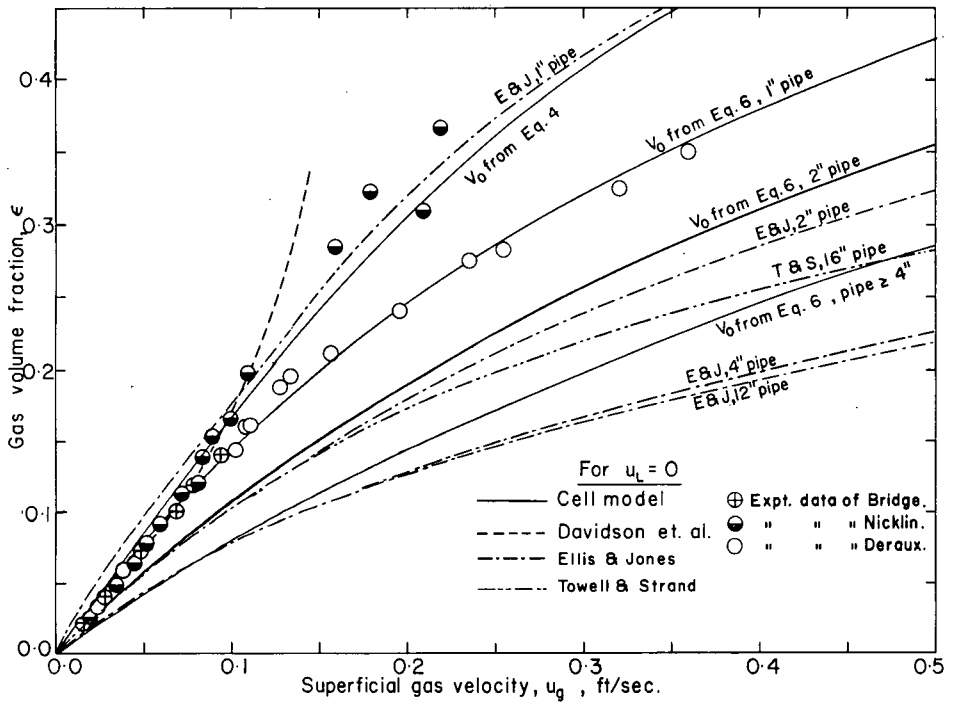

Fig. 2. Gas holdup for noncirculating air-water system.

will therefore predict higher gas holdup than actually observed in columns where recirculation is prevalent. This is illustrated by the large column data of Ellis and Jones and of Towell and Strand, which are plotted in Figure 2 and fall below that predicted by the cell model. It may be mentioned here that since the bubble diameter in the swarm is increasing gradually with the gas rate, it is not possible to satisfy the experimental data with a single bubble size in the cell model equation for all gas rates. Therefore to predict the gas holdup in large diameter columns, one must know both the bubble size and the liquid recirculation velocity as a function of gas rate.

We can also use Equation (4) to predict gas holdup for cocurrent gas-liquid flow. Baker and Chao (*17*) reported that the relative velocity for bubble rise in a turbulently flowing liquid is the same as for a quiescent liquid. Thus V_o for cocurrent gas-liquid flow could be obtained from Equations (1) and (4). For cocurrent gas-liquid flow Patrick (*18*) reported the average bubble diameter, d_e, to be a function of true liquid velocity V_T.

$$d_e = 0.52/V_T^{0.666} \quad (0.5 < V_T < 5.0) \qquad (9)$$

where

$$V_T = u_L/(1-\epsilon) \qquad (10)$$

Dukler, et. al. (*16*) compiled all the existing data on two-phase flow and checked the validity of various proposed empirical correlations. They found that Hughmark's (*2*) correlation represents the existing data better than any other correlation. Therefore it was decided to check the above theory with Hughmark's correlation. Figure 3 shows this comparison, as well as Ostergaard's Equation (1) and Deraux's data for a superficial liquid velocity of 0.569 ft./sec. The present method, using the correlation for bubble diameter reported by Patrick, agrees reasonably well with Hughmark's correlation for higher liquid velocities. We should use Equation (4) for the bubble flow regime and Equation (6) for the slug flow regime. Deraux (*13*) reported that slugs begin to appear at a gas volume fraction of about 0.2, whereas Patrick (*18*) observed that no slug formation occurs until $\epsilon = 0.4$. Using the proper equation for each regime we see that the deviation between the present correlation and Hughmark's correlation is reduced appreciably.

CONCLUSIONS

A method has been derived to predict the gas holdup of a swarm of bubbles based on the cell technique for representing a swarm, using the bubble velocity in bounded media as developed by Mendelson (*5*). The method is applicable to low viscosity and comparatively pure gas-liquid systems. The presence of any interfacial impurity will tend to make the gas bubbles behave like solids and the equation will not be applicable. The model shows good agreement with existing experimental data

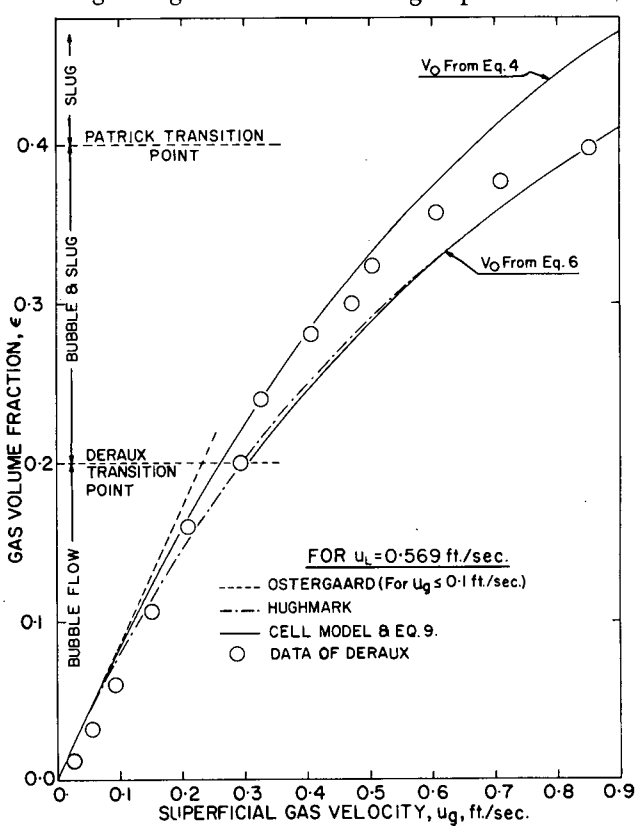

Fig. 3. Gas holdup for cocurrently flowing air-water system.

for the air-water system and gives better insight into rising bubble swarms than models based on the hindered settling of rigid particles. To check the general validity of the above model, systematic data for average bubble diameter, gas holdup, and flow regime as a function of gas and liquid velocities are needed.

ACKNOWLEDGMENT

The author wishes to express his gratitude to Dr. Norman Epstein for reading and criticizing the original manuscript. The continuing financial assistance from the National Research Council of Canada and the University of British Columbia is gratefully acknowledged.

NOTATION

D = diameter of tube, ft.
d_e = average bubble diameter, cm.
g = acceleration of gravity, ft./sec.^{2}
N_{Eo} = Eötvös number based on tube radius, $g\rho r^2/\sigma$
r = tube radius, ft.
r_e = equivalent bubble radius based on a sphere of equal volume, ft.
u_g = superficial gas velocity based on empty tube area, ft./sec.
u_L = superficial liquid velocity based on empty tube area, ft./sec.
V = rise velocity of single bubble in a tube, ft./sec.
V_o = energy destroying velocity of bubble swarm, ft./sec.
V_B = velocity of bubbles relative to wall for steady co-current gas-liquid flow, ft./sec.
V_∞ = rise velocity of single bubble in infinite media ft./sec.
V_s = slug rise velocity, ft./sec.
V_T = true liquid velocity as defined by Equation (10), ft./sec.

Greek Letters

ρ = density of liquid phase, lb./cu.ft.
σ = surface tension, poundals/ft.
λ = ratio of radii, r_e/r
ϵ = gas volume fractions
$\Delta\rho$ = difference between liquid and gas density, lb./cu.ft.

LITERATURE CITED

1. Ostergaard, K., and M. L. Michelsen, paper presented at AIChE meeting, Tampa, Fla. (May, 1968).
2. Hughmark, G. A., *Chem. Eng. Progr.*, **58**, 62 (1962).
3. Uno, S., and R. C. Kintner, *AIChE J.*, **2**, 3 (1956).
4. Harmathy, T. Z., *ibid.*, **6**, 281 (1960).
5. Maneri, C. C., and H. D. Mendelson, *ibid.*, **14**, 295 (1968).
6. Mendelson, H. D., *ibid.*, **13**, 250 (1967).
7. Marrucci, Giuseppe, *Ind. Eng. Chem. Fundamentals*, **4**, 224 (1964).
8. Happel J., and H. Brenner, "Low Reynolds Number Hydrodynamics," p. 387ff., Prentice-Hall, Englewood, Cliffs, N.J. (1965).
9. ———, and P. A. Ast, *Chem. Eng. Sci.*, **11**, 286 (1960).
10. Nicklin, D. J., *ibid.*, **17**, 693 (1962).
11. Dumitrescu, D. T., *Z. angew. Math U. Mech.*, **23**, 139 (1943).
12. Bridge, A. G., L. Lapidus, and J. C. Elgin, *AIChE J.*, **10**, 819 (1964).
13. Deraux, R., *Argonne Natl. Lab Trans.*, **61** (1964).
14. Levich, G. V., "Physical Hydrodynamics," p. 435ff., Prentice-Hall, Englewood Cliffs, N.J. (1962).
15. Davidson, J. F., and D. Harrison., *Chem. Eng. Sci.*, **21**, 731 (1966).
16. Dükler, A. E., Moyce Wicks, III, and R. G. Cleveland, *AIChE J.*, **10**, 38 (1964).
17. Baker, James L. L., and B. T. Chao, *ibid.*, **11**, 268 (1965).
18. Patrick, M., *Argonne Natl. Lab. Rept. 6581* (1962).
19. Ellis, J. E., and E. L. Jones, *Two Phase Flow Symposium*, Exeter, England (June 1965).
20. Towell, G. D., and C. P. Strand, Proc. Symposium Mixing, London, England, (June, 1965).

Reprinted from I&EC PROCESS DESIGN & DEVELOPMENT, Vol. 11, Page 151, January 1972

CORRESPONDENCE

Effect of Solids Wettability on Expansion of Gas-Liquid Fluidized Beds

SIR: In their recent paper on "Bed Porosities in Gas-Liquid Fluidization," Dakshinamurti et al. (1971) have reported some data on the expansion characteristics of three-phase fluidized beds. They used air as the gas, and both water and kerosine as the liquid, the air-liquid surface tension of their kerosine being approximately one-third that of water. Their results with water were similar to those found by previous investigators (Turner, 1964; Stewart and Davidson, 1964; Ostergaard, 1965) inasmuch as their beds contracted rather than expanded, on first introducing gas at most of their liquid flow rates, for the smaller lighter particles. However their results with kerosine for the same particles, plotted in their Figures 2 and 6, show no such contractions whatsoever (despite contrary statements by the authors in their abstract and text), and, in fact, show higher expansion rates with gas flow than any of their other systems. The authors vaguely suggest that there may be some connection between this exceptional behavior of kerosine and the fact that a small fraction of the 1.3-mm rockwool shot particles (the smallest particles used in kerosine), when fluidized by the kerosine, "formed a thin, more or less stagnant, layer on the walls of the tube," but they do not spell out the connection mechanistically.

It is our contention that the stabilization of particles at the walls of the tube implies that traces of impurities were present in the kerosine (the authors describe no special purification procedures of what was probably commercial-grade kerosine),

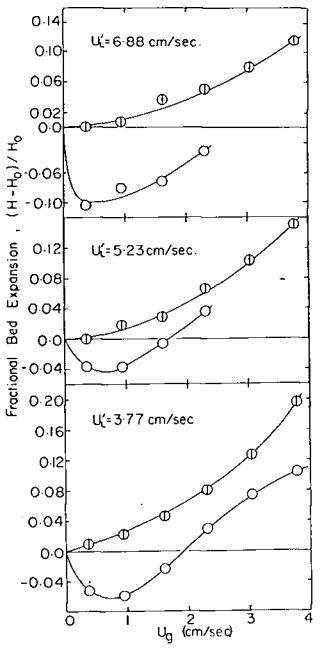

Figure 1. Effect of solids wettability on expansion of a gas-liquid fluidized bed

○ Clean glass beads. ⦶ Teflon-coated glass beads

which rendered the particles nonwettable or only partially wettable by the liquid. Earlier studies of gas-liquid-solid systems (Guha et al., 1964) have shown the importance of wettability in determining the hydrodynamic behavior of such systems. In the case of cocurrent gas-liquid fluidization of small solid particles, previous studies have been confined to wettable solids. It has been postulated by Stewart and Davidson (1964) and subsequently by Ostergaard (1965) that contraction of the bed occurs on introducing gas at a fixed liquid rate because of the formation of liquid wakes behind the gas bubbles, which do not contact the solid particles, as the solids are entirely immersed in the liquid. Since the gas bubbles and their accompanying liquid wakes move faster than the remaining liquid, it follows that the latter must slow down to conserve the fixed average liquid velocity, and, hence, the immersed bed of solids is caused to contract. One experimental test of this hypothesis would be to render the solid particles nonwettable by the liquid, in which case they would no longer remain wholly immersed in the liquid but would be able to contact the gas as well. The result should then be an attenuation, elimination, or even reversal of the bed contraction phenomenon. We have performed just such a test.

Three-phase fluidization experiments were carried out in a 2-cm. diameter bench-top glass column using clean air as the gas phase, distilled water as the liquid phase, and 30–40 grams of 1-mm glass beads (density = 2.82 g/cc) as the fluidized solids. Details of the experimental setup are given by Evans (1970). Runs were performed on the clean glass beads at three values of the superficial liquid velocity, U_L', for an appreciable range of superficial gas velocity, U_g. The glass beads were then thoroughly coated with Teflon spray and, after determining that the coating added negligibly to the weight of the beads while rendering them almost nonwettable by water, the experiments were repeated at similar conditions with the coated beads. The results are shown in Figure 1, in which H_0 represents the bed height at zero gas flow, while H represents the bed height at any gas flow. Whereas the clean wettable beads first undergo distinct bed contraction with increasing gas flow before undergoing subsequent expansion, the Teflon-coated nonwettable beads give rise to bed expansion from the lowest gas velocities onward.

If one accepts that the work of adhesion, W_{SLV}, represents the energy that must be expended per unit interfacial area to effect separation between a solid and a liquid phase (in the presence of a gas or vapor) at the interface between them, and that this work is given by Dupré's equation (Adamson, 1967),

$$W_{SLV} = \sigma_{LV}(1 + \cos\theta) \quad (1)$$

where σ_{LV} is the liquid-gas surface tension, and θ is the contact angle of the liquid on the given solid surface in the presence of the given gas, then the above results can be mathematically rationalized. Thus the increase of θ from 0° for a perfectly wettable solid to almost 180° for a nonwettable solid brings about a continuous decrease in the value of cos θ from +1 to almost −1, so that W_{SLV} is reduced accordingly. A secondary effect via Equation 1 may be that of surface tension. Thus the considerably lower liquid-air surface tension of kerosine than that of water may make kerosine even more amenable than water to bed expansion (rather than contraction) by gas flow.

Literature Cited

Adamson, A. W., "Physical Chemistry of Surfaces" p. 353, Wiley, New York, N.Y., 1967.
Dakshinamurti, P., Subrahamanyam, V., Rao, J. N., *Ind. Eng. Chem. Process Des. Develop.*, **10**, 332 (1971).
Evans, K. A., B. A. Sc. Thesis, University of British Columbia, Vancouver, B.C., Canada, 1970.
Guha, D. K., Roy, N. K., Rao, M. N., *Chem. Eng. Sci.*, **19**, 215 (1964).
Ostergaard, K., *Chem. Eng. Sci.*, **20**, 165 (1965).
Stewart, P. S. B., Davidson, J. F., *Chem. Eng. Sci.*, **19**, 319 (1964).
Turner, R., "Fluidization," p 47, Society of Chemical Industry, London, England 1964.

Vinay K. Bhatia
Kenneth A. Evans
Norman Epstein

Department of Chemical Engineering
The University of British Columbia
Vancouver 8, B.C., Canada

SIR: It is true that in the abstract, owing to an oversight, statements contrary to the graphs are presented regarding the reduction of bed porosity for rockwoolshot and small glass beads with kerosine. Only commercial-grade kerosine without any further purification was used in the experiments.

It has been proved that the rockwoolshot is wettable both by water and kerosine, but the surface tension of kerosine to air is approximately one-third that of water. Hence adhesion in the case of kerosine is lower than for water and this may be responsible for bed expansion (instead of bed contraction) in the case of kerosine with rockwoolshot and small glass beads.

P. Dakshinamurty

Chem. Eng. Dept.
Andhra Univ.
Waltair, India

APPENDIX 8.9

Error Estimation

The experimental errors in various measured primary quantities were estimated to be the following:

Primary Quantities			Max. Error
H	=	manometer reading	± 0.2 cm
W	=	height of solid particles in the column	± 5.0 gm
L_b	=	expanded bed height	± 0.5 cm
ρ_3	=	density of solid particles	± 0.01 gm/cc
ρ_1	=	density of liquid	± 0.005 gm/cc
ρ_M	=	density of manometer fluid	± 0.01 gm/cc
D	=	diameter of column	± 0.2 cm
Z	=	distance between manometer taps	± 0.2 cm
L	=	length of various sections of the column	± 0.2 cm

If a result, R, is dependent on the variables X_1, X_2 $\cdots$, X_n, then the uncertainty, δ_R, in the calculated result is given by

$$\delta_R = \left[\left(\frac{\partial R}{\partial X_1}\,\delta_1\right)^2 + \left(\frac{\partial R}{\partial X_2}\,\delta_2\right)^2 + \cdots + \left(\frac{\partial R}{\partial X_n}\,\delta_n\right)^2\right]^{1/2} \qquad (8.9.1)$$

where

$$R = f(X_1, X_2 \cdots X_n) \qquad (8.9.2)$$

and $\delta_1, \delta_2, \cdots, \delta_n$ are the errors in the variables $X_1, X_2, \cdots, X_n$ [109].

Applying equation 8.9.1 to the appropriate expressions used in calculating the results, the experimental errors in the main computed quantities were estimated and are presented in Table 8.9.1.

TABLE 8.9.1

ESTIMATED ERRORS IN EXPERIMENTAL RESULTS

Variable	Formula Used	% Error (max.)
Solids holdup, ε_3	(1) $\varepsilon_3 = W/\rho_3 A L_b$	± 3.0%
	(2) $\varepsilon_3'' = H(\rho_M-\rho_l)/Z(\rho_3-\rho_l)$	± 5.0%
Gas holdup in gas-liquid flow	(1) $\varepsilon_2'' = L_{ig}/L_i$ for i = E or C	± 1.0% to ± 6.5%
	(2) $\varepsilon_2'' = -H(\rho_M-\rho_l)/Z\ \rho_l$	± 5.5%
Gas holdup in three-phase fluidized bed	(1) $\varepsilon_2''' = \varepsilon_{2P}'' + (\varepsilon_{2EC}-\varepsilon_{2P}'')\frac{L_E}{L_b}$	± 6.0% to ± 20%
	(2) $\varepsilon_2''' = \frac{\varepsilon_3(\rho_3-\rho_l)-S_I(\rho_M-\rho_l)}{\rho_l}$	± 6.5% to ± 20%

Terms defined either in nomenclature or Appendix 8.2.

APPENDIX 8.10

CALCULATIONS

The methods used to treat the experimental data are illustrated by sample calculations. All such calculations were performed on the IBM-360 digital computer. Some of the equations used for obtaining the results are presented in the following sections (for others see Section 3.4 or Appendix 8.2), but the actual computer programs, which are straightforward and unexceptional, are neither presented nor discussed. The run for fluidization of 1/2 mm glass beads by a cocurrent stream of air ($\langle j_2 \rangle$ = 9.94 cm/sec) and water ($\langle j_1 \rangle$ = 4.55 cm/sec), with corresponding runs for gas-liquid flow and liquid-solid fluidization, will be used for illustrating the procedure.

(1) Free settling terminal velocity and Reynolds number of 1/2 mm glass beads

For calculating the free-settling velocity of particles, the simple method recommended by Wallis [27] was used. Accordingly, the drag coefficient of particles, $C_{D\infty}$, is related to the free settling particle Reynolds number, Re_p, by the following equations:

$$C_{D\infty} = \frac{24}{Re_p}\left(1 + 0.15\ Re_p^{0.687}\right) \qquad (8.10.1)$$

for $Re_p < 1000$, and

$$C_{D\infty} = 0.44 \qquad (8.10.2)$$

for $Re_p > 1000$. It can be easily seen that

$$C_{D\infty}\ Re_p = \frac{4}{3}\ \frac{d_p^3\ \rho_1\ g(\rho_3-\rho_1)}{\mu_1^2} \qquad (8.10.3)$$

since by definition,

$$Re_p = \frac{d_p\ V_\infty\ \rho_1}{\mu_1}$$

On obtaining the physical properties of water at 70°F from Perry [106] and the physical properties of glass beads from Table 8.6.1, the free settling velocity of 1/2 mm glass beads was calculated from these equations by trial and error. Then

$$V_\infty = 7.37 \text{ cm/sec}$$

$$Re_p = 28.0$$

(2) Voidage and solids holdup in liquid-solid fluidization

Solids holdup was calculated from

$$\varepsilon_3 = \frac{W}{\rho_3 A L_b} \qquad (3.1)$$

$W = 566.5$ gm

$\rho_3 = 2.935$ gm/cm^3

$A = \pi R^2 = \pi(2.54)^2 = 20.268$ cm^2

$L_b = 72.2$ cm

Then from equation 3.1,

$$\varepsilon_3 = \frac{566.5}{2.935 \times 20.268 \times 72.2} = 0.132$$

Solids holdup was also calculated from

$$\varepsilon_3 = S_I \frac{(\rho_M - \rho_l)}{(\rho_3 - \rho_l)} \qquad (3.7)$$

where S_I is the slope of the best straight line through the pressure drop data of H (cm of CCl_4) versus Z (distance from tap 1 in inches), for $Z < Z_{max}$. It was found that

$S_I = 1.099$ cm of CCl_4/inch of bed length

Then from equation 3.7,

$$\varepsilon_3 = \frac{1.099}{2.54} = \frac{1.595-1}{2.935-1} = 0.133$$

Then average solids holdup $\varepsilon_3 = 0.133$

and voidage $\varepsilon = (1-\varepsilon_3) = 0.867$.

The voidage was predicted by the Richardson - Zaki correlation, equation 2.46, with exponent n evaluated from equation 2.49a. Thus

$$n = [4.45 + 18\, d_p/D]\, Re_p^{-0.1} = [4.45 + \frac{18 \times 0.456}{5.08}]\, (28.0)^{-0.1}$$

$$= 3.31$$

and voidage

$$\varepsilon = \left\{\frac{\langle j_1 \rangle}{V_\infty}\right\}^{1/n} = \left\{\frac{4.55}{7.37}\right\}^{1/3.31} = 0.864$$

(3) Gas holdup in gas-liquid flow

From experimental measurements, the following observations were recorded for the valve shut-off technique:

$L_{Ag} = 11.6$ cm, $L_{Eg} = 37.75$ cm, $L_{Cg} = 26.8$ cm

$h_1 = 11.0$ cm of Hg, $h_2 = 8.99$ cm of Hg,

$h_3'' = 12.56$ cm of Hg

Now the gas holdups in the three sections of the column were calculated from equations 8.2.26 - 8.2.28. Thus

$$\varepsilon_{2A} = 0.230, \quad \varepsilon_{2E} = 0.240, \quad \varepsilon_{2C} = 0.170$$

Similarly, from the recorded pressure drop in these sections, the gas holdup in each section was obtained by using equation 8.2.17. Then

$$H_C = -49.8 \text{ cm of } CCl_4, \quad L_C = 148.1 \text{ cm}$$

$$\varepsilon_{2CP} = -\frac{H(\rho_M - \rho_L)}{Z\ \rho_l} = \frac{49.8 \times 0.595}{148.1} = 0.200$$

In the test section, several pressure drop measurements (normally 5 - 15) were recorded and the gas holdups calculated from these measurements were averaged. In this case the average was

$$\varepsilon_{2EP} = 0.238$$

Similarly, in the section of column above the test section, two pressure drop measurements were recorded and the mean of gas holdups calculated from them was

$$\varepsilon_{3AP} = 0.240$$

It was shown in Appendix 8.2 that the pressure at different locations in the column varied; therefore, for comparing the gas holudps measured in different sections of the column, it is necessary that they all be referred to the same pressure. The procedure for obtaining these pressure corrections was discussed in detail in Appendix 8.2 and therefore only the results are presented. Thus the pressure at which the gas was collected (from h_1, h_2 and h_3'' in valve shut-off measurements)

in the test section = PSC = 8.46 cm of Hg

and below the test section = PCC = 22.06 cm of Hg

The pressure at the mid-point under running conditions (from equations 8.2.25 and 8.2.23)

in the test section = PME $\{\equiv (\bar{P})_A''\}$ = 7.45 cm of Hg

and below the test section = PMC $\{\equiv (\bar{P})_B''\}$ = 16.59 cm of Hg

As was noted in Appendix 8.2, the pressure at which the gas was collected in the test section, PSC, was only slightly greater than the pressure at the mid-point of the section, $(\bar{P}_A)''$.

Now the gas holdup can be corrected as follows:

$$\varepsilon_{2CC} = \varepsilon_{2C} \left(\frac{PCC + 76}{76} \right) = 0.220$$

Thus the gas holdups corrected to 760 mm of Hg (no correction was applied to gas holdups measured above the test section) are

$$\varepsilon_{2A} = 0.230, \quad \varepsilon_{2EC} = 0.266, \quad \varepsilon_{2CC} = 0.220$$

and $$\varepsilon_{2AP} = 0.240, \quad \varepsilon_{2EPC} = 0.261, \quad \varepsilon_{2CPC} = 0.241$$

The average of such corrected values of gas holdup was taken to represent the gas holdup in two-phase gas-liquid flow. Thus

$$\varepsilon_2 = 0.246 \quad \text{at } \langle j_1 \rangle = 4.55 \text{ cm/sec and } \langle j_2 \rangle = 9.94 \text{ cm/sec}$$

(4) Gas and solids holdup in three-phase fluidized beds

From experimental measurements the following observations were recorded for the valve shut off technique as before:

$$L_{Ag} = 10.95 \text{ cm}, \quad L_{Eg} = 29.55 \text{ cm}, \quad L_{Cg} = 25.85 \text{ cm}$$

$$h_1 = 11.00 \text{ cm of Hg}, \quad h_2 = 9.17 \text{ cm of Hg}, \quad h_3''' = 13.10 \text{ cm of Hg}$$

Now the gas holdup in the three sections of the column were calculated from equations 8.2.26 - 8.2.28. Thus

$$\varepsilon''_{2A} = 0.217, \quad \varepsilon_{2E} = 0.188, \quad \varepsilon''_{2C} = 0.162$$

Similarly, from the recorded pressure drops in these sections, the gas holdup in each section was obtained by using equation 8.2.17. Thus

$$\varepsilon''_{2AP} = 0.209, \quad \varepsilon''_{2EP} = 0.182, \quad \varepsilon''_{2CP} = 0.194$$

Note that ε''_{2EP} was obtained from the slope of the pressure drop profile (line I + II of Figure 8.2.2) above the bed and represents the gas holdup in the two-phase region of the test section, unlike ε_{2E}, which represents the combined gas holdup in the two-and three-phase regions.

Before a comparison between these gas holdups could be attempted, it was necessary that they all be referred to the same pressure. The procedure for correcting them was exactly the same as described above, and also outlined in Appendix 8.2. Thus, summarizing, the pressure at which the gas was collected (from h_1, h_2, and h'''_3 of valve shut-off measurements)

in the test section = PSC = 8.35 cm of Hg

and below the test section = PCC = 23.96 cm of Hg

The pressure at the mid-point under running conditions (from equations 8.2.23 and 8.2.24)

in the test section = PME $\{\equiv (\bar{P})'''_A\}$ = 7.92 cm of Hg

and below the test section = PMC $\{\equiv (\bar{P})'''_B\}$ = 16.59 cm of Hg

It can be seen that PME in three-phase fluidized beds of 1/4 mm glass beads is not much different from that in gas-liquid flow. However, in three-phase fluidized beds of large heavy particles, e.g. lead shot and steel shot, PME was considerably larger than that in gas-liquid flow.

The pressure correction was then applied and the gas holdups, corrected to 760 mm of Hg, are

$$\varepsilon''_{2A} = 0.217, \quad \varepsilon_{2EC} = 0.208, \quad \varepsilon''_{2CC} = 0.212$$

$$\varepsilon''_{2AP} = 0.219, \quad \varepsilon''_{2EPC} = 0.197, \quad \varepsilon''_{2CPC} = 0.241$$

From the measured longitudinal pressure drop profile, the following quantities were obtained (see Figure 8.2.2):

S_I = 1.139 cm of CCl_4/inch of three phase bed

H_{max} = 15.13 cm of CCl_4

Z_{max} = 12.6 inches

Then the expanded bed height from equation 3.6 is

$$L_b = (Z_{max})_{cm} + 8.7 = 2.54 \times 12.6 + 8.7$$

$$= 40.7 \text{ cm}$$

and

$$\% \text{ bed contraction} = \left(\frac{72.2 - 40.7}{72.2}\right) \times 100 = 43.6\%$$

Now solids holdup was calculated from equation 3.1:

$$\varepsilon_3 = \frac{566.52}{20.268 \times 40.7 \times 2.935} = 0.234$$

and the bed voidage from equation 1.3:

$$\varepsilon = 1-\varepsilon_3 = 0.766$$

The gas holdup in the three-phase fluidized bed from valve shut-off measurements was then calculated from equation 8.2.33. Thus

$$\varepsilon_2''' = 0.209 + [0.208 - 0.209] \frac{157.5}{40.7} = 0.205$$

The gas holdup was also calculated from the measured longitudinal pressure drop profiles as follows:

1. For $Z < Z_{max}$, equation 8.2.12 was used for calculating the gas holdups from pressure drop measurements. Normally 5-10 readings were recorded and the average gas holdup in the bed was taken as the mean value of the gas holdups so calculated. Thus, in this case

$$\varepsilon_2''' = 0.155$$

2. From the slope of the best straight line through the data, S_I, the gas holdup in the bed was obtained from equation 3.8. Thus

$$\varepsilon_2''' = [0.234 \times 1.935 - (\frac{1.139}{2.54}) \times 0.595] = 0.186$$

3. From the point of intersection of the two straight lines, the gas holdup was obtained from equation 3.9. Thus

$$\varepsilon_2''' = [\frac{0.234 \times 1.935 \times (2.54 \times 12.6) - 15.13 \times 0.595}{2.54 \times 12.6}]$$

or $\varepsilon_2''' = 0.172$

Although a significant variation occurred in this instance amongst the four values of gas holdup measured by the two techniques, better agreement was observed in deeper beds at higher liquid flow rates. The gas holdup values reported as data in Appendix 8.7 are an average of these four values, except when ε_{2E} is not measurable (at small gas flow rates). Thus the average gas holdup in the present three-phase fluidized bed is

$$\varepsilon_2''' = 0.179$$

The average gas holdup in the two-phase gas-liquid regions of the column was obtained, as before, by averaging

the measured values in different sections of the column, excluding ε_{2E} in this case. Thus the average gas holdup in the two-phase regions was

$$\varepsilon_2'' = 0.215$$